Solutions for Innovation

JMS-S3000 SpiralTOF™ series

Polymers, Materials, & Chemistry Applications Notebook

Edition June 2020

JEOL Ltd.

JMS-S3000 SpiralTOF™ series

Polymers, Materials, & Chemistry Applications Notebook

Edition June 2020

Table of Contents

- For any question or inquiry regarding this Applications Notebook, please contact your local JEOL representative, or use the Product Information Request form on our Global Web Site: https://www.jeol.co.jp/en/support/support_system/contact_products.html
  - The contact information on each applications note is that at the time of the initial publication and might not be current.
  - The contact information and affiliations of the authors on the JEOL News articles are those at the time of the initial publication and might not be current.
- Irganox is either a registered trademark or a trademark of BASF SE in the United States and other countries.
- SpheriCal is a trademark of Polymer Factory Sweden AB.
- Cadenza is a trademark of Imtakt Co., Ltd.
- Polymerix is a trademark of Sierra Analytics, Inc.

Development of JMS-S3000: MALDI-TOF/TOF Utilizing a Spiral Ion Trajectory

Takaya Satoh

MS Business Unit, JEOL Ltd.

We have developed the JMS-S3000, matrix assisted laser/desorption ionization time-of-flight mass spectrometer (MALDI-TOFMS). An innovative ion optical system, which achieved a spiral ion trajectory, surpassed basic specification of the reflectron ion optical system presently used in most commercially available TOFMSs. Furthermore, we have developed the TOF-TOF option for the JMS-S3000. In the case of attaching the TOF-TOF option, a spiral ion optical system is adopted for the first TOFMS, whereas a reflectron ion optical system with offset parabolic reflectron is adopted for the second one. Utilizing the spiral trajectory ion optical system, the JMS-S3000 provides unprecedentedly high mass resolution and high precursor ion selectivity. In this paper, we demonstrate not only the high mass resolution of more than 60,000 (FWHM) at *m/z* 2093 but also achievement of high mass resolution over a wide mass range. In addition, we present the high selectivity that enables selection of monoisotopic ions of precursor ions. By selecting only monoisotopic ions of precursor ions, one signal peak corresponding to each fragmentation channel is observed on a product ion spectrum. Consequently, the analysis of the product ion spectrum is made clearer.

Introduction

The time-of-flight mass spectrometer (TOFMS) is one of mass spectrometry techniques, which include the quadrupole mass spectrometer, the magnetic sector mass spectrometer, the ion trap mass spectrometer and the Fourier transform ion cyclotron resonance mass spectrometer. In the case of TOFMS, ions of various m/z values, which are generated in the ion source, are accelerated to the detection plane by a pulse voltage applied from a starting time of data acqisition. Since the time-of-flight of ions at the detection plane are proportional to the square root of their m/z values, the ions generated in the ion source can be separated. One of the TOFMS feature is fast measurement, which is due to the unnecesity of scan for any physical parameters such as electric or magnetic fields. Recently, not only a single type mass spectrometer, but also a tandem type mass spectrometer connected with the quadrupole mass spectrometer (Q/TOF) or tandemly connected two TOFMSs (TOF/TOF) are available.

The mass resolution of TOFMS is expressed by $T/2\Delta T$, where ΔT is the time-of-flight distribution of the ion group with the same m/z value(ion packet) at the detection plane (that is, spatial distribution of the ion packet in the flight direction at the detection plane) and, T is centroid of the time-of-flight distribution. Since TOFMS was invented in 1964 [1], its mass resolution has been improved by increasing T and decreasing ΔT. In 1955, a unique acceleration technique was developed, which focuses the initial space and energy distributions at the detector surface in the flight direction. Applying this technique, the mass resolution was increased by decreasing ΔT [2]. Furthermore, in the early 1970s, a new technique was developed. In this technique, the focus position defined by the above-mentioned acceleration technique is chosen as the start point, and an ion optical system that is composed of ion mirror [3] or elerctrostatic sectors [4] is placed at the post stage. This innovation made it possible to increase the time-of-flight T without increasing ΔT, and led to a dramatic improvement of the mass resolution. Recently, most of commercially available TOFMS instruments use ion mirrors, and their flight paths are 1 to 3 m. For further improvement in the mass resolution of TOFMS, another types of ion optical systems have been proposed. They are the multi-reflecting type [5] and the multi-turn type [6-7] ion optical system where ions fly multiple times on the certain trajectory. These two ion optical systems theoretically achieve an infinitely long flight path in a compact space, and impoved the mass resolution. However, they have the limitation of the mass range because ions with large speed (ions with small m/z) lap the ions with small speed (ions with large m/z) when the ions flying on the same trajectory multiple times.

We have developed an original ion optical system that utilizes a spiral ion trajectory. This ion optical system can overcome the "lap" problem present in multi-reflecting and multi-turn type ion optical systems. In addition, it is possible to achieve mass resolution and mass accuracy higher than those of widely used reflectron ion optical systems. In this paper, we describe the design of the spiral trajectory

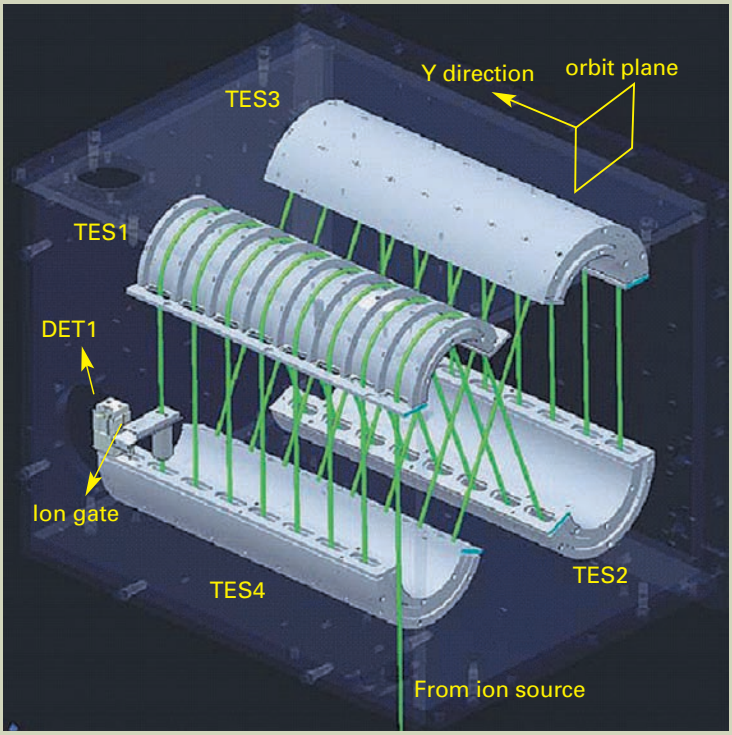

Fig. 1 Spiral ion trajectory ion optical system.

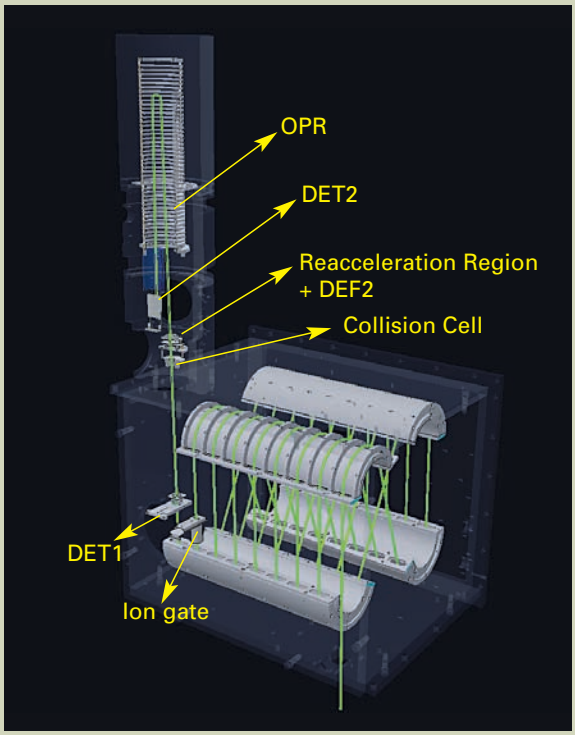

Fig. 2 MALDI-TOF/TOF utilizing the spiral ion trajectory ion optical system.

type ion optical system, and basic performance of a MALDI-TOF/TOF system applying it. The system consistsed of the spiral trajectory type ion optical system and reflectron type ion optical system using offset parabolic reflectron for the first and second TOFMSs, respectively. The instrument achieves higher mass resolution, mass accuracy and precursor ion selectivity due to utilizing a spiral ion optical system for the first TOFMS, thus enabling more precise analysis.

Design of the spiral trajectory ion optical system

Multi-turn type ion optical system technique was applied for development of the spiral trajectory ion optical system. Especially, a combination of the "perfect focusing" and "multi-turn" [12] techniques developed at Osaka University, which achieved highest mass resolution in the world, was considered the most suitable for development of the spiral trajectory ion optical system. For conversion of a multi-turn type ion optical system for a spiral trajectory ion optical system, it is necessary to move ion trajectory perpendicular to the orbit plane. In order to achieve this, we have designed the system so that ion injection is slightly tilted to the orbit plane. The advantage of the design is that there is no need for the mechanism to transfer the ions to the next layer. There are concerns about degradation of mass resolution due to the trajectory deviation from a multi-turn type ion optical system. However, the effect should be negligible by keeping the injection angle to several degrees.

Practically, we have designed the spiral trajectory ion optical system based on MULTUM II [7] construction, which consists of four toriodal electrostatic sectors (cylindrical electrodes with two Matsuda plates). The schematic of the ion optical system is shown in **Fig. 1**. To achieve a spiral trajectory, we have constructed a layered toriodal electric field (TES) by placing (number of cycles +1) Matsuda plates into the cylindrical electrostatic sectors. The Matsuda plates are arranged within certain equal distances L_y in the space L_x between the external and internal electrodes. The three types of voltages applied on TESs 1 to 4 is that of the internal electrode, external electrodes and Matsuda plates. Corresponding voltages are supplied to every Matsuda plates, internal and external electrodes of TESs 1 to 4.

Also, four TESs were placed so that they correspond to MULTUM II when looked from the orbit plane. Y direction was set perpendicular to the periodic orbit plane. In development of the MALDI-TOF/TOF, we have made Y direction to horizontal. The TES1 in the Fig. 1 shows the external electrode is removed so that it can be seen the Matsuda plates are equally spaced. Ions fly through the center of the space, formed by L_x and L_y. Ion passes the same layer of TESs 1 to 4, and after passing the TES 4, it enters to the next layer of TES 1. The process is repeated for several cycles; the ion thus draws a spiral trajectory and reaches the detector (DET1) (Green line in the Figure 1 represents the ion trajectory). The injection angle θ into the layered toriodal electric field can be expressed as follows,

$$\tan\theta = (L_y + L_m) / L_c \quad \cdots\cdots\cdots (1)$$

where, L_m is the thickness of a Matsuda plate and L_c is the one cycle length.

As mentioned above, owing to the usage of four TESs of the same structure in it's construction, the ion optical system can achieve a complicated trajectory within a simple structure.

Production of MALDI-TOF/TOF utilizing spiral trajectory ion optical system

We have developed MALDI-TOF/TOF utilizing the spiral trajectory ion optical system. It consisted of the first TOFMS using the spiral trajectory ion optical system and the second TOFMS using the reflectron ion optical system. The mass spectrum measurement in the first TOFMS is referred as spiral mode, and the product ion spectrum measurement in the second TOFMS as TOF/TOF mode.

An schematic of the system is shown in **Fig. 2** (ion source and the detector DET1 of the first TOFMS are omitted). Spiral trajectory is set to eight cycles of 2.093 m per each. A distance between central trajectories of the adjacent layers is 58 mm, an injection angle is 1.6 degree according to equation (1). Y direction is set as horizontal, so the injection angle is achieved by tilting the extraction direction of the ion source 1.6 degrees from a horizontal plase.

In the spiral mode, ions fly a spiral trajectory and are detected with the spiral mode detector (though not specified in Fig. 2, it is located similarly to DET1 in Fig. 1). Ion gate is placed in the 7th cycle. It allows eliminating high-intensity matrix ions , which are outside of the data acquisition m/z range.

In TOF/TOF mode, selection width of the ion gate is made narrower and monoisotopic ions of precursor ions are selected out of all isotpic ions of them. It is possible to mechanically move the spiral mode detector out of the trajectory so that precursor ions can be introduced into the collision cell. Ions, that entered a collision cell, collide with rare gas inside of the cell with a kinetic energy of approximately

20 keV, and generate fragment ions. Precursor ions and fragment ions are mass-separated in a reflectron ion optical system that combines an offset parabolic reflectron (OPR) [13] and a reacceleration mechanism. OPR is a reflectron connecting a linear and parabolic electric fields. It allows simultaneous observation of ions, from low *m*/*z* fragment ions up to precursor ions. In addition, in order to increase transmission of ions, fine adjustment of the ion trajectory is enabled by installing two deflectors (DEF1 and DEF2) on both sides of the collision cell.

Evaluation of MALDI-TOF/TOF with spiral trajectory ion optical system utilized

Figure 3 shows mass spectrum of six types of peptide mixtures (in order of *m*/*z* increase: Bradykinin fragment 1-7, Angiotensin II, Angiotensin I, P14R, ACTH fragment 1-17, ACTH fragment 18-39). The mass spectrum of Angiotensin II and ACTH fragment 1-17 are also displayed as an enlarged image. Mass resolution is 58000 (FWHM) and 73000 (FWHM) respectively. The mass error of ACTH fragment 1-17 is 0.16 ppm, when internal calibration is performed among five peptides except ACTH fragment 1-17. It became clear from the above mentioned facts that distance of flight for spiral trajectory ion optical system is 17 m, which is 5 times longer than that of the conventional reflectron type ion optical systems. This allows enhancement of mass resolution and mass accuracy.

Figure 4 shows the relation between *m*/*z* value and mass resolution when mass resolution is adjusted with ACTH fragment 1-17. Figure 4 shows that it is possible to achieve high mass resolution simultaneously in a wide *m*/*z* range. This overcomes the problem of MALDI-TOFMS utilizing conventional reflectron type ion optical system that could achieve high mass resolution only in a narrow *m*/*z* range.

Figure 5.a shows a product ion spectrum diagram of Poly (oxypropylene), acquired in TOF/TOF mode. Selected precursor ions are monoisotopic ions from $[M+Na]^+$ series with *m*/*z* 1027. A numbers of fragmentation channels from sodium ions as fragment ion to precursor ion ion are observed. The enlarged spectrum around *m*/*z* 780 is shown in Fig. 5.b. The system is able to select only monoisotopic ions of precursor ions, therefore each fragment channels can be observed as one peak without any isotopic peaks. Two peaks in Fig. 5.b indicate different fragmentation channels. It indicates that 2u different fragmentation channels can be clearly separated. Figure 5.c displays an image of the same *m*/*z* range as in Fig. 5.b when measured with conventional MALDI-TOF/TOF. Pecursor ion selectivity of traditional TOF/TOF is insufficient so that the fragment ions from all isotopic ions of precursor ions are analyzed in the second TOFMS. Thus every fragmentation channels of product ion spectrum include isotopic peaks. As a result, when *m*/*z* values of monoisitopc ions of two fragment channels are close, such as 2 u, their isotopic peaks are overlapped and are impossible to be clearly identified. The high precursor ion selectivity originated from the spiral trajectory ion optical system used in this system makes the structual analysis of chemical compounds much easier.

Conclusion

This paper reports on the development of the spiral trajectory ion optical system. Also, the paper describes the development of MALDI-TOF/TOF, which combines a spiral trajectory ion optical system and reflectron type ion optical system utilizing offset parabolic ion mirrors. Innovative ion optical system introduced to the JMS-S3000 has overcome preexisting problems related to conventional MALDI-TOF and MALDI-TOF/TOF. Thus, the JMS-S3000 is expected to play a significant role in various areas.

References

[1] W. E. Stephens. *Phys. Rev.*, **69**, 691 (1946)

[2] W.C.Wiley and I. H. McLaren, *Rev. Sci. Instrum.*, **26**, 1150 (1955).

[3] B. A .Mamyrin, V. I. Karataev, D. V. Shmikk and V. A. Zagulin, *So. Phys. JETP*, 3745(1973).

[4] W. P. Poschenrieder, *Int. J. Mass Spectrom. Ion. Phys.*, **6**, 357 (1972).

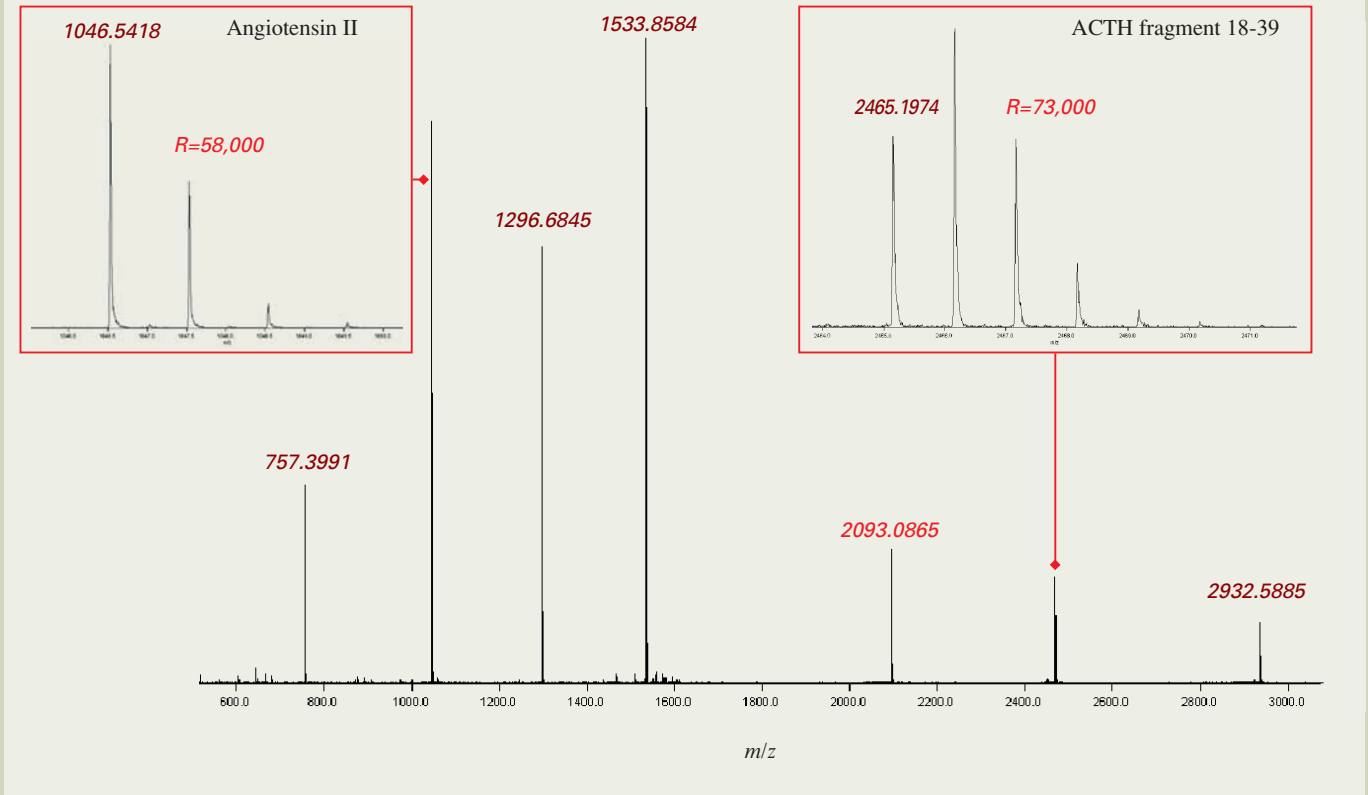

Fig. 3 Mass spectrum of peptide mixtures.

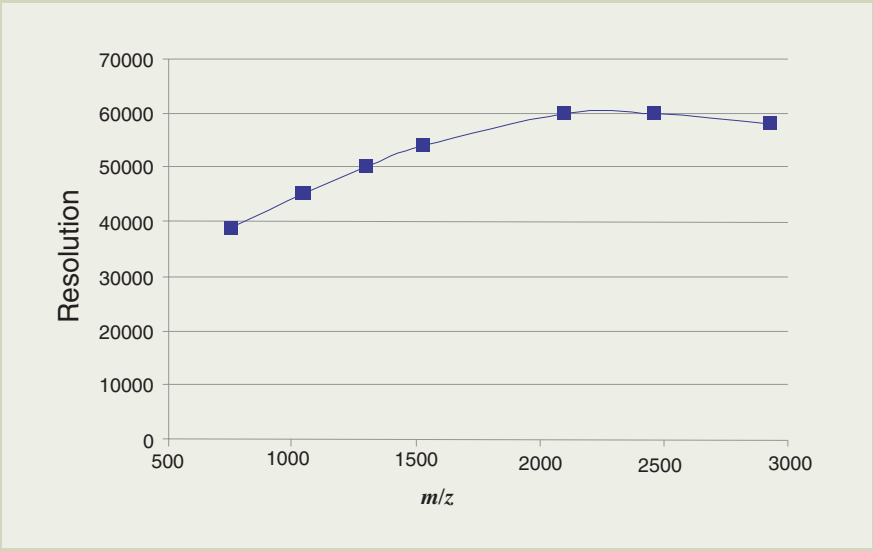

Fig. 4 Relation between *m*/*z* value and mass resolution.

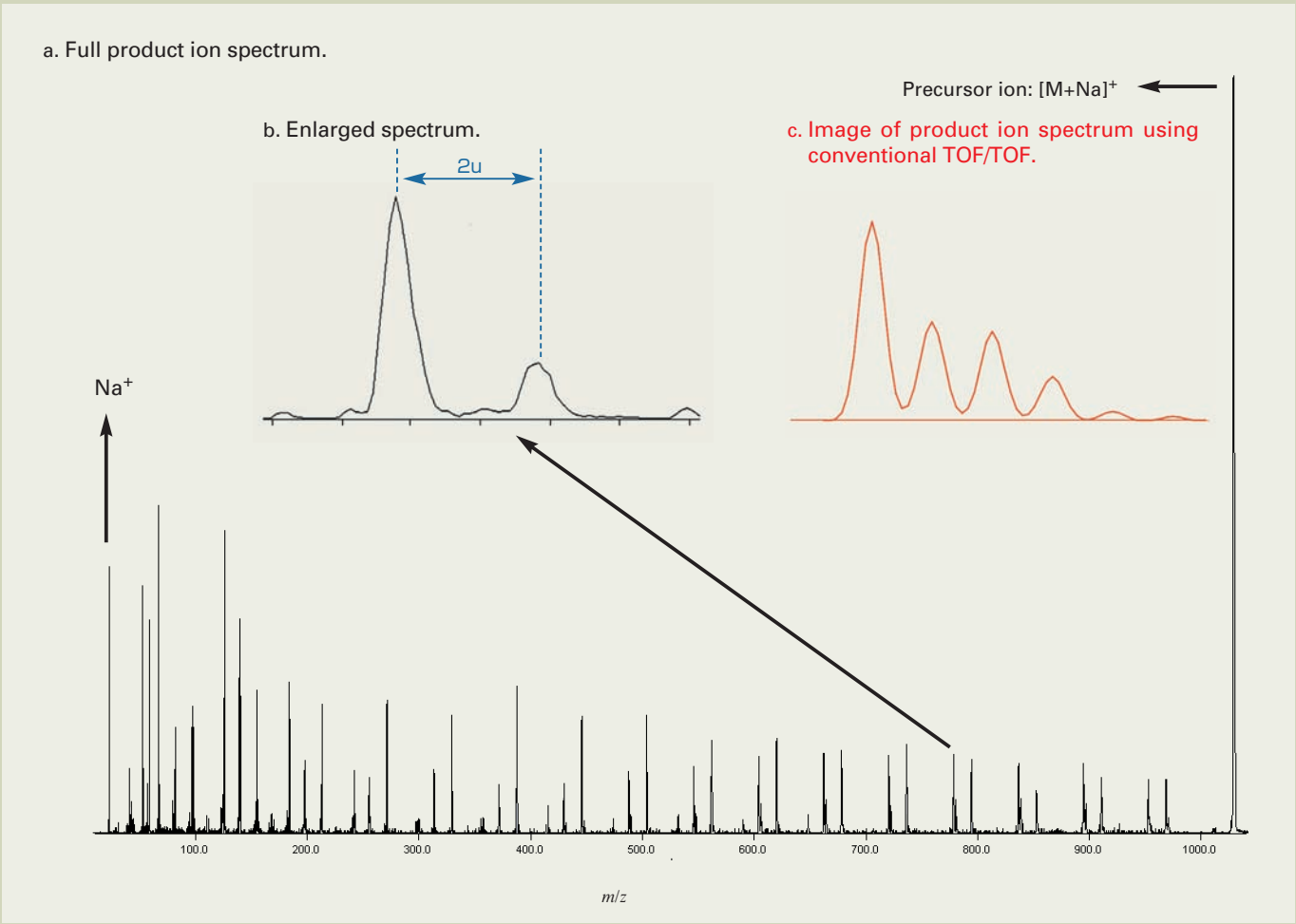

Fig. 5 Product ion spectrum of Poly(oxypropylene).

[5] H. Wollnik and A. Casares, *Int. J. Mass Spectromety,* **227**, 217 (2003).
[6] M. Toyoda, M. Ishihara, S. Yamaguchi, H. Ito, T. Matsuo, R. Reinhard and H. Rosenbauer, *J. Mass Spectrom.,* **35**, 163 (2000).
[7] D. Okumura, M. Toyoda, M. Ishihara and I. Katakuse, *J. Mass Spectom. Soc. Jpn.,* **51**, 349 (2003).
[8] M. Yavor, A. Verentchikov, J. Hasin, B. Kozlov, M. Gavrik and A. Trufanov, Physics Procedia 1 391 (2008)
[9] T. Satoh, H. Tsuno, M. Iwanaga, Y. Kammei, *J. Am. Soc. Mass Spectrom.,* **16**, 1969 (2005).
[10] T. Satoh, H. Tsuno, M. Iwanaga, and Y. Kammei, *J. Mass Spectrom. Soc. Jpn.,* **54**, 11 (2006).
[11] T. Satoh, T. Sato, and J. Tamura, *J. Am. Soc. Mass Spectrom.* **18**, 1318 (2007).
[12] M. Ishihara, M. Toyoda and T. Matsuo, *Int. J. Mass Spectrom.,* **197**, 179 (2000).
[13] E. N. Nikolaev, A. Somogyi, D. L. Smith, C. Gu, V. H. Wysocki, C. D. Martin and G. L. Samuelson, *Int. J. Mass Spectrom.,* **212**, 535 (2001)

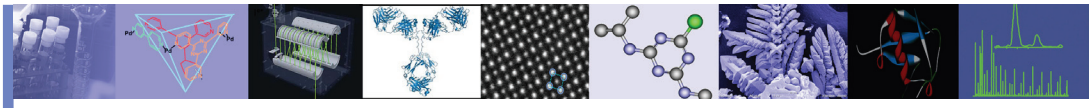

Applications Note

SpiralTOF™

The Relationship between Crystal Condition and Mass Resolving Power, Mass Accuracy

Introduction

The JMS-S3000 SpiralTOF™ has a unique 17 m flight path that offers the highest resolution MALDI-TOF MS system currently available. With an extended flight distance, the SpiralTOF reduces topographic effect of matrix crystal to a minimum and achieves highly reproducible mass resolving power and high mass accuracy with external mass calibration.

In this work, we demonstrate the measurement of a polymer standard with 4 types of matrices that are typically used for MALDI polymer measurement by using the JEOL SpiralTOF system. Additionally, we looked at the crystal condition using the JEOL JSM-7600F thermal field emission scanning electron microscope (FE-SEM).

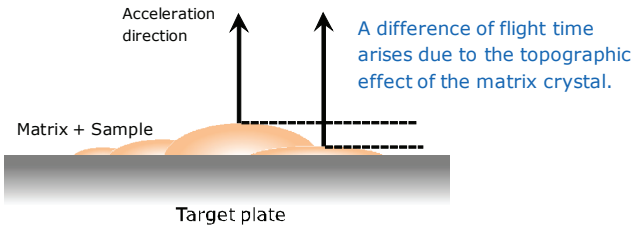

Figure 1. Reduced topographic effect of matrix crystal.

Experimental

Sample information and preparation conditions are shown in Table 1. PEG1500 was dissolved in water at a concentration of 10 mg/mL. Each matrix was dissolved in THF at a concentration of 10 mg/mL. NaI used as the cationization agent was dissolved in THF at a concentration of 1 mg/mL. Next, the PEG1500, NaI and matrix solutions were mixed together 1:1:2 (1:1:4 for DIT) by volume. Afterwards, 0.75 µL of this mixture was placed on the hairline finish stainless steel plate (MTP format, 384 spots for samples and 96 spot for calibrant). Finally, the dried sample was measured using the JMS-S3000 SpiralTOF MS system. We also obtained SEM images for each crystal condition with the JSM-7600F.

Polymer standard	Conc.	Solvent
Polyethylene glycol (PEG) 1500	10 mg/mL	Water
Cationization agent		
NaI	1 mg/mL	Water
Matrix		
α-Cyano-4-hydroxycinnamic acid (CHCA)	10 mg/mL	Tetrahydrofuran (THF)
2,5-Dihydroxybenzoic acid (DHB)	10 mg/mL	THF
Dithranol (DIT)*	10 mg/mL	THF
trans-3-Indoleacrylic acid (IAA)	10 mg/mL	THF
Sample		
PEG1500/NaI/Matrix = 1/1/2 (v/v) * PEG1500/NaI/DIT = 1/1/4 (v/v)		
0.75 µL of this sample solution mixture was placed on the MALDI target plate		
JSM-7600F conditions		
Sample preparation	Uncoated	
Acceleration voltage	1 kV	
Magnification	x500 and x2,000	

Table 1. Sample information and preparation conditions.

Figure 3. JMS-3000 SpiralTOF.

Figure 4. JSM-7600F Thermal FE-SEM.

MS-0328A

Results & discussion:

The MALDI mass spectra of PEG1500 are shown in Figure 4 for each matrix. We set the delay time to achieve the maximum mass resolving power at *m/z* 1537.9. Therefore, the resolving power was approximately 70,000 for the $[HO(C_2H_4O)_{34}H + Na]^+$ peaks, well in excess of that needed to separate isotope peaks. Additionally, we observed excellent mass distributions.

We determined the average mass resolving power (n=10) and external mass accuracy (n=8) for *m/z* 1097.6, *m/z* 1537.9 and *m/z* 1978.2 for each matrix. The results are shown in Figure 5 and 6, respectively. We achieved high mass resolving power for the three selected ions with each matrix. In addition, we obtained excellent mass error (less than 10 ppm) with external calibration for each matrix.

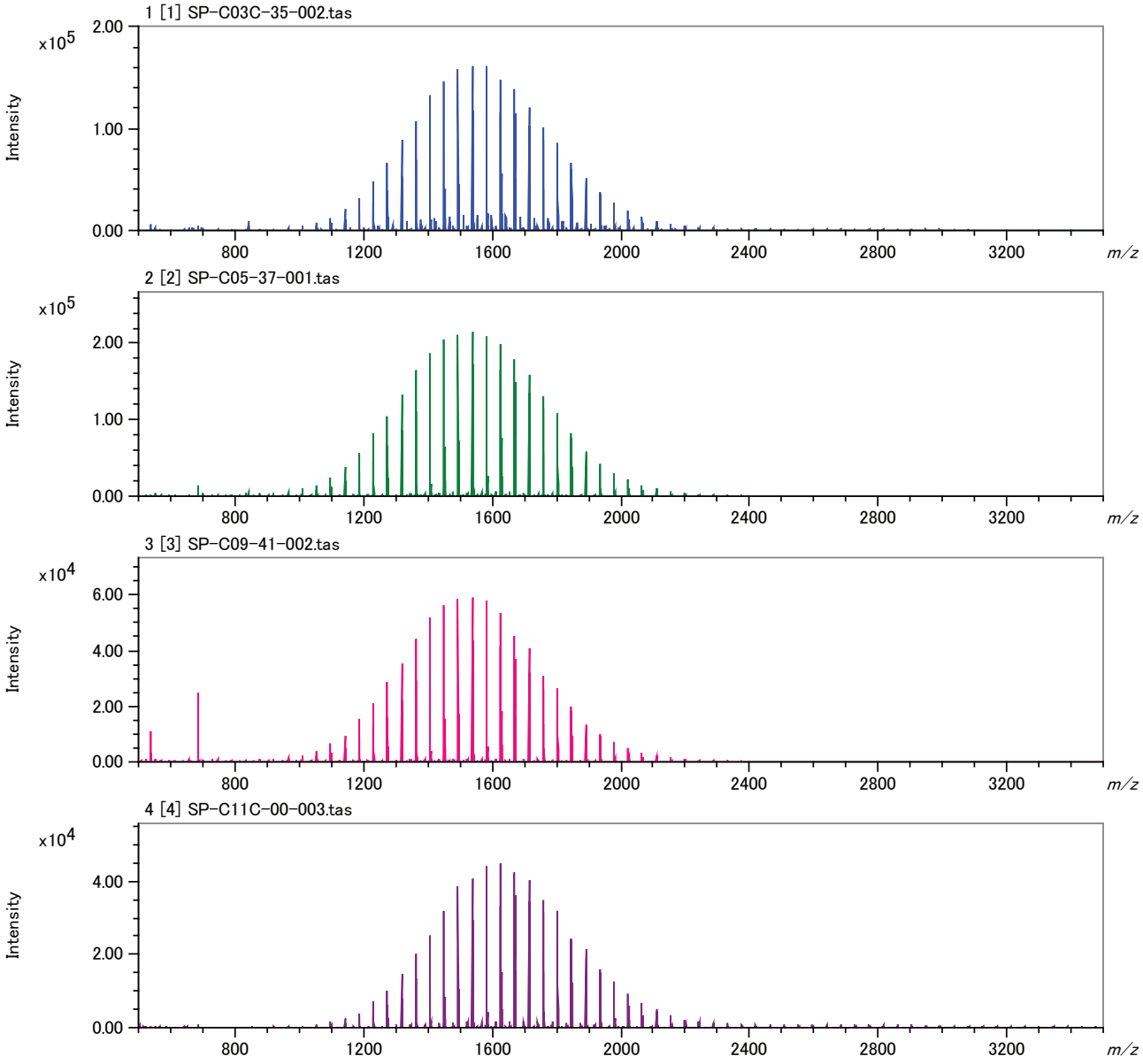

Figure 4. MALDI mass spectra of PEG1500.

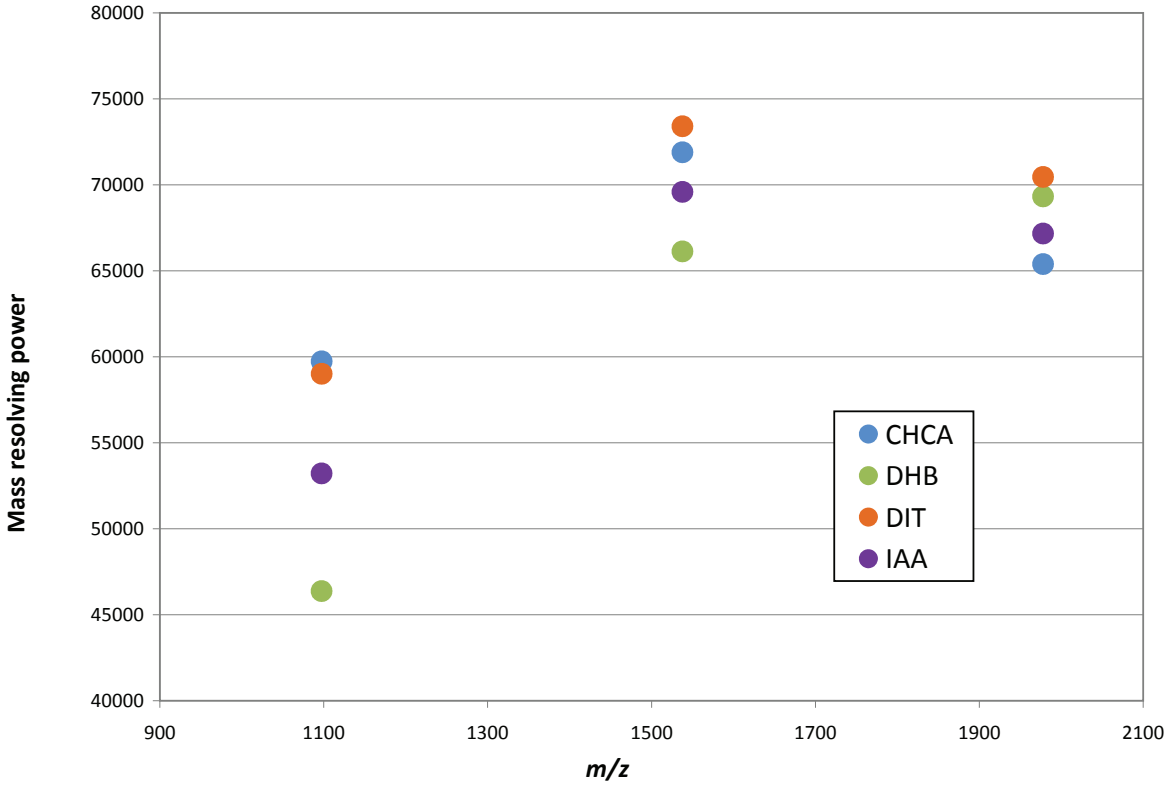

Figure 5. Averaged mass resolving power (n=10) for *m/z* 1097.6, *m/z* 1537.9 and *m/z* 1978.2.

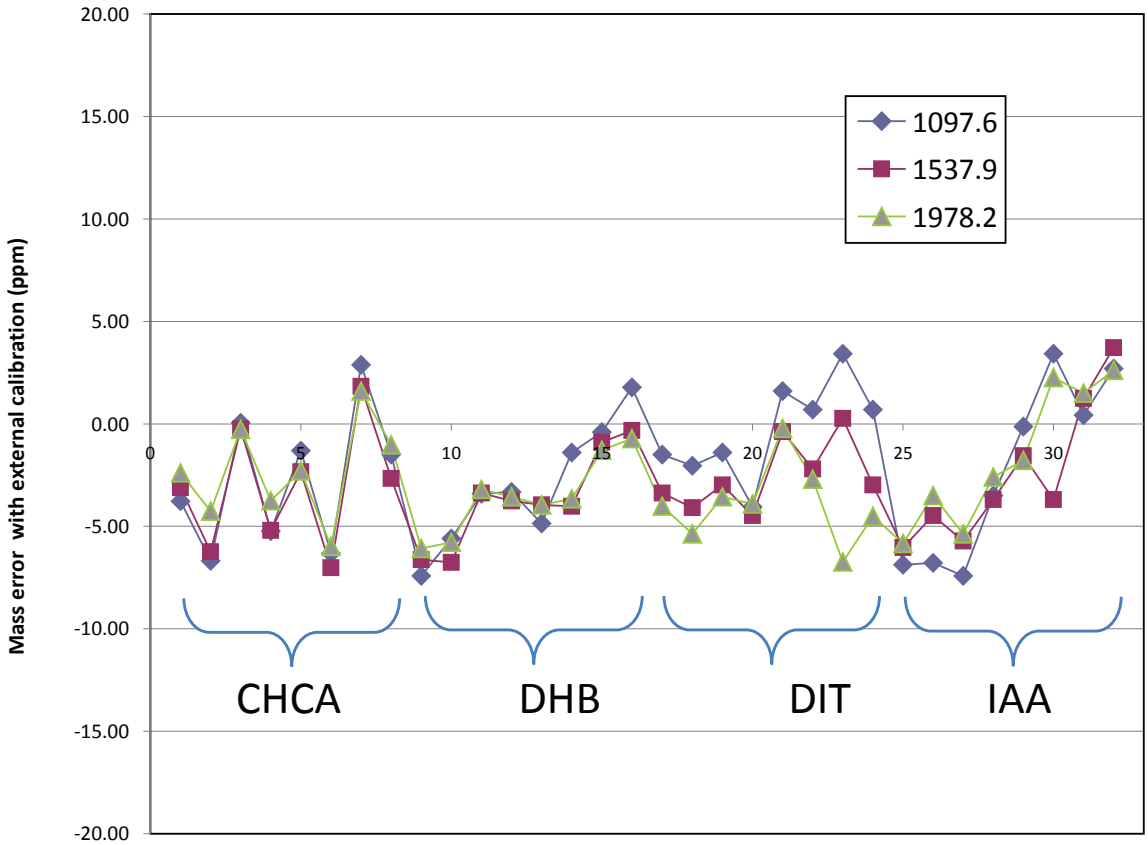

Figure 6. Mass error with external calibration (n=8) for *m/z* 1097.6, *m/z* 1537.9 and *m/z* 1978.2.

We examined the crystal condition with the JEOL JSM-7600F thermal field emission scanning electron microscope. The SEM images are shown Figures 7-10. The crystal shape, size and dispersion were quite different in each matrix crystal. However, SpiralTOF performance was not affected by the topographic effects because these spatial differences were a negligible fraction of the 17 m flight path.

Conclusions

SpiralTOF achieved highly reproducible mass resolving power and high mass accuracy with external mass calibration for all samples. These values were not significantly influenced by the different crystal morphologies for the different matrices. This is attributed to the SpiralTOF's very long (17 meter) flight path.

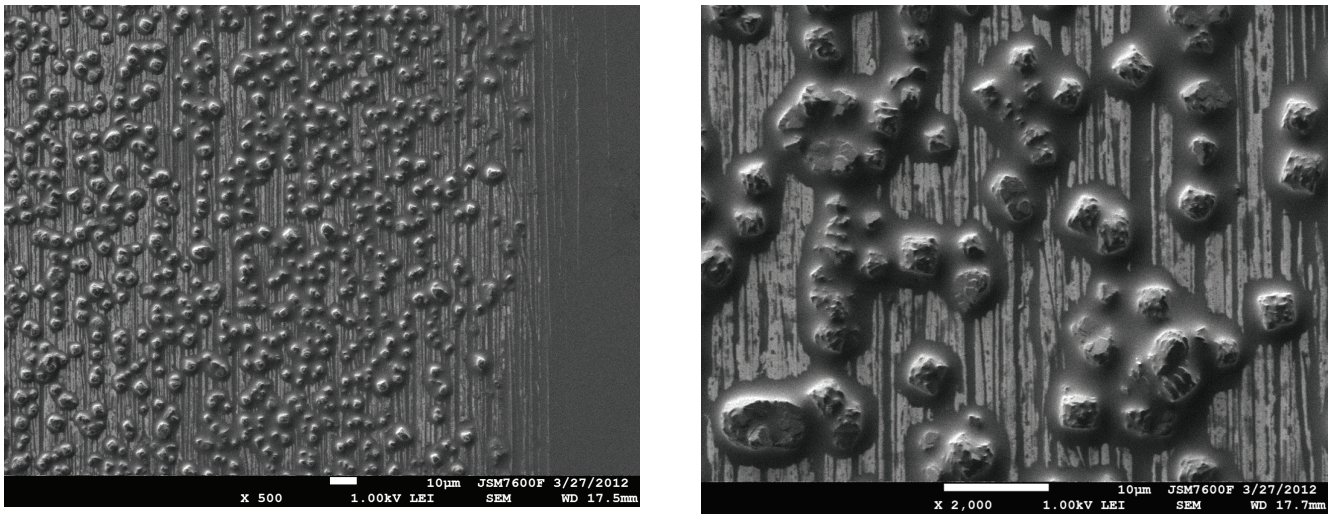

Figure 7. SEM images of CHCA crystal with PEG1500: left: x500, right: x2,000.

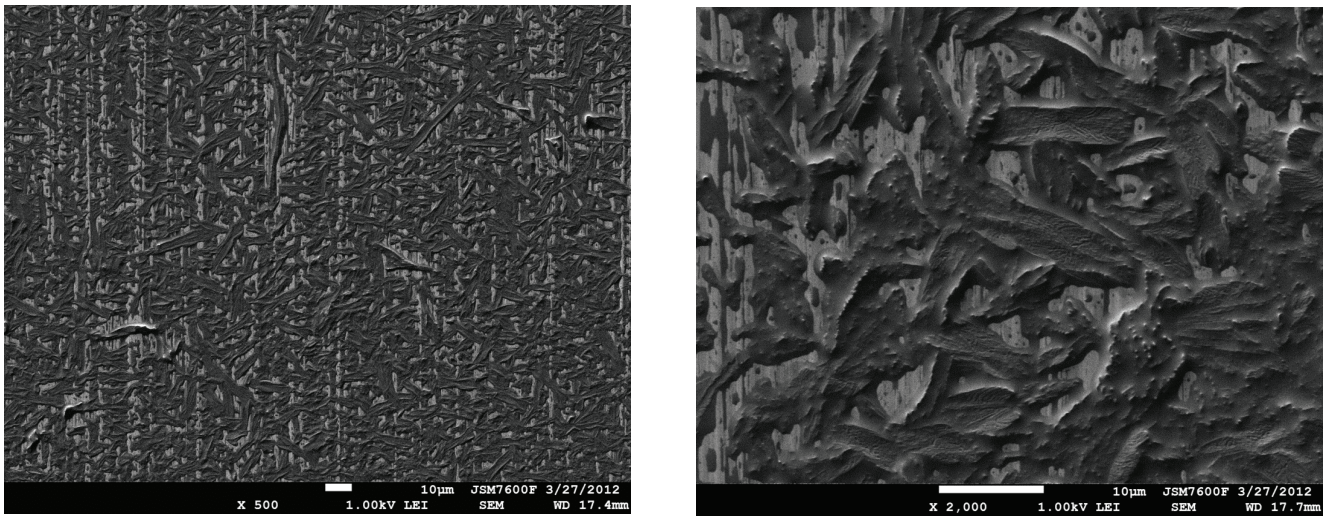

Figure 8. SEM images of DHB crystal with PEG1500: left: x500, right: x2,000.

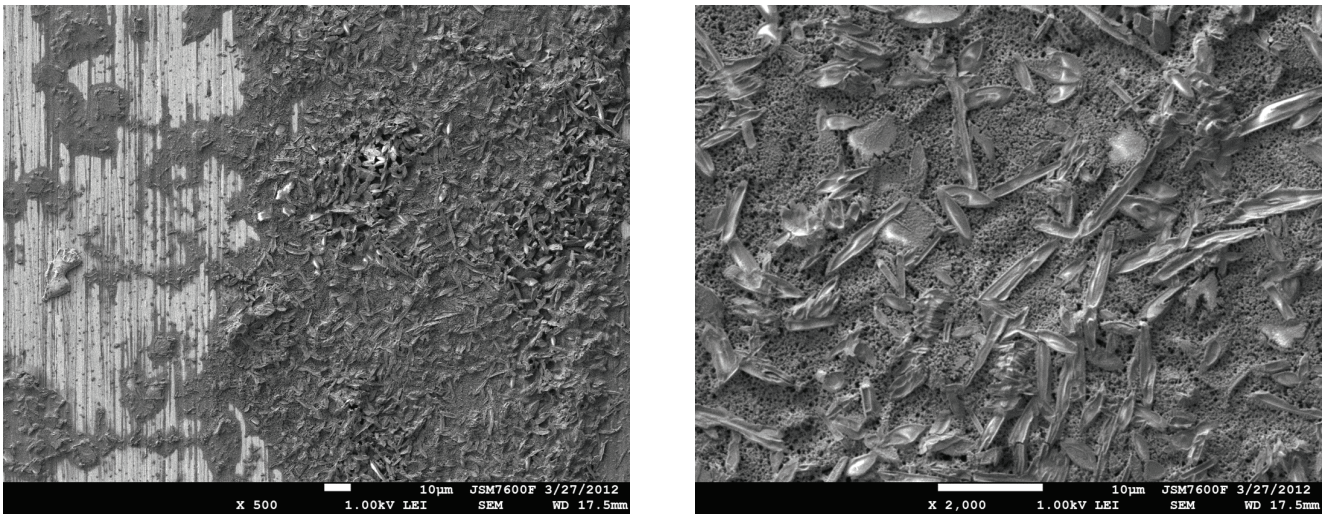

Figure 9. SEM images of DIT crystal with PEG1500: left: x500, right: x2,000.

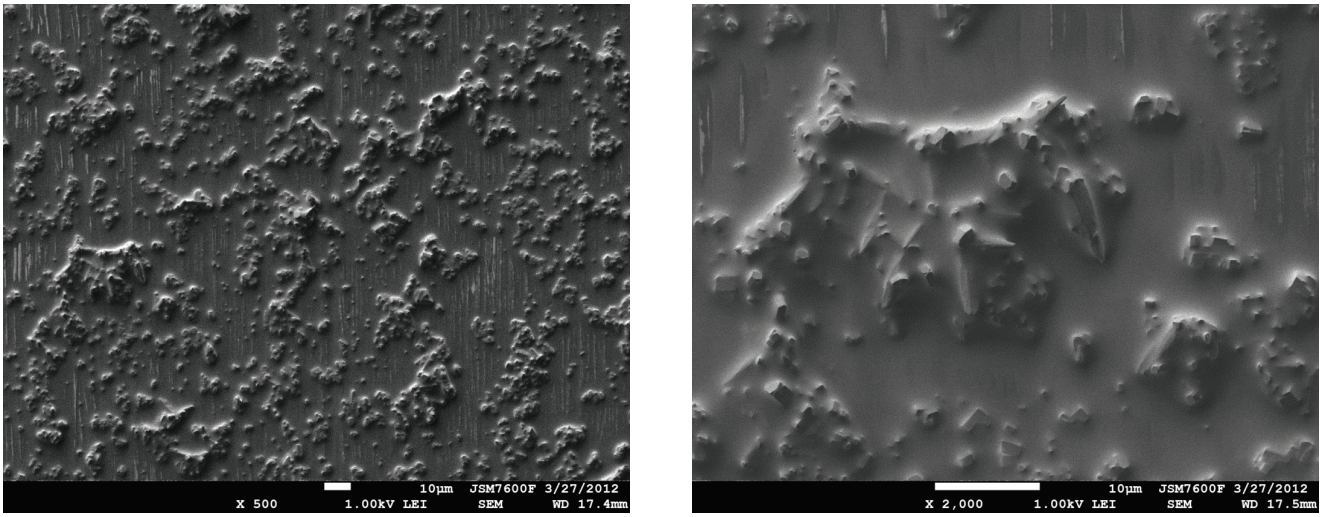

Figure 10. SEM images of IAA crystal with PEG1500: left: x500, right: x2,000.

Detailed Structural Characterization of Polymers by MALDI-TOFMS with a Spiral Ion Trajectory

Hiroaki Sato National Institute of Advanced Industrial Science and Technology

Introduction

Detailed structural characterization of polymers is important because molecular properties of polymers strongly influence the material properties. Structural characterization of polymers have been performed by various instrumental analyses such as spectroscopic techniques (nuclear magnetic resonance spectroscopy: NMR, infrared spectroscopy: IR), chromatographic techniques ((pyrolysis-)gas chromatography: (Py-)GC , high performance liquid chromatography: HPLC, size exclusion chromatography: SEC), as well as mass spectrometry. Matrix-assisted laser desorption ionization time-of-flight mass spectrometry (MALDI-TOFMS) can observe molar mass of each polymer chain without fragmentation. Therefore, it exhibits its power for the determination of detailed polymer structures such as repeating units, end-groups, molecular weight distribution, and copolymer compositions. However, characterization of industrial complicated polymers such as copolymers and polymer blends are difficult by conventional MALDI-TOFMS, because a mass of polymer chains within complex polymeric materials increases the likelihood of isobaric interference, in which the peaks of different chemical compositions with the same nominal mass overlap. Peak separation of isobaric components requires high-resolution mass spectrometry. This report first describes brief features of high-resolution MALDI-TOFMS with a spiral ion trajectory, termed "MALDI spiral-TOFMS", and then some applications of MALDI spiral-TOFMS for a detailed structural characterization of complicated polymers are presented.

Fundamental: Time-of flight mass spectrometer with a spiral ion trajectory

The combination of a MALDI source and a time-of-flight mass spectrometer is better suited for mass spectrometry of the ions generated by pulsed laser irradiation. MALDI-TOFMS system is typically composed of a UV pulse laser, a MALDI source, a flight tube, and a detector. Ions generated by pulsed laser irradiation are accelerated by electrical potential between a target plate and a grid electrode about 20 kV. Accelerated ions are pushed into an electric-field-free flight tube and finally detected. When ions with mass m flight along with the flight tube with L (m) at a velocity of v (m/s), the flight time t (s) can be calculated as,

$$t = L/v \quad \cdots\cdots (1)$$

The velocity v can be obtained according to the law of conservation of energy,

$$ezV_0 = \frac{1}{2} muv^2 \quad \cdots\cdots (2)$$

or

$$v = 2ezV_0/mu \quad \cdots\cdots (3)$$

where, z is a charge of ion, V_o is an accelerating voltage, e is the elementary charge (=1.6×10^{-19} C), and u is unified atomic mass unit (=1.66 ×10^{-27} kg), respectively.

The velocity v is substituted into eq. (1), giving,

$$t = L\sqrt{\frac{u}{2eV_0}} \times \sqrt{\frac{m}{z}} \quad \cdots\cdots (4)$$

Thus, the flight time t of ion is directly proportional to the square root of mass-to-charge ratio (m/z). To improve the resolving power, the flight time t should be elongated. Variable parameters in Eq. (4) are limited to the flight path L and the accelerating voltage V_o. Here, decreasing of V_o causes lowering of the efficiency of ion extraction and expands a variation of the initial velocity. Extension of the flight path L results in increasing size of instruments and loss of transparent ions caused by diffusion of ions. To overcome these problems, a new type of high-resolution TOFMS based on a spiral ion trajectory in a compact space has been developed. **Figure 1** shows a schematic of the ion optical system of a SpiralTOF™ mass spectrometer (JEOL JMS-S3000). This system has a long flight path of approximately 17 m (2.1 m × 8 turns) along the spiral ion trajectory within a compact space [1], [2]. Because ion beams are focused at every turns, loss of transparent ions can be prevented. As a result, spiral TOFMS can achieve a high mass-resolving power over 60,000 at full width at half maximum (FWHM) and provide high mass precision and accuracy at a milli mass unit.

〉〉 16-1 Onogawa, Tsukuba, 305-8569, Japan | E-mail: sato-hiroaki@aist.go.jp

Structural characterization of polymers by MALDI-TOFMS

Polymer samples with a simple structure would give a series of peaks with regular intervals on the MALDI mass spectra. The *m/z* values observed on the MALDI mass spectra can be calculated according to Eq. (5),

$$m/z = M_{monomer} \times n + M_{end} + M_{cation} \cdots\cdots (5)$$

where, $M_{monomer}$ is the mass of repeating unit, n is the numbers of repeating units, M_{end} is the mass of end-groups, and M_{cation} is the mass of cation (*e.g.* Na^+), respectively. $M_{monomer}$ can be determined by the peak interval and M_{cation} can be easily speculated from the used cationization reagents. Therefore, the end-group structures can be speculated from the mass M_{end}.

The chemical structures of a simple homopolymer can easily be determined by MALDI-TOFMS. However, most industrial polymers are complex materials such as copolymers, polymer blends, and composites. Furthermore, various additives such as flame-retardants, anti-oxidants, stabilizers, surfactants, pigments, and so on, are usually added to the industrial polymeric materials. A variety of chemical structures in the complicated polymer samples would give extremely intricate mass spectra observed by a conventional MALDI-TOFMS, resulting in increasing the likelihood of isobaric interference.

Peak separation of isobaric components within complicated polymer samples requires high-resolution mass spectrometry. One might thought that Fourier transform ion cyclotron mass spectrometry (FTICR-MS) would be useful to characterize such polymer samples. Although FTICR-MS is the most powerful tool for separating isobaric components at an ultrahigh resolution, it requires special skills for operation and careful maintenance of FTICR-MS, especially in the case of combination with a MALDI source. Limitation of the amount of trapped ions in the ICR cell is a disadvantage for the measurements of polymer samples composed of various polymer chains. Furthermore, the requirement of long ion life-times (second level) to record long free induction decay (FID) signal would also be disadvantage for the detection of polymer ions generated by MALDI, because ion life-time of polymers by MALDI would be shorter than the FID recording time. The advantage of spiral-TOFMS over FTICR-MS is that high-resolution mass spectrometry can be readily performed using basically the same procedure as with conventional TOFMS instruments. This report describes representative applications of MALDI spiral-TOFMS for the characterization of complicated polymers.

Application of MALDI spiral-TOFMS for the structural characterization of copolymers

Copolymers are types of polymers composed of two or more monomers. To modify the properties and functions of polymeric materials, copolymers have been widely used in industrial materials. Improvement of copolymer materials has been accomplished by detailed characterization of copolymers, including copolymer composition and comonomer sequences, as well as end-group structures, molecular weights, and their distributions. This report presents the structural characterization of free radical polymerized methacrylate ester copolymers [3].

The sample used in this study is a copolymer composed of methyl methacrylate (MMA) and tartly butyl methacrylate (tBMA). This polymer was synthesized by free radical polymerization using 2,2-azobis(2,4-dimethylvaleronitrile) (AVN) as an initiator in ethyl lactate (EL) solvent acting as a chain transfer agent. Under this condition, polymerization would

Fig.1

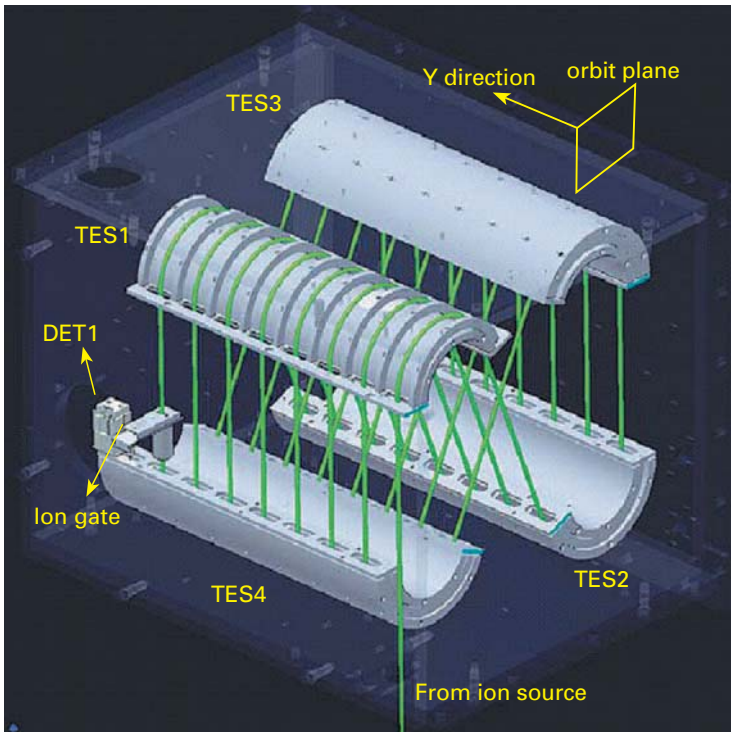

Spiral ion trajectory ion optical system. (Courtesy of JEOL)

start both from AVN initiator and solvent, resulting in two types of initial ends. The polymerization reaction would be terminated by disproportion resulting in saturated and unsaturated ends. As another termination, recombination of two radical chains would also occur. As a result, a total of seven different types of end-group combinations would be possible as shown in **Fig. 2**(a).

Figure 2(b) shows the high-resolution MALDI mass spectra of poly(MMA-*co*-tBMA) with a feed ratio of MMA/tBMA = 45/55 (mol/mol). This copolymer would be composed of various polymer chains having different end group combinations and copolymer compositions. The peak resolution of about 60,000 by MALDI spiral-TOFMS could be achieved up to *m/z* 3000, and therefore, the isobaric peaks could be separated. From the obtained precious mass values, the combination of end-group and the copolymer composition of each component could be identified. For example, isobaric peaks observed around *m/z* 1218 could be separated. Among these, the peak at *m/z* 1218.714 could be assigned as the molecule composed of MMA/tBMA

Fig. 2

(a)

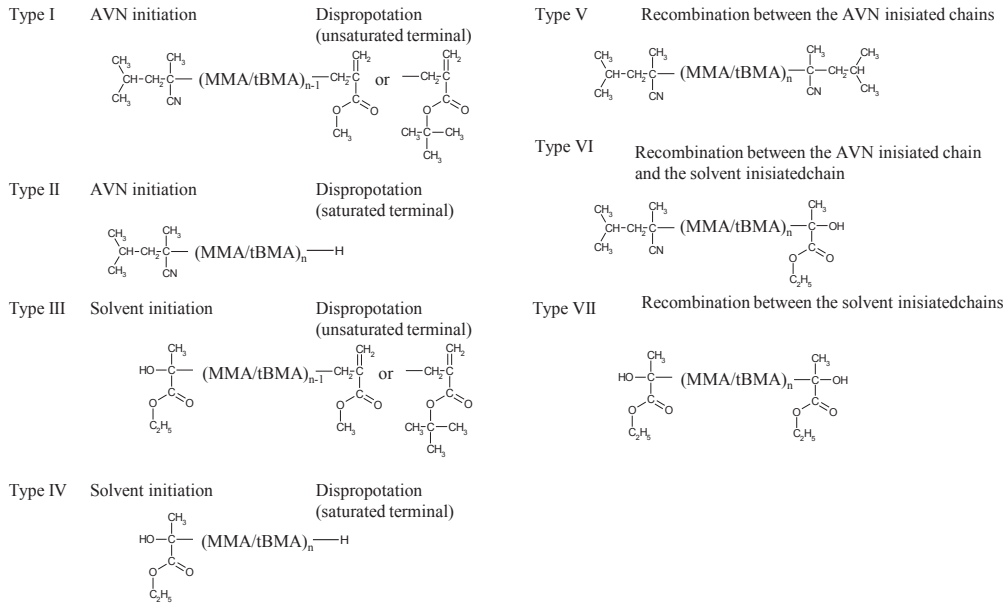

(b)

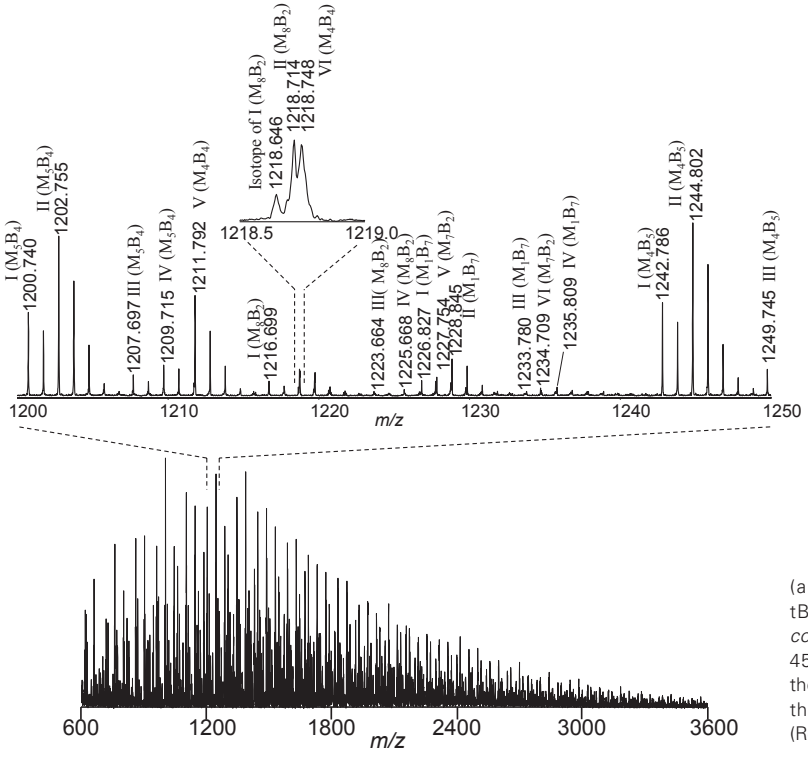

(a) Possible structures of poly(MMA-*co*-tBMA) and (b) mass spectra of poly(MMA-*co*-tBMA) with a feed ratio of MMA/tBMA = 45/55 (mol/mol). Roman numerals indicate the structure types in (a) and (M_mB_n) indicates the compositions of MMA and tBMA units. (Reprints with permission from ref. [3].)

= 8/2 units with type II end-group combination (AVN-initiated and saturated terminus), denoted as II(M_8B_2). Similarly, the peak at *m/z* 1218.748 could be assigned as III(M_4B_4) having EL initiated and unsaturated terminus. Here, the adjacent peak at *m/z* 1218.646 could be assigned as the isotope peak of I(M_8B_2).

Figure 3 shows a comparison of expanded mass spectra of the poly(MMA-*co*-tBMA) with different copolymer compositions in the range of *m/z* 1226-1232. As for the sample with MMA/TBMA=12/88 (mol/mol), two components of I(M_1B_7) and II(M_1B_7) are mainly observed at *m/z* 1226.832 and *m/z* 1228.844. With rising MMA composition, the relative peak intensities of these components decrease, whereas the peaks of III(M_7B_1) increase. The mass differences between these peaks have only ca. 0.08 Da. Conventional reflector type TOFMS could not separate such peaks as shown in the bottom figure, where three peaks of I(M_1B_7), II(M_1B_7), and III(M_7B_2) were not discriminated. Therefore, the high resolving power of spiral-TOFMS should be needed for the precious peak assignments. The results obtained by MALDI spiral-TOFMS could give an insight into the mechanisms of copolymer synthesis based on the information such as bivariate distributions in copolymer composition and compositional distributions of the different end group combinations (data not shown , see Ref [3]). These results are difficult to obtain by other method, so, MALDI spiral-TOFMS is a powerful tool for the structural and compositional characterization of complicated copolymers.

Compositional analysis using Kendrick mass defect analysis

Although MALDI spiral-TOFMS is possible to characterize complicated polymers based on a complete peak assignment, it should deal with an enormous collection of peak data. Therefore, an effective data processing method without relying on peak assignments is required. Here, this report describes "Kendrick mass defect (KMD) analysis" applied for the characterization of complicated polymers. KMD analysis is, in fact, an old technique proposed by Kendrick [4] in 1963, and it has been used chiefly to characterize petroleum and lipid samples by means of ultra-high-resolution FT-ICRMS. The KMD analysis, however, have not been applied for the polymer characterization, probably due to the limitation of the polymer measurements by MALDI-FT-ICRMS as described in the former section. The high resolving power of spiral-TOFMS, which can determine precious mass with a high-mass accuracy within a few ppm error, opens the way to KMD analysis in the field of polymer characterization. Here, this report explains the details of KMD analysis and several applications.

This has been proposed to discriminate homologous series differing only by a number of base units based on the "mass defect". Here, we consider the differences in nominal mass and accurate mass of various atoms containing in organic compounds. The accurate masses of hydrogen and nitrogen are larger than their nominal mass, whereas the masses of oxygen, sulfur, and phosphorus are deficient. In organic compounds, the mass of CH_2, corresponding to saturated hydrocarbons, shows the largest mass sufficiency. KMD is defined as the exact Kendrick mass subtracted from the nominal Kendrick mass.

The Kendrick mass (M_K) can be converted from the IUPAC mass (M_{IUPAC}) according to Eq.(6),

$$M_k = M_{IUPAC} \times \frac{\textit{nominal mass of base unit}}{\textit{IUPAC mass of base unit}} \cdots\cdots (6)$$

Originally, the methylene unit (-CH_2-) giving the maximum mass sufficiency is set as the base unit, i.e., *nominal mass of base unit* = 14 and *IUPAC mass of base unit* = 14.01565. In

Fig. 3

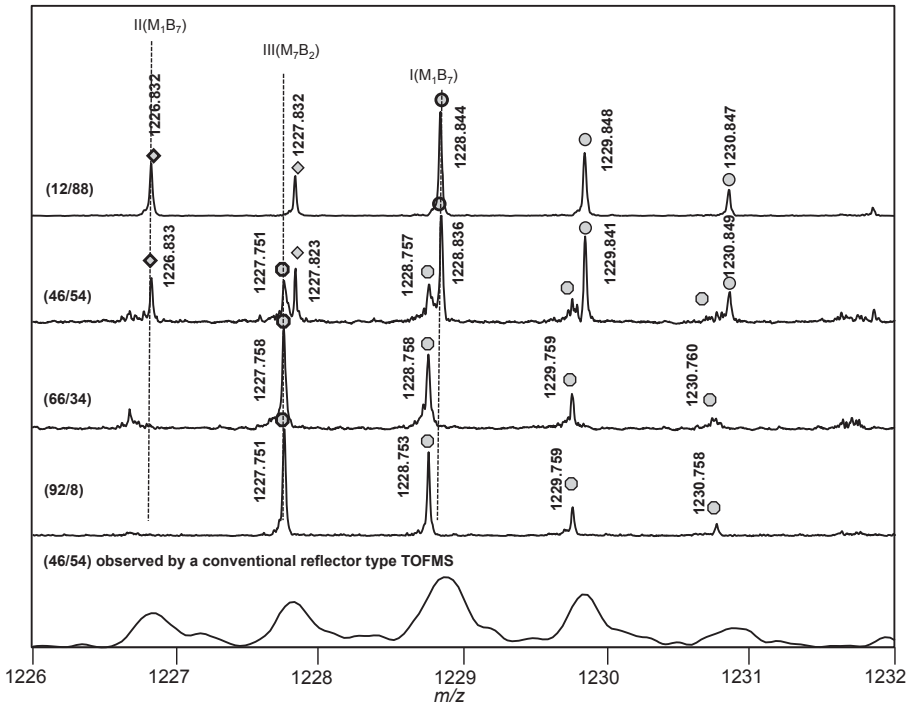

Comparison of the expanded mass spectra of poly(MMA-*co*-tBMA) with different copolymer compositions. The figures in the parentheses indicate the feed composition of (MMA/tBMA) in mol%. The bottom mass spectrum was observed using a conventional reflector type TOFMS.

polymer characterization, we set repeating unit of the polymer as the base unit.

Figure 4 explains the data processing procedures to make the KMD plot using a simple example. The sample of this example is a commercial detergent, which is a mixture of polyoxyethylene lauryl ether (C_{12}-PEO) and sodium dodecylbenzenesulfonate (LAS). The mass spectra of this detergent observed by MALDI spiral-TOFMS shows a distribution of the peaks of $[M+Na]^+$ ions of (C_{12}-PEO) over *m/z* 900 together with the peaks of LAS having different alkyl chain length (C_{11}-C_{13}). The observed *m/z* values were converted to M_K according to Eq. (6). In this case, ethylene oxide (EO) unit was set as the base unit (i.e. C_2H_4O = 44.0261 Da was converted to 44). For example, the peak observed at *m/z* 429.3181 was converted to 429.0634 in Kendrick mass scale based on EO unit. The M_K values consist of nominal and decimal parts. That is, 429 as nominal M_K and 0.0634 as KMD. A set of M_K and KMD of each observed peak was plotted on the two-dimensional graph (the KMD plot), where the components having common repeat units line up in the horizontal direction, whereas the components having different structures shift to the vertical direction. In this case, C_{12}-PEO chains having EO repeating units line up in the horizontal direction, whereas three LAS components having different numbers of CH_2 units line up obliquely.

The next application represents the case of more complicated samples. The samples of this application are different grades of commercial laundry detergents produced by the same company. **Figure 5** compares MALDI mass spectra and the KMD plots. Because several series of peak distributions have ca. 44 Da interval, it can be easily speculated that most components would contain the surfactants h aving EO repeating units. Setting EO unit as the base unit in KMD analysis, the m/z values of all observed peaks were converted to M_K, and the resulting nominal M_K and KMD values were plotted. (Here, the KMD values in y-axis were omitted to avoid the specification of the samples). The general views of two plots are very similar, in which several lines distributing to the horizontal direction indicate that these detergents are the mixture of at least three different types of surfactants having EO units. By comparing two plots, it can be easily found out the differences in the chain length distribution of each components having EO chain. The EO chain length of the components in detergent B (for strong stain) seems to be longer than that in detergent A (for normal stain). Because a compound has a specific combination of KMD and nominal M_K values, the visual identification of each compound would be performed, if the database of KMD values of various compounds is prepared. Based on the plot patterns, one might be able to have an insight into a basic design concept of these detergents. If one has interests in specific lines in the KMD plots, then detailed structural characterization can be proceeded based on their precious masses of the corresponding peaks in the observed mass spectra. Thus, the KMD analysis would be useful for the extraction of characteristic compounds in a complex material.

Displaying the compositional distribution of copolymers on the KMD plot

The next application of the KMD analysis is relating to the characterization of copolymers [5]. **Figure 6** shows the mass spectra of a block copolymer composed of poly(ethylene oxide) and poly(propylene oxide) [P(EO-*b*-PO)]. A peak distribution can be observed with a maximum at *m/z* ca. 1900. The copolymers composed of EO and PO units theoretically give a peak series with ca. 2 Da interval corresponding to the mass differences in EO_xPO_y and $EO_{x+4}PO_{y-3}$, together with their isotope peaks. In this case, the monoisotope peaks of $EO_{x+4}PO_{y-3}$

Fig. 4

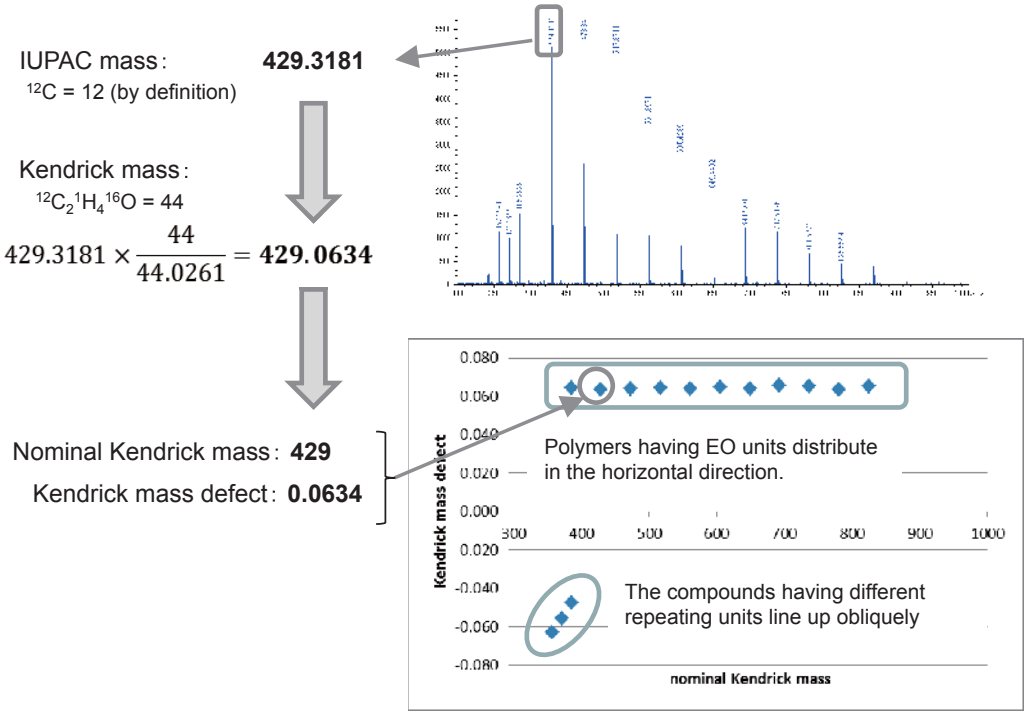

Explanation of the data processing procedures to make the KMD plot of a commercial detergent.

Fig. 5

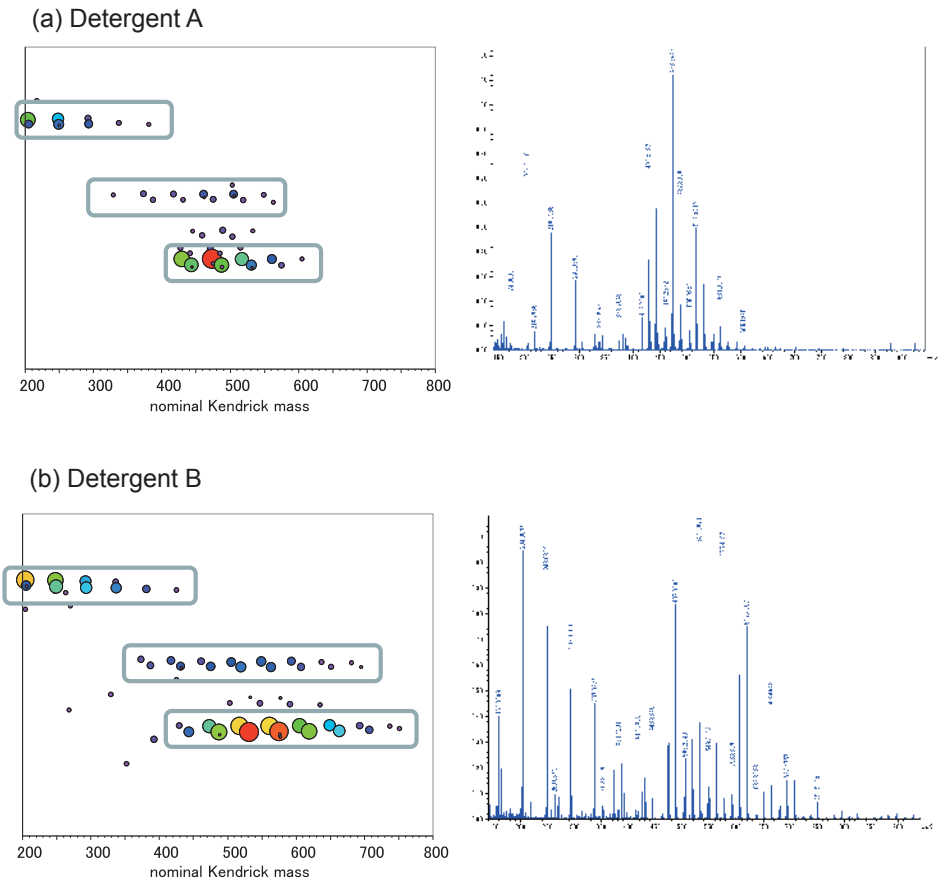

Comparison of the KMD plots and original mass spectra of two different grades of commercial laundry detergents. The size of each dot indicates peak intensity. Note: the KMD values in y-axis were omitted to avoid the specification of the samples.

Fig. 6

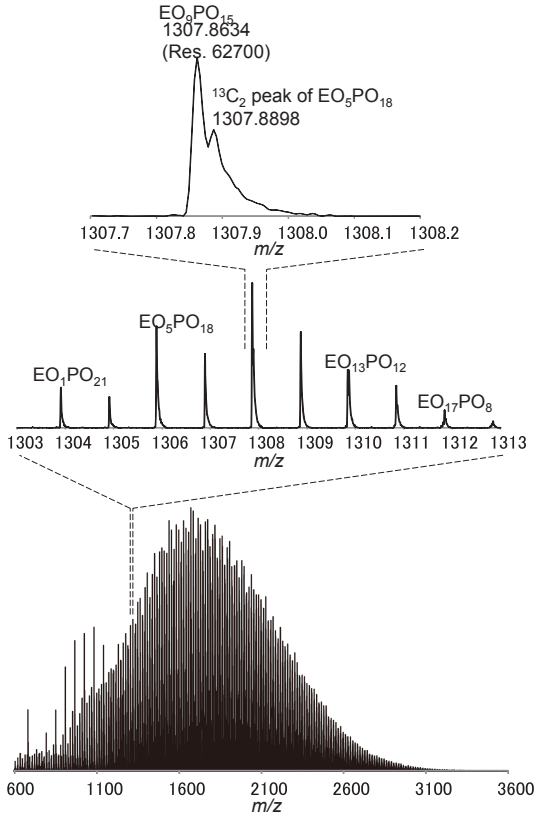

Mass spectra of P(EO-*b*-PO). The broad-band mass spectrum (bottom) and the expanded mass spectrum in the range of *m/z* 1303-1313 (middle) and *m/z* 1307.7-1308.2 (top). Reprints from ref. [5] (open access).

should be accompanied with closely adjacent peaks of the second isotope (mainly due to $^{13}C_2$) of EO_xPO_y with only 0.027 Da differences as shown in Fig. 6. Spiral-TOFMS can resolve these peaks. The observed *m/z* values of all peaks were then converted to the M_K values based on PO unit (C_3H_6O, 58.0419 Da to 58), and plotted to make the KMD plot as shown in **Fig. 7**.

In the plot, the distribution of PO units line up in a horizontal distribution at intervals of 58. On the other hand, the distribution of EO units line up obliquely, where nominal M_K increases by 44 and KMD value increases by 0.0055. Theoretical lines of EO/PO compositions are also indicated in Fig. 7 as a guide. By reading the plot patterns, the compositional distribution of P(EO-*b*-PO) sample could be characterized, where EO distributes 0-35 units and PO distributes 13-23 units. The dots on the lines of EO = 0 indicated the existence of poly(propylene oxide) homopolymers. These results suggest that this polymer was synthesized by elongation of EO chains from the both ends of core poly(propylene oxide) chains.

The reports demonstrated that MALDI spiral-TOFMS made it possible to perform KMD analysis for polymer characterization. One of the key advantages of this method is that the KMD plot visually represents patterns in the structural distribution of a given polymer without the need to perform peak assignment or peak picking. This feature is potentially useful for high-throughput profiling (or typing) of industrially-produced polymers, to inspect how the polymer was made and processed.

Conclusions

MALDI-TOFMS would have seemed to ensure the strong position as a powerful characterization tool. Actually, however, complicated polymers have been difficult to be characterized by conventional MALDI-TOFMS instruments mainly due to insufficient resolution. The new type of TOFMS with a spiral ion trajectory (SpiralTOF™) has a potential to make a breakthrough in the characterization of complicated polymers. This report presented the features of MALDI spiral-TOFMS and its applications for the characterization of complicated polymers. The first application was relating to the detailed structural characterization of copolymers. High-resolution mass spectrometry of spiral-TOFMS can avoid isobaric interference of the observed mass spectra, and it enables us to almost completely identify copolymer compositions and end-group combinations. The second application was the visualization of the high-resolution mass spectra composed of a huge numbers of peaks. By introducing KMD analysis, compositional distributions of complicated polymers such as blends and copolymers can visually be understood without any peak assignments. In conclusion, MALDI spiral-TOFMS has a great potential as a powerful tool for the structural and compositional characterization of complicated polymers.

References

[1] Satoh, T., Tsuno, H., Iwanaga, M., Kammei, Y.: The design and characteristic features of a new time-of-flight mass spectrometer with a spiral ion trajectory. *J. Am. Soc. Mass Spectrom.* **16**, 1969-1975 (2005).

[2] Satoh, T., Sato, T., Tamura, J.: Development of a high-performance MALDI-TOF mass spectrometer utilizing a spiral ion trajectory. *J. Am. Soc. Mass Spectrom.* **18**, 1318-1323 (2007).

[3] Sato, H., Ishii, Y., Momose, H., Sato, T., Teramoto, K.: Structural characterization of free radical polymerized methacrylate ester copolymers using high-resolution MALDI-TOFMS with a spiral ion trajectory. *Mass Spectrometry* **2**, A0014 (2013).

[4] Kendrick, E.: A mass scale based on CH2=14.0000 for high resolution mass spectrometry of organic compounds. *Anal. Chem.* **35**, 2146-2154 (1963).

[5] Sato, H., Nakamura, S., Teramoto, K., Sato, T.: Structural characterization of polymers by MALDI spiral-TOF mass spectrometry combined with Kendrick mass defect analysis. *J. Am. Soc. Mass Spectrom.* **25**, 1346-1355 (2014). Open access.

Fig. 7

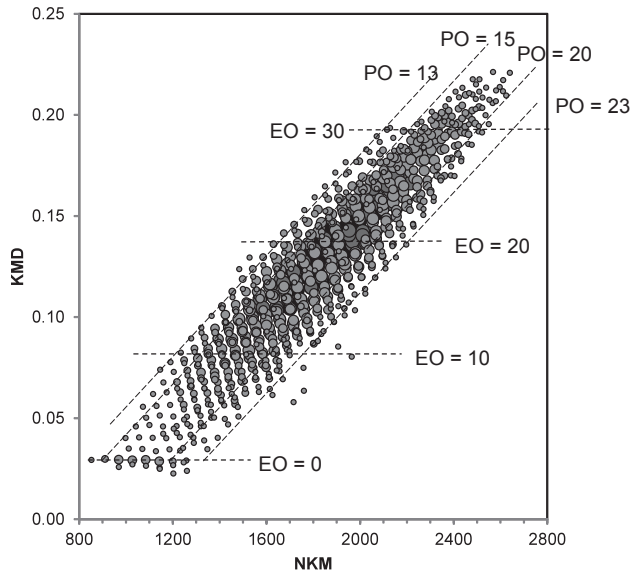

The KMD plot of P(EO-*b*-PO). The lines indicate the theoretical distribution of the homologue having the same numbers of EO or PO compositions. The size of each dot indicates peak intensity. Reprints from ref. [5] (open access).

Research Article

Rapid Communications in Mass Spectrometry

Received: 15 December 2015 Revised: 22 January 2016 Accepted: 1 February 2016 Published online in Wiley Online Library

Rapid Commun. Mass Spectrom. **2016**, *30*, 973–981
(wileyonlinelibrary.com) DOI: 10.1002/rcm.7525

MALDI SpiralTOF high-resolution mass spectrometry and Kendrick mass defect analysis applied to the characterization of poly(ethylene-*co*-vinyl acetate) copolymers

Thierry Fouquet*, Sayaka Nakamura and Hiroaki Sato*

National Institute of Advanced Industrial Science and Technology (AIST), Environmental Measurement Technology Group, Environmental Management Research Institute (EMRI), Tsukuba, Ibaraki, Japan

RATIONALE: Poly(ethylene-*co*-vinyl acetate) copolymers – usually referred to as EVA – are first class industrial polymers used for applications ranging from padding to photovoltaics as encapsulant for the silicon solar cells. Various techniques have been used for their characterization but the analysis of intact EVA chains using mass spectrometry (MS) has not been reported so far.
METHODS: Three copolymers containing 18, 25 and 40 wt% vinyl acetate (VA) have been characterized using an off-line coupling of size-exclusion chromatography (SEC) and matrix-assisted laser desorption/ionization (MALDI) spiral-time-of-flight (TOF) high-resolution mass spectrometry (HRMS). The representativeness of those results for the entire samples has been checked using ^{13}C NMR spectroscopy. Lastly, Kendrick mass defect analysis has been proposed as an alternative and user-friendly data treatment method.
RESULTS: The shortest chains isolated by SEC fractionation and mass-analyzed by HRMS have been thoroughly described in terms of end-groups (found to be hydrogens) and co-monomeric composition. The VA content was successfully derived from the peak assignments in MS spectra for the EVA 40 wt% and 25 wt% while it tended to be overestimated for the latest EVA 18 wt% (increasing poly(ethylene) character). Similar results have been found using a faster data treatment method relying on the Kendrick mass defect analysis of the MS data.
CONCLUSIONS: EVA low molecular weight intact oligomers have been extensively characterized by MS for the first time and the structural features confidently extended to the full sample according to NMR data. The Kendrick mass analysis finally constituted an efficient method for a fast evaluation of their VA content with no need for manual assignment. © 2016 The Authors. *Rapid Communications in Mass Spectrometry* Published by John Wiley & Sons Ltd.

Poly(ethylene-*co*-vinyl acetate), also known as ethylene-vinyl acetate or ethylene vinyl acetate copolymer – further noted EVA for sake of clarity – designates a class of copolymers of prime importance for various industrial and high-technology applications. EVA is produced by the copolymerization of ethylene (E) and vinyl acetate (VA) monomers, usually under high pressure and high temperature (high-pressure ethylene polymerization, e.g. autoclave process[1]). Varying the content in VA repeating units will result in different properties (flexibility, crystallinity, melting temperature, softness…) which will further dictate the applications of the copolymer. Low VA content EVA (<10 wt%) are typically used as additives to bitumen.[2] The major EVA formulation consists nevertheless of 28–33 wt% VA[3–6] and finds applications as padding (EVA foam[7]), as part of hot melt adhesives,[8,9] or as encapsulating material for silicon solar cells, protecting the photovoltaic module from moisture, oxygen and mechanical stress.[3] Such importance in the industrial landscape thus requires specific analytical techniques and methodologies to be developed to ensure a proper characterization of the materials at every step of the process. In particular, the starting EVA copolymer (before cross-linking or blending with other polymers) should be thoroughly described in terms of end-groups, branching and VA content. If several techniques have been proposed in the literature – ranging from NMR[10–14] to rheological or thermal measurements[15,16] and Fourier transform infrared spectroscopy (FTIR)[17] to X-ray photoelectron spectroscopy (XPS),[18] the use of mass spectrometry has been mentioned in the form of pyrolysis-gas chromatography MS fingerprints[19] or time-of-flight secondary ion mass spectrometry (TOF-SIMS)[20] only – inducing in both cases a cleavage of the polymeric backbone. To the best of our

* *Correspondence to*: T. Fouquet and H. Sato, National Institute of Advanced Industrial Science and Technology (AIST), Environmental Measurement Technology Group, Environmental Management Research Institute (EMRI), Tsukuba, Ibaraki, Japan.
E-mail: thierry.fouquet@aist.go.jp; sato-hiroaki@aist.go.jp

knowledge and despite its increasing use for the characterization of polymeric materials,[21–26] especially with soft ion sources (electrospray ionization (ESI), matrix-assisted laser desorption/ionization (MALDI)) to preserve the integrity of the polymeric chains, no report has dealt with the analysis of *intact* EVA copolymers by MS. ESI- or MALDI-MS configurations allow the mass measurement of each individual chain, highlighting the occurrence of different distributions and allowing an accurate description of the samples in terms of repeating units, degrees of polymerization or end-groups.[27] The present article proposes a full analytical strategy relying on the use of size-exclusion chromatography (SEC) and high-resolution mass spectrometry (HRMS) to gain insight into the microstructure of three commercial EVA samples varying by their VA content (40 wt%, 25 wt% and 18 wt%, further noted EVA40, EVA25 and EVA18) with the aim of deciphering the terminations of the chain and evaluate the VA content from the MS data. The preliminary fractionation of polymeric samples by SEC and the subsequent analysis of the collected fractions by MALDI-MS – often referred to as 'off-line coupling'[28,29] – has been reported by several authors as an efficient analytical technique for polydisperse samples.[30] Kendrick mass defect (KMD) analysis, recently proposed as a user-friendly MS data visualization from polymer mass spectra,[31] will be finally applied for the fast and reliable discrimination of the EVA samples. The three VA contents have been specifically chosen (a) to mimic the 28–33 wt% VA content mainly used in the industry (EVA25)[3] and (b) as reference (EVA40) sample and limit sample (EVA18), easily and hardly analyzable, respectively.

EXPERIMENTAL

Chemicals

Poly(ethylene-*co*-vinyl acetate) copolymers (abbreviated as EVA) and {(2*E*)-2-methyl-3-[4-(2-methyl-2-propanyl)phenyl]-2-propen-1-ylidene}malononitrile (known as DCTB) were purchased from Sigma Aldrich (St. Louis, MO, USA). Chloroform ($CHCl_3$) used in SEC and tetrahydrofuran (THF) were from Wako Pure Chemical Industries (Osaka, Japan). The poly(methyl methacrylate) standard (M_p = 1310 g mol^{-1}) used for the external calibration of the MALDI mass spectra was purchased from Polymer Laboratories (Church Stretton, UK).

Size-exclusion chromatography

Size-exclusion chromatography (SEC) measurements and fractionations were performed using a HLC8220 GPC system (Tosoh, Tokyo, Japan) equipped with a refractive index detector (RID). Separation was carried out using two TSKgel multipore H_{XL}-M columns (7.8 mm × 300 mm) connected in series following a multipore Hxl guard column. $CHCl_3$ was used as the mobile phase at a flow rate of 1 mL min^{-1}. EVA samples were dissolved in $CHCl_3$ at 2 mg mL^{-1}, filtered using Millex syringe-driven filter units (Merck Millipore, Carrigtwohill, Ireland) and 200 µL of the so-formed solution were injected for the SEC elutions. Fractionation of the polymeric samples was done by collecting aliquots of 0.5 mL (30 s) into vials directly after the RID, further allowed to air dry for a couple of hours and submitted to mass analysis. Following this re-concentration procedure, the sensitivity of the mass spectrometer allowed satisfactory mass spectra to be recorded from one single analytical SEC run only. The fractions of interest in the present study were collected after 18′30″–19′00″ (fraction #1), 19′00″–19′30″ (fraction #2) and 19′30″–20′00″ (fraction #3) of elution. Fractions of higher molecular weights were also collected (16′30″–18′30″) and mass-analyzed (see Supporting Information).

Mass spectrometry

MALDI mass spectra were recorded using a JMS-S3000 SpiralTOF™ mass spectrometer (JEOL, Tokyo, Japan). A Nd:YLF laser irradiated the spots made from the deposition of 1 µL of a matrix/salt/sample solution (5 µL of DCTB at 20 mg mL^{-1} in THF, 1 µL of NaTFA at 2 mg mL^{-1} in THF and 1 µL of the aliquot from a SEC single elution) on a target plate and allowed to air-dry. DCTB has been expressly chosen as it provides the best signal-to-noise (S/N) ratios at a low laser fluence, then allowing high resolution to be achieved. In addition, it has been found that the use of alternative matrices such as dithranol or 2,5-DHB not only dramatically deteriorates the S/N ratios but also favors the detection of the VA-rich oligomers detrimentally to the E-rich species, leading to overestimations of the VA content (data not shown). The so-generated ions were accelerated by a 20 kV high voltage and went through the SpiralTOF analyzer along a spiral trajectory (approximate path length: 17 m) before their detection.[32] The delay time was set according to the mass range of the sample (230 ns for fractions #3, 240 ns for fractions #2 and 350 ns for fractions #1) to keep the peak width $\Delta M < 0.03$ Da at FWHM over the mass range of interest. Calibration was performed externally using the sodium adducts of a poly(methyl methacrylate) standard (DCTB, no salt added).

^{13}C NMR

^{13}C and DEPT135 NMR spectra were recorded using a JNM-ECX400 spectrometer (JEOL, Tokyo, Japan) at the ^{13}C resonance frequency of 100 MHz. Samples were dissolved in deuterated chloroform ($CDCl_3$) at 50°C and analyzed at 30°C (accumulated spectra: 3000 for ^{13}C NMR and 1440 for DEPT135 NMR) using a TH5ATFG2 5 mm probe. Assignment of ^{13}C NMR signals was done according to values referenced in the literature.[10]

Kendrick mass defect analysis

As proposed by Sato *et al.*,[31] using the repeating unit of a polymeric backbone as the base unit for the Kendrick masses (further noted KM) allows a fast visualization of homologue series in a Kendrick mass defect plot (shortened in KMD plot). In the case of EVA copolymers, KM could be indifferently calculated using E or VA as the base unit. The E unit (C_2H_4, m_{IUPAC} = 28.03130 Da) has been chosen here for the sake of simplicity as a simple extension of the methylene unit (CH_2, m_{IUPAC} = 14.01565 Da) traditionally used for fuels.[33] Accurate mass measurements on the IUPAC

scale of the co-oligomeric adducts from EVA samples are converted into Kendrick masses with E as the base unit as follows:

$$\mathrm{KM(oligomer)} = m_{\mathrm{IUPAC}}(\mathrm{oligomer}) \cdot \frac{28}{28.03130} \quad (1)$$

The KM values are then decomposed in the nominal Kendrick mass (the rounded KM to the next highest integer, noted NKM) and the Kendrick mass defect (noted KMD) calculated as follows:

$$\mathrm{KMD(oligomer)} = \mathrm{NKM(oligomer)} - \mathrm{KM(oligomer)} \quad (2)$$

The KMD plot displays the KMD of the detected oligomeric adducts as a function of their NKM using a 'bubble chart' where each disk expresses a data triplet (NKM, KMD, abundance). The size of the disk reflects the abundance of the associated oligomer in the mass spectrum. Species containing the same number of VA units within their skeleton will line up horizontally (variation of the number of E units only) while points will shift to the oblique direction if varying their content of VA units (with the number of E units being constant).

RESULTS AND DISCUSSION

Comments on the mass analysis of EVA copolymers

EVA copolymers are composed of a varying number of ethylene units (C_2H_4, 28.0313 Da) and vinyl acetate units ($C_4H_6O_2$, 86.0368 Da). The generic structure of an EVA copolymer with undefined initiating and terminating end-groups (noted α and ω) is depicted on the left in Fig. 1. A rapid inspection of the masses of these repeating units provides evidence of two overlapping issues which will further dictate the requirements for a proper mass analysis.

Starting from a hypothetic E_mVA_n co-oligomer (i.e. a copolymeric chain containing m ethylene units and n vinyl acetate units, regardless of the end-groups and the adducted cation), adding one VA unit induces a +86 Da mass shift while adding *three* E units increases the *m/z* ratio of 84 Da (Fig. 1, right). $E_{m+3}VA_n$ and E_mVA_{n+1} are thus spaced by 2 *m/z* only. In the high-mass range, the resolution of MS devices is lower than 1 Da (e.g. TOF in linear mode for *m/z* exceeding 10,000) and one would thus fail at assigning the detected peaks to $E_{m+3}VA_n$ and/or E_mVA_{n+1} for long polymeric chains. In addition, the $^{13}C_2$ isotope of the $E_{m+3}VA_n$ co-oligomer will interfere with the monoisotopic peak of E_mVA_{n+1}, both shifted by +86 Da from the first E_mVA_n chain. The exact masses of $E_{m+3}VA_n(^{13}C_2)$ and E_mVA_{n+1} differ by 0.06 Da. Generally speaking, for species whose carbon content exceeds 100 atoms, the ^{13}C isotope is more intense than the monoisotopic peak and the $^{13}C_2$ isotope is half the ^{12}C intensity. To ensure once more a correct peak assignment in the mass spectra of EVA copolymers for co-oligomers exceeding 1500 g mol^{-1}, isotopes should be properly differentiated using a high-resolution mass analyzer to avoid severe biases (R >25,000 at *m/z* 1500 for the isotope separation mentioned above). In summary, a satisfactory mass analysis of EVA would hence be limited to (a) co-oligomers of low molecular weight and (b) using a mass analyzer of high resolving power. A preliminary fractionation of commercial EVA samples by SEC followed by the MALDI mass analysis of the shortest chains using a SpiralTOF analyzer[31,32] constitutes a full analytical strategy expected to overcome the two pitfalls listed above.

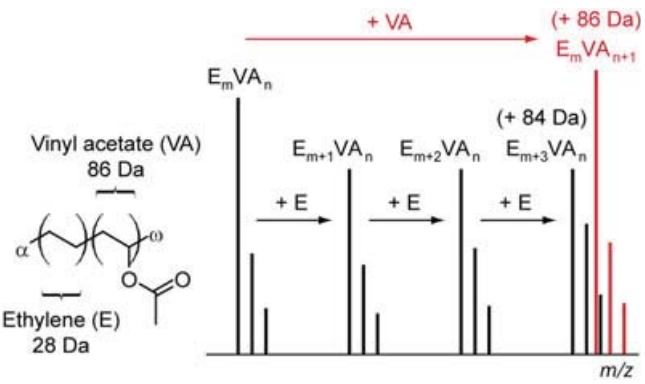

Figure 1. Left: generic structure of an EVA copolymer with undefined α/ω terminations. Right: Schematic representation of the isobaric issue arising from the masses of the repeating units. Adding one VA unit or three E units to an E_mVA_n oligomer leads to +86 Da shifted E_mVA_{n+1} or +84 Da shifted $E_{m+3}VA_n$, respectively. The $^{13}C_2$ isotope of $E_{m+3}VA_n$ and the monoisotopic peak of E_mVA_{n+1} are isobaric.

SEC-MALDI of EVA copolymers

The solubility of EVA samples in $CHCl_3$ at room temperature has been found to depend on the VA content. EVA40 and EVA25 readily solubilize at a working concentration of 2 mg mL^{-1} while EVA18 is clearly partly insoluble at the same concentration after several days in solution. The decrease in the number of polar VA groups concomitantly with the increase in the poly(ethylene) (PE) character of EVA accounts for this behavior. The SEC chromatograms recorded for the three EVA samples (targeted concentration: 2 mg mL^{-1}) are depicted in Fig. 2(A) (EVA40, solid line; EVA25: short dashed line; EVA18: long dashed line). The peak intensity clearly decreases from EVA40 to EVA18. This variation in peak intensity probably reflects the variation in sample solubility in $CHCl_3$, but alternative reasons cannot be dismissed. The decrease in the VA content potentially yields a decrease in the refractive index increment (dn/dc) (found to vary with the co-monomeric composition under certain conditions[34]) or a stronger interaction with the stationary phase. The following MS data support nevertheless the solubility variation as a highly probable hypothesis. In addition, if the elution of EVA40 and EVA25 lead to SEC chromatograms with similar shapes (number average molecular weight M_n = 42,200 g mol^{-1} for EVA40, M_n = 43,600 g.mol^{-1} for EVA25 PS equivalent), EVA18 strongly departs from this fingerprint with the detection of a peak strongly shifted towards the longer retention times (i.e. the lower molecular weights), which indicates the shortest chains only have been solubilized (M_n = 11,200 g mol^{-1} PS equivalent). The use of chlorinated/aromatic solvents such as trichlorobenzene and SEC at high temperature would allow this solubility issue to be overcome but raises the problem of the highly specific SEC system and columns to be used – not to mention the

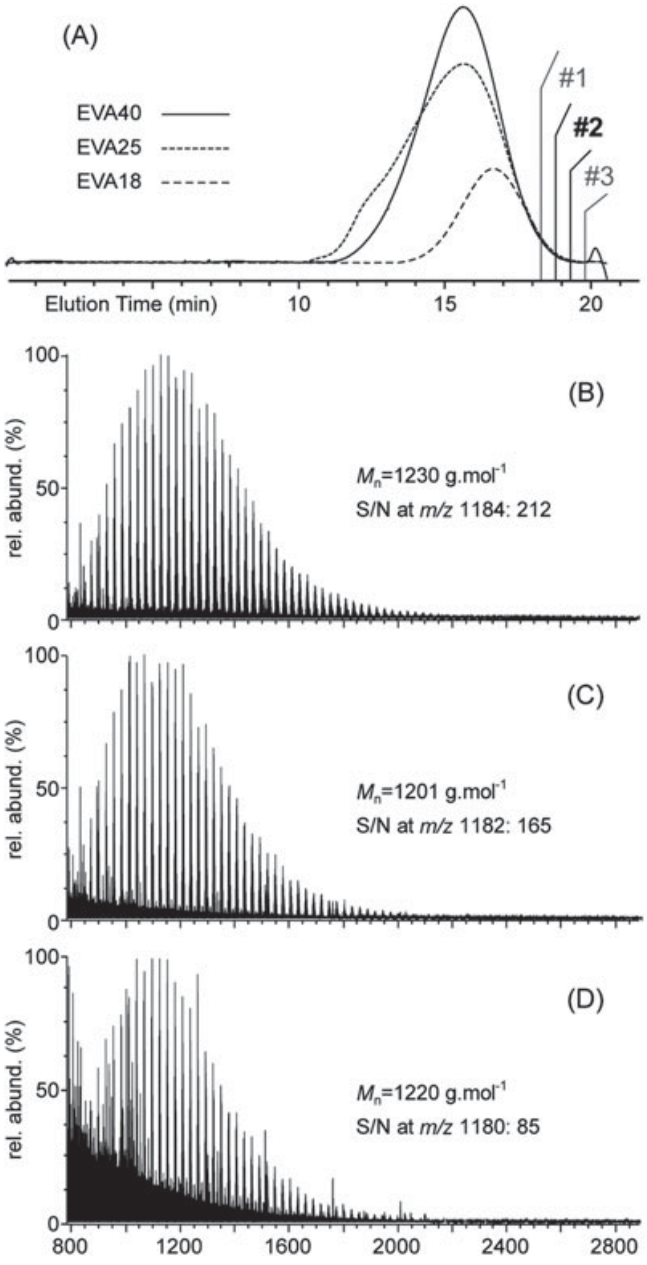

Figure 2. (A) SEC chromatogram of the three EVA samples in $CHCl_3$ at a targeted 2 mg mL^{-1} concentration (solid line: EVA40; short dashed line: EVA25; long dashed line: EVA18). The three collected fractions #1–#3 further mass analyzed are highlighted. (B–D) MALDI mass spectra of fractions #2 collected from the SEC elution of EVA40, EVA25 and EVA18, respectively. The number average molecular weights M_n and signal-to-noise (S/N) ratios are listed in insets. MALDI mass spectra of fractions #3 and #1 are depicted in the Supplementary Figs. S1 and S2, respectively (Supporting Information).

tedious evaporation step for the MALDI analysis, putting a damper on the applicability of the below-described procedure in any laboratory. Since the mass analysis will be limited to the low molecular weight fractions following the analytical strategy commented in the first section, such a solubility issue using $CHCl_3$ does nevertheless not constitute a drawback for the forthcoming characterization by MALDI-MS. As mentioned in the introduction, the samples of interest for industrial applications are also mostly composed of more than 25 wt% VA.[3] If EVA40 is a 'reference' material, EVA18 acts as the 'limit' sample highlighting the apparent limitations of the presently reported methodology.

The EVA chains have then been fractionated by collecting 30-s aliquots directly after the RI detector. Of particular interest for the forthcoming high-resolution mass analysis, the shortest chains eluting in the last minutes (18'30'' to 20' of total elution) have been collected in three aliquots numbered #1 to #3. Those fractions are highlighted in Fig. 2(A). The MALDI mass spectra subsequently recorded from the fractions #2 of the three EVA samples are depicted in Figs. 2(B) (EVA40), 2(C) (EVA25) and 2(D) (EVA18). Fractions #2 will be used throughout the text while results from fractions #1 and #3 will be systematically reported in the Supporting Information for the sake of simplicity. Contrary to the SEC fingerprints which differ between samples, the SEC-MALDI-MS off-line coupling leads to similar mass spectra in terms of mass range and shape, with three Gaussian-like distributions centered around 1220 g mol^{-1} (EVA40: M_n = 1230 g mol^{-1}; EVA25: M_n = 1201 g mol^{-1} and EVA18: M_n = 1220 g mol^{-1}). However, a clear deterioration of the S/N ratio is observed from EVA40 to EVA18. Matrix adducts and background peaks are detected with great abundance in the latter case. Values of S/N ratios calculated at a given *m/z* ratio (the maximum of the pattern, see Fig. 4) are listed in Figs. 2(B)–2(D), found at 212 at *m/z* 1184 for EVA40, 165 at *m/z* 1182 for EVA25 and 65 at *m/z* 1180 for EVA18. As for the solubility issue, the increasing PE-like character of EVA when decreasing the content of VA makes the mass analysis of highly apolar chains[35] more tedious by affecting the desorption and the ionization efficiencies. The S/N ratios calculated from the MALDI mass spectra of fractions #3 and #1 (Supplementary Figs. S1 and S2, Supporting Information) are also decreasing concomitantly with the content of VA, corroborating the above mentioned findings.

Structural characterization of EVA chains

The following discussion is focused on the 'reference' EVA40 for the sake of clarity. Owing to the complexity of the recorded mass spectra displayed in Fig. 2, a restricted spectrum (*m/z* range: 1140–1260) is depicted in Fig. 3(A). A set of four patterns is detected and mass shifts of 28 Da (i.e. ethylene unit E) and 86 Da (i.e. vinyl acetate unit VA) are readily evidenced. Starting from a first oligomer at *m/z* 1156.0, adding one, two and three E units leads to peaks detected at *m/z* 1184.0, 1212.0 and 1240.0, respectively, while adding one VA unit produces a peak at *m/z* 1242.0. Note the similarity of such patterns with the simulated mass spectrum depicted in Fig. 1. Looking even closer at the MS data (Fig. 3(B), *m/z* range: 1238–1243), two isobaric species clearly contribute to the signal of some peaks. The high resolving power of the SpiralTOF analyzer hence allows the expected contributions of the ^{13}C isotopes to be separated from the monoisotopic peaks (as presented in Fig. 1) and ensures correct peak picking and associated assignments.

Elemental compositions have been evaluated based on the accurate mass measurements listed in Supplementary Table S1 (Supporting Information). All the detected peaks could be assigned to sodiated adducts of EVA oligomers with hydrogen as both initiating and terminating end-group. The

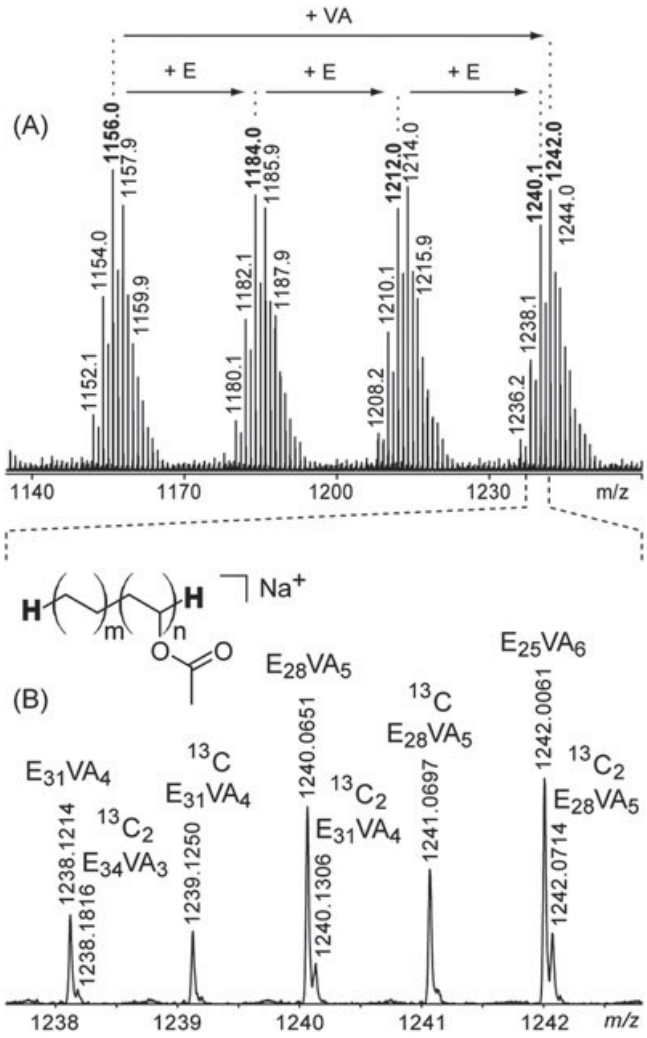

Figure 3. (A) Restricted mass spectrum of fraction #2 from EVA40 (*m/z* range: 1140–1260). (B) Magnification of (A) (*m/z* range: 1238–1243). Peaks are annotated with their composition in E and VA units (E_mVA_n). The generic structure with H as end-groups derived from the accurate mass measurements is depicted in the inset.

generic structure of oligomers found in the fraction #2 of EVA40 is depicted in the inset of Fig. 3(B). No other species with alternative terminations have been found in the mass spectrum. All the peaks detected in Fig. 3(B) could be further labelled with their respective E and VA content (in the form of E_mVA_n) and discriminated as either monoisotopic or $^{13}C_x$ isotopic peaks. For instance, the peak at *m/z* 1240.0651 is assigned to a $[H\text{-}E_{28}\text{-}VA_5\text{–}H+Na]^+$ adduct (shortened as $E_{28}VA_5$ in Fig. 3(B)) and is properly differentiated from the $^{13}C_2$ isotope of $[H\text{–}E_{28}\text{–}VA_5\text{–}H+Na]^+$ detected at *m/z* 1240.1306. Similar results have been obtained for EVA25 and EVA18 in terms of end-groups with a unique $H\text{-}E_mVA_n\text{-}H$ structure adducted with a sodium cation in both cases.

Restricting the mass analysis to those low molecular weight fractions allows the high resolving power of the SpiralTOF to be exploited and the pitfalls mentioned in the first section to be overcome but it puts into question the extension of these structural assessments to the entire EVA sample. NMR experiments have thus been conducted on the whole sample to check the representativeness of the MS results. The ^{13}C and DEPT135 NMR spectra have been recorded for the EVA40 sample and are depicted in Fig. 4.

The NMR spectra of EVA40 are extremely similar to the NMR data reported in the literature[10–14] and the peak assignment has been done following the reported nomenclature.[10] Aliphatic carbons from the VA unit are detected at 74.3 and 34.1 ppm and noted as A1 (-CH-, positive phase in DEPT135) and A2 ($-CH_2-$, negative phase in DEPT135). The quaternary carbon B1 and the methyl groups of VA, noted B2, are detected at 170.8 (unseen in the DEPT135 spectrum) and 21.2 ppm ($-CH_3$, positive phase in DEPT135), respectively. The two carbon atoms constituting an ethylene monomer unit linked to a VA unit are seen at 25.3 (noted A3) and 29.6 ppm (noted A4), both of negative phase in DEPT135 ($-CH_2-$ groups). E units not surrounded by VA units would be detected by a chemical shift similar to A4. The peak of noticeable abundance at 14.1 ppm has been assigned to another methyl group ($-CH_3$, positive phase in DEPT135) acting as chain termination and noted α. The generic structure of EVA accounting for such an NMR fingerprint is depicted in the inset at the top of Fig. 4(B). Another representation of the same EVA copolymer with methyl groups as initiating and terminating groups is depicted in the inset at the bottom of Fig. 4(B) with the VA units surrounded by E units. From the NMR point of view, such a polymeric backbone is methyl/methyl-terminated, i.e. $\mathbf{CH_3}\text{-}CH_2\text{-}E_m\text{-}VA_n\text{-}CH_2\text{-}\mathbf{CH_3}$, which is strictly identical to H/H as end-groups from the MS point of view. The first and last carbon atoms from the first and last E units could also be seen as parts of the backbone as in $\mathbf{H\text{-}CH_2}\text{-}CH_2\text{-}E_m\text{-}VA_n\text{-}CH_2\text{-}\mathbf{CH_2\text{-}H}$ which

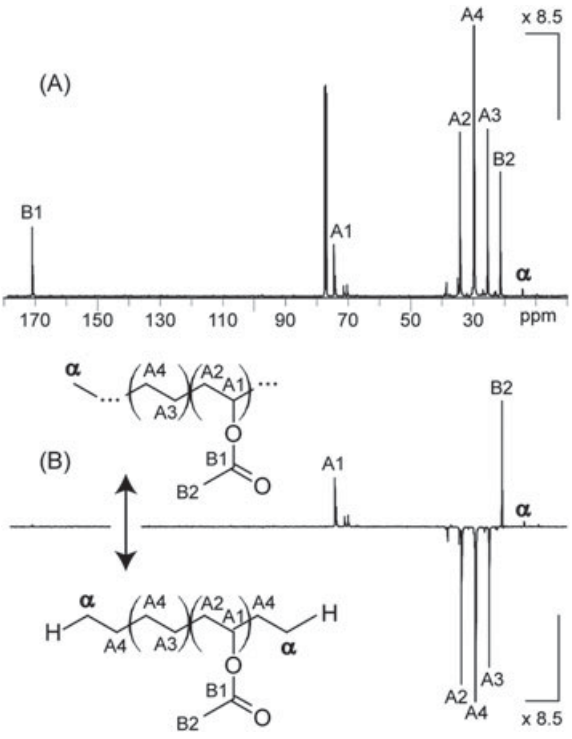

Figure 4. (A) ^{13}C NMR spectrum and (B) DEPT135 NMR spectrum of EVA40 solubilized in $CDCl_3$. Carbons from the polymeric backbone are designated with the letters A and B while the proposed methyl end-group is designated with α.

corresponds to **H**-E_{m+1}-VA_n-E-**H**. This structure is isomeric to the generic H-E_{m+2}-VA_n-H depicted in Fig. 3(B). In other words, the structure of EVA40 proposed from NMR is consistent with the structure derived from the SEC-MALDI-MS analysis, validating the latter as a technique in its own right to characterize the EVA copolymers scrutinized in the present study from their low molecular weight fractions only with satisfactory representativeness. Consequently, the last step for a complete characterization of these commercial EVA samples which consists of the evaluation of the VA content (mol% or wt % for the molar and weight fractions, respectively) could be meaningfully conducted from the MS results only.

Evaluation of the VA content from the native MS data

Magnifications of the SEC-MALDI mass spectra of the three commercial EVA samples (*m/z* range: ~1170–1200) are depicted in Fig. 5 (A: EVA40, B: EVA25 and C: EVA18). Echoing the results from the previous section, all the detected peaks are assigned to sodium adducts of EVA oligomers with a varying number of E units (m) and VA units (n) and hydrogen atoms as end-groups. The E_mVA_n compositions are mentioned in Fig. 5 and listed in Table 1. Highlighting the performance of the SpiralTOF mass analyzer, the average error value for the assignments has been found to be +0.2 ppm.

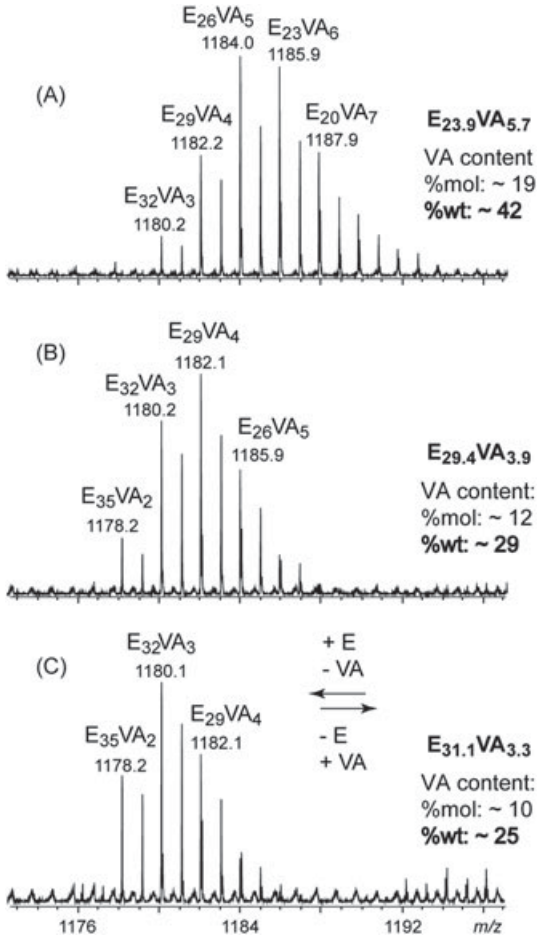

Figure 5. Restricted MALDI mass spectra of the fractions #2 collected from the SEC elution of (A) EVA40, (B) EVA25 and (C) EVA18 (mass range: 1173–1197). Composition in terms of ethylene (E) and vinyl acetate (VA) units are mentioned for each major peak as E_mVA_n considering H as end-group. Average compositions and computed VA contents (molar and weight) are mentioned alongside the spectra.

If the general shape of the whole mass spectrum is similar regardless of the EVA sample (Fig. 2), the magnifications depicted in Fig. 5 greatly differ between EVA40, EVA25 and EVA18. A clear shift in the pattern towards lower *m/z* ratios is observed from EVA40 to EVA18, which corresponds to an increase (resp. decrease) in the number of E (resp. VA) units within the detected oligomeric backbones (Table 1). Qualitatively speaking, MS thus allows the three samples to be discriminated. To gain more quantitative insights, the VA content has been tentatively evaluated considering the composition E_mVA_n of each peak convoluted by their relative abundance to calculate an average $E_{m\ av}VA_{n\ av}$ composition. The molar content (mol%) and weight content (wt%) of VA are then derived from this average composition according to $mol\%(VA) = n_{av}/(m_{av} + n_{av})$ and $wt\%(VA) = 86*n_{av}/(28*m_{av} + 86*n_{av})$. Results from such calculations applied to the restricted mass spectra are mentioned for each spectrum in Fig. 5 and listed in Table 1.

VA contents of approximatively 42 wt%, 29 wt% and 25 wt% have been found for EVA40, EVA25 and EVA18, respectively. A decrease in the weight fraction of VA is thus highlighted from EVA40 to EVA18 and the values are in good agreement with the contents provided by the supplier for EVA40 and EVA25. A bias tends to appear for the last EVA18 with an overestimation of the VA content (+40% as compared to the value provided by the supplier). As for the SEC and MS measurements, EVA18 acts as the limit sample for the evaluation of the VA content. The limited solubility of EVA18 in $CHCl_3$ concomitantly to desorption and ionization issues undoubtedly account for such bias. The VA content has been previously found not to vary with the molecular weight using high-performance liquid chromatography (HPLC) measurements[36] and we obtained similar results with a steady VA content calculated for fractions #1 and #3 (as shown in Supplementary Figs. S3 and S4, Supporting Information). A unique value for the VA content regardless of the degree of polymerization ensures once more the representativeness of the results from the low molecular weight oligomers for the whole sample. Interestingly, the calculation of the VA content conducted on the whole mass spectra gave similar results (43 wt% for EVA40, 29 wt% for EVA25 and 24 wt% for EVA18). The complete data are listed in Supplementary Tables S2–S4 (Supporting Information). Limiting the evaluation to a single pattern in lieu of the whole mass spectrum thus does not bias the VA content calculation but drastically speeds up the procedure (4 to 7 values to be treated vs. 100 to 200 values for the whole mass spectra). The composition in E and VA units has nevertheless to be evaluated manually for each point. The last section of this paper deals with the use of the Kendrick masses and KMD plots to both easily interpret the MS data in a user-friendly representation and instantaneously calculate the VA content of any sample.

Kendrick mass defect plots as an alternative data treatment method

The Kendrick masses are calculated according to the procedure described in the Experimental section from the

Table 1. Accurate mass measurements and assignments of peaks detected in the restricted MALDI mass spectra of EVA40, EVA25 and EVA18 (Fig. 5)

	Elemental Comp.	$(m/z)_{exp}$	δ (ppm)	Assignment	Ab. (%)	Average Comp.	VA (%wt)
EVA40	$C_{76}H_{148}NaO_6^+$	1180.1168	+0.0	$[H\text{-}(E_{32}VA_3)\text{-}H + Na]^+$	18	$E_{23.9}VA_{5.7}$	42+/-1
	$C_{74}H_{142}NaO_8^+$	1182.0589	-0.6	$[H\text{-}(E_{29}VA_4)\text{-}H + Na]^+$	55		
	$C_{72}H_{136}NaO_{10}^+$	1184.0030	+0.4	$[H\text{-}(E_{26}VA_5)\text{-}H + Na]^+$	100		
	$C_{70}H_{130}NaO_{12}^+$	1185.9461	+0.5	$[H\text{-}(E_{23}VA_6)\text{-}H + Na]^+$	96		
	$C_{68}H_{124}NaO_{14}^+$	1187.8886	+0.2	$[H\text{-}(E_{20}VA_7)\text{-}H + Na]^+$	57		
	$C_{66}H_{118}NaO_{16}^+$	1189.8312	+0.0	$[H\text{-}(E_{17}VA_8)\text{-}H + Na]^+$	28		
	$C_{64}H_{112}NaO_{18}^+$	1191.7737	-0.3	$[H\text{-}(E_{14}VA_9)\text{-}H + Na]^+$	12		
EVA25	$C_{78}H_{154}NaO_4^+$	1178.1739	+0.0	$[H\text{-}(E_{35}VA_2)\text{-}H + Na]^+$	26	$E_{29.4}VA_{3.9}$	29+/-2
	$C_{76}H_{148}NaO_6^+$	1180.1167	-0.1	$[H\text{-}(E_{32}VA_3)\text{-}H + Na]^+$	77		
	$C_{74}H_{142}NaO_8^+$	1182.0595	-0.2	$[H\text{-}(E_{29}VA_4)\text{-}H + Na]^+$	100		
	$C_{72}H_{136}NaO_{10}^+$	1184.0023	-0.2	$[H\text{-}(E_{26}VA_5)\text{-}H + Na]^+$	55		
	$C_{70}H_{130}NaO_{12}^+$	1185.9429	-2.2	$[H\text{-}(E_{23}VA_6)\text{-}H + Na]^+$	18		
EVA18	$C_{78}H_{154}NaO_4^+$	1178.1744	+0.4	$[H\text{-}(E_{35}VA_2)\text{-}H + Na]^+$	49	$E_{31.1}VA_{3.3}$	25+/-2
	$C_{76}H_{148}NaO_6^+$	1180.1178	+0.8	$[H\text{-}(E_{32}VA_3)\text{-}H + Na]^+$	100		
	$C_{74}H_{142}NaO_8^+$	1182.0606	+0.8	$[H\text{-}(E_{29}VA_4)\text{-}H + Na]^+$	71		
	$C_{72}H_{136}NaO_{10}^+$	1184.0068	+3.6	$[H\text{-}(E_{26}VA_5)\text{-}H + Na]^+$	28		

VA content is derived from the composition in E and VA units of each peak convoluted by their abundance.

accurate mass measurements. Plotting the Kendrick mass defect (KMD) as a function of the nominal Kendrick masses (NKM) congeners with a varying number of base units *only* will line up horizontally.[31] Considering E as the base unit, PE adducts would line up horizontally (same KMD value regardless of the degree of polymerization, NKM increasing by one 28 Da monomer unit at a time) while a pure VA would lead to an oblique plot, each addition of a VA unit increasing the KMD value of 0.0593 and the NKM value of 86 Da (see Fig. 6(A) for hypothetic KMD plots of pure PE and pure VA). Plotting KMD vs. NKM for an EVA copolymer for which the number of E *and* VA units vary will lead to a scatter plot with an elliptic shape, as schematically represented in Fig. 6(A) (grey spot). Such representation of the MS data allows a rapid interpretation, the dimensions of the plot in the horizontal and oblique directions giving information about the degree of polymerization in terms of E and VA units, respectively (Fig. 6(A)). An ellipse-shaped plot with its major axis along the horizontal direction would correspond to an E-rich aliquot while an ellipse along the oblique direction would be associated with a VA-rich sample. The coordinates of the centroid of the KMD plot (weighted average of the NKM and KMD values) noted (NKM(centroid); KMD(centroid)) are also linked to the average n and m compositions of E and VA as follows:

$$NKM(centroid) = NKM(\alpha + \omega + cation) + NKM(E)\cdot m_{centroid} + NKM(VA)\cdot n_{centroid} \quad (3)$$

$$KMD(centroid) = KMD(\alpha + \omega + cation) + KMD(VA)\cdot n_{centroid} \quad (4)$$

The number of VA units at the centroid $n_{centroid}$ is obtained from Eqn. (4) according to:

$$n_{centroid} = (KMD(centroid) - KMD(\alpha + \omega + cation)/KMD(VA) \quad (5)$$

and the number of E units at the centroid $m_{centroid}$ is then calculated from Eqn. (3) as follows:

$$m_{centroid} = NKM(centroid) - NKM(\alpha + \omega + cation) - NKM(VA)\cdot n_{centroid})/NKM(E) \quad (6)$$

In the present case, α = ω=H and cation=Na^+, KMD(α + ω + cation) = 0.0225, KMD(VA) = 0.0593, NKM(α + ω + cation)=25, NKM(E) = 28 and NKM(VA) = 86. Note that these equations are valid for any point in the KMD plot, which means one could use the KMD and NKM values found for any oligomer adduct to decipher its co-monomeric composition instantaneously.

The KMD plots for the fractions #2 of EVA40, EVA25 and EVA18 are depicted in Figs. 6(B)–6(D) and the associated centroids are highlighted by a red dot. Each point of the plot corresponds to a given E_mVA_n co-oligomer. The $E_{m+1}VA_n$ congener is aligned on the same horizontal line (same KMD since the VA content does not change) with a NKM shift of +28 Da. The E_mVA_{n+1} congener is shifted by +86 Da in terms of NKM and +0.0593 in terms of KMD, hence aligned in the oblique direction. The shapes of the plots are in accordance with the expected nature of the EVA aliquots. From EVA40 to EVA18, the elliptic shape tends to flatten with its major axis being closer and closer to the horizontal direction, i.e. closer to a pure PE sample. Elliptic approximations of the KMD plots for EVA40 and EVA25 are reproduced in Fig. 6(D) for sake of comparison (light and dark grey, respectively). The flattening of the plots from EVA40 to EVA18 is concomitant with a decrease in their dimension in the horizontal direction, highlighting the increasing difficulty to detect the E-rich chains. The average compositions for EVA40, EVA25 and EVA18 calculated from the centroids have been found at $E_{24.5}VA_{5.4}$, $E_{28.8}VA_{3.5}$ and $E_{31.4}VA_{3.1}$, in other words 40 wt%, 27 wt% and 23 wt%, respectively. As an alternative *visualization*

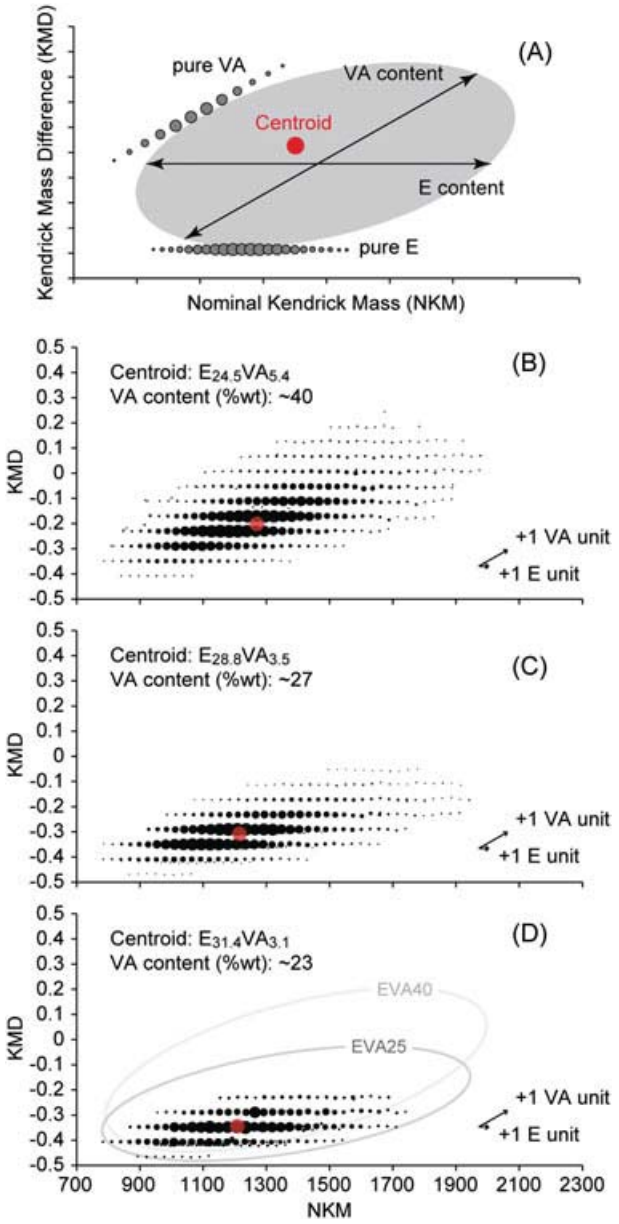

Figure 6. (A) Generic representation of KMD plotted as a function of NKM (so-called KMD plot) for hypothetic pure VA and pure E polymers (oblique and horizontal lines, resp.) and EVA copolymer (grey spot). VA content is calculated from the composition in E and VA units at the centroid of the plot. The size of each disk reflects the relative abundance of the associated oligomeric adduct in the mass spectrum (so-called bubble chart). (B)-(D) KMD plots for the fractions #2 collected from the SEC elution of EVA40, EVA25 and EVA18 with the calculated VA content (centroid: red dot). Schematic KMD plots for EVA40 and EVA25 are reproduced in (C) for the sake of comparison (light grey and dark grey ellipses, respectively).

method of the native MS data, the VA contents computed from the KMD plot are similar to those computed from the MALDI mass spectra and in good agreement with the values provided by the supplier for EVA40 and EVA25, while a bias still arises for EVA18 with a noticeable overestimation. At least the correct trend (i.e. a decrease in VA content) is highlighted using either native MA data or KMD plots in a qualitative manner. Since EVA25 is the sample of interest for many industrial applications (typical VA content: 28–33 wt%), the bias observed for EVA18 should not call into question the analytical procedure proposed here. As a short digression, the KMD plots for the fractions #1 and #3 are depicted in Supplementary Figs. S5 and S6 (Supporting Information). No variation is observed over the mass range covered by the three collected fractions (*m/z* 700–3000) with VA contents (wt%) found at 41 (#1) and 40 (#3) for EVA40, 28 (#1) and 27 (#3) for EVA25 and 22 (#1) and 22 (#3) for EVA18.

It is worth mentioning that four aliquots from EVA25 collected *before* the fraction #1 discussed in the present paper have been submitted to MALDI-MS analysis. The associated mass spectra are depicted in Supplementary Fig. S7 (Supporting Information) and display clean Gaussian-shaped distributions (M_n = 3600, 4900, 7500 and 10,900 g mol^{-1}). However, the resolution in such a high mass range is not high enough to overcome the assignment pitfalls mentioned in the first section (+2 Da between $E_{m+3}VA_n$ and E_mVA_{n+1}, isobaric $E_{m+3}VA_n(^{13}C_2)$ and E_mVA_{n+1}). Proper peak assignment (composition in E and VA units) is not possible, nor is the evaluation of the VA content from either the native MS data or KMD plots. Oligomers of higher molecular weight collected from the SEC elution of EVA samples could hence be mass analyzed, but the information extracted from the so-recorded mass spectra should be limited to the molecular weights only.

CONCLUSIONS

First results about the characterization of commercial EVA copolymers with different VA contents using high-resolution mass spectrometry have been reported. As a major structural feature for polymeric chains, the end-groups of the low molecular weight oligomers were successfully characterized using a MALDI SpiralTOF apparatus following a preliminary fractionation by SEC, regardless of the VA content of the aliquots. Such VA content was also satisfactorily evaluated from the mass data for the EVA samples of industrial interest (VA content >25%) while it tended to be overestimated for the samples with low VA content owing to their increasing PE-like character. Lastly, Kendrick mass defect analysis was proposed as an alternative data treatment method for the discrimination of the EVA samples and the evaluation of their VA content. A major advantage of the KMD plot relies on the speed of data treatment especially for copolymers. Once the end-groups have been characterized, spectra with correct calibration can be automatically converted into KMD plots using automatic peak picking, the centroid and its associated E_mVA_n determined instantaneously, that is to say the VA content, in addition to the degrees of polymerizations (shape of the KMD plot). Such a user-friendly data treatment method would be of high interest for time-consuming routine or comparative studies for which many samples must be analyzed.

Acknowledgements

K. Kobayashi (JEOL Resonance) is gratefully acknowledged for the NMR measurements. T. Fouquet and H. Sato also acknowledge the ongoing financial support by the Japan Society for the Promotion of Science (JSPS) under the "Postdoctoral Fellowship for Overseas Researchers" program. This project was also supported by a Grant-in-Aid "JSPS KAKENHI" (Grant No 15F15344) and by the New Energy and Industrial Technology Development Organization (NEDO).

REFERENCES

[1] I-L. Chien, T. W. Kan, B.-S. Chen. Dynamic simulation and operation of a high pressure ethylene-vinyl acetate (EVA) copolymerization autoclave reactor. *Comput. Chem. Eng.* **2007**, *31*, 233.
[2] D. Doran, B. Cather. *Construction Materials Reference Book*. Routledge, Taylor and Francis Group, Oxford, **2013**.
[3] H.-Y. Li, R. Theron, G. Röder, T. Turlings, Y. Luo, R.F.M. Lange, C. Ballif, L.-E. Perret-Aebi. Insights into the encapsulation process of photovoltaic modules: GCMS analysis on the curing step of poly(ethylene-co-vinyl acetate) (EVA) encapsulant. *Polym. Polym. Compos.* **2012**, *20*, 665.
[4] A. Arsac, C. Carrot, J. Guillet. Rheological characterization of ethylene vinyl acetate copolymers. *J. Appl. Polym. Sci.* **1999**, *74*, 2625.
[5] T. Kuila, H. Acharya, S. K. Srivastava, A. K. Bhowmick. Synthesis and characterization of ethylene vinyl acetate/Mg–Al layered double hydroxide nanocomposites. *J. Appl. Polym. Sci.* **2007**, *104*, 1845.
[6] F. J. Pern. Luminescence and absorption characterization of ethylene-vinyl acetate encapsulant for PV modules before and after weathering degradation. *Polym. Degrad. Stab.* **1993**, *41*, 125.
[7] J. K. Fink. *Handbook of Engineering and Specialty Thermoplastics: Polyolefins and Styrenics*. John Wiley, New York, **2010**.
[8] NPCS Board of Consultants and Engineers. *The Complete Technology Book on Adhesives, Glues and Resins*. Asia Pacific Business Press Inc., New Delhi, **2007**.
[9] NPCS Board of Consultants and Engineers. *The Complete Technology Book on Industrial Polymers, Additives, Colourants and Fillers*. Asia Pacific Business Press Inc., New Delhi, **2006**.
[10] Z. Su, Y. Zhao, Y. Xu, X. Zhang, S. Zhu, D. Wang, J. Wu, C. Han, D. Xu. Characterization of the sequence distribution and crystalline structure of poly(ethylene-co-vinyl acetate) copolymers with high-resolution NMR spectroscopy. *Polymer* **2004**, *45*, 3693.
[11] T. K. Wu, D. W. Ovenall, G. S. Reddy. Nuclear magnetic resonance studies on microstructure of ethylene copolymers. VI. Carbon-13 spectra of ethylene-vinyl acetate copolymers. *J. Polym. Sci.: Polym. Phys.* **1974**, *12*, 901.
[12] K. Besdah. Microstructure analysis of ethylene-vinyl acetate copolymer by 2D NMR spectroscopy. *Macromolecules* **1992**, *25*, 5597.
[13] N. Gospodinova, L. Terlemezyan, M. Mihailov, U. M. Han, K. B. Du. Microstructure of ethylene-(vinyl acetate) copolymers prepared by emulsion copolymerization. *Eur. Polym. J.* **1992**, *28*, 961.
[14] L. Wang, P. Fang, C. Ye, J. Feng. Solid-state NMR characterizations on phase structures and molecular dynamics of poly(ethylene-co-vinyl acetate). *J. Polym Sci., Part B: Polym. Phys.* **2006**, *44*, 2864.
[15] W. Stark, M. Jaunich, W. Bohmeyer, K. Lange. Investigation of the crosslinking behaviour of ethylene vinyl acetate (EVA) for solar cell encapsulation by rheology and ultrasound. *Polym. Test.* **2012**, *31*, 904.
[16] B. Rimez, H. Rahier, G. Van Assche, T. Artoos, M. Biesemans, B. Van Mele. The thermal degradation of poly(vinyl acetate) and poly(ethylene-co-vinyl acetate), Part I: Experimental study of the degradation mechanism. *Polym. Degrad. Stab.* **2008**, *93*, 800.
[17] S.P. Tambe, S.K. Singh, M. Patri, Dhirendra Kumar. Ethylene vinyl acetate and ethylene vinyl alcohol copolymer for thermal spray coating application. *Prog. Org. Coat.* **2008**, *62*, 382.
[18] R. L. McEvoy, S. Krause, P. Wut. Surface characterization of ethylene-vinyl acetate (EVA) and ethylene-acrylic acid (EAA) co-polymers using XPS and AFM. *Polymer* **1998**, *39*, 5223.
[19] S. Tsuge, H. Ohtani, C. Watanabe. *Pyrolysis–GC/MS Data Book of Synthetic Polymers: Pyrograms, Thermograms and MS of Pyrolyzates*. Elsevier, Amsterdam, **2011**.
[20] A. A. Galuska. Surface characterization of EVA copolymers and blends using XPS and ToF-SIMS. *Surf. Interface Anal.* **1994**, *21*, 703.
[21] C. A. Jackson, W. J. Simonsick. Application of mass spectrometry to the characterization of polymers. *Curr. Opin. Solid State Mater. Sci.* **1997**, *2*, 661.
[22] S. D. Hanton. Mass spectrometry of polymers and polymer surfaces. *Chem. Rev.* **2001**, *101*, 527.
[23] Giorgio Montaudo, Robert P. Lattimer. *Mass Spectrometry of Polymers*. CRC Press, Taylor and Francis Group, Oxford, **2001**.
[24] H. Pasch, W. Schrepp. *MALDI-TOF Mass Spectrometry of Synthetic Polymers*. Springer-Verlag, Berlin Heidelberg New York, **2003**.
[25] T. Gruendling, S. Weidner, J. Falkenhagen, C. Barner-Kowollik. Mass spectrometry in polymer chemistry: a state of the art up-date. *Polym. Chem.* **2010**, *1*, 599.
[26] M. Hakkarainen. *Mass Spectrometry of Polymers – New Techniques*. Springer-Verlag, Berlin Heidelberg New York, **2012**.
[27] L. Charles. MALDI of synthetic polymers with labile end-groups. *Mass Spectrom. Rev.* **2014**, *33*, 523.
[28] X. Lou, J. L. J. van Dongen, E. W. Meijer. Off-line size-exclusion chromatographic fractionation–matrix assisted laser desorption ionization time-of-flight mass spectrometry for polymer characterization: Theoretical and experimental study. *J. Chromatogr. A* **2000**, *896*, 19.
[29] H. Pasch, W. Schrepp. *MALDI-TOF Mass Spectrometry of Synthetic Polymers*. Springer-Verlag, Berlin Heidelberg, **2003**, pp. 209–287.
[30] R. Murgasova, D. M. Hercules. Polymer characterization by combining liquid chromatography with MALDI and ESI mass spectrometry. *Anal Bioanal Chem* **2002**, *373*, 481.
[31] H. Sato, S. Nakamura, K. Teramoto, T. Sato. Structural characterization of polymers by MALDI SpiralTOF mass spectrometry combined with Kendrick mass defect analysis. *J. Am. Soc. Mass Spectrom.* **2014**, *25*, 1346.
[32] T. Satoh, H. Tsuno, M. Iwanaga, Y. Kammei. The design and characteristics features of a new time-of-flight mass spectrometer with a spiral ion trajectory. *J. Am. Soc. Mass Spectrom.* **2005**, *16*, 1969.
[33] E. Smit, C. P. Rüger, M. Sklorz, S. De Goede, R. Zimmermann, E. R. Rohwer. Investigating the trace polar species present in diesel using high-resolution mass spectrometry and selective ionization techniques. *Energy Fuels* **2015**, *29*, 5554.
[34] D. C. Bugada, R. Gagnon, A. Rudin. Specific refractive index increments of ethylene-vinyl acetate copolymers in trichlorobenzene solutions at 145°C. *J. Appl. Polym. Sci.* **1987**, *34*, 501.
[35] O. Y. Alothman. Processing and characterization of high density polyethylene/ethylene vinyl acetate blends with different VA contents. *Adv. Mater. Sci. Eng.* **2012**, Article ID 635693, DOI: 10.1155/2012/635693.
[36] N. Kagawa, R. Okazaki, A. Itou. Characterization of ethylene-vinyl acetate copolymer by eluent gradient HPLC. *Bunseki Kagaku* **2010**, *59*, 793.

SUPPORTING INFORMATION

Additional supporting information may be found in the online version of this article at the publisher's website.

Applications note MS
MSTips No. 284
MALDI Application

"Fraction base" KMD plots for a high molecular weight poly(3-hydroxybutyrate-*co*-3-hydroxyvalerate) copolyester following its on-plate alkaline degradation and SpiralTOF™ analysis

Product used : Mass spectrometer (MS)

Introduction

High molecular weight polymers are often MS-silent due to their inherent high dispersity ($Đ_M$) or detected in the high mass range with low resolving power. High-resolution mass spectrometry (HRMS) is indeed limited to the low mass range (< 3000 Da) for an unambiguous evaluation of the nature of repeating units and/or end-groups or the isolation of isobaric compounds. An "on-plate" alkaline degradation has thus been developed as a sample pre-treatment on the MALDI target with tenths of ng of polymer to cut long industrial polyester chains into short oligomers amenable to MALDI-HRMS [1]. The complexity of the associated mass spectra can be greatly reduced with the appropriate resolution-enhanced Kendrick mass defect (KMD) analysis using the "fraction base" option of msRepeatFinder to produce compositional maps.

Experimental

Poly(3-hydroxybutyrate-*co*-3-hydroxyvalerate) (PHBV, 12 mol% 3HV, M_n=1.4×10^5 g mol^{-1}, $Đ_M$=2.5) was from Sigma-Aldrich (St. Louis, MO, USA) while all other chemicals and solvents were from FUJIFILM Wako Pure Chemical Corporation unless otherwise mentioned. 1 µL of PHBV (1 mg mL^{-1} in THF) was drop-casted on a disposable MALDI target plate (Hudson Surface Technology, NJ, USA). 1 µL of sodium hydroxide in methanol-d4 at 10 mg mL^{-1} was further deposited and left to air-dry. The excess alkaline reagent was washed with distilled water. 1 µL of 2,4,6-trihydroxyacetophenone (Protea Biosciences, WV, USA) in THF at 20 mg mL^{-1} was applied on the sample spot. Mass spectra were recorded with a JMS-S3000 SpiralTOF™ mass spectrometer. Plots were computed using msRepeatFinder 3.0 from the peak list exported using msTornado™.

MS and regular KMD analyses

The alkaline on-plate degradation of PHBV releases up to six short copolyester series readily detected in MALDI-MS [1]. (**Fig. 1A**). With the variation of end-groups, 3HB and 3HV contents within one given series and the isotopic patterns, peak assignments are non-trivial neither from the mass spectrum nor the regular KMD plot [2] as series overlap (**Fig. 1B**).

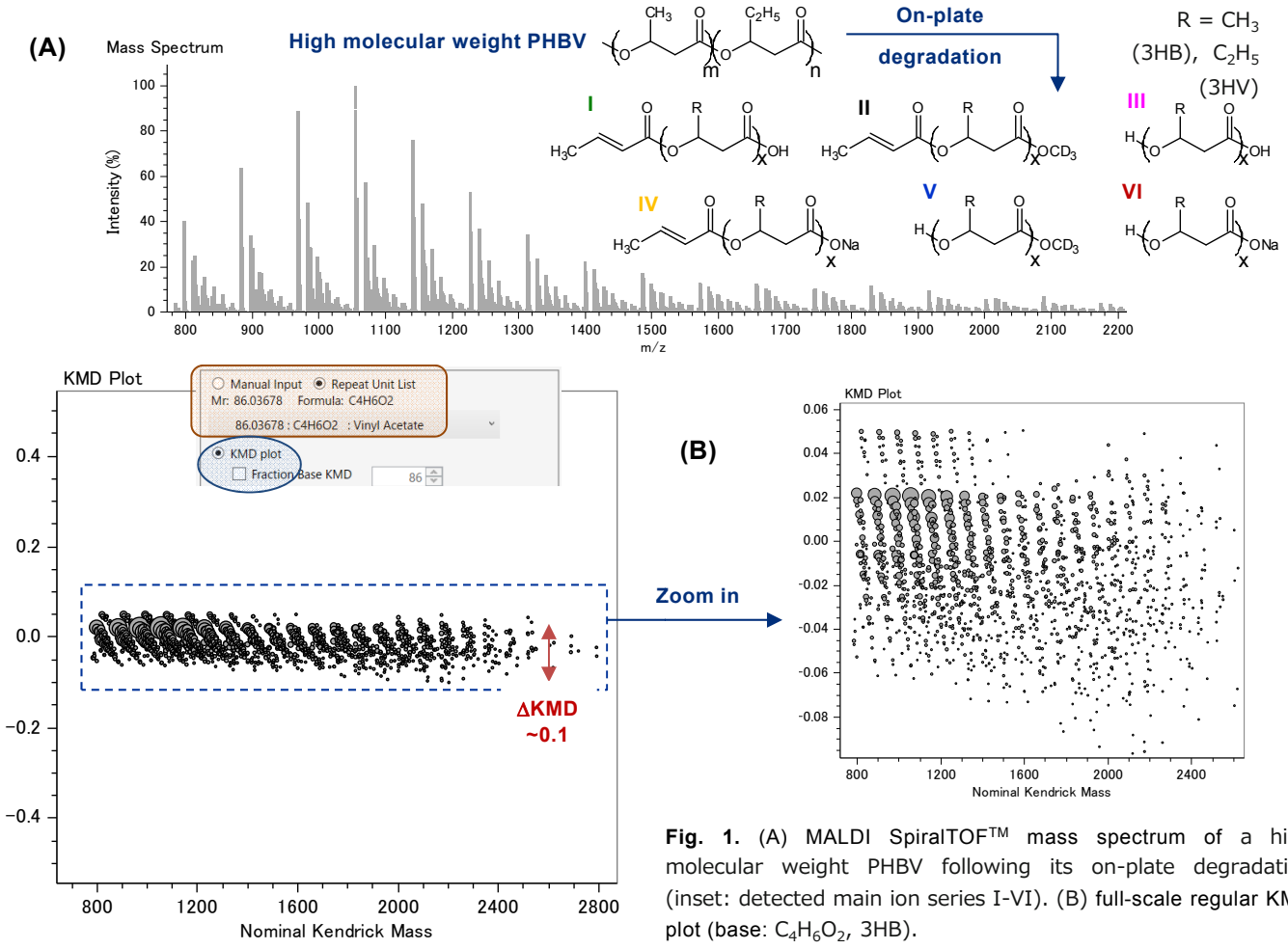

Fig. 1. (A) MALDI SpiralTOF™ mass spectrum of a high molecular weight PHBV following its on-plate degradation (inset: detected main ion series I-VI). (B) full-scale regular KMD plot (base: $C_4H_6O_2$, 3HB).

“One-shot” resolution-enhanced KMD analysis

Contrary to the condensed regular KMD plot, the different ion series cover the entire range of KMD (from -0.5 to 0.5) in the fraction base KMD plot computed with 3HB/135 (**Fig. 2**) [3]. Within one cluster, points differ by their content in 3HB (horizontal alignment, base unit) and in 3HV (oblique alignment) while the isotopic composition is different from one cluster to the other (^{12}C or $^{13}C_x$, **Fig. 2** with color coding). All the peaks detected in the mass spectrum are thus advantageously separated or grouped for a rapid assignment.

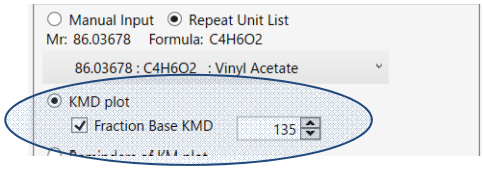

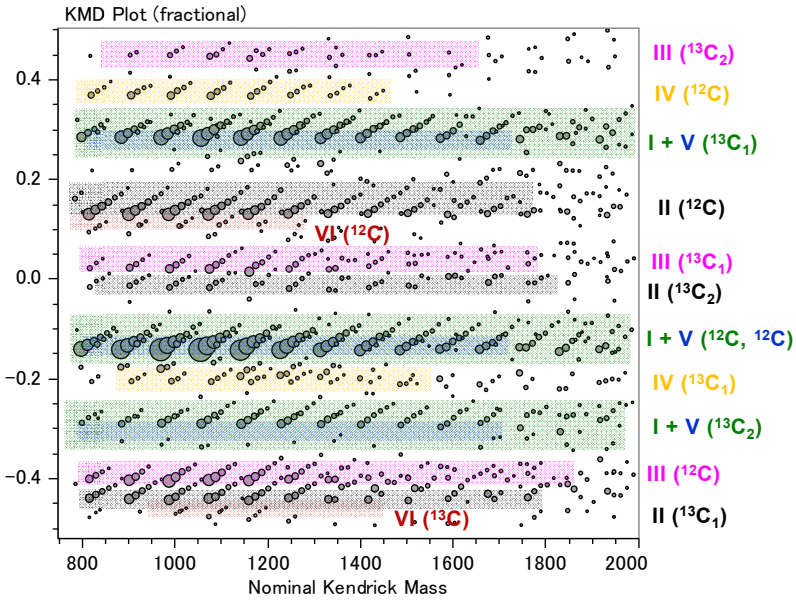

Fig. 2. “Fraction Base KMD” plot with a fractional base unit 3HB/135 using msRepeatFinder.

“Sequential” resolution-enhanced KMD analysis [4]

The series I and V almost overlap in the previous fraction base KMD plot (**Fig. 2**) preventing their separation/isolation. To circumvent this issue, the monoisotopic cluster is extracted (grouping mode, **Fig. 3A**) while the other points are hidden to enhance the visualization (**Fig. 3B**). The two monoisotopic ion series are deconvoluted by changing the fraction (3HB/117, **Fig. 3C**). All the points are fully separated, being monoisotopic co-oligomers (^{12}C) with a varying content in 3HB (horizonal alignment) and 3HV (oblique alignment, structures in insets).

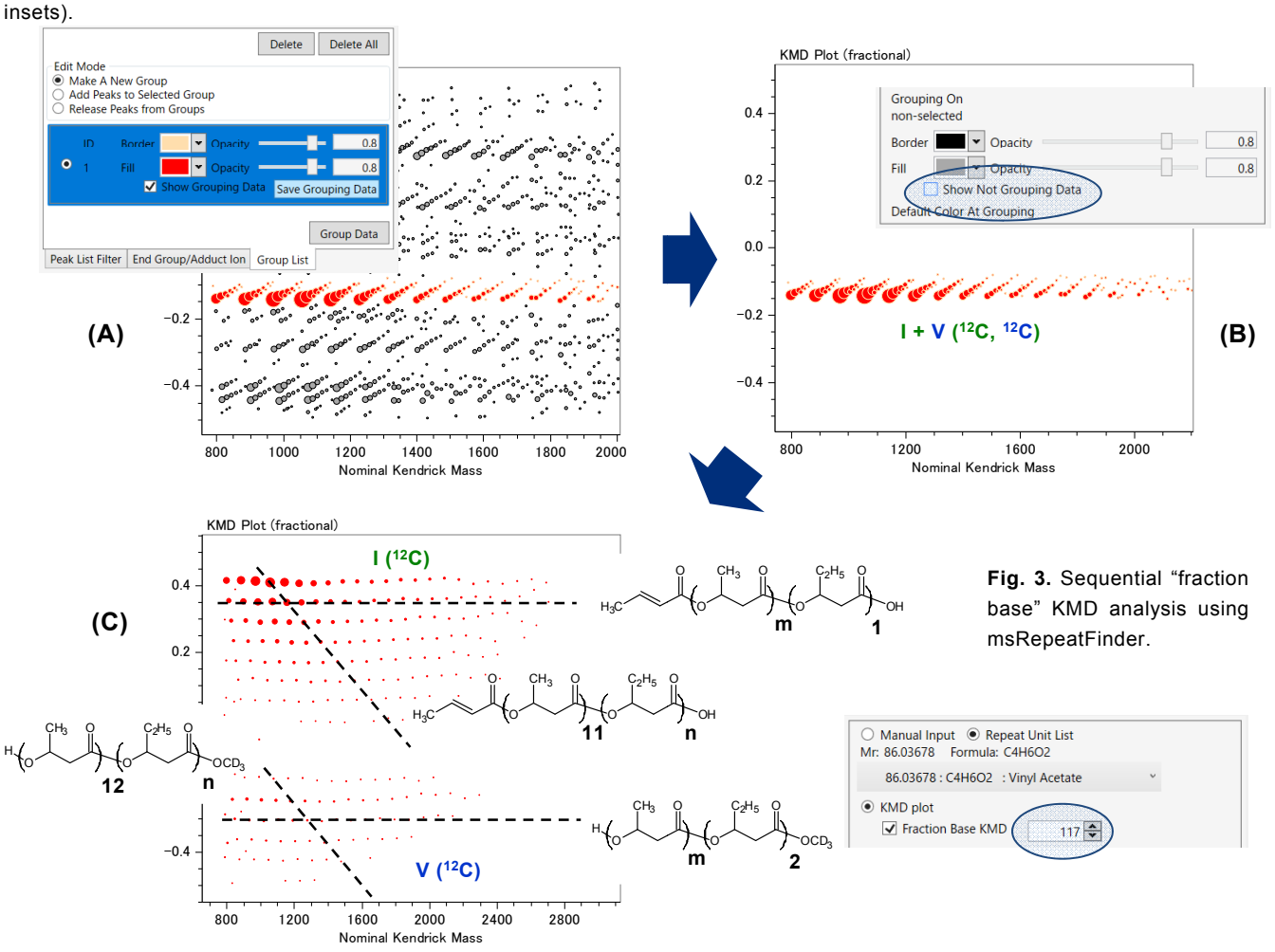

Fig. 3. Sequential “fraction base” KMD analysis using msRepeatFinder.

Alternative data processing: deisotoped mass spectrum (msTornado™)

Using the full dataset reduces the risk of missing minor ion series but the isotopes complicate the data processing with several clusters for a given copolymeric series (**Fig. 2**). The mass spectrum may be instead automatically deisotoped using msTornado™ to simplify the visualization. However, and in spite of deisotoping, the regular KMD plot still fails at separating the ion series (**Fig. 4A**). Instead, the fraction base KMD plot computed with another fractional unit 3HB/92 (**Fig. 4B**) greatly separates the six copolymeric ion series in a single plot further allowing a rapid selection/assignment of co-oligomers with unrivalled viewability [1]. The fraction base differs from the previous case (135 or 117 to 92) as the need for separation is different (content in 3HB, 3HV and end-groups only, no isotopes) [5].

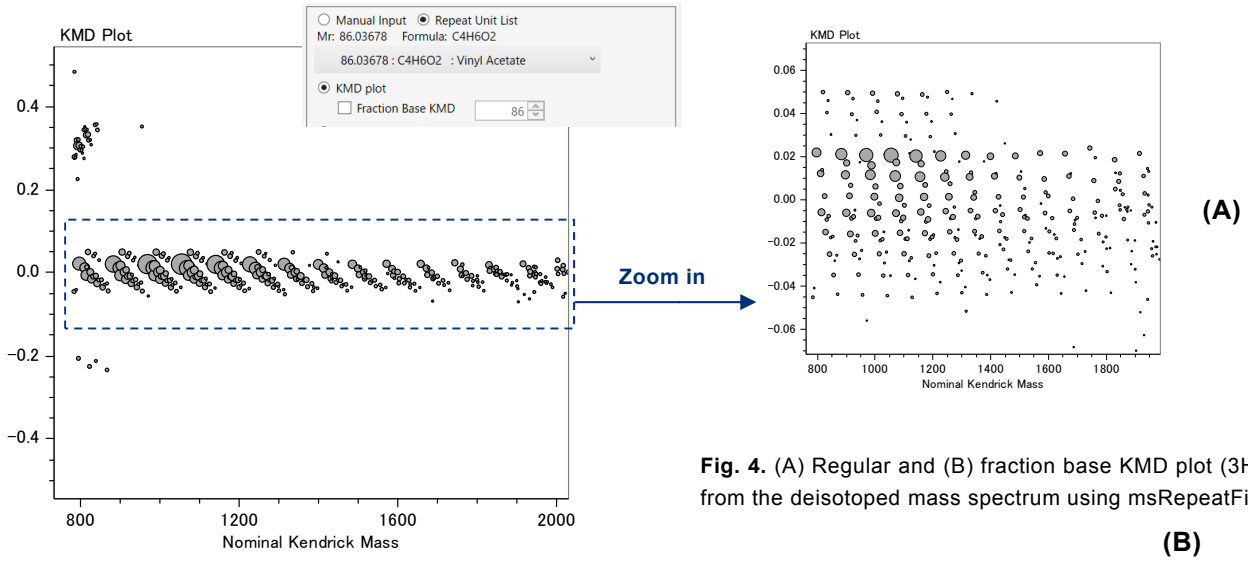

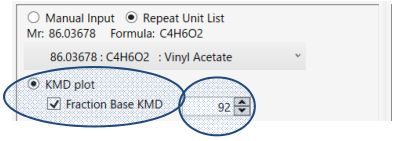

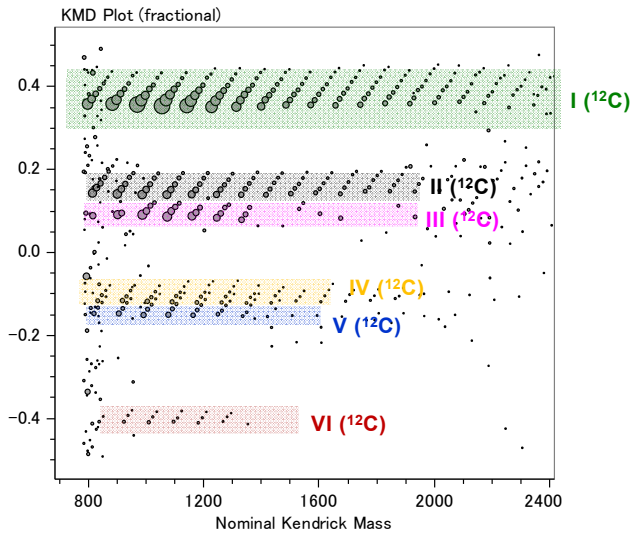

Fig. 4. (A) Regular and (B) fraction base KMD plot (3HB/92) from the deisotoped mass spectrum using msRepeatFinder.

TIP **Alternative separation powers are available by varying the fraction iteratively** from the rounded repeating unit. The best fractions for any expected variations of composition are easily picked from a simple graphical tool [5].

Conclusions

Different KMD plots are computed from the same mass spectrum by varying the fractions to produce favorable compositional maps, depending on the needs for visualization (e.g. separation by ^{13}C isotopes, end-groups, co-monomeric content, or their combination). Using the on-plate alkaline degradation (sample pre-treatment for high molecular weight samples) and the msRepeatFinder filtering capabilities (data processing), the “fraction base KMD” analysis is a very versatile tool suitable for numerous copolymeric datasets.

Acknowledgements

This application note is written based on the results of a joint research project with Sayaka Nakamura, Thierry Fouquet and Hiroaki Sato from the Research Institute for Sustainable Chemistry, National Institute of Advanced Industrial Science and Technology (AIST).

References

[1] S. Nakamura, T. Fouquet, H. Sato. *J. Am. Soc. Mass Spectrom.* **2019**, *30*, 355.
[2] H. Sato, S. Nakamura, K. Teramoto, T. Sato. *J. Am. Soc. Mass Spectrom.* **2014**, *25,* 1346.
[3] T. Fouquet, H. Sato. *Anal. Chem.* **2017**, *89*, 2682.
[4] Q. Zheng, M. Morimoto, H. Sato, T. Fouquet. *Fuel* **2019**, *235*, 944.
[5] S. Nakamura, R. B. Cody, H. Sato, T. Fouquet. *Anal Chem.* 10.1021/acs.analchem.8b04371

JEOL Ltd.
3-1-2 Musashino Akishima Tokyo 196-8558 Japan Sales Division Tel. +81-3-6262-3560 Fax. +81-3-6262-3577
www.jeol.com ISO 9001 • ISO 14001 Certified
▼ Local office
• AUSTRALIA & NEW ZEALAND • BELGIUM • BRAZIL • CANADA • CHINA • EGYPT • FRANCE • GERMANY • GREAT BRITAIN & IRELAND • ITALY • KOREA • MALAYSIA • MEXICO • RUSSIA • SCANDINAVIA • SINGAPORE • TAIWAN • THE NETHERLANDS • USA

MALDI Application: “Fraction base" KMD plots for a high molecular weight poly(3-hydroxybutyrate) polyester following its on-plate alkaline degradation and SpiralTOF™ analysis"

Product used：Mass spectrometer (MS)

Introduction: mathematical background

High molecular weight polymers are often MS-silent due to their inherent high dispersity ($Đ_M$) or detected in the high mass range with low resolving power. An “on-plate” alkaline degradation has thus been developed as a sample pre-treatment on the MALDI target with tenths of ng of polymer to cut long industrial polyester chains into short oligomers amenable to MALDI-HRMS [1]. The complicated mass spectrum of P3HB oligomers was analyzed by fraction base Kendrick mass defect (KMD) plot [2]. Fraction base KMD analysis has been developed from the regular KMD analysis to modify the aspect and separation capabilities of the KMD plots depending on a divisor (noted X) in addition to the base unit (noted R) via a fraction base R/X [3].

Regular rescaling factor

Regular KMD analysis [1]: $KM(R) = m/z \cdot \frac{round(R)}{R}$

Fraction base KMD analysis [2]: $KM(R,X) = m/z \cdot \frac{round(R/X)}{R/X}$

Fraction base rescaling factor

$KMD = round(KM) - KM$

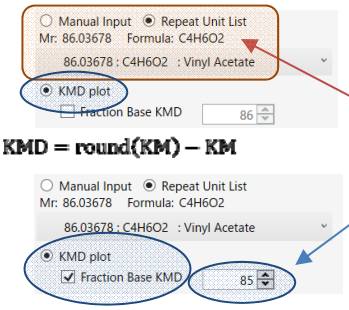

R: exact mass of a repeating unit (unified atomic mass unit)

X: positive integer modifying the rescaling factor

Experimental

Poly(3-hydroxybutyrate) (P3HB, M_n = 2.6 × 10^5 g mol^{-1}, $Đ_M$=2.7) was from Sigma-Aldrich (St. Louis, MO,USA). All other chemicals and solvents were from FUJIFILM Wako Pure Chemical Corporation (Osaka, Japan) unless otherwise mentioned. 1 µL of P3HB in THF at 1 mg mL^{-1} was drop-casted on a disposable MALDI target plate (Hudson Surface Technology, New Jersey, USA) to form a polymer thin layer. 1 µL of sodium hydroxide in methanol (10 mg mL^{-1}) was deposited on the sample layer and left to air-dry for 5 min. The excess amount of alkaline reagent was washed with distilled water. After drying, 1 µL of 2,4,6-trihydroxyacetophenone (THAP, Protea Biosciences, West Virginia, USA) in THF (20 mg mL^{-1}) was applied on the sample spot as matrix. Mass spectra were recorded with a JMS-S3000 SpiralTOF™ mass spectrometer. Plots were computed using msRepeatFinder 3.0 from the peak list exported using msTornado™.

MALDI mass analysis

Intense ion series of P3HB oligomers are observed in MALDI-MS (**Fig. 1A**). Six main series varying by their end-groups are detected (**Fig. 1B**) but assigning and visualizing all congeners remains time-consuming and poorly intuitive.

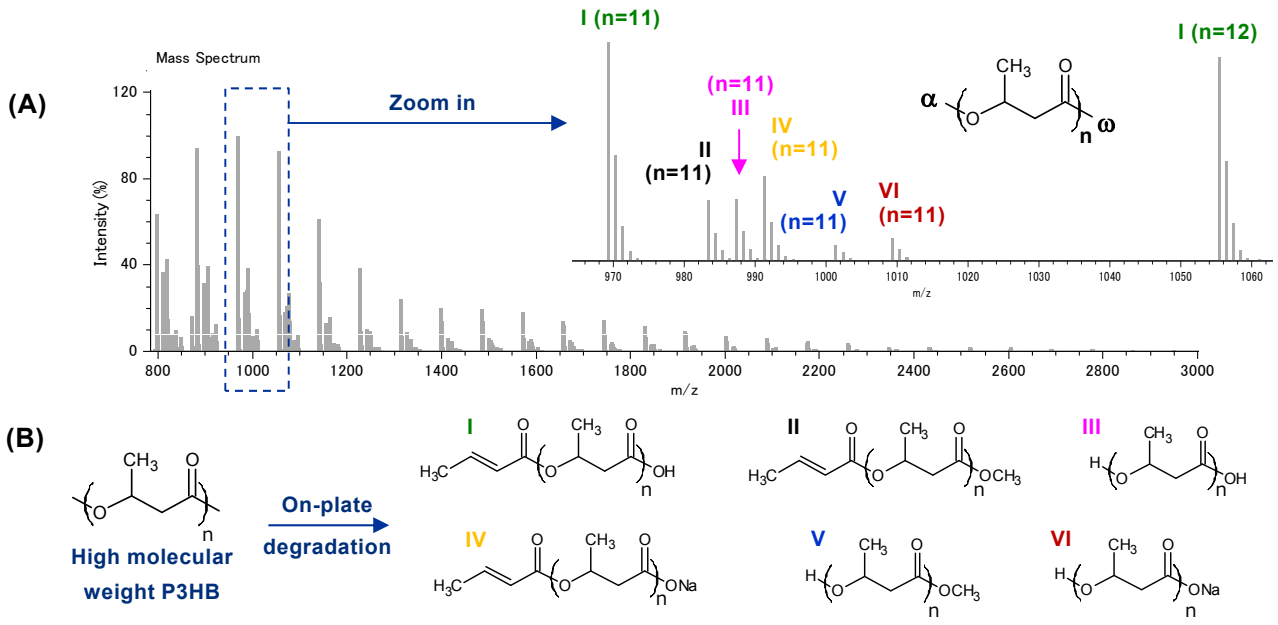

Fig. 1. (A) MALDI SpiralTOF mass spectrum of a high molecular weight P3HB following its on-plate degradation (inset: zoom shot with assignments). (B) P3HB ion series noted I-VI.

Regular and resolution-enhanced KMD plots

The regular KMD plot computed from the MALDI mass spectrum displays a cloud of points aligned horizontally (**Fig. 2A**). Zooming in is mandatory as the points are clustered within a restricted portion of the plot due to a very limited change of KMD with the variation of isotope or end-group composition [4]. Two poorly resolved groups of points are seen (**Fig. 2B**) while six series are expected considering the mass spectral data.

Fig. 2. Full-scale regular KMD plot from the mass spectrum of P3HB with $C_4H_6O_2$ as base unit using msRepeatFinder.

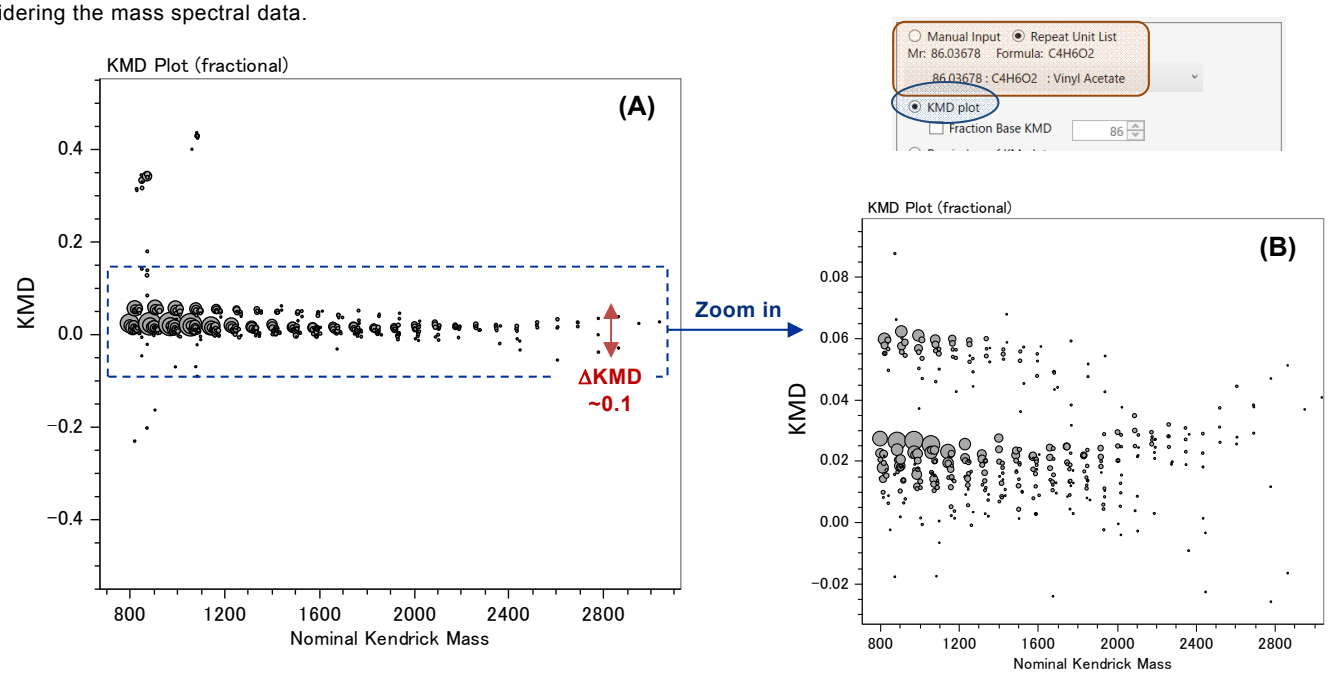

Activating the "Fraction Base KMD" option in msRepeatFinder and decreasing the value of X from 86 (regular KMD plot) to 85, the resolution-enhanced KMD plot greatly separates the six P3HB series at full scale thanks to a greater variation of KMD by the change of composition (**Fig. 3A**). Decreasing X of one unit at X=84, the resolution-enhanced KMD plot additionally resolves the isotopic patterns (1st line: ^{12}C, 2nd line: $^{13}C_1$, ...) and discriminates the six series even better (**Fig. 3B**, X=84).

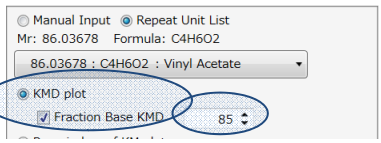

TIP **Decreasing / increasing the fraction iteratively** will separate the ^{13}C isotopes more and more. The best fractions for any expected variation of composition are easily picked from a simple graphical tool [4].

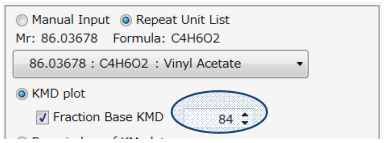

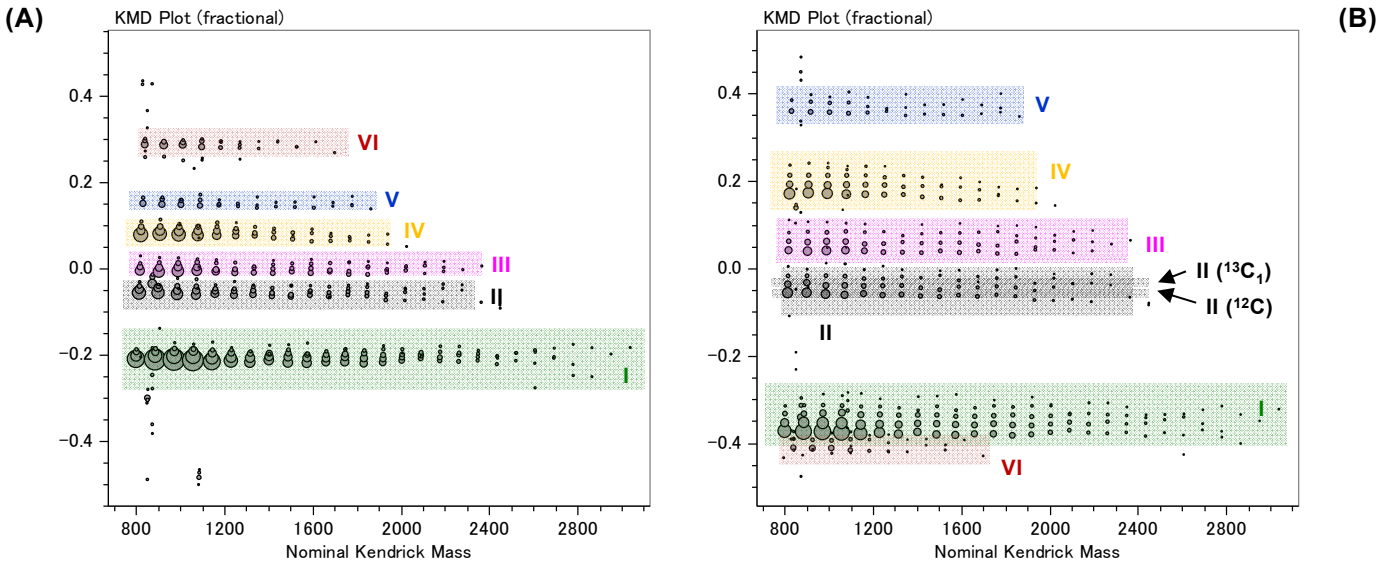

Fig. 3. Full scale fraction base KMD plots computed with the fractional base units (A) 3HB/85 and (B) 3HB/84 using msRepeatFinder.

Grouping mode with the resolution-enhanced KMD plot

The “grouping mode” in msRepeatFinder combined with the fraction base KMD analysis allows each ion series to be labelled in the mass spectrum and the plot with visual color coding via a simple selection of points (**Fig. 4**). The high separating power reached with 3HB/84 further allows the selection of monoisotopic peaks (^{12}C, light green dots) from the main series I (dark green dots). Unselected ion series can also be hidden to further help at visualizing the polymeric series from the background peaks.

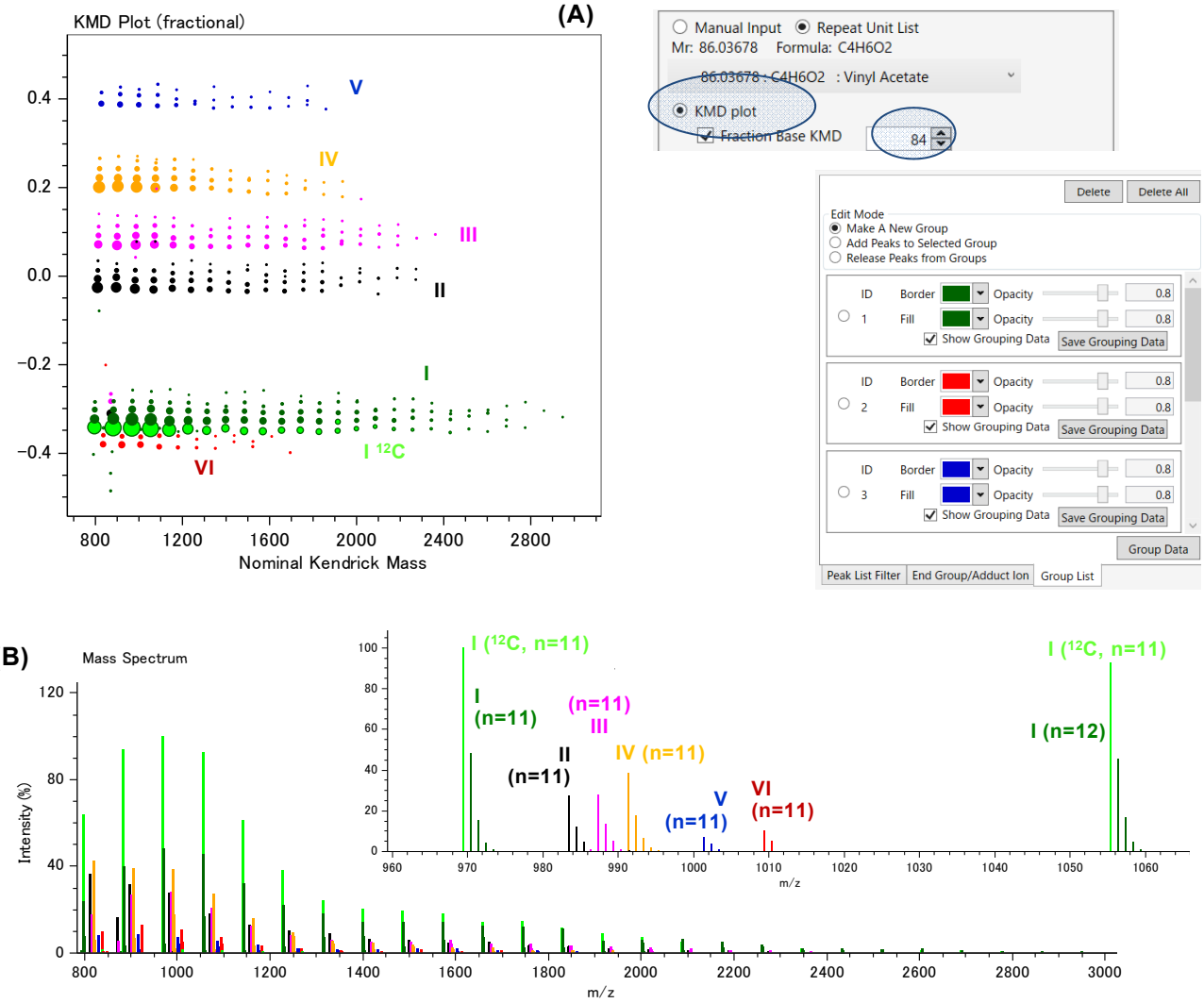

Fig. 4. (A) Fraction base KMD plot computed with the fractional base unit 3HB/84 in grouping mode to label the series in the mass spectrum (B).

Conclusions

The KMD analysis becomes dynamic with the introduction of the “Fraction Base KMD” relying on the resolution-enhanced methodology. It is a highly versatile tool as decreasing or increasing the value of the fraction leads to numerous favorable separations of ion series varying by their isotopic composition, end-groups or adducted ion. It can be successfully adapted to any type of homopolymers and any type of mass spectral data of medium to ultrahigh accuracy.

Acknowledgements

This application note is written based on the results of a joint research project with Sayaka Nakamura, Thierry Fouquet and Hiroaki Sato from the Research Institute for Sustainable Chemistry, National Institute of Advanced Industrial Science and Technology (AIST).

References

[1] S. Nakamura, T. Fouquet, H. Sato. *J. Am. Soc. Mass Spectrom.* **2019**, *30*, 355.
[2] H. Sato, S. Nakamura, K. Teramoto, T. Sato. *J. Am. Soc. Mass Spectrom.* **2014**, *25*, 1346.
[3] T. Fouquet, H. Sato. *Anal. Chem.* **2017**, *89*, 2682.
[4] S. Nakamura, R. B. Cody, H. Sato, T. Fouquet. *Anal Chem.* 10.1021/acs.analchem.8b04371

JEOL Ltd.
3-1-2 Musashino Akishima Tokyo 196-8558 Japan Sales Division Tel. +81-3-6262-3560 Fax. +81-3-6262-3577
www.jeol.com ISO 9001 • ISO 14001 Certified

• **AUSTRALIA & NEW ZEALAND** /JEOL(AUSTRALASIA) Pty.Ltd. Suite 1, L2 18 Aquatic Drive - Frenchs Forest NSW 2086 Australia • **BELGIUM** /JEOL (EUROPE) B.V. Planet II, Gebouw B Leuvensesteenweg 542, B-1930 Zaventem Belgium • **BRAZIL** /JEOL Brasil Instrumentos Cientificos Ltda. Av. Jabaquara, 2958 5° andar conjunto 52 ; 04046-500 Sao Paulo, SP Brazil • **CANADA** /JEOL CANADA, INC. 3275 1ere Rue, Local #8 St-Hubert, QC J3Y-8Y6, Canada • **CHINA** /JEOL(BEIJING) CO., LTD. Zhongkeziyuan Building South Tower 2F, Zhongguancun Nansanjie Street No. 6, Haidian District, Beijing, P.R.China • **EGYPT** /JEOL SERVICE BUREAU 3rd Fl. Nile Center Bldg., Nawal Street, Dokki, (Cairo), Egypt • **FRANCE** /JEOL (EUROPE) SAS Espace Claude Monet, 1 Allee de Giverny 78290, Croissy-sur-Seine, France • **GERMANY** /JEOL (GERMANY) GmbH Gute Aenger 30 85356 Freising, Germany • **GREAT BRITAIN & IRELAND** /JEOL (U.K.) LTD. JEOL House, Silver Court, Watchmead, Welwyn Garden City, Herts AL7 1LT, U.K. • **ITALY** /JEOL (ITALIA) S.p.A. Palazzo Pacinotti - Milano 3 City, Via Ludovico il Moro, 6/A 20080 Basiglio(MI) Italy • **KOREA** /JEOL KOREA LTD. Dongwoo Bldg. 7F, 1443, Yangjae Daero, Gangdong-Gu, Seoul, 05355, Korea • **MALAYSIA** /JEOL(MALAYSIA) SDN.BHD. 508, Block A, Level 5, Kelana Business Center, 97, Jalan SS 7/2, Kelana Jaya, 47301 Petaling Jaya, Selangor, Malaysia • **MEXICO** /JEOL DE MEXICO S.A. DE C.V. Arkansas 11 Piso 2 Colonia Napoles Delegacion Benito Juarez, C.P. 03810 Mexico D.F., Mexico • **RUSSIA** /JEOL (RUS) LLC. Krasnoproletarskaya Street, 16, Bld 2, 127473, Moscow, Russian Federation • **SCANDINAVIA** /SWEDEN JEOL (Nordic) AB Hammarbacken 6A, Box 716, 191 27 Sollentuna Sweden • **SINGAPORE** /JEOL ASIA PTE.LTD. 2 Corporation Road #01-12 Corporation Place Singapore 618494 • **TAIWAN** /JIE DONG CO., LTD. 7F, 112, Chung Hsiao East Road, Section 1, Taipei, Taiwan 10023 (R.O.C.) • **THE NETHERLANDS** /JEOL (EUROPE) B.V. Lireweg 4, NL-2153 PH Nieuw-Vennep, The Netherlands • **USA** /JEOL USA, INC. 11 Dearborn Road, Peabody, MA 01960, U.S.A.

Applications note

MS
MSTips No. 269
MALDI Application

“Remainders of KM” plot for polymers using msRepeatFinder: compositional mapping over a broad mass range

Product used：MS

Mass Spectrometry (MS) with soft ionization such as matrix-assisted laser desorption ionization (MALDI) allows the compositional analysis of polymers (repeating units, chain terminations) of low dispersity. Combining a size exclusion chromatography (SEC) fractionation with a high-resolution MALDI SpiralTOF™ MS analysis enables the evaluation of the composition of polydisperse polymeric samples over a broad mass range (high-resolution/high-accuracy mass measurements in the low mass range <4 kDa, isotopic resolution in higher mass range < 30kDa). However, the higher the resolution the more the peaks detected in the mass spectrum with one spectrum per fraction, making the interpretation of mass spectral data the rate-limiting step of the whole analytical procedure. A “remainders of Kendrick mass” analysis (RKM) is proposed as a rapid post-acquisition data processing using visual maps from concatenated low/high-accuracy and low/high mass range data.

Experimental

A 1 mg mL^{-1} solution of poly(ε-caprolactone) (PCL, Polymer Source, P1302-CL) in $CHCl_3$ was fractionated by SEC (HLC8220 GPC system, Tosoh, TSKgel multipore HXL-M columns, flow rate: 1 mL min^{-1}, 0.5 mL per fraction). Mass spectra were recorded with a JMS-S3000 SpiralTOF™ mass spectrometer (matrix: DCTB, no salt added). Plots were computed using msRepeatFinder 3.0.

SEC-MALDI-MS

Five fractions are collected from the SEC elution turning the PCL sample into aliquots of low dispersity (Fig. 1A). The main distributions in the last fraction (*m/z* 2000 to 5000, Fig. 1B) are assigned to sodiated (H, OH)-ended PCL (red circles) and (H, C_3H_7O)-ended PCL (blue triangle) taking full advantage of the high resolution of the analyzer. The SpiralTOF™ analyzer is still capable of producing mass spectra for the four other fractions of increasing molecular weight up to 20000 Da with a neat isotopic resolution (Fig. 2A). Mass spectra are concatenated using msRepeatFinder3.0 to display the full mass spectral data in one graph (Fig. 2B).

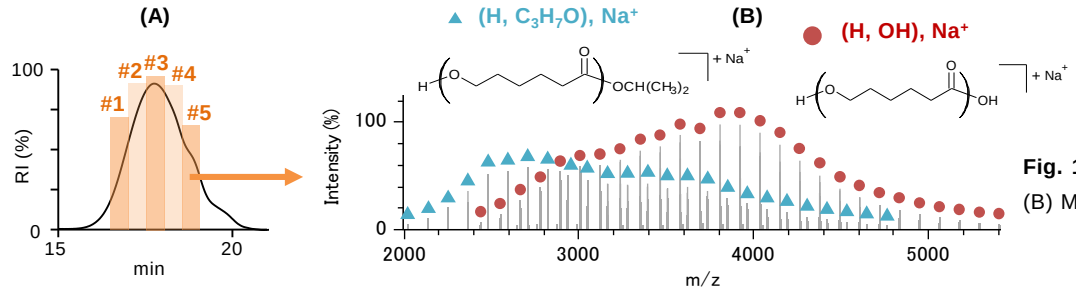

Fig. 1. (A) SEC chromatogram. (B) Mass spectrum of fraction 5.

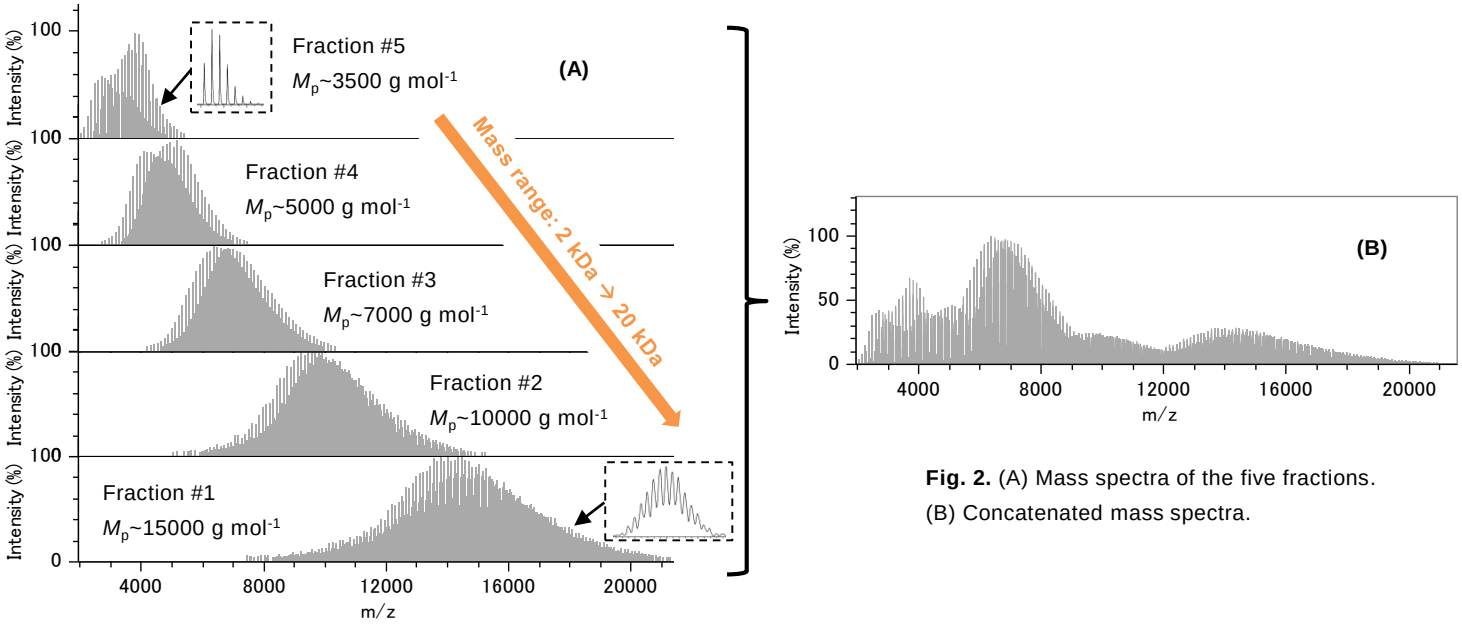

Fig. 2. (A) Mass spectra of the five fractions. (B) Concatenated mass spectra.

Kendrick mass defect (KMD) plots

The regular KMD plot from the concatenated mass spectra barely separates the sodiated (H, OH)- and (H, C_3H_7O)-ended oligomers in the lowest mass range but the plot becomes unresolved while increasing the chain length (Fig. 3). In spite of the isotopic resolution reached by the SpiralTOF™ analyzer, the mass accuracy is not high enough for a regular KMD analysis. The resolution-enhanced KMD plot using a fractional base unit CL/113 (Fig. 4) successfully separates the four main distributions (sodiated and potassiated (H, OH)- and (H, C_3H_7O)-ended oligomers) over the whole mass range. The separating power is nevertheless decreasing while the molecular weight is increasing and the plot becomes fuzzy with a low quality of point alignment.

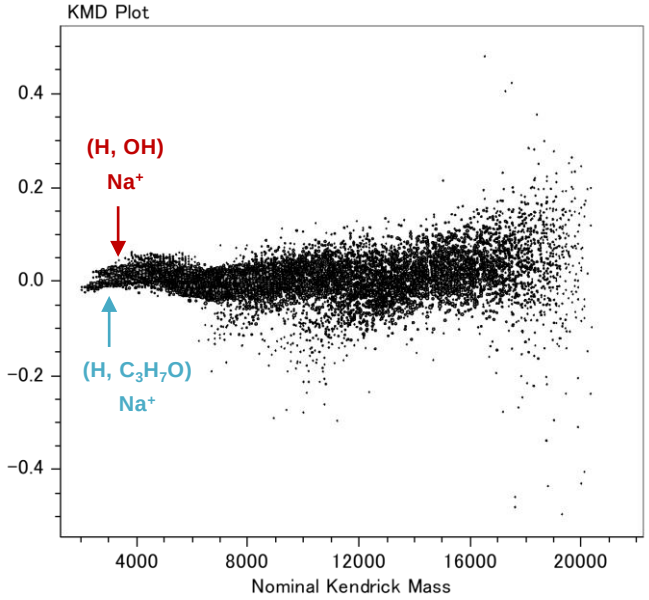

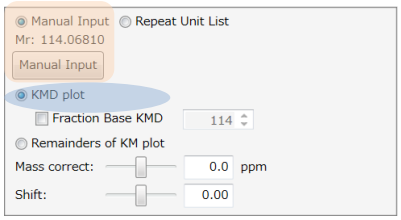

Fig. 3. Regular KMD plot [1] from the concatenated mass spectra of the five fractions (base unit: CL, $C_6H_{10}O_2$, 114.0681).

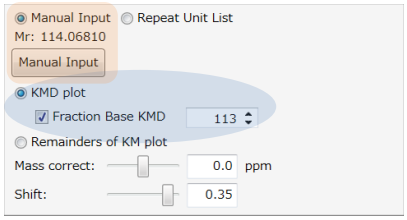

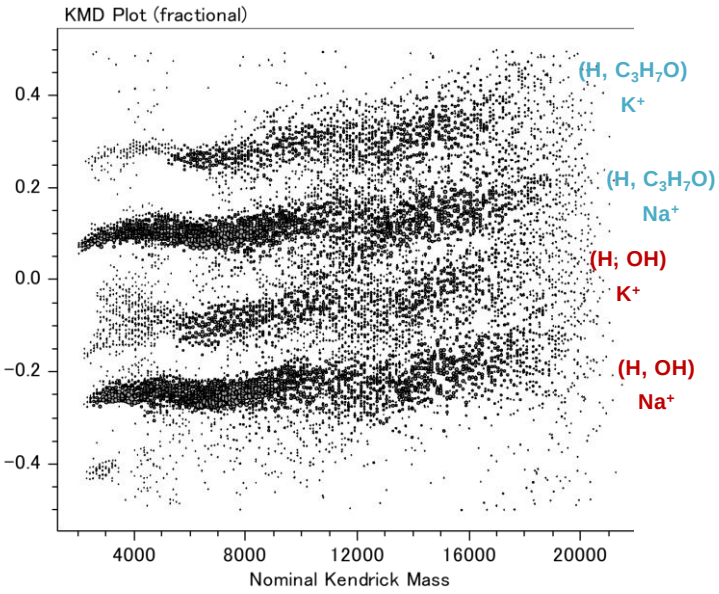

Fig. 4. Resolution-enhanced KMD plot [2] from the concatenated mass spectra of the five fractions using the “fraction base KMD” option (base unit: CL/113).

Remainders of KM (RKM) plot

The RKM plot of the concatenated mass spectra reveals a great compositional homogeneity of PCL throughout a broad 20 kDa mass range with (H, OH)- and (H, C_3H_7O)-ended chains (sodium and potassium adduction, Fig. 5A). An additional cyclic ion series is observed in the lowest mass range (fraction #5, blue square) typical of ring-opening and polycondensation synthesis routes. The detection of (H, ONa)-ended oligomers seen in the fraction #5 (violet square) further validates the presence of a COOH acidic end-group and confirms the (H, OH) assignment. As compared to the unresolved or fuzzy KMD plots, points are perfectly aligned in the RKM plot throughout the whole mass range in spite of using different external calibrants (one per fraction). The isotopic shift ($^{12}C \rightarrow {}^{13}C$) is clearly seen while increasing the chain length (from ^{12}C to $^{13}C_{16}$ for the largest chains, Fig. 5B). The high separating power of the RKM plot allows a rapid filtering of a given ion series (full series or fixed isotopic composition) over the whole mass range using the “Grouping Mode” of msRepeatFinder (Fig. 6, red bars assigned to (H, OH)-ended PCL from 2 kDa to 20 kDa).

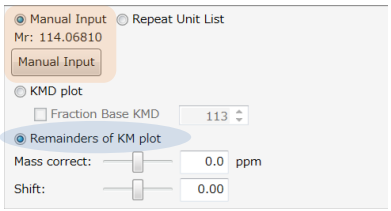

Fig. 5. RKM plots from the concatenated mass spectra. (A) Full plot with assignments of end-groups. (B) Detail of the sodiated (H, OH) ion series.

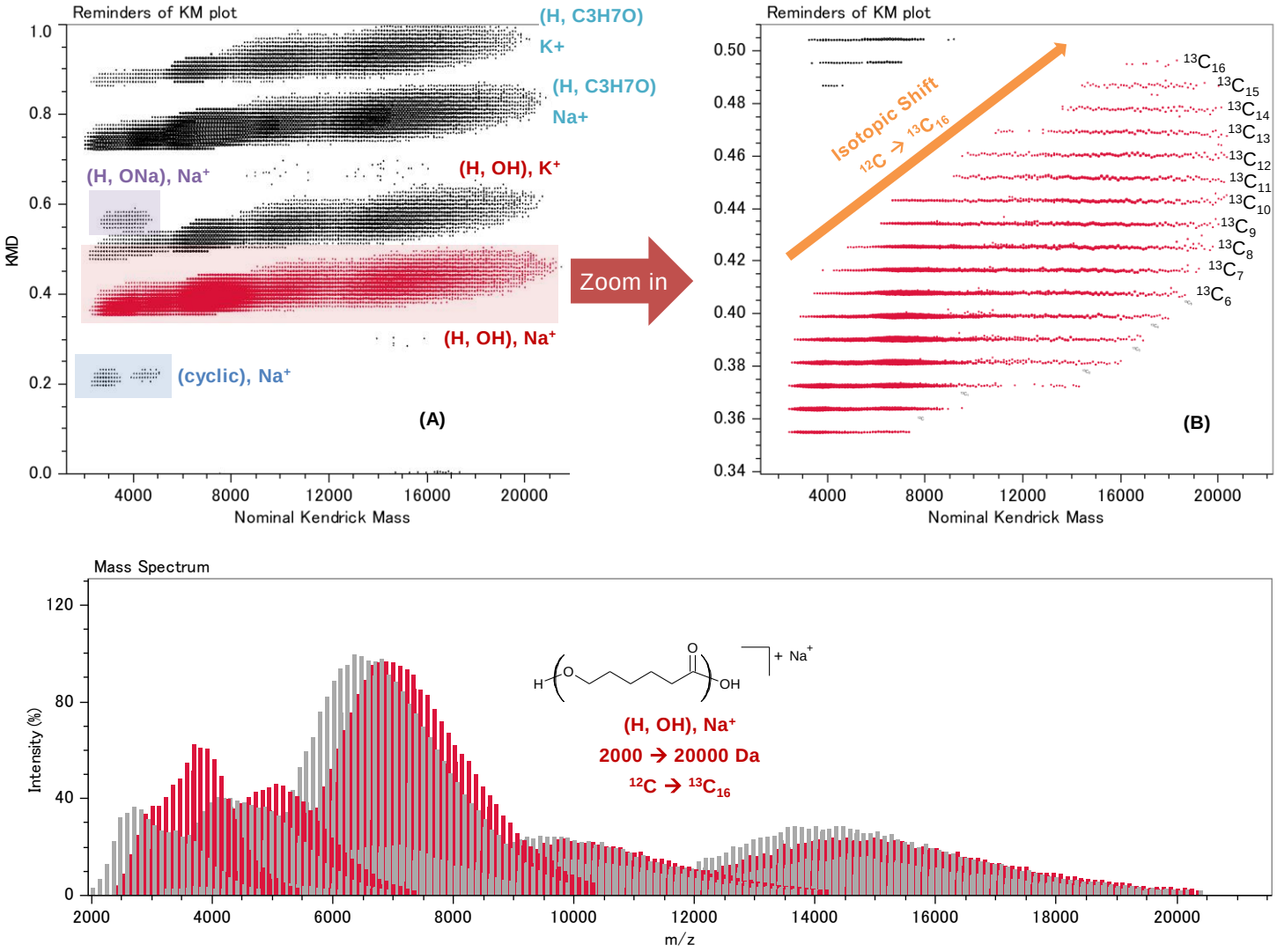

Fig. 6. Instant selection of the whole sodiated (H, OH)-PCL series throughout the 20kDa mass range (five fractions at once) using the "grouping mode" of msRepeatFinder.

Prospects

The RKM plots are compatible with high-accuracy and low-accuracy mass spectral data from the SpiralTOF™ analyzer (isotopic resolution) and the linear TOF analyzer (oligomeric resolution) of the JMS-S3000 mass spectrometer [3]. It is also compatible with multiple charging potentially observed in the MALDI-MS analysis of high molecular weight polymers [4].

Acknowledgment

This application note is written based on the results of a joint research project with Dr. Hiroaki Sato and Dr. Thierry Fouquet in Research Institute for Sustainable Chemistry, National Institute of Advanced Industrial Science and Technology (AIST).

References

[1] H. Sato, S. Nakamura, K. Teramoto, T. Sato. *J. Am. Soc. Mass Spectrom.* **2014**, *25*, 1346–1355.
[2] T. Fouquet, H. Sato. *Anal. Chem.* **2017**, *89*, 2682−2686.
[3] T. Fouquet, T. Satoh, H. Sato. *Anal. Chem.* **2018**, *90*, 2404–2408.
[4] T. Fouquet, R. B. Cody, Y. Ozeki, S. Kitagawa, H. Ohtani, H. Sato. *J. Am. Soc. Mass Spectrom.* **2018**, 29, 1611-1626.

JEOL Ltd.
3-1-2 Musashino Akishima Tokyo 196-8558 Japan Sales Division Tel. +81-3-6262-3560 Fax. +81-3-6262-3577
www.jeol.com ISO 9001 • ISO 14001 Certified

• **AUSTRALIA & NEW ZEALAND** /JEOL(AUSTRALASIA) Pty.Ltd. Suite 1, L2 18 Aquatic Drive - Frenchs Forest NSW 2086 Australia • **BELGIUM** /JEOL (EUROPE) B.V. Planet II, Gebouw B Leuvensesteenweg 542, B-1930 Zaventem Belgium • **BRAZIL** /JEOL Brasil Instrumentos Cientificos Ltda. Av. Jabaquara, 2958 5° andar conjunto 52 ; 04046-500 Sao Paulo, SP Brazil • **CANADA** /JEOL CANADA, INC. 3275 1ere Rue, Local #8 St-Hubert, QC J3Y-8Y6, Canada • **CHINA** /JEOL(BEIJING) CO., LTD. Zhongkeziyuan Building South Tower 2F, Zhongguancun Nansanjie Street No. 6, Haidian District, Beijing, P.R.China • **EGYPT** /JEOL SERVICE BUREAU 3rd Fl. Nile Center Bldg., Nawal Street, Dokki, (Cairo), Egypt • **FRANCE** /JEOL (EUROPE) SAS Espace Claude Monet, 1 Allee de Giverny 78290, Croissy-sur-Seine, France • **GERMANY** /JEOL (GERMANY) GmbH Gute Aenger 30 85356 Freising, Germany • **GREAT BRITAIN & IRELAND** /JEOL (U.K.) LTD. JEOL House, Silver Court, Watchmead, Welwyn Garden City, Herts AL7 1LT, U.K. • **ITALY** /JEOL (ITALIA) S.p.A. Palazzo Pacinotti - Milano 3 City, Via Ludovico il Moro, 6/A 20080 Basiglio(MI) Italy • **KOREA** /JEOL KOREA LTD. Dongwoo Bldg. 7F, 1443, Yangjae Daero, Gangdong-Gu, Seoul, 05355, Korea • **MALAYSIA** /JEOL(MALAYSIA) SDN.BHD. 508, Block A, Level 5, Kelana Business Center, 97, Jalan SS 7/2, Kelana Jaya, 47301 Petaling Jaya, Selangor, Malaysia • **MEXICO** /JEOL DE MEXICO S.A. DE C.V. Arkansas 11 Piso 2 Colonia Napoles Delegacion Benito Juarez, C.P. 03810 Mexico D.F., Mexico • **RUSSIA** /JEOL (RUS) LLC. Krasnoproletarskaya Street, 16, Bld. 2, 127473, Moscow, Russian Federation • **SCANDINAVIA** /SWEDEN JEOL (Nordic) AB Hammarbacken 6A, Box 716, 191 27 Sollentuna Sweden • **SINGAPORE** /JEOL ASIA PTE.LTD. 2 Corporation Road #01-12 Corporation Place Singapore 618494 • **TAIWAN** /JIE DONG CO., LTD. 7F, 112, Chung Hsiao East Road, Section 1, Taipei, Taiwan 10023 (R.O.C.) • **THE NETHERLANDS** /JEOL (EUROPE) B.V. Lireweg 4, NL-2153 PH Nieuw-Vennep, The Netherlands • **USA** /JEOL USA, INC. 11 Dearborn Road, Peabody, MA 01960, U.S.A.

Applications note

MS
MSTips No. 235
MALDI Application

Analysis of low molecular weight polyethylene with solvent-free method using JMS-S3000 "SpiralTOF™"

Product used : Mass spectrometer (MS)

Matrix assisted laser desorption ionization (MALDI) time-flight mass spectrometer (TOMFS) is a powerful tool to identify the repeat units and end groups of polymers. The mass spectra of polymers can be easily interpreted because MALDI can generate singly-charged ions over a wide mass range. MALDI is a soft ionization method that uses "matrix" compounds and "cationization agents" to assist the ionization process of polymers. Typically, sample, matrix and cationization agent are dissolved in the same solvent. These solutions are pre-mixed and placed drop-wise on the target plate to make cocrystals (dried droplet method). However, this procedure cannot be applied to polymers that are insoluble or only slightly soluble. To solve this problem, solvent-free methods have been developed [1-4] for these situations. In this report, we analyzed low molecular weight polyethylene by using a solvent-free method and then using a high mass-resolution MALDI-TOFMS "SpiralTOF™" system for the analysis.

Experiments

Sample : Polyethylene analytical standard, for GPC, 1,000
(Sigma aldrich PN 81219) (PE1000)

Matrix: trans-2-[3-(4-tert-Butylphenyl)-2-methyl-2-propenylidene]malononitrile (DCTB)

Cationization Agent: Silver Trifluoroacetate (AgTFA)

Preparation: PE1000, DCTB、and AgTFA powders were mixed in Agate mortar. The mixed powder was then pressed onto the target plate using a spatula (Note 1). (See Figure 1)

Measurement: The mass spectra were acquired by using SpiralTOF™ positive ion mode.

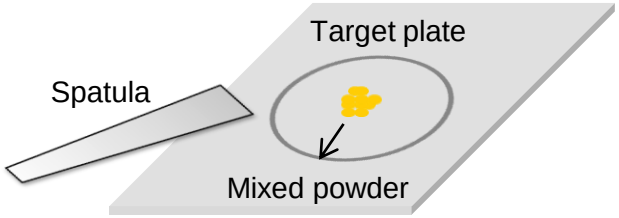

Figure 1 Solvent-free sample preparation.

Results

The PE1000 mass spectrum is shown in Figure 2. The polymer distribution of $[H(C_2H_4)_nH+Ag]^+$ was observed from 600 – 1,800 where the apex is at *m/z* 1000(Figure 2a). The enlarged mass spectrum at *m/z* 890 - 960, where $[H(C_2H_4)_nH+Ag]^+$ (n = 28 - 30) were observed, is shown in Figure 2b. The peaks had a mass resolution of more than 50,000, and the mass difference 28.031 u±0.001 u corresponded with mass of polyethylene repeat unit C_2H_4. In the solvent-free method used in this report, the mixed powder of sample, matrix, and cationization agent were pressed onto the target plate. The sample surface roughness is much larger than for the dried droplet method. Even so, the SpiralTOF™ was able to achieve high mass-resolution and mass accuracy using the system's 17m flight path in order to overcome the adverse effects of sample roughness.

References

[1] R. Sketlton, F. Doubois, K. Zenobi, *Anal. Chem*. 72 (7) (2000) 1707–1710
[2] L. Przybilla, J. D. Brand, K. Yoshimura, H.J. Räder, K. Müllen, *Anal. Chem*. 72 (2000) 4591–4597
[3] A. Marie, F. Fournier, J.C. Tabet, *Anal. Chem*. 72 (2000)5106–5114
[4] S. Trimpin, A. Rouhanipour, R. Az, H.J. Räder, K. Müllen, *Rapid Commun. Mass Spectrom.*15 (2001) 1364–1373

(Note 1) Please press the powder firmly onto the plate in order to prevent ion source contamination from the scattering of powders.

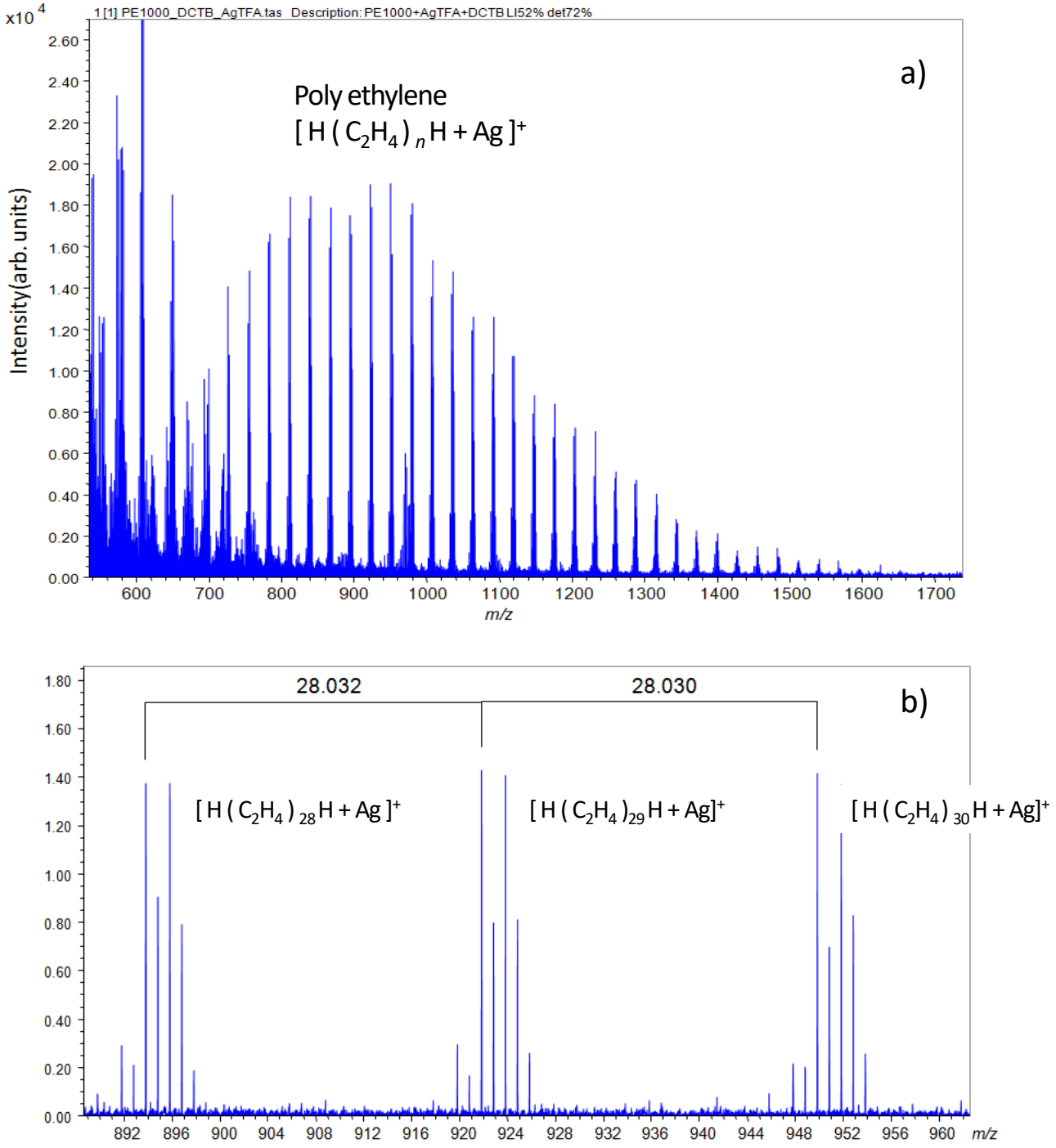

Figure 2 a) Mass spectrum of PE1000. b) Distribution of $[H (C_2H_4)_n H + Ag]^+$ was observed around *m/z* 1000.

JEOL Ltd.
3-1-2 Musashino Akishima Tokyo 196-8558 Japan Sales Division Tel. +81-3-6262-3560 Fax. +81-3-6262-3577
www.jeol.com ISO 9001 • ISO 14001 Certified
• AUSTRALIA & NEW ZEALAND • BELGIUM • BRAZIL • CANADA • CHINA • EGYPT • FRANCE • GERMANY • GREAT BRITAIN & IRELAND • ITALY • KOREA • MALAYSIA • MEXICO • RUSSIA • SCANDINAVIA • SINGAPORE • TAIWAN • THE NETHERLANDS • USA
▼ Local offces

Application note

MS
MSTips No.220

Analysis of cyanoacrylate adhesive using the JMS-S3000 "SpiralTOF™" — Application of Kendrick Mass Defect plot analysis —

Product used : Mass spectrometry (MS)

Introduction

SpiralTOF™ has been used previously for the detailed characterization of polymers and lipids. Due to the high mass- resolution of SpiralTOF™, slight mass difference between CH_4 and O (Δ 0.036 Da) can be easily discriminated. However, the analysis of complicated compounds by high mass-resolution MS requires an effective data processing method. Recently, Kendrick mass defect (KMD) plot analysis has been proposed as an effective data processing technique for SpiralTOF™ which allows for the structural characterization of complicated compounds[1, 2]. Here, a commercial acrylic adhesive containing cyanoacrylate was characterized using a SpiralTOF™ combined with KMD plot analysis.

Experiment

A solution of the acrylic adhesive was prepared by dissolving 10 mg of the sample in 1 ml of acetone. The matrix (2,5-dihydroxybenzoic acid, DHB) at concentration of 10 mg/ml in tetrahydrofuran (THF) was used as a matrix solution. Sodium iodide was used as the cationization reagent. MALDI mass spectra were measured by SpiralTOF™ (R=75000). The KMD plots were constructed using the msRepeatFinder software (JEOL).

Results and discussion

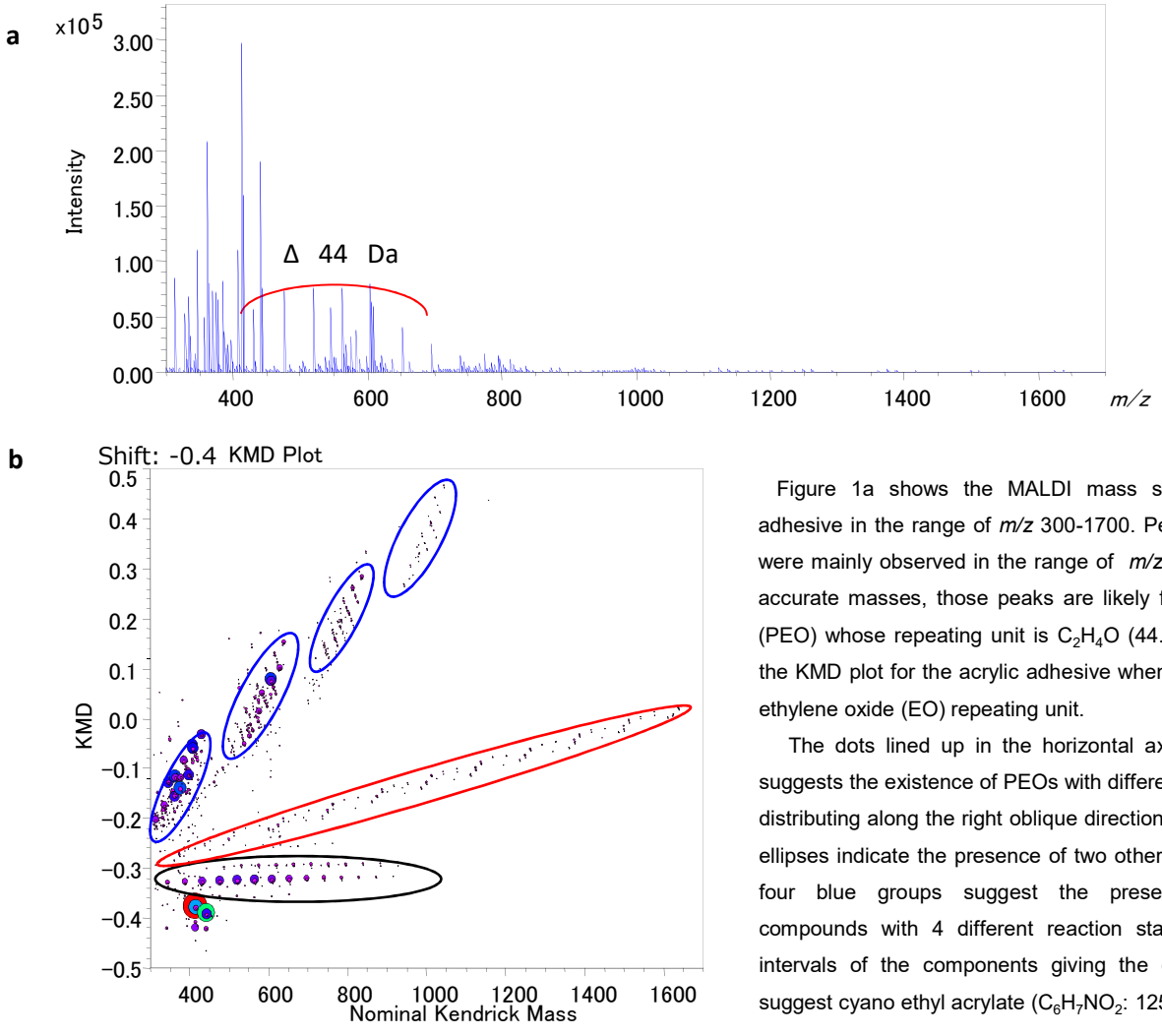

Figure 1. MALDI mass spectrum of an acrylate adhesive (a) and KMD plot of the adhesive using a mass scale based on EO unit (b).

Figure 1a shows the MALDI mass spectrum of the acrylic adhesive in the range of *m/z* 300-1700. Peak intervals with 44 Da were mainly observed in the range of *m/z* 400-700. Based on the accurate masses, those peaks are likely from polyethylene oxide (PEO) whose repeating unit is C_2H_4O (44.026). Figure 1b shows the KMD plot for the acrylic adhesive when the base unit is set for ethylene oxide (EO) repeating unit.

The dots lined up in the horizontal axis inside a black circle suggests the existence of PEOs with different end groups. The dots distributing along the right oblique directions marked by red or blue ellipses indicate the presence of two other types of polymers. The four blue groups suggest the presence of multibranched compounds with 4 different reaction starting points. The peak intervals of the components giving the dots in the red ellipse suggest cyano ethyl acrylate ($C_6H_7NO_2$: 125.047).

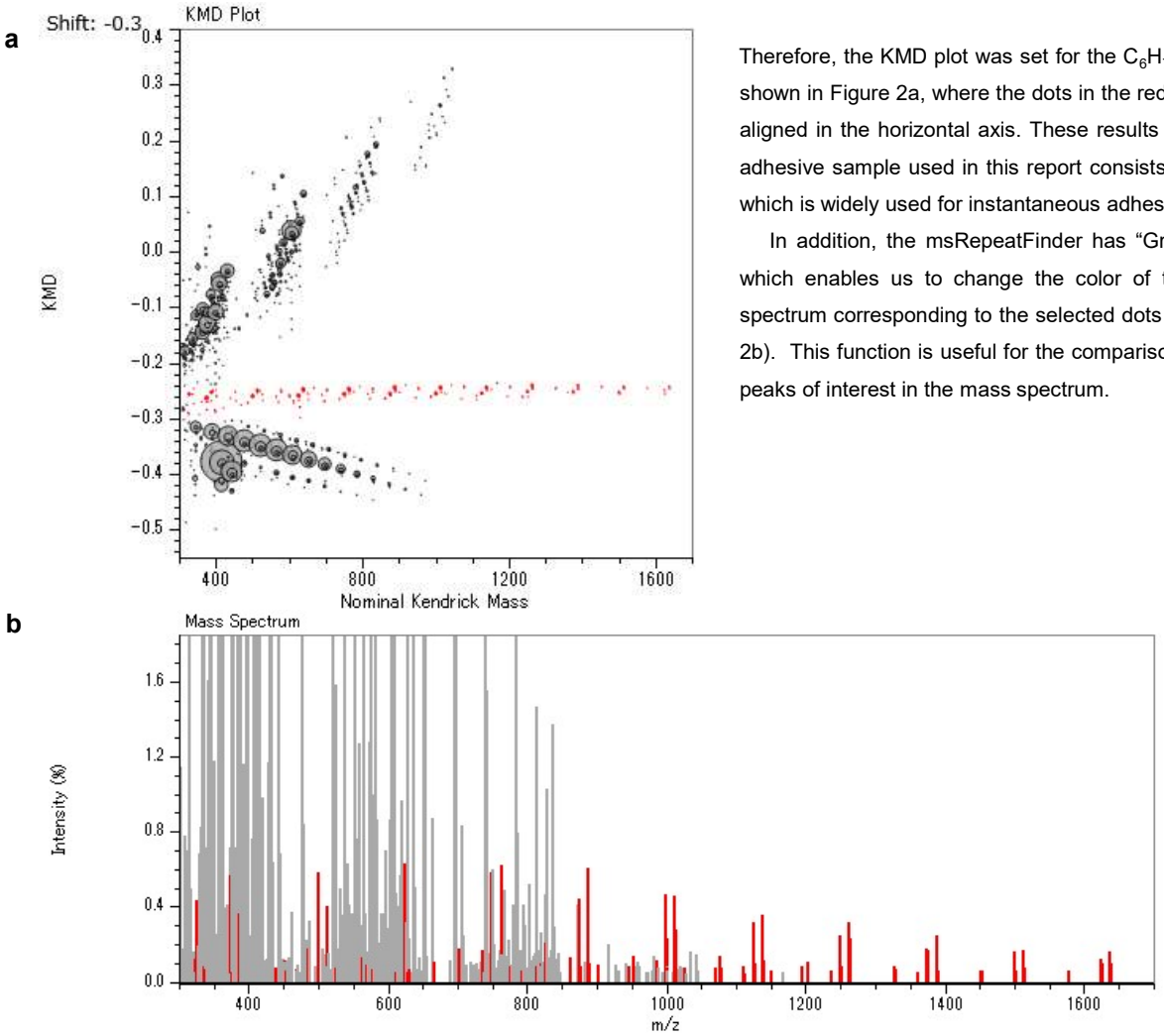

Figure 2. KMD plot of the adhesive using a mass scale based on $C_6H_7NO_2$ unit (a) and MALDI mass spectrum of an acrylate adhesive (b). Peaks and dots corresponding to cyanoacrylic acid ethyl ester are indicated in red color.

Therefore, the KMD plot was set for the $C_6H_7NO_2$ repeating unit as shown in Figure 2a, where the dots in the red ellipse in Figure 1b are aligned in the horizontal axis. These results suggest that the acrylic adhesive sample used in this report consists of cyano ethyl acrylate which is widely used for instantaneous adhesives.

In addition, the msRepeatFinder has “Grouping Mode” function, which enables us to change the color of the peaks in the mass spectrum corresponding to the selected dots in the KMD plot (Figure 2b). This function is useful for the comparison of KMD plots and the peaks of interest in the mass spectrum.

Conclusion

Here, acrylic adhesive was characterized using a combination of high-resolution SpiralTOF™ measurements and KMD plot analysis. The KMD plot allows us to visualize the distribution of weak peaks corresponding to polymers which are hidden within a complicated mass spectrum. Since the KMD plot analysis does not require peak assignment and is able to be constructed by selecting a monomer unit or entering the calculated- or observed-mass of the monomer unit, this technique enables the quick and easy visualization of the homologue distribution for different chemical structures. The combination of the SpiralTOF™ instrument and “msRepeatFinder” KMD plot analysis software is an effective tool for the characterization of industrial products containing a variety of materials.

References

1) Sato,H. *et al*., Structural characterization of polymers by MALDI spiral-TOFMS combined with Kendrick mass defect analysis, *J. Am. Soc. Mass Spectrom.*, **25**, 1346 (2014).
(Open access: http://link.springer.com/article/10.1007%2Fs13361-014-0915-y)

2) Zheng, Q. *et al.,* Molecular composition of extracts obtained by hydrothermal extraction of brown coal, *Fuel*, **159**, 751 (2015).

Acknowledgement

We would like to acknowledge Dr. H. Sato of Environmental Management Research Institute, National Institute of Advanced Industrial Science and Technology（AIST）, for his comments and suggestions.

JEOL Ltd.
1-2 Musashino 3-chome Akishima Tokyo 196-8558 Japan Sales Division Tel. +81-3-6262-3560 Fax. +81-3-6262-3577
www.jeol.com ISO 9001 • ISO 14001 Certified

• **AUSTRALIA & NEW ZEALAND** /JEOL(AUSTRALASIA) Pty.Ltd. Suite 1, L2 18 Aquatic Drive - Frenchs Forest NSW 2086 Australia • **BELGIUM** /JEOL (EUROPE) B.V. Planet II, Gebouw B Leuvensesteenweg 542, B-1930 Zaventem Belgium • **BRAZIL** /JEOL Brazil Instrumentos Cientificos Ltda. Av. Jabaquara, 2958 5° andar conjunto 52 ; 04046-500 Sao Paulo, SP Brazil • **CANADA** /JEOL CANADA, INC. 3275 1ere Rue, Local #8 St-Hubert, QC J3Y-8Y6, Canada • **CHINA** /JEOL(BEIJING) CO., LTD. Zhongkeziyuan Building South Tower 2F, Zhongguancun Nansanjie Street No. 6, Haidian District, Beijing, P.R.China • **EGYPT** /JEOL SERVICE BUREAU 3rd Fl. Nile Center Bldg., Nawal Street, Dokki, (Cairo), Egypt • **FRANCE** /JEOL (EUROPE) SAS Espace Claude Monet, 1 Allee de Giverny 78290, Croissy-sur-Seine, France • **GERMANY** /JEOL (GERMANY) GmbH Gute Aenger 30 85356 Freising, Germany • **GREAT BRITAIN & IRELAND** /JEOL (U.K.) LTD. JEOL House, Silver Court, Watchmead, Welwyn Garden City, Herts AL7 1LT, U.K. • **ITALY** /JEOL (ITALIA) S.p.A. Palazzo Pacinotti - Milano 3 City, Via Ludovico il Moro, 6/A 20080 Basiglio(MI) Italy • **KOREA** /JEOL KOREA LTD. Dongwoo Bldg. 7F, 1443, Yangjae Daero, Gangdong-Gu, Seoul, 134-814, Korea • **MALAYSIA** /JEOL(MALAYSIA) SDN.BHD. 508, Block A, Level 5, Kelana Business Center, 97, Jalan SS 7/2, Kelana Jaya, 47301 Petaling Jaya, Selangor, Malaysia • **MEXICO** /JEOL DE MEXICO S.A. DE C.V. Arkansas 11 Piso 2 Colonia Napoles Delegacion Benito Juarez, C.P. 03810 Mexico D.F., Mexico • **RUSSIA** /JEOL (RUS) LLC. Krasnoproletarskaya Street, 16, Bld. 2, 127473, Moscow, Russian Federation • **SCANDINAVIA** /SWEDEN JEOL (Skandinaviska)AB Hammarbacken 6A, Box 716, 191 27 Sollentuna Sweden • **SINGAPORE** /JEOL ASIA PTE.LTD. 2 Corporation Road #01-12 Corporation Place Singapore 618494 • **TAIWAN** /JIE DONG CO., LTD. 7F, 112, Chung Hsiao East Road, Section 1, Taipei, Taiwan 10023 Republic of China • **THE NETHERLANDS** /JEOL (EUROPE) B.V. Lireweg 4, NL-2153 PH Nieuw-Vennep, The Netherlands • **USA** /JEOL USA, INC. 11 Dearborn Road, Peabody, MA 01960, U.S.A.

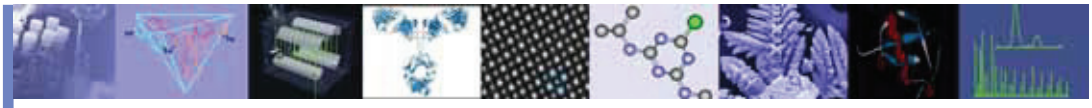

Applications Note

SpiralTOF™

Measurement of a Dendritic MS Reference Standard

Introduction:

A high-quality mass calibration is required to achieve highly accurate mass measurements by mass spectrometry. A polymer or a mixture of peptides is commonly used to calibrate a MALDI-TOF MS system. However, peptides do not necessarily have long-term stability, and a monodisperse polymer does not have a wide *m/z* range. Sometimes these standards are not well suited for calibration over a wide *m/z* range.

We used a new dendritic MS calibrant (SpheriCal®) to resolve these issues. Here we demonstrate measurement and calibration using the new calibrant with the JEOL SpiralTOF MALDI mass spectrometer.

Experimental:

The new SpheriCal® High Range dendritic MS reference standard was obtained from the Polymer Factory (http://www.polymerfactory.com/). The sample was dissolved in tetrahydrofuran at a concentration of 10 mg/mL. A 0.5 µL sample was deposited and dried on the MALDI target plate. An additional matrix was not required because it is already included in the SpheriCal® reference standard mixture.

Results:

The MALDI mass spectrum is shown in Figure 1, and the comparison of measured and theoretical isotopic distribution for *m/z* 6000 are shown in Figure 2. The delay time was set to achieve the highest mass resolving power at *m/z* 6000. Therefore, the resolving power was approximately 85,000 for the $[C_{320}H_{372}O_{110}Na]^+$ peak, well in excess of that needed to separate isotope peaks.

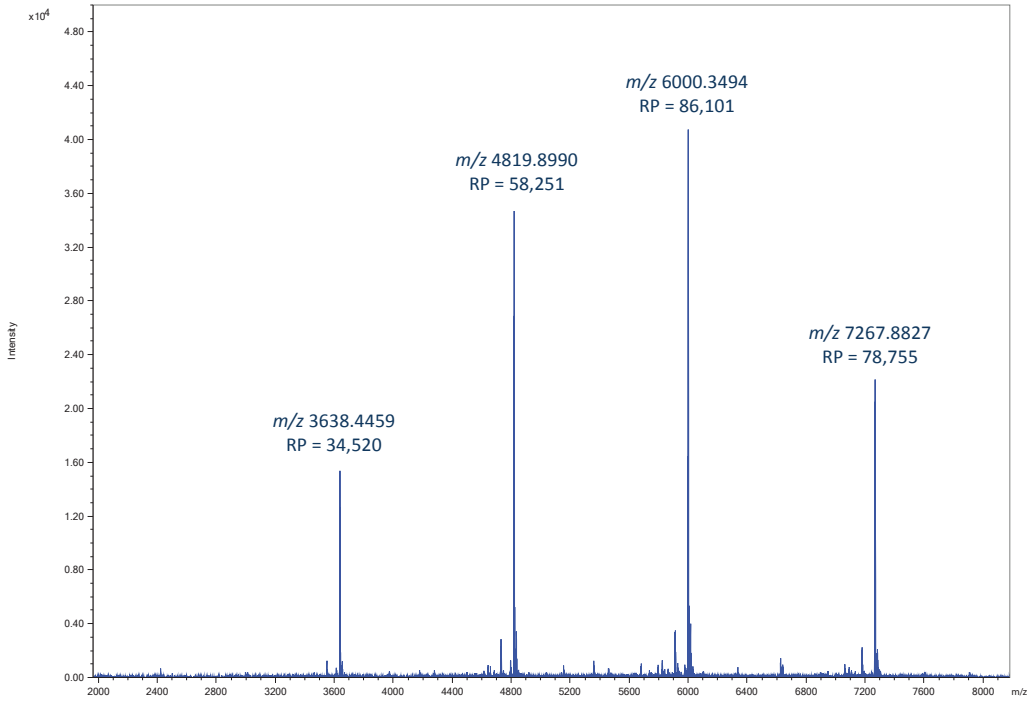

Figure 1. MALDI mass spectrum of SpheriCal® High Range standard.

MS-111227A

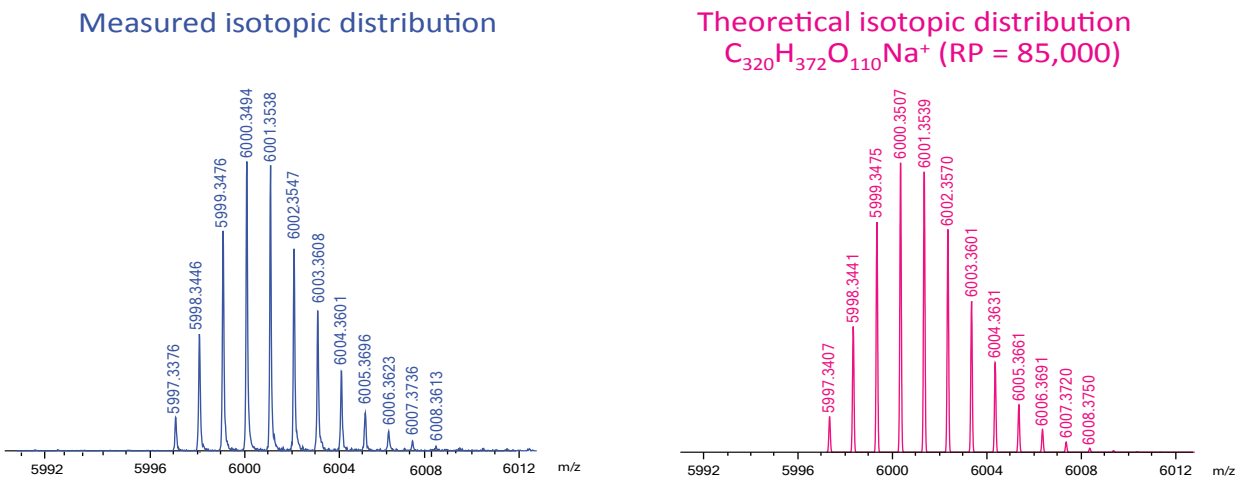

Figure 2. The comparison of measured and theoretical isotopic distribution.

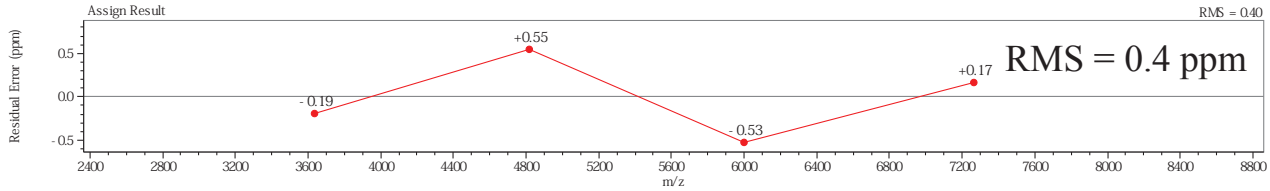

Figure 3. The residual plot for the calibration curve obtained by using the SpheriCal® High Range standard.

A residual plot for the calibration curve is shown in Figure 3. We were able to calibrate the system by using the monoisotopic ions for each dendrimer because the SpiralTOF is able to detect these species with enough intensity to achieve a high-quality mass calibration (see Figure 2). The Root Mean Square (RMS) mass error of actual measured *m/z* value against the calibration curve was just 0.4 ppm with this calibrant.

Conclusion:

In this study we demonstrated measurement and calibration using a new dendritic mass reference standard with the JEOL SpiralTOF MALDI mass spectrometer.

The SpiralTOF provides:

- Ultra high resolving power sufficient to separate isotopic ions and signal-to-noise ratios sufficient to detect monoisotopic ions in the high *m/z* region.
- Routine high mass accuracy (less than 1ppm)

A high-quality mass calibration curve over a wide *m/z* range was achieved by using the new dendritic calibrant and the JEOL SpiralTOF.

Reference:

1. Yeija Li, Jessica N. Hoskins, Subramanya G. Sreerama, Michael A. Grayson and Scott M. Grayson. *The identification of synthetic homopolymer end groups and verification of their transformations using MALDI-TOF mass spectroscopy.* J. Mass Spectroscopy, 2010, 45, 587-611.

2. http://www.polymerfactory.com/images/articles/Grayson-Universal_MS_calibrants_ASMS%202011.pdf

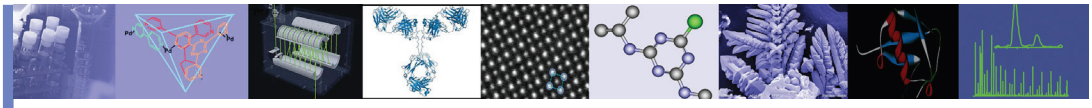

Applications Note

SpiralTOF™

Analysis of EO-PO Random Copolymer by Using a Conventional HPLC and MALDI SpiralTOF MS

Introduction

Ethylene oxide (EO) – propylene oxide (PO) copolymers have been used as components of various functional materials. Detailed analyses of them, however, still remain challenging. As it turns out, it is difficult to detect all of the components by using mass spectrometry alone without chromatographic separation due to ion suppression effects. In this work we analyzed an EO-PO random copolymer by using an LC – MALDI-SpiralTOF MS system, with the expectation of detecting more components as a result of reduced ion suppression effects.

Experimental

A commercially available EO-PO random copolymer (Mn ~ 2,500) as shown in Fig. 1 was dissolved in water and used for the analyses. The mass spectrum shown in Fig. 2 was obtained by analyzing the sample solution with MALDI – SpiralTOF MS without HPLC separation.

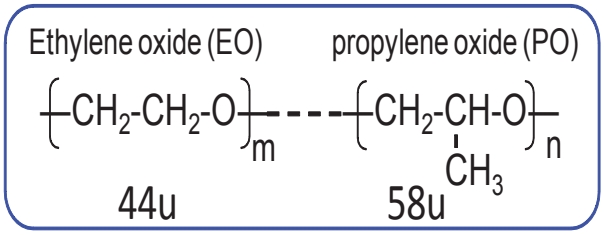

Figure 1. EO-PO copolymer

Analytical conditions:

- HPLC system: Agilent 1200SL
- Mobile phase: A: water, B: Methanol
- Flow rate: 0.2 mL/min
- Injection volume (to the HPLC): 20 µL
- HPLC column: Imtakt Cadenza CD-C18 (150 x 2.0 mm)
- Fractionation: every 15 seconds (50 µL/fraction)
- Mass spectrometer: JMS-S3000 SpiralTOF (automated analysis with Spiral, Positive Ion mode)
- Amount of sample used for MS analysis: 1 µL from each fraction (no further concentration performed)
- Matrix / cationization agent: CHCA/NaI (in methanol)
- Target plate: HST µFocus 900 µm

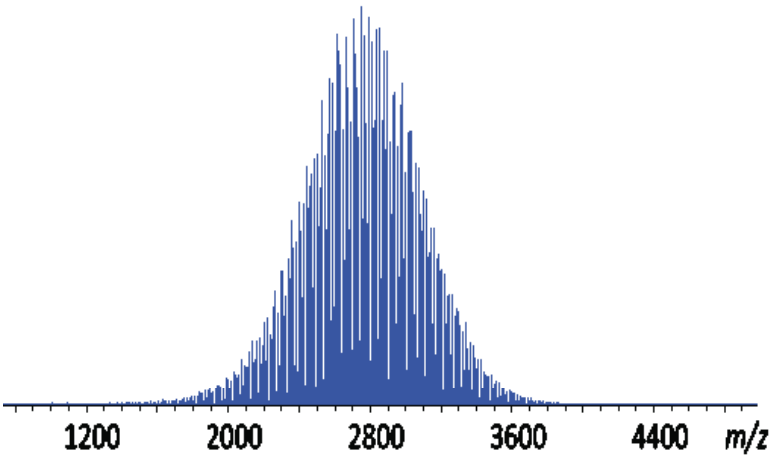

Fig.2 MALDI mass spectrum of EO-PO copolymer

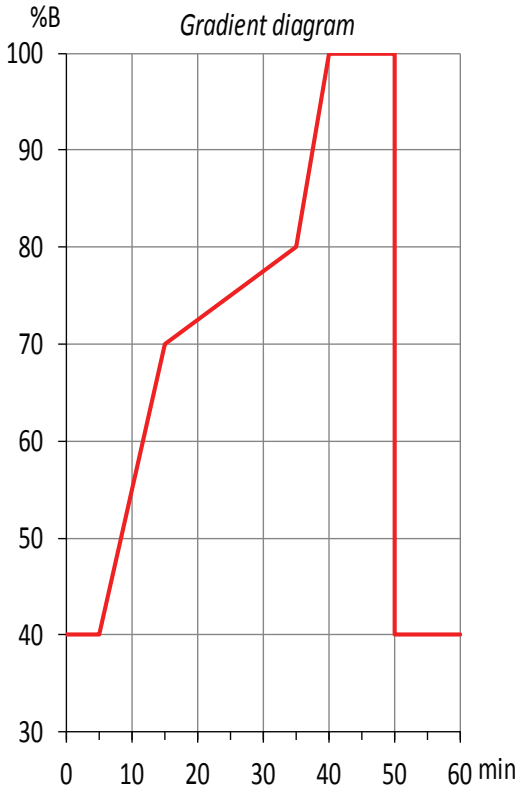

Fig.3 Solvent gradient condition

MS-030113A

Results and Discussion

Mass spectra acquired through automated measurements are shown in the "Survey View" of the msTornado Analysis software (Fig. 4). By assigning the signals in the data, it was found that the components were separated by HPLC according to the number of PO units in the components; the more PO units, (which are hydrophobic), present in a component, the later the observed retention time. Components with different numbers of PO units were separated by retention time; whereas components with different numbers of EO units were detected as peaks that are separated by m/z 44 in each mass spectrum.

At retention times before 22 min, hydrophilic components with more EO units and less PO units were detected below m/z 1,600. These hydrophilic components were not observed on Fig. 2 and were detected only after HPLC separation. Since detection of these components had not been expected, the gradient profile (Fig. 3) was not optimum for separating them according to the number of PO units present in them.

A comparison between with and without HPLC separation is shown on Fig. 5. Based on the peak pattern in the mass spectrum before separation (top), it is easy to surmise that the most abundant component EO47-PO11 (red) and another component EO39-PO17, which is 2 Da lower, are overlapping. However, peaks derived from a minor component EO39-PO17 (green) are barely discernible from the baseline noise. With HPLC separation, all overlapping minor components, including EO51-PO8 (purple) and EO55-PO5 (blue) are clearly observed with good S/N.

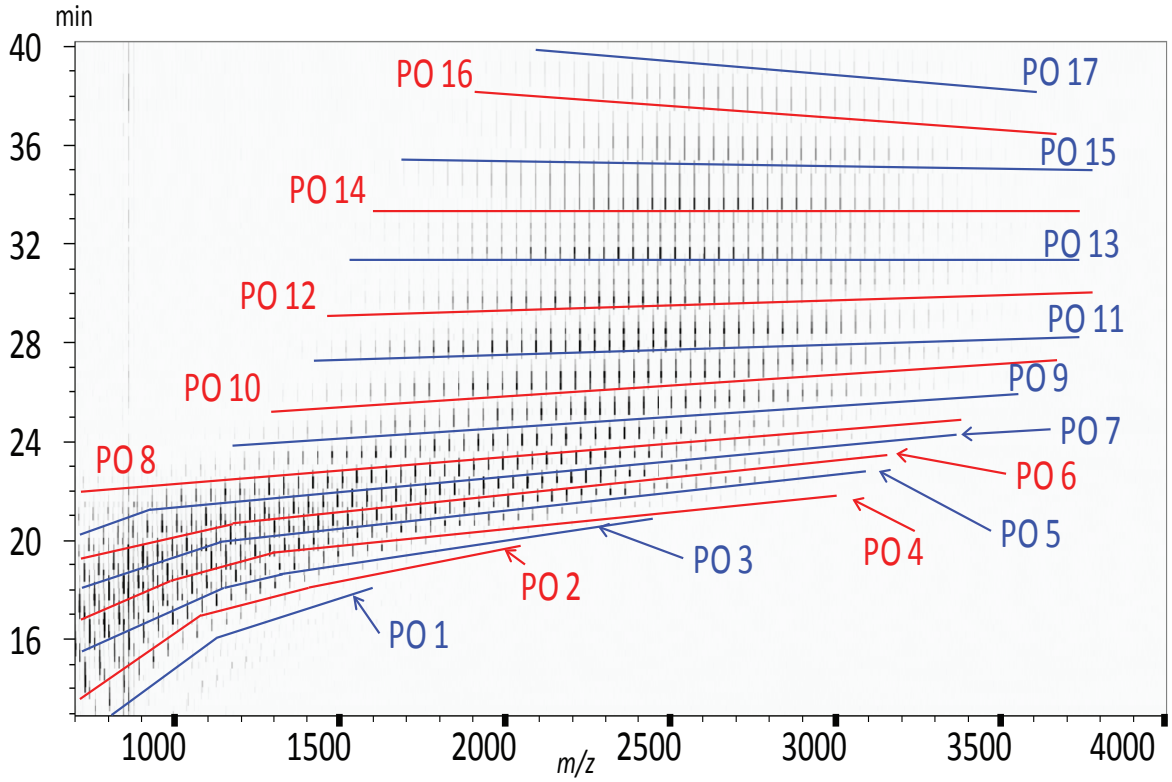

Fig 4. Signal assignments on the "Survey View" of the msTornado Analysis software.

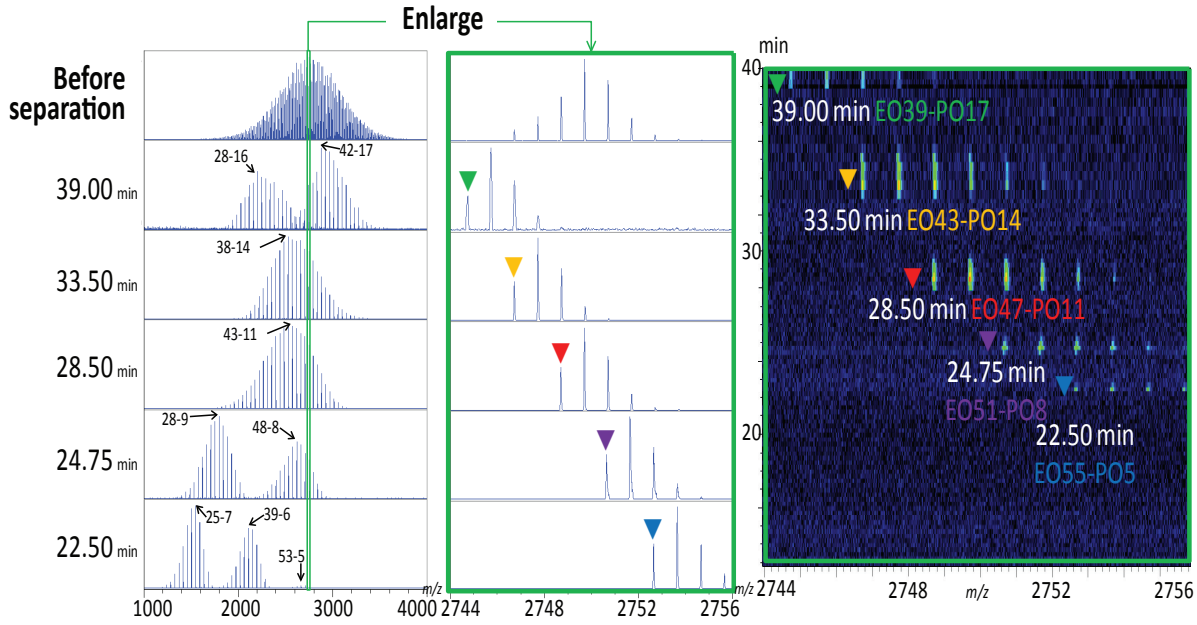

Fig.5 HPLC separation effect to reduced ion suppression (m/z 2744-2756)

Conclusion

Using a combination of conventional HPLC and MALDI-SpiralTOFMS is more effective in detecting the components of a complex EO-PO random copolymer than MALDI-TOF alone. Additionally, since MALDI predominantly produces single-charge ions, the distribution for the large number of components present in the sample was observed intuitively through the "Survey View" of the msTornado Analysis software.

Analysis of high molecular weight polystyrene standards by using JMS-S3000 "SpiralTOF™" with Linear TOF option.

Product used : Mass Spectrometry (MS)

An example of the analysis of low molecular weight Polystyrene (PS) by using JMS-S3000 SpiralTOF™ MALDI-TOFMS was already shown in MS Tips No.163. This time, high molecular weight polystyrene standards (TSKgel Standard Polystyrene F-4 (Mw = 3.72×10^4), F-10 (Mw = 9.89×10^4), and F-20 (Mw = 1.89×10^5), Tosoh Corporation) were analyzed by using JMS-S3000 SpiralTOF™ with Linear TOF option(Fig. 1). For F-4, peaks were observed at every 104 u, which is the repeating unit of PS. For both F-10 and F-20, expected distributions around their respective average molecular weights were obtained (Fig. 2). Wide applications of the Linear TOF option for the analyses of high molecular weight synthetic polymers are expected.

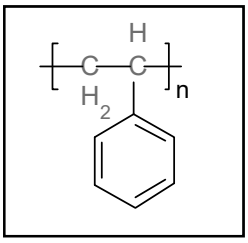

Fig.1 Repeating unit
(C_8H_8=104.0626)

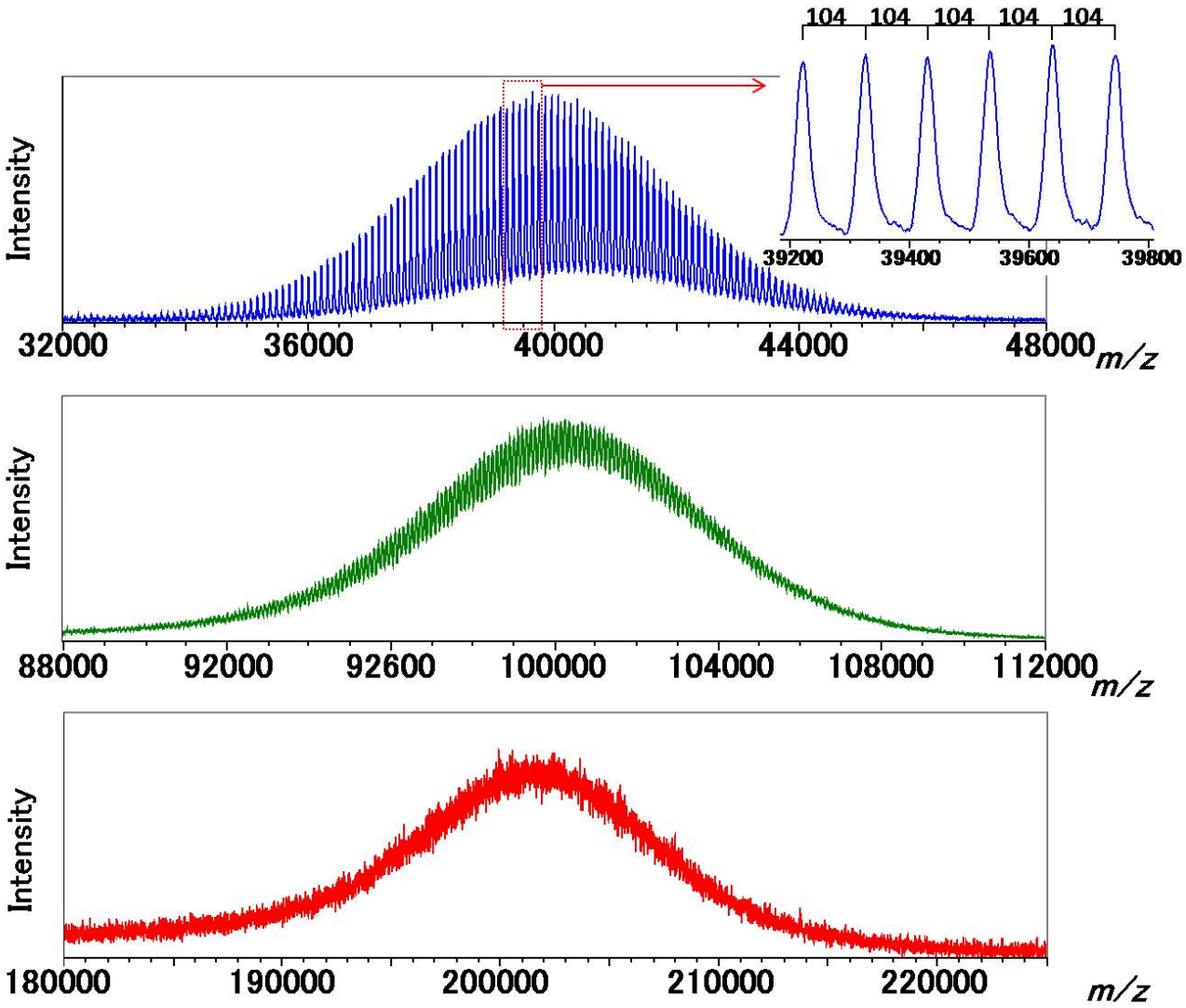

Fig.2 Mass spectra of PS using LinearTOF option.

JEOL Ltd.
3-1-2 Musashino Akishima Tokyo 196-8558 Japan Sales Division Tel. +81-3-6262-3560 Fax. +81-3-6262-3577
www.jeol.com ISO 9001 • ISO 14001 Certified
▼Local office
• AUSTRALIA & NEW ZEALAND • BELGIUM • BRAZIL • CANADA • CHINA • EGYPT • FRANCE • GERMANY • GREAT BRITAIN & IRELAND • ITALY • KOREA • MALAYSIA • MEXICO • RUSSIA • SCANDINAVIA
• SINGAPORE • TAIWAN • THE NETHERLANDS • USA

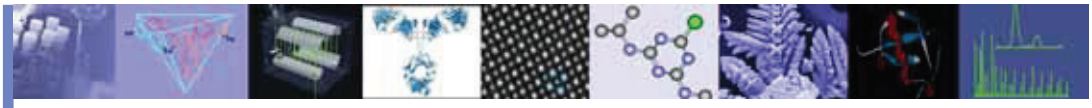

JEOL

Applications Note

SpiralTOF™

Measurement of synthetic polymers

Polystyrene

Polystyrene (PS)1000 and 2400 were measured using the JMS-S3000 SpiralTOF. The $[M+H]^+$ peaks of PS with the basic monomer units of 104u (Fig.1) were observed for each sample. The mass spectrum of PS1000 and an expanded view around *m/z* 1000 are shown in Fig. 2. The resolving power at *m/z* 1101 was approximately 50,000 (FWHM). The mass difference between 8, 9 and 10-mers showed a very good match with the theoretical mass number (104.0626) calculated from the elemental composition of the repeating unit (C_8H_8). The mass spectrum of PS2400 and the expanded view of the isotopic pattern of 23-mer are shown in Fig 3. The observed isotopic pattern of the 23-mer is in very good agreement with the simulated isotopic distribution (R 60,000).

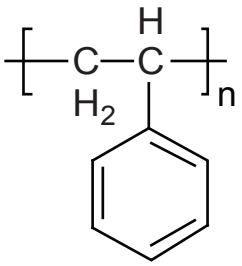

Figure 1. PS repeat unit (C_8H_8=104.0626).

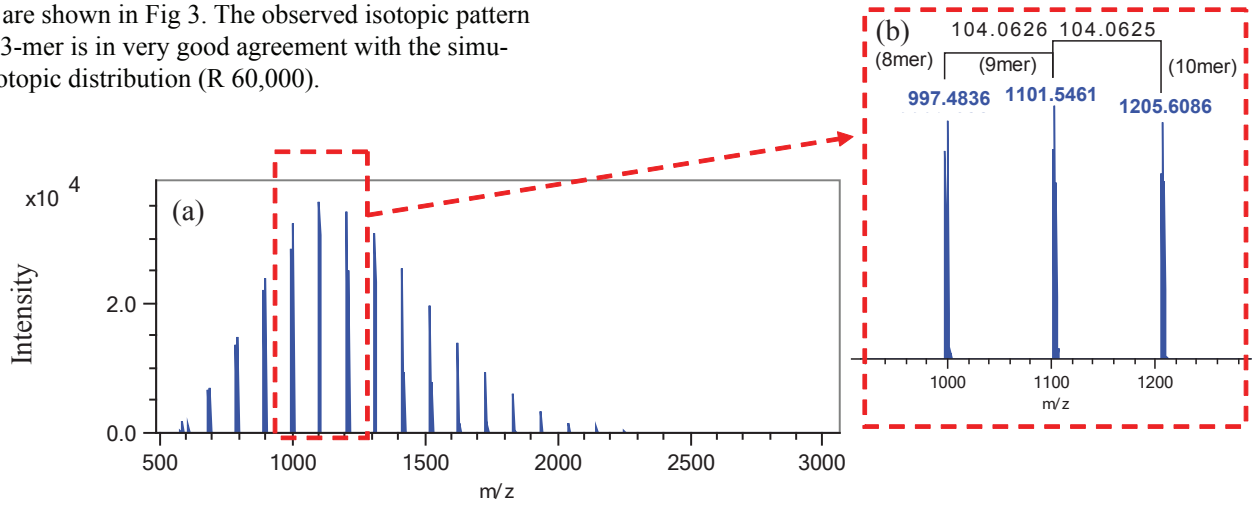

Figure 2. Mass spectrum of (a) PS1000 and (b) 8-10mer.

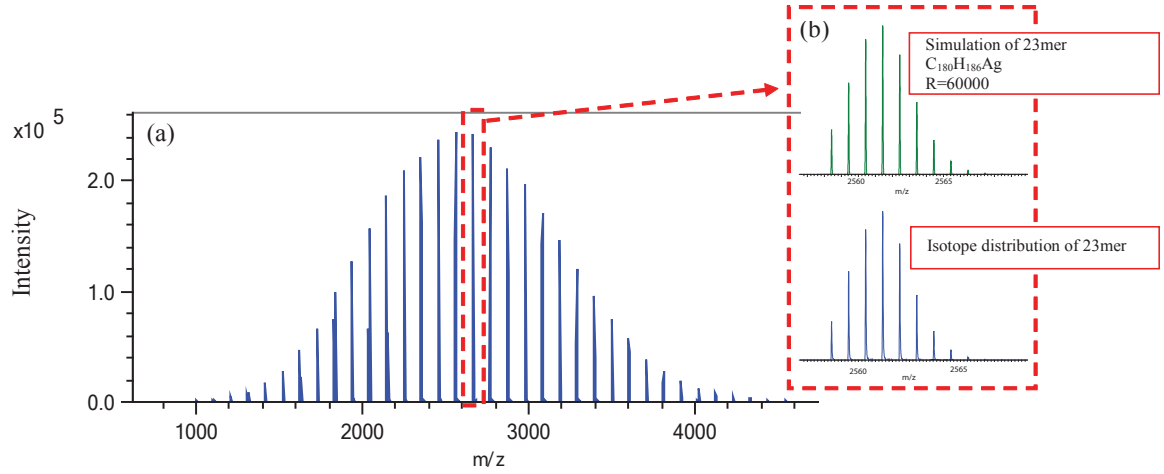

Figure 3. Mass spectrum of (a) PS2400 and (b) the 23mer with its corresponding isotopic simulation.

MS-Tips #163

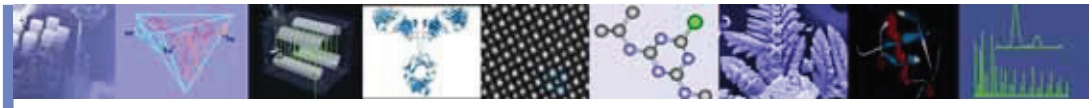

Applications Note

SpiralTOF™

Measurement of synthetic polymers

Polymethyl methacrylate

Polymethyl methacrylate (PMMA) 4000 was measured by using the JMS-S3000 SpiralTOF. The $[M+H]^+$ peaks for PMMA with the basic monomer units of 100u (Fig.1) were observed for this sample. The full PMMA mass spectrum and an expanded view around *m/z* 4000 are shown in Fig. 2(a) and (b), respectively. The resolving power at *m/z* 4,000 was approximately 45,000 (FWHM). Also, the mass differences between the 39, 40, and 41-mers had a very good match with the theoretical mass number (100.0524) of the PMMA repeat unit ($C_5H_8O_2$). A comparison between the 40-mer's observed and simulated isotopic patterns is shown in Fig. 2(c). The observed isotopic pattern is in very good agreement with the calculated isotopic distribution.

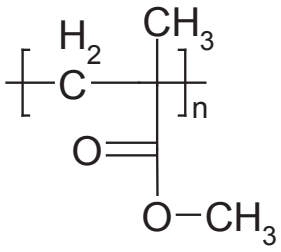

Figure 1. PMMA repeat unit ($C_5H_8O_2$=100.0524)

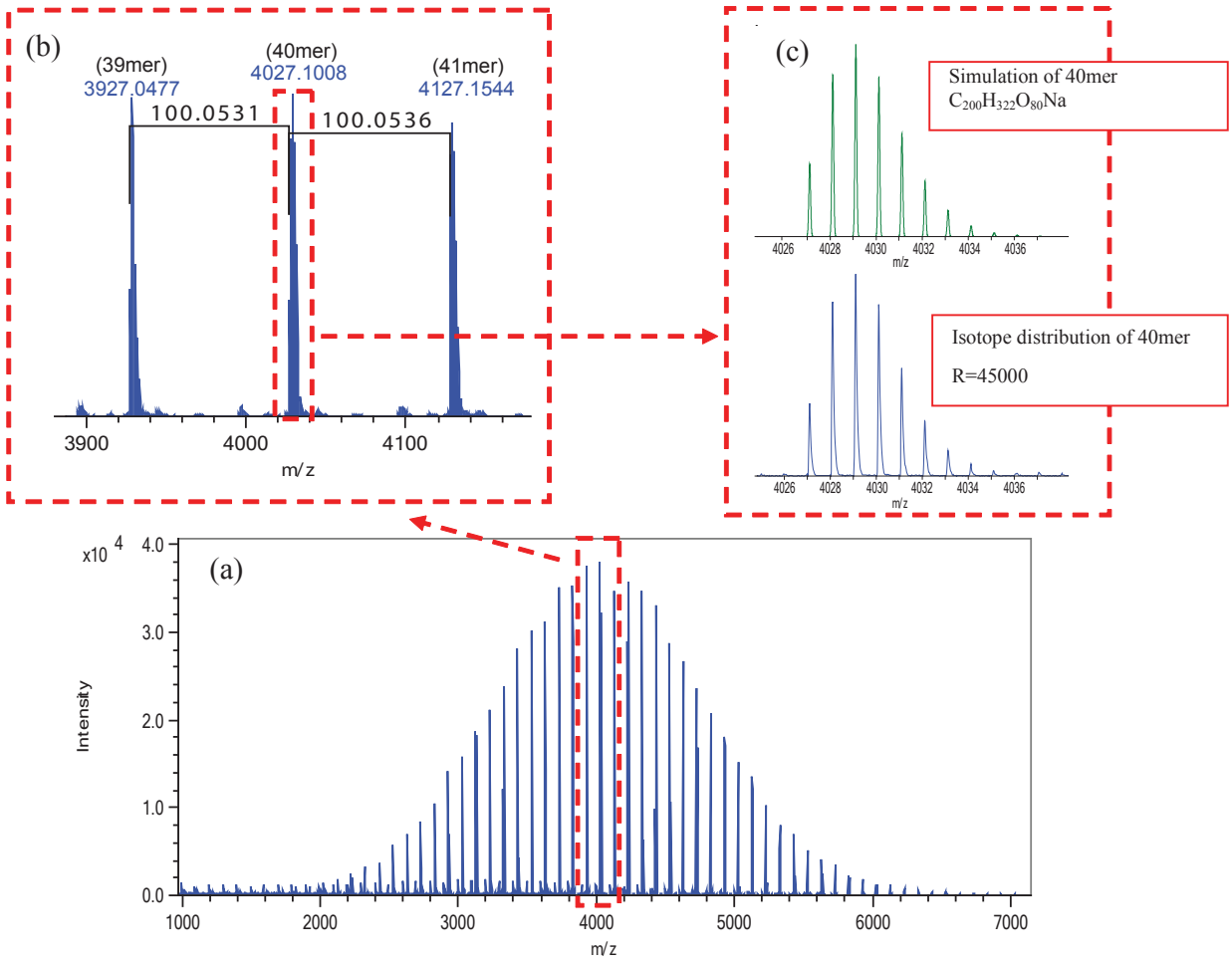

Figure 2. Mass spectrum of (a) PMMA4000, (b) the 39-41mer and (c) the 40mer with its corresponding isotopic simulation.

MS-Tips #164

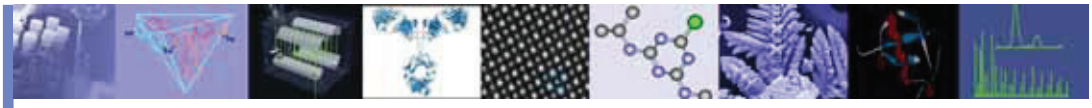

JEOL

Applications Note

SpiralTOF™

Measurement of synthetic polymers

Polyethylene Glycol

Polyethylene glycol (PEG) 1000 and 8000 were measured by using the JMS-S3000 SpiralTOF. The $[M+H]^+$ peaks for PEG with the basic monomer units of 44u (Fig. 1) were observed for each sample. The mass spectrum for PEG1000 and an expanded view around *m/z* 1,000 are shown in Fig. 2. The resolving power at *m/z* 1009 is approximately 60,000 (FWHM). The mass difference between the 21, 22 and 23-mers showed very good agreement with the theoretical mass of the PEG monomer. The full mass spectrum for PEG8000 is shown in Fig. 3(a). The comparison between the observed and simulated isotopic pattern (R 35,000) for the 226mer are shown in Fig. 3(b). The observed isotopic pattern is in very good agreement with the calculated isotopic distribution.

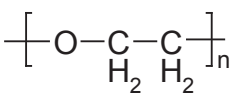

Figure 1. PEG repeat unit (C_2H_4O=44.0262).

Figure 2. Mass spectrum of (a) PEG1000 and (b) the 21-23mer.

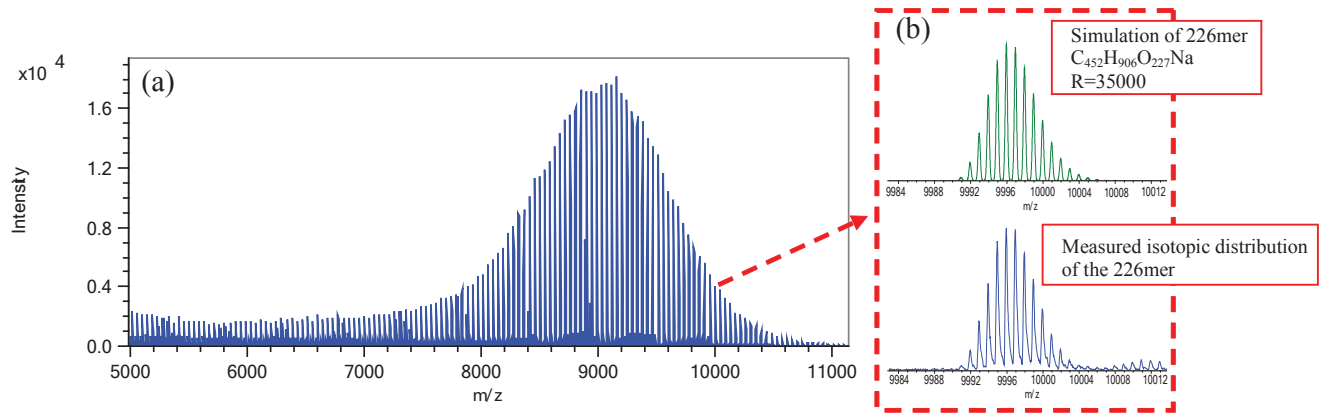

Figure 3. Mass spectrum of (a) PEG8000 and (b) the 226mer with its corresponding isotopic simulation.

MS-Tips #165

Applications note

MS
MSTips No. 311
MALDI Application

Structural analysis of polyethylene terephthalate combining an on-plate alkaline degradation method and tandem time-of-flight mass spectrometry

Product：Mass spectrometry(MS)

Introduction

Matrix assisted laser desorption/ionization (MALDI) mass spectrometry is a powerful tool for the analysis of synthetic polymers. This technique, when combined with a high-resolution time-of-flight mass spectrometer, can be used to identify differences in monomer, polymer end groups, and their molecular weight distributions. However, there are limitations to doing accurate mass analysis of high molecular weight polymers. For example, as the polymer molecular weight increases, the ionization efficiency, detection sensitivity, and ratio of monoisotopic ions used for accurate mass analysis all decrease. One way to address this is to use an “on-plate alkaline degradation” method [1] that was previously published in which high molecular weight polyester or polycarbonate are partially hydrolyzed by an alkaline reagent to form smaller oligomers that can then be analyzed by high-resolution MALDI-TOFMS. This degradation into oligomers is not only advantageous for accurate mass analysis but also for structural analysis by using tandem time-of-flight mass spectrometry (TOF-TOF). In this report, we investigated the structural analysis of the polyethylene-terephthalate (PET) polymer exposed to the on-plate alkaline degradation method by using the JMS-S3000 "SpiralTOF™-plus" with TOF-TOF option. The SpiralTOF™-plus uses an ultra-high resolution TOF for MS1 which allows monoisotopic precursor selection and a reflectron TOF for MS2 to analyze the product ion spectra produced from high energy collisional induced dissociation (HE-CID).

Experiment

PET (film) was dissolved in hexafluoro-2-propanol (HFIP) solution at a concentration of 10 mg/ml. The matrix compound 2,4,6-trihydroxyacetophenone (THAP) was dissolved in HFIP/tetrahydrofuran (THF) at a concentration of 10 mg/ml. Sodium hydroxide (NaOH) 10 mg/ml methanol solution was used for on-plate alkaline degradation. The high resolution mass spectra were measured by using SpiralTOF positive ion mode, and HE-CID measurements were performed in TOF-TOF positive ion mode.

[Sample treatment for on-plate alkaline degradation]

1. Spot the sample solution on the target plate.
2. Spot and dry the NaOH solution on the sample spot.
3. After on-plate decomposition, the sample spot was desalted with purified water.
4. Spot the THAP HFIP/THF solution on the dried sample spot.

Results

Figure 1 shows the mass spectra before and after applying the on-plate alkaline degradation method. Before the on-plate alkaline degradation, there were two characteristic cyclic oligomer series observed in the mass spectrum. However, after the on-plate decomposition, there were 10 different series observed in the sample. The proposed structures for peaks 1-3 are shown in Figure 1C.

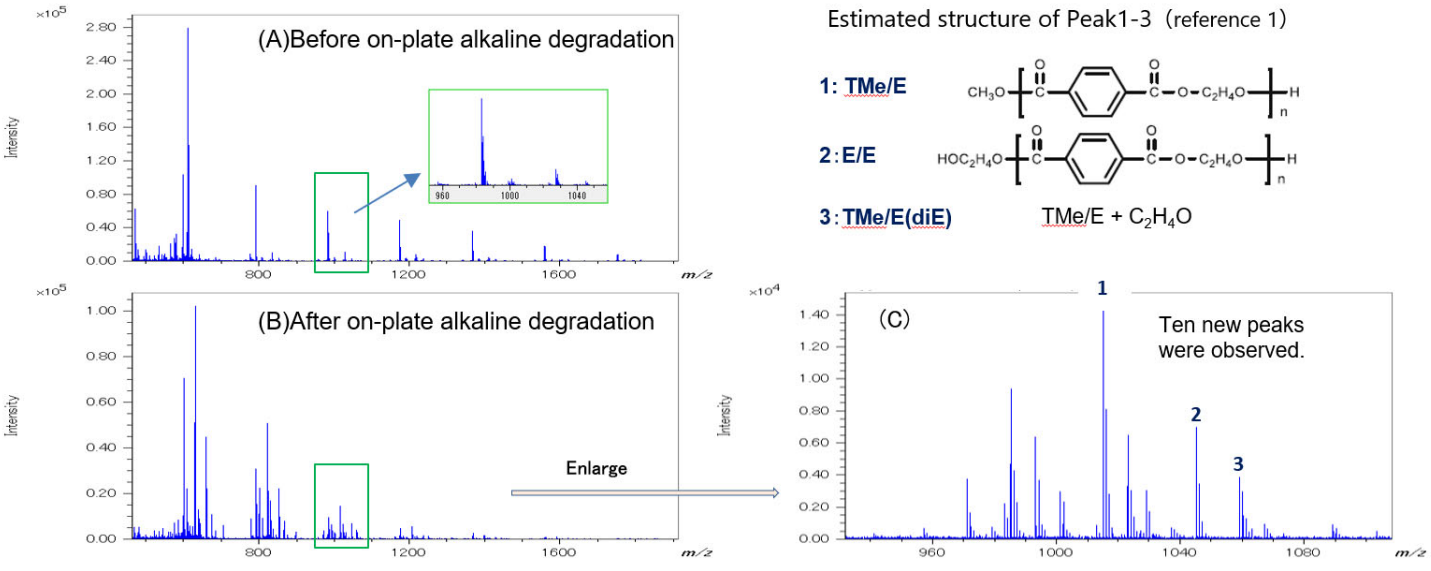

Figure 1. The mass spectra of PET oligomer (A) before and (B) after on-plate alkaline degradation treatment.
(C) Enlarged mass spectrum of PET after on-plate alkaline degradation.

Next, the $C_{10}H_8O_4$ KMD plots for the before and after on-plate alkaline degradation mass spectra are shown in Figure 2A and 2B, respectively. The before degradation sample showed two distinct series (blue: Cyclic, red: Cyclic + C_2H_4O). However, the after degradation sample showed a lower intensity for the original series as well as the emergence of several new series in the sample. The three series discussed in Figure 1C are colored as green: TMe/E, yellow: E/E, and orange: TMe/E(diE),.

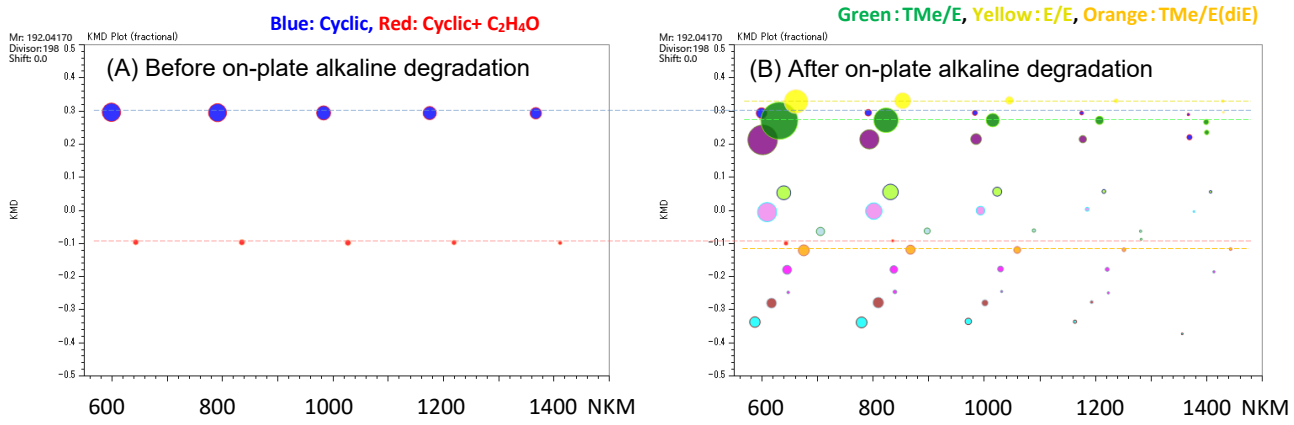

Figure 2. The KMD plots of PET before(A) and after(B) on-plate alkaline degradation（base unit $C_{10}H_8O_4$:192.04, x=198）

Three oligomers generated by on-plate alkaline degradation were selected for TOF-TOF analysis: TMe/E (*m/z* 1015), E/E (*m/z* 1045) and TMe/E(diE) (*m/z* 1059). Figures 3 and 4 show the product ion spectra for these ions. The product ion spectra showed common ions as well as several mass spectral peaks with separation intervals of 192u, which all suggest that these ions have similar structures. The estimated structure (n=5) and the fragmentation position are shown in each product ion spectrum. First, the E/E product ion spectrum (Figure 3A), which has the same end-group structure at both ends, was analyzed, and the product ions highlighted with blue arrows were used to support the estimated structure. Next, the product ion spectrum of TMe/E (Figure 3B), which has one end-group that is different from E/E, showed unique ions that were labeled with red arrows. The red and blue arrows highlight all of the product ions that supported this structure.

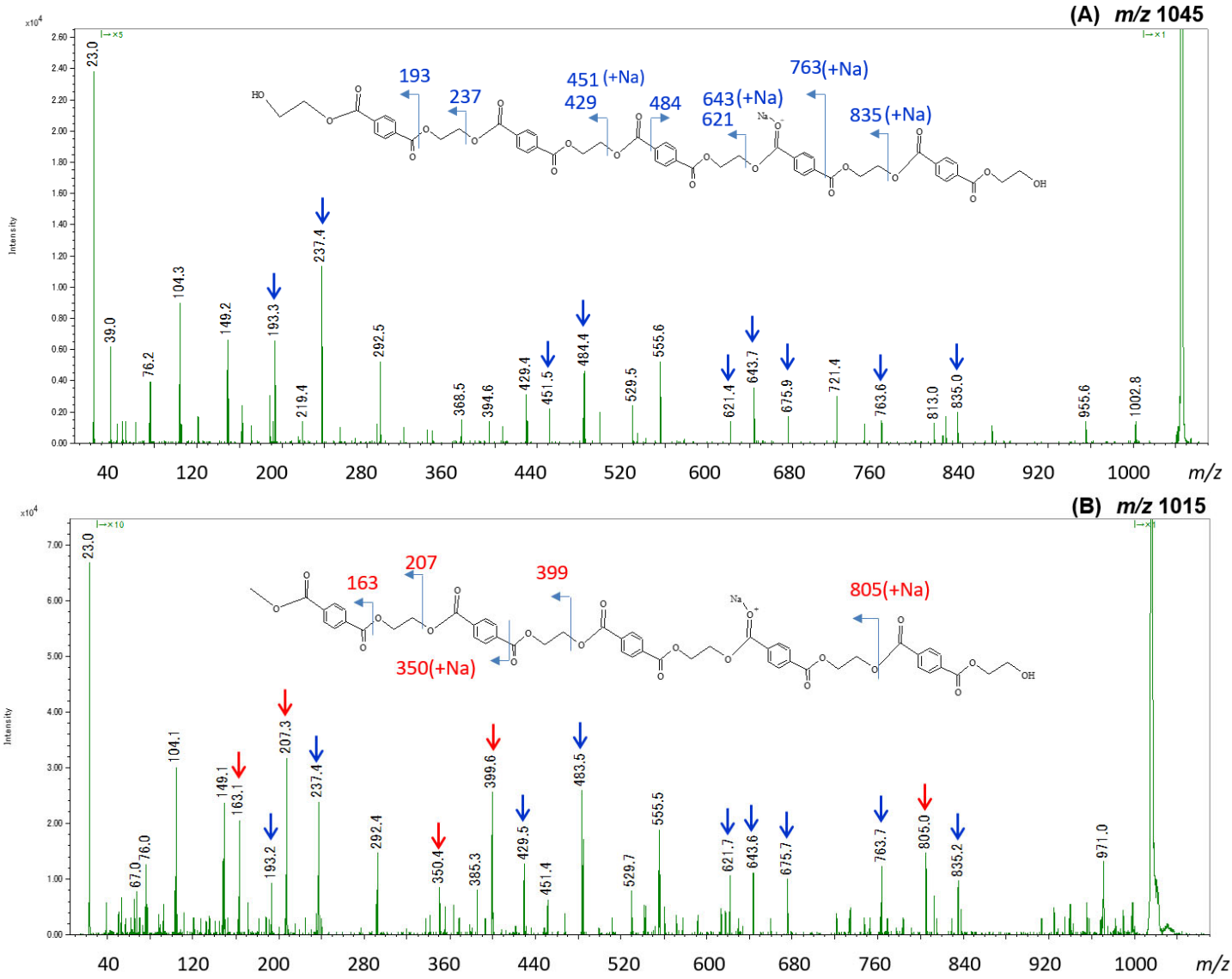

Figure 3. The PET product ion spectra for (A) *m/z* 1045 and (B) *m/z* 1015 after on-plate alkaline degradation.

Next, the product ion spectrum of TMe/E(diE), which is estimated to have the [C_2H_4O] unit inside the repeat unit, was analyzed by using TOF-TOF mode. In addition to the peaks observed in Figure 3A and B (blue and red arrows), the characteristic peaks highlighted with green arrows in Figure 4 support the estimated structure shown. Since the peaks common to Figure 3A and B (*m/z* 163, 193, 207 and 237) correspond to the fragmentation channel near the end-group, it can be inferred that the [C_2H_4O] unit exists in the main chain.

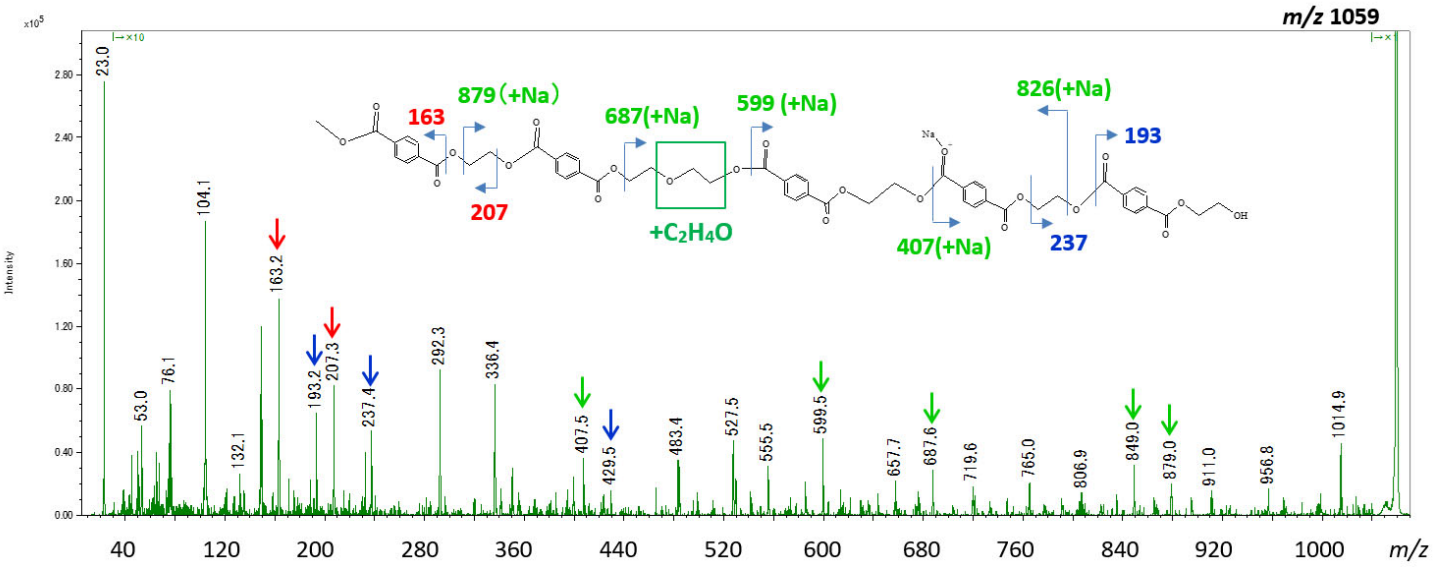

Figure 4. The PET product ion spectrum for *m/z* 1059 after on-plate alkaline degradation.

Conclusion

Structural analysis by TOF-TOF using HE-CID were performed on PET oligomers generated by on-plate alkaline degradation method. The results supported the estimated structures shown in Reference 1 and show that using a combination of on-plate polymer degradation with MS/MS structural analysis provides complementary information to accurate mass analysis.

Reference

1) S. Nakamura, T. Fouquet, H. Sato: *J. Am. Soc. Mass Spectrom.,* 30, 355 (2018).

JEOL Ltd.
3-1-2 Musashino Akishima Tokyo 196-8558 Japan Sales Division Tel. +81-3-6262-3560 Fax. +81-3-6262-3577
www.jeol.com ISO 9001 • ISO 14001 Certified
▼ Local office
• AUSTRALIA & NEW ZEALAND • BELGIUM • BRAZIL • CANADA • CHINA • EGYPT • FRANCE • GERMANY • GREAT BRITAIN & IRELAND • ITALY • KOREA • MALAYSIA • MEXICO • RUSSIA • SCANDINAVIA
• SINGAPORE • TAIWAN • THE NETHERLANDS • USA

Visualizing fragmentation channels of polyethylene oxide with different end groups using the JMS-S3000 SpiralTOF™ with TOF–TOF option

Product used: Mass Spectrometry (MS)

Tandem mass spectrometry is a powerful tool for polymer characterization. It can obtain information about polymer end groups, repeating structures (linear, cyclic, or branched), and copolymerization. High-energy collision–induced dissociation (HE-CID) is a fragmentation method that is available only in tandem time-of-flight mass spectrometry (TOF–TOF). The informative fragmentation channels, which are difficult to observe with commonly used low-energy CID, are often observable in HE-CID spectra. In MSTips 270, we proposed a method to visualize this abundant structural information and enable intuitive analysis using the “Remainders of KM” (RKM) plot method. In this report, we applied the method to analyze polyethylene oxide (PEO) with different end groups.

Experiment

We dissolved polypropylene glycol HO $(C_2H_4O)_nH$, polyethylene glycol monolauryl ether HO $(C_2H_4O)_nC_{12}H_{25}$, and polyoxyethylene monocetyl ether HO $(C_2H_4O)_nC_{16}H_{33}$ in methanol (10 mg/mL). We used α-cyano-4-hydroxycinnamic acid (α-CHCA; 10 mg/mL in methanol) and sodium trifluoroacetate (NaTFA; 10 mg/mL in methanol) as matrix and cationizing agent, respectively. The sample, α-CHCA, and NaTFA were mixed at 1:10:1 (v/v/v), spotted on a target plate, and air dried. Product-ion spectra were acquired in positive-ion mode using JMS-S3000 SpiralTOF™ with the TOF–TOF option. We analyzed the data using msRepeatFinder version 3.0.

Product ion spectra

All product-ion spectra showed strong sodium-adduct ions $[M+Na]^+$. The HE-CID spectra were acquired by selecting $[HO(C_2H_4O)_{28}H+Na]^+$ (*m/z* 1273.7), $[HO(C_2H_4O)_nC_{12}H_{25}+Na]^+$ (*m/z* 1265.8) and $[HO(C_2H_4O)_nC_{16}H_{33}+Na]^+$(*m/z* 1277.9) as precursor ions (Fig. 1). The red arrows in each product-ion spectrum in Figure 1 represent the mass difference corresponding to 44u (C_2H_4O). Several fragmentation channels with 44u interval were observed in each product ion spectrum; however, it is time consuming to assign each series one by one. Also note that the differences between the three polymers cannot be understood intuitively.

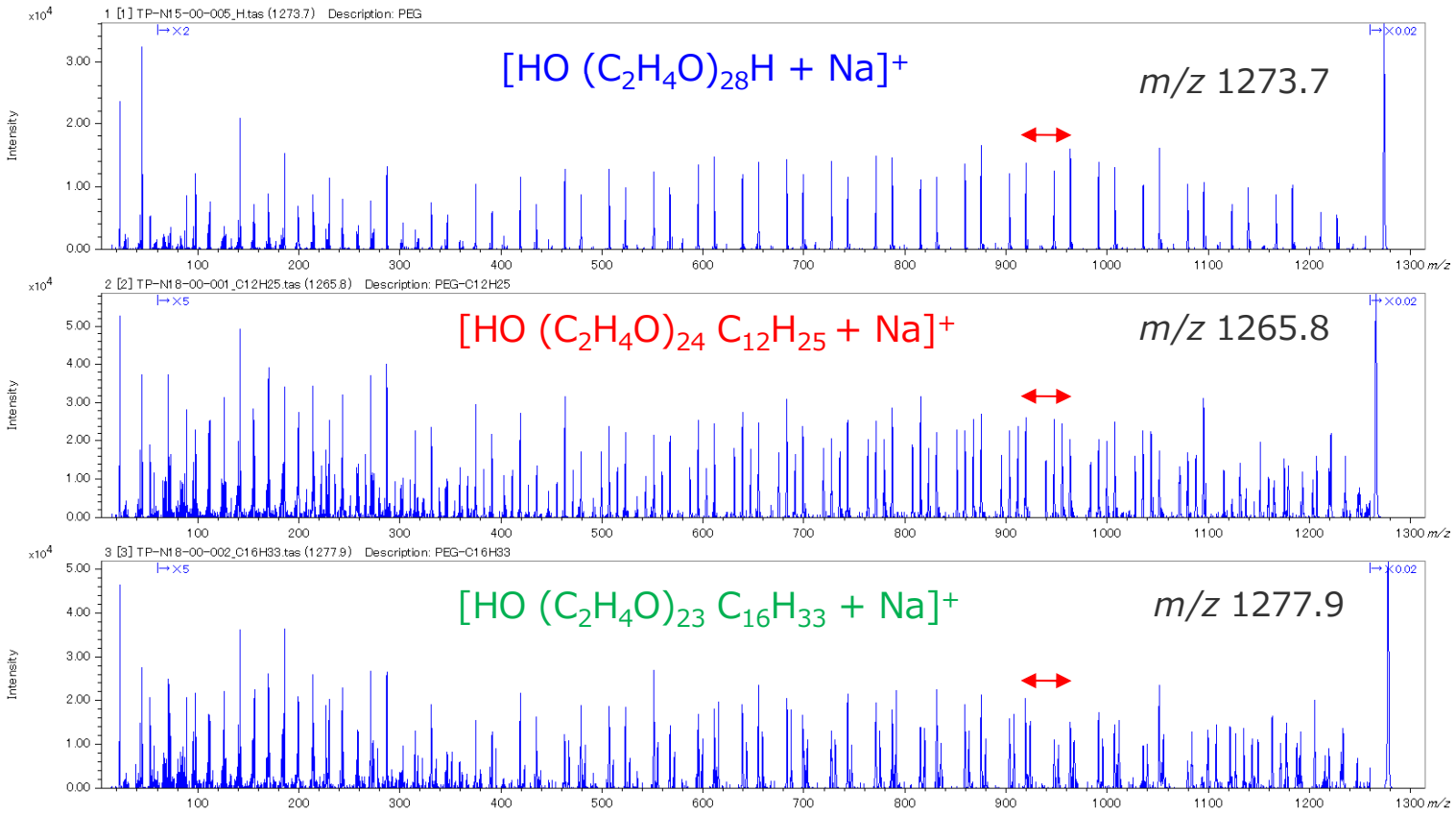

Figure 1. Product ion spectra of three types of polyethylene oxides.

Visualization of polymer series with Remainders of KM (RKM) plot

In Figure 2 below, product ion spectra of three types of PEO are overlaid in an RKM plot (base unit EO). We excluded the precursor and sodium ions from the display region in order to clarify the fragmentation channels of the repeating structures. In this figure, the peak colors of $[HO(C_2H_4O)_nH+Na]^+$, $[HO(C_2H_4O)_nC_{12}H_{25}+Na]^+$, and $[HO(C_2H_4O)_nC_{16}H_{33}+Na]^+$ are overlaid as blue, red, and green, respectively. The peak series displayed in black denote fragment ions commonly observed in all three types of PEOs. The fragmentation peak series in the RKM plot of Figure 2 are divided into three characteristic parts, each of which is confirmed in Figures 3–5, respectively.

$[HO\ (C_2H_4O)_{28}H + Na]^+$ $[HO\ (C_2H_4O)_{24}\ C_{12}H_{25} + Na]^+$ $[HO\ (C_2H_4O)_{23}\ C_{16}H_{33} + Na]^+$

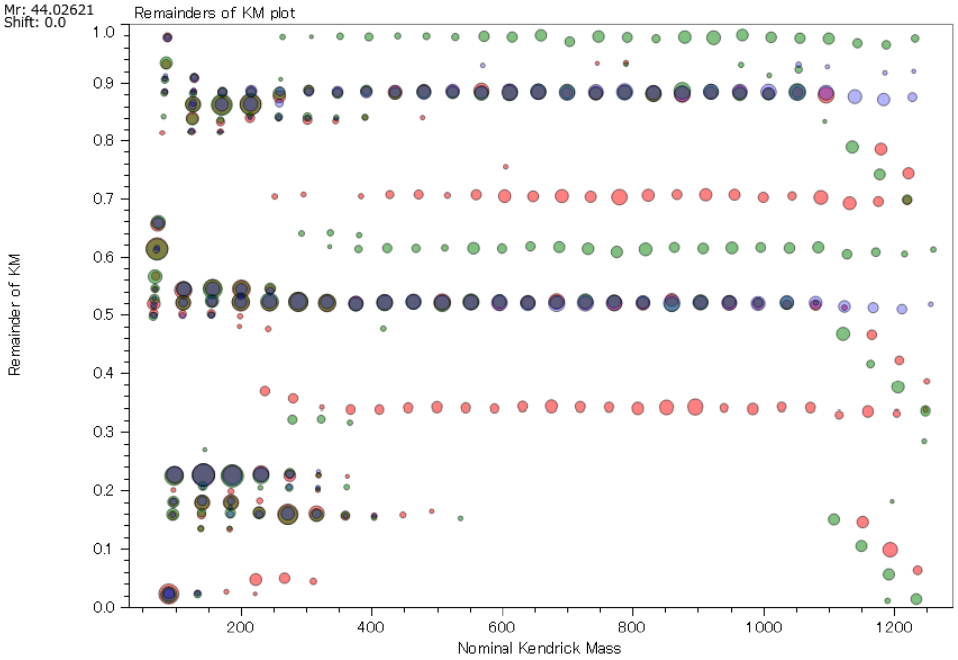

Figure 2. Overlaid RKM plot (base unit: propylene oxide C_2H_4O from the repeat unit list) of three PEO types

First, we focused on the black series (Fig. 3), i.e., the series commonly observed in all product ion spectra. These two series were considered to be fragmentation channels that did not include different end-group structures. We confirmed them to be the fragmentation channels shown in Figure 3, which we observed as $[M+Na]^+$.

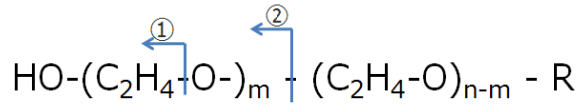

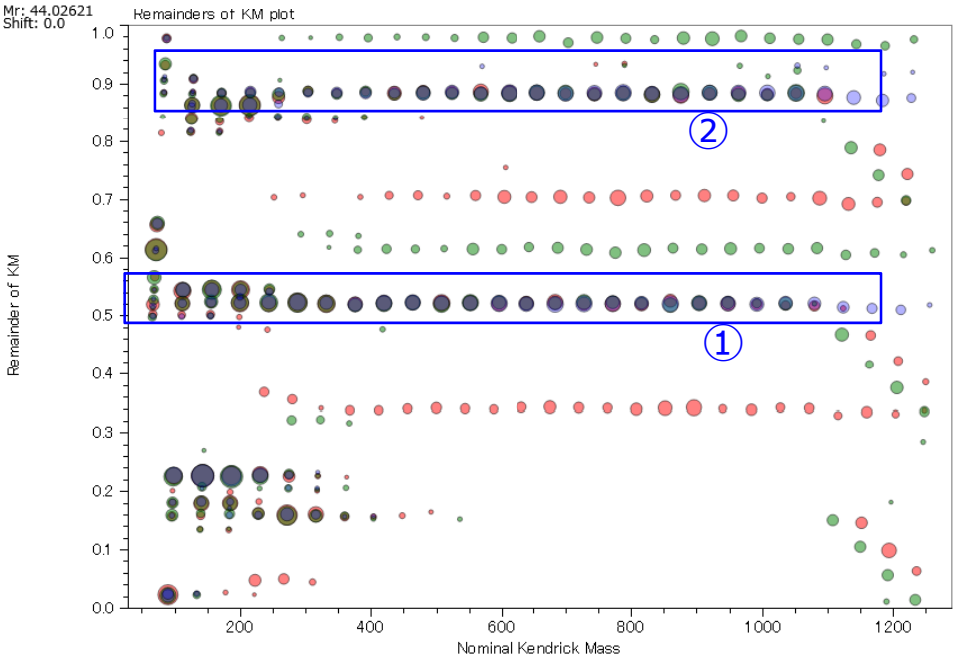

Figure 3. Common peaks in RKM plot of three types of polyethylene oxides.

Second, we focused on the series of red and green (Fig. 4). These four series were considered to be fragmentation channels, which included different end-group structures. We confirmed these as the fragment channels shown in Figure 4, which we observed as $[M+Na]^+$. Third, we focused on the series with slope (Fig. 5), which we observed in the part near the precursor ion (right side of RKM plot). “Series with slope” are series without 44u intervals. They have 14u (CH_2) intervals and are assigned to be the alkyl chain cleavage, which is a unique fragmentation channel in HE-CID.

Conclusion

It is easy to visualize the fragmentation channels of polymer series using an RKM plot. By overlapping product-ion spectra obtained from precursor ions with different end groups in an RKM plot, fragmentation channels common to all PEOs can be distinguished from fragmentation that is dependent on end-group composition. This is a proven method for helping to analyze different series of end groups observed in the mass spectra of polymers in real samples.

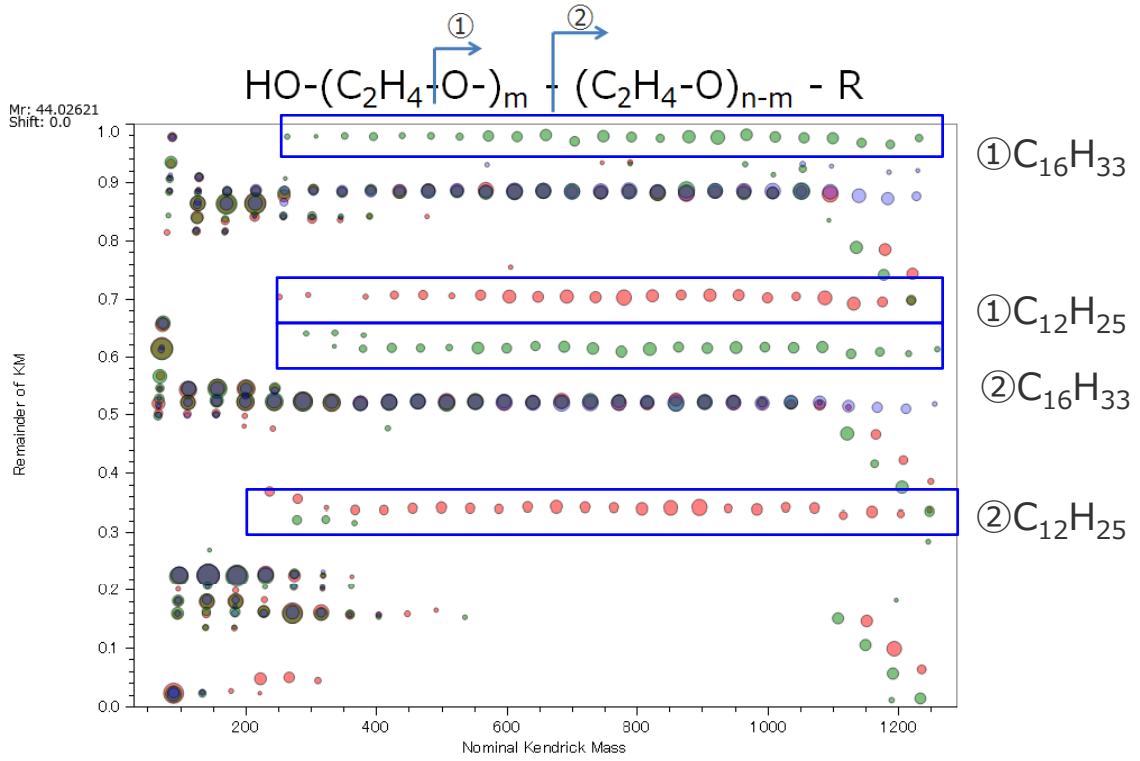

Figure 4. Peaks that are dependent on end group composition.

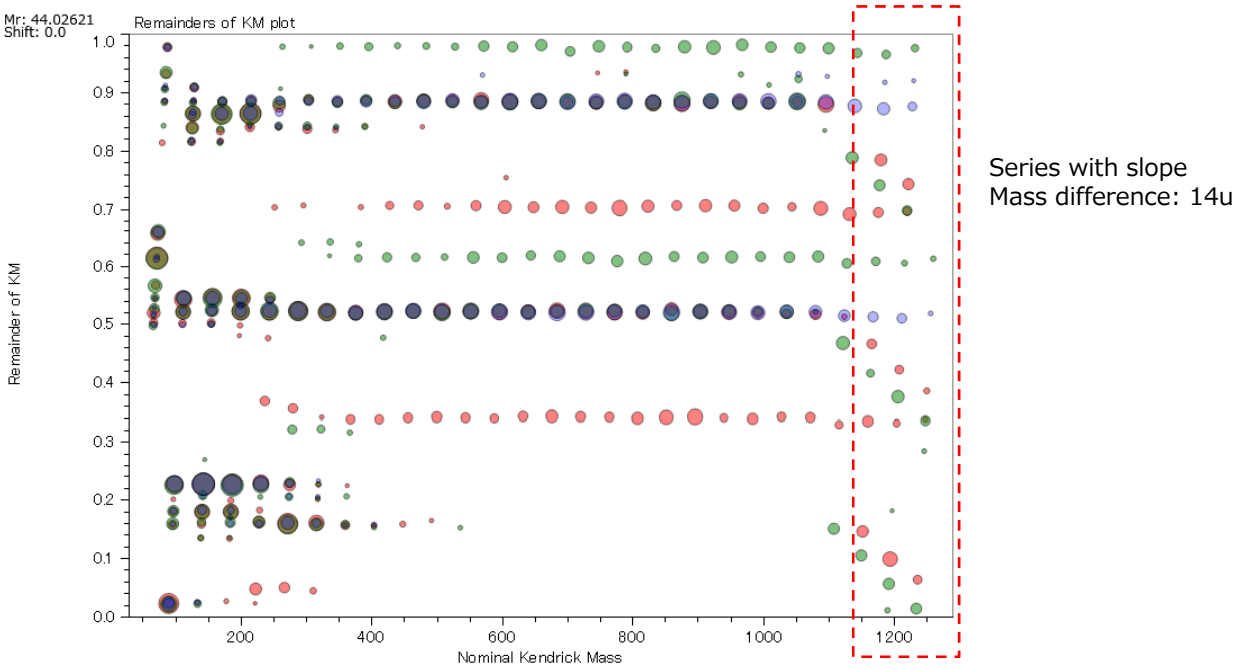

Figure 5. Peaks originating from charge-remote fragmentation of the alkyl chain in the end group.

JEOL Ltd.
3-1-2 Musashino Akishima Tokyo 196-8558 Japan Sales Division Tel. +81-3-6262-3560 Fax. +81-3-6262-3577
www.jeol.com ISO 9001 • ISO 14001 Certified
▼Local office
• AUSTRALIA & NEW ZEALAND • BELGIUM • BRAZIL • CANADA • CHINA • EGYPT • FRANCE • GERMANY • GREAT BRITAIN & IRELAND • ITALY • KOREA • MALAYSIA • MEXICO • RUSSIA • SCANDINAVIA • SINGAPORE • TAIWAN • THE NETHERLANDS • USA

Applications note

MS
MSTips No. 270
MALDI Application

“Remainders of KM” plot for polymers using msRepeatFinder: Intuitive display of High energy collision induced dissociation mass spectra acquired by SpiralTOF™/TOF

Product used：Mass spectrometer (MS)

Tandem mass spectrometry of polymer ions provides valuable information about the nature of individual end-groups, chain architecture (linear / cyclic / branched) or copolymeric microstructure. A high energy collision-induced dissociation (HE-CID) tandem time-of-flight analysis (TOF/TOF) advantageously follows a matrix-assisted laser desorption ionization (MALDI) TOF analysis. However, the interpretation of the resulting mass spectrum is not obvious with numerous ion series and signals of low intensity. A “remainders of Kendrick mass” analysis (RKM) is proposed as a rapid post-acquisition data processing of TOF/TOF mass spectra to visualize and filter the ion series instantly via intuitive point alignments.

Experimental

Poly(propylene oxide) (PPO 1000 g mol^{-1}) was used for an analyte. Product ion spectra were recorded with a JMS-S3000 SpiralTOF™ mass spectrometer (CHCA 10 mg mL^{-1}, PPO 10 mg mL^{-1}, NaTFA 1 mg mL^{-1}, 10:1:1 in MeOH). KMD and RKM plots were computed using msRepeatFinder 3.0.

HE-CID mass spectrum

A typical HE-CID mass spectrum of a (OH, H)-ended PPO 30-mer with isotopic selection of the precursor ion at *m/z* 1782 displays two main product ion series detected with low intensity (**Fig. 1**) while several minor series are also barely observed in the background. Visualizing and interpreting such type of mass spectral data remains inconvenient and time-consuming as a manual assignment of each peak one by one as well as a tedious artwork are necessary to label all the product ions in a quite unclear figure.

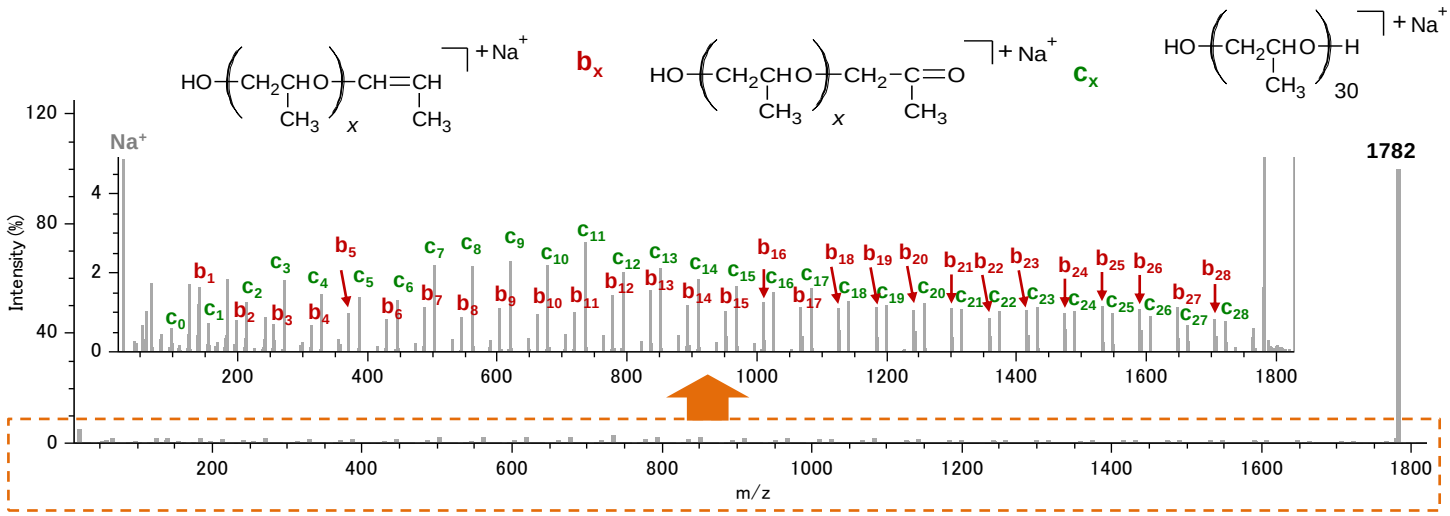

Fig. 1. HE-CID mass spectrum with two main product ion series noted b_x and c_x (adapted from Wesdemiotis et al [1] – structures in inset).

Kendrick mass defect (KMD) plot

The KMD plot [2] computed from the HE-CID mass spectrum displays a cloud of points barely aligned horizontally (**Fig. 2**). As the resolution of a TOF/TOF mass spectrum is unitary with limited mass accuracy for the mass measurements of the product ions, accurate mass defects cannot be evaluated and the resulting KMD plot is unresolved with no separation of the product ion series.

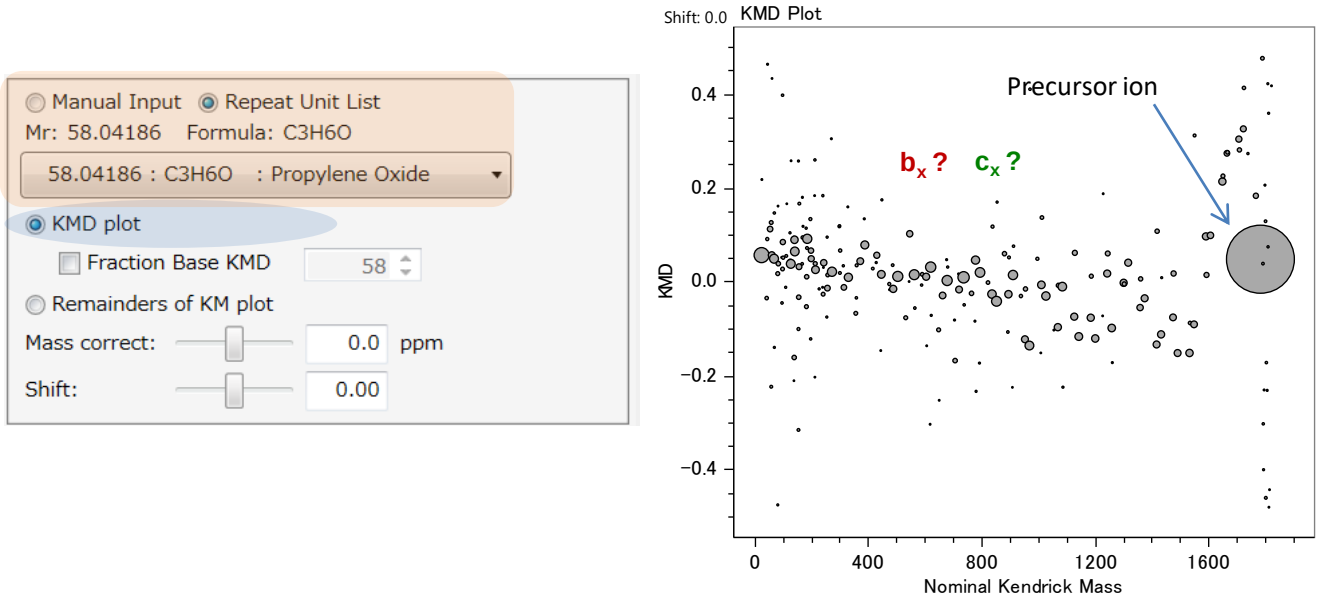

Fig. 2. "Regular" KMD plot (base unit: propylene oxide C_3H_6O from the repeat unit list) using msRepeatFinder.

Remainders of KM (RKM) plot

A "remainders of KM" plot [3] (base unit: C_3H_6O, PO repeating unit) is readily computed by checking the corresponding option in msRepeatFinder (**Fig. 3**). Instead of the unresolved cloud of points in the KMD plot, several series of points are clearly visualized in the RKM plot which does not require high-accuracy mass measurement to display horizontal alignments. Each line is instantly assigned to the main product ion series (c_x: green dots; b_x: red dots) and the minor series barely seen in the HE-CID mass spectrum.

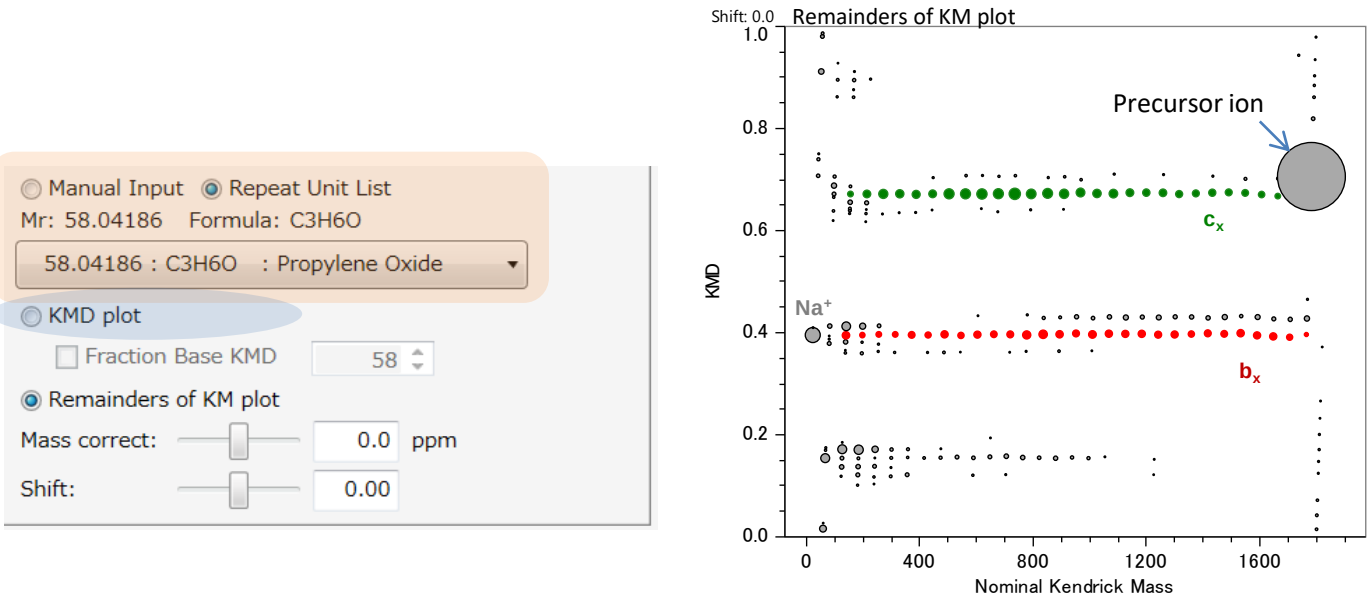

Fig. 3. RKM plot (base unit: propylene oxide C_3H_6O from the repeat unit list) using msRepeatFinder.

The “grouping mode” in msRepeatFinder further allows each ion series to be instantly label in the HE-CID mass spectrum with visual color coding by a simple selection of a given point series horizontally aligned in the RKM plot (**Fig. 4**). Unselected ion series can be hidden for an ever more visual mapping of complex mass spectral data (**Fig. 5**).

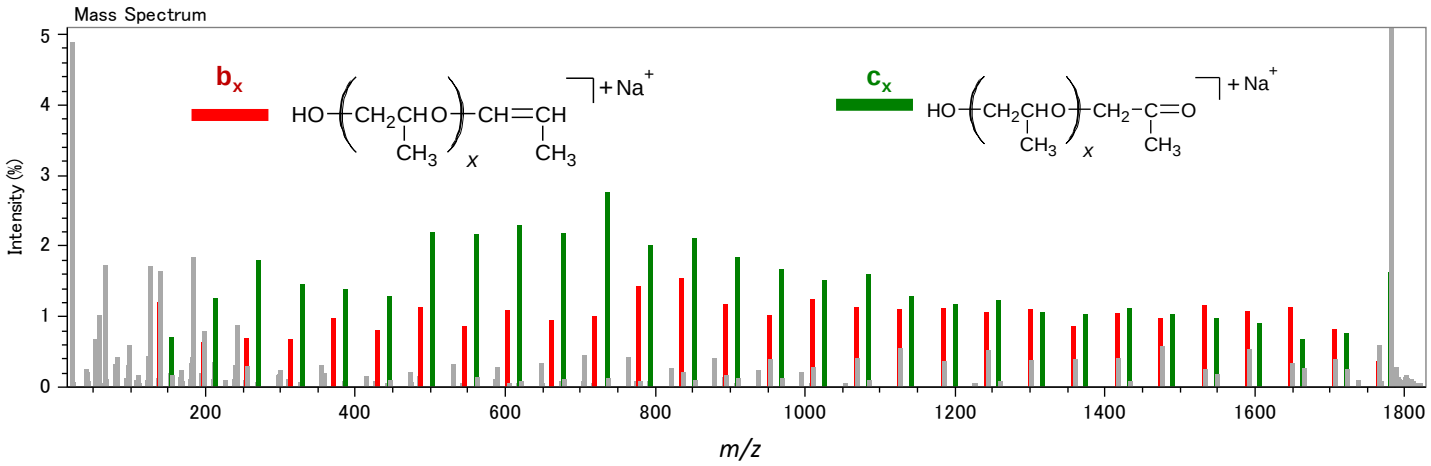

Fig. 4. Visualization of the two main product ion series (green bars: c_x; red bars: b_x) by grouping points horizontally aligned in the RKM plot.

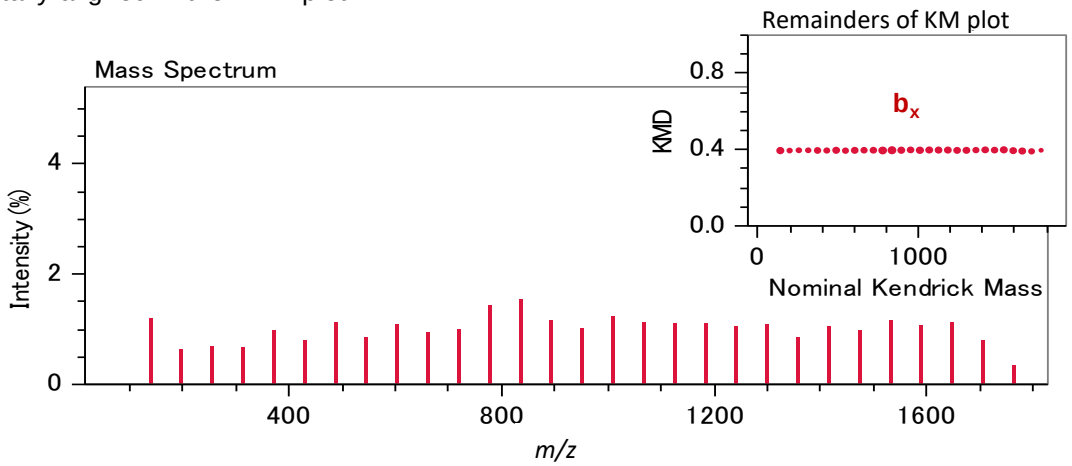

Fig. 5. Visualization of one ion series only by hiding the unselected points.

Prospects

The RKM plots are compatible with HE-CID mass spectra of homopolymers and copolymers using one of the repeating units (different end-groups of ion series and/or architecture block/random) or the expelled neutrals (filiations) [4].

Acknowledgment

This application note is written based on the results of a joint research project with Dr. Hiroaki Sato and Dr. Thierry Fouquet in Research Institute for Sustainable Chemistry, National Institute of Advanced Industrial Science and Technology (AIST).

References

[1] C. Wesdemiotis, N. Solak, M. J. Polce, D. E. Dabney, K. Chaicharoen, B. C. Katzenmeyer. *Mass Spec. Rev.* **2011**, *30*, 523-559.

[2] H. Sato, S. Nakamura, K. Teramoto, T. Sato. *J. Am. Soc. Mass Spectrom.* **2014**, *25,* 1346–1355.

[3] T. Fouquet, T. Satoh, H. Sato. *Anal. Chem.* **2018**, *90,* 2404–2408.

[4] T. Fouquet, H. Sato. *Rapid Commun. Mass Spectrom.* **2016**, *30*, 1361–1364.

JEOL Ltd.
3-1-2 Musashino Akishima Tokyo 196-8558 Japan Sales Division Tel. +81-3-6262-3560 Fax. +81-3-6262-3577
www.jeol.com ISO 9001 • ISO 14001 Certified

• **AUSTRALIA & NEW ZEALAND** /JEOL(AUSTRALASIA) Pty.Ltd. Suite 1, L2 18 Aquatic Drive - Frenchs Forest NSW 2086 Australia • **BELGIUM** /JEOL (EUROPE) B.V. Planet II, Gebouw B Leuvensesteenweg 542, B-1930 Zaventem Belgium • **BRAZIL** /JEOL Brasil Instrumentos Cientificos Ltda. Av. Jabaquara, 2958 5° andar conjunto 52 ; 04046-500 Sao Paulo, SP Brazil • **CANADA** /JEOL CANADA, INC. 3275 1ere Rue, Local #8 St-Hubert, QC J3Y-8Y6, Canada • **CHINA** /JEOL(BEIJING) CO., LTD. Zhongkeziyuan Building South Tower 2F, Zhongguancun Nansanjie Street No. 6, Haidian District, Beijing, P.R.China • **EGYPT** /JEOL SERVICE BUREAU 3rd Fl. Nile Center Bldg., Nawal Street, Dokki, (Cairo), Egypt • **FRANCE** /JEOL (EUROPE) SAS Espace Claude Monet, 1 Allee de Giverny 78290, Croissy-sur-Seine, France • **GERMANY** /JEOL (GERMANY) GmbH Gute Aenger 30 85356 Freising, Germany • **GREAT BRITAIN & IRELAND** /JEOL (U.K.) LTD. JEOL House, Silver Court, Watchmead, Welwyn Garden City, Herts AL7 1LT, U.K. • **ITALY** /JEOL (ITALIA) S.p.A. Palazzo Pacinotti - Milano 3 City, Via Ludovico il Moro, 6/A 20080 Basiglio(MI) Italy • **KOREA** /JEOL KOREA LTD. Dongwoo Bldg. 7F, 1443, Yangjae Daero, Gangdong-Gu, Seoul, 05355, Korea • **MALAYSIA** /JEOL(MALAYSIA) SDN.BHD. 508, Block A, Level 5, Kelana Business Center, 97, Jalan SS 7/2, Kelana Jaya, 47301 Petaling Jaya, Selangor, Malaysia • **MEXICO** /JEOL DE MEXICO S.A. DE C.V. Arkansas 11 Piso 2 Colonia Napoles Delegacion Benito Juarez, C.P. 03810 Mexico D.F., Mexico • **RUSSIA** /JEOL (RUS) LLC. Krasnoproletarskaya Street, 16, Bld. 2, 127473, Moscow, Russian Federation • **SCANDINAVIA** /SWEDEN JEOL (Nordic) AB Hammarbacken 6A, Box 716, 191 27 Sollentuna Sweden • **SINGAPORE** /JEOL ASIA PTE.LTD. 2 Corporation Road #01-12 Corporation Place Singapore 618494 • **TAIWAN** /JIE DONG CO., LTD. 7F, 112, Chung Hsiao East Road, Section 1, Taipei, Taiwan 10023 (R.O.C.) • **THE NETHERLANDS** /JEOL (EUROPE) B.V. Lireweg 4, NL-2153 PH Nieuw-Vennep, The Netherlands • **USA** /JEOL USA, INC. 11 Dearborn Road, Peabody, MA 01960, U.S.A.

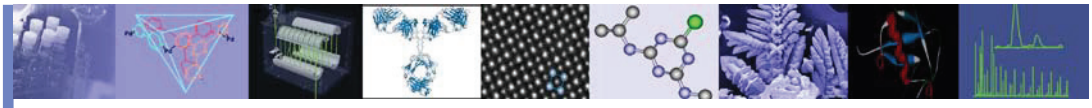

Applications Note

SpiralTOF-TOF

Synthetic Polymer Structure Analysis
Poly Propylene Glycol (PPG)

Introduction:
The JMS-S3000 "SpiralTOF™" is a MALDI-TOFMS that incorporates an innovative SpiralTOF ion optics system (Fig.1). The JMS-S3000 is available with a TOF-TOF option that can acquire high-energy collision-induced dissociation (CID) product ion spectra for monoisotopically selected precursor ions. This monoisotopic precursor selection is made possible by the fact that the distance to the ion gate is 15 m, which is more than one order of magnitude longer than that of conventional MALDI TOF-TOF instruments. Additionally, the second TOF MS incorporates a re-acceleration mechanism and an offset parabolic reflectron, another innovative ion optical design developed by JEOL. This unique design enables seamless observation of product ions ranging from very low *m/z* up to that of the precursor ion.

Figure 1. JMS-S3000 "SpiralTOF" with TOF-TOF attachment.

In this work, we analyzed Polypropylene Glycol (PPG) by using the JMS-S3000 SpiralTOF with the TOF-TOF option. The resulting high-energy CID data was then processed using the Polymerix™ (Sierra Analytics, Inc., http://massspec.com/) analysis software.

Samples:
Polymer: PPG
Matrix agent: α-Cyano-4-hydroxycinnamic acid (CHCA)
Cationization agent: NaI

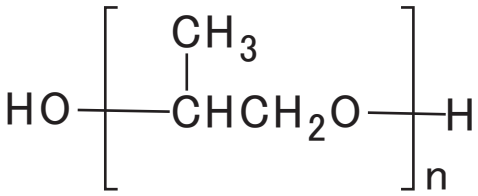

Figure 2. Structural formula of PPG.

Results and Discussion:
The MALDI mass spectrum of PPG and the *m/z* 1027.7 (n=17, $[M+Na]^+$) product ion spectrum are shown in Fig. 3. The MS-MS spectrum shows the full range of ions from *m/z* 23.0 for $[Na^+]$ to *m/z* 1027.7 for the precursor ion. Also worth noting, these product ions are all monoisotopic because the precursor ion was monoisotopically selected, which greatly simplified the resulting MS-MS spectrum.

The enlarged region (*m/z* 580-630) in Fig. 3 shows that there are five different product ions present that could result from the monomer repeat unit (58u, C_3H_6O). Therefore, this high-energy CID data for PPG suggests that there are five possible fragmentation pathways.

Based on previously published work[1], we hypothesized that the structural formulas for these different product ion series were most likely the structures shown in Fig. 4a-e. These formulas were then used in the Polymerix™ software which resulted in the product ion series assignments shown in Fig. 5. These results supported our hypothesis for each structure and showed that the JMS-S3000 high-energy CID data fully represents the structural fragmentation expected for PPG.

Conclusions:

Structural analysis of synthetic polymers such as PPG can easily be done by using the JMS-S3000 TOF-TOF method (high-energy CID, monoisotopic precursor selection) with the Polymerix™ analysis software.

Reference:

(1) Liang Li, "MALDI Mass Spectrometry for Synthetic Polymer Analysis", John Wiley & Sons, Inc., United States of America (2010).

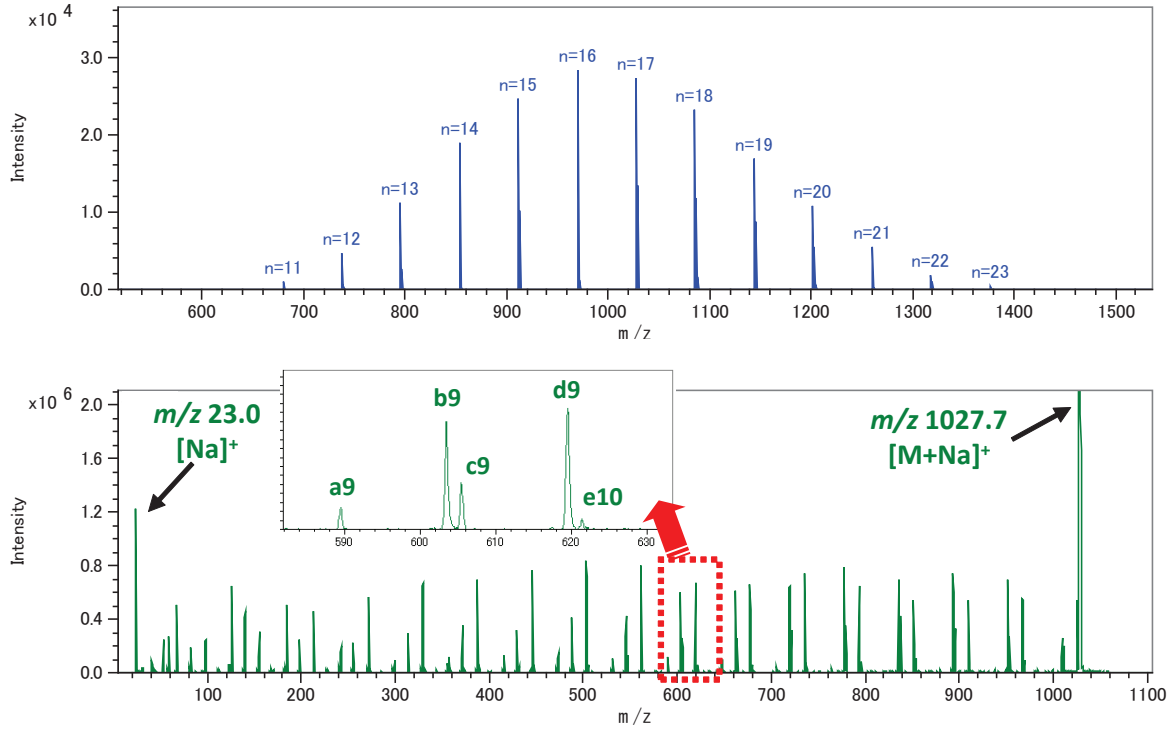

Figure 3. MALDI mass spectrum of PPG (upper) and product ion spectrum of *m/z* 1027.7 (n=17, $[M+Na]^+$) (lower).

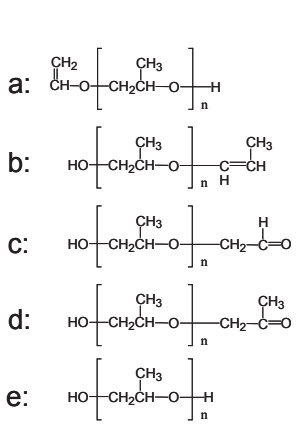

Figure 4. Structural formula of product ions series.

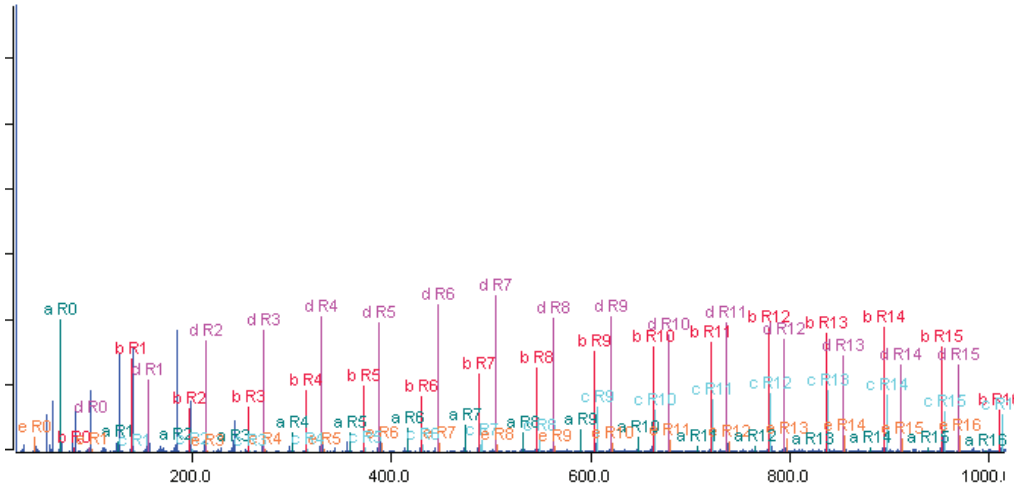

Figure 5. Polymerix™ analysis result of of *m/z* 1027.7 (n=17, $[M+Na]^+$).

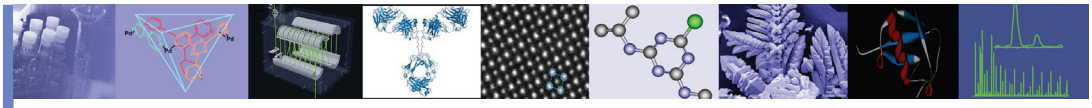

Applications Note

SpiralTOF-TOF

Synthetic Polymer Structure Analysis
Poly Methal Methacrylate (PMMA)

Introduction:
The JMS-S3000 "SpiralTOF™" is a MALDI-TOFMS that incorporates an innovative SpiralTOF ion optics system. This system is available with a TOF-TOF option that can acquire high-energy collision-induced dissociation (CID) product ion spectra for monoisotopically selected precursor ions.

In this work, we analyzed Poly Methyl Methacrylate (PMMA) shown in Fig. 1 by using the JMS-S3000 SpiralTOF with the TOF-TOF option. The resulting high-energy CID data was then processed using the Polymerix™ (Sierra Analytics, Inc., http://massspec.com/) analysis software.

Samples:
Polymer: PMMA
Matrix agent: 2,5-Dihydroxybenzoic acid (DHB)
Cationization agent: NaI

Results and Discussion:
The MALDI mass spectrum of PMMA and the product ion spectra for *m/z* 1525.8 (n=15, $[M+Na]^+$) and *m/z* 2326.2 (n=23, $[M+Na]^+$) are shown in Fig. 2. These product ion spectra show the full range of ions from *m/z* 23.0 for $[Na^+]$ to the precursor ion *m/z* 1027.7 and *m/z* 2326.2, respectively. Also worth noting, these product ions are all monoisotopic because the precursor ion was monoisotopically selected, which greatly simplified the resulting MS-MS spectrum.

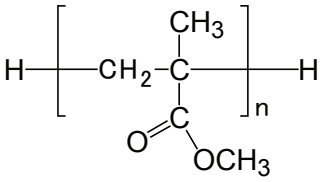

Figure 1. Structural formula of PMMA.

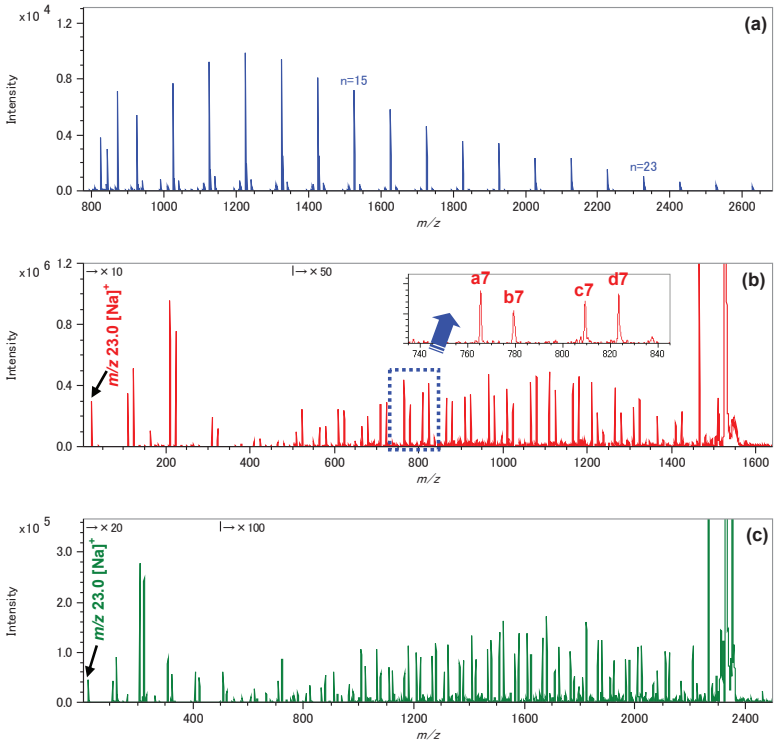

Figure 2. MALDI mass spectrum of a) PMMA, b) product ion spectrum of *m/z* 1525.8 (n=15, $[M+Na]^+$), and c) product ion spectrum of *m/z* 2326.2 (n=23, $[M+Na]^+$).

MS Tips 172

The enlarged region (*m/z* 730-850) in Fig. 2b shows that there are at least four different product ions present that could result from the monomer repeat unit (100u, $C_5H_8O_2$). Therefore, this high-energy CID data for PMMA suggests that there are four possible fragmentation pathways.

Based on previously published work[1], we hypothesized that the structural formulas for these different product ion series were most likely the structures shown in Fig. 3a-d. These formulas were then used in the Polymerix™ software which resulted in the product ion series assignments shown in Fig. 5. These results supported our hypothesis for each structure and showed that the JMS-S3000 high-energy CID data fully represents the structural fragmentation expected for PMMA.

Conclusions:
Structural analysis of synthetic polymers such as PMMA can easily be done by using the JMS-S3000 TOF-TOF method (high-energy CID, monoisotopic precursor selection) with the Polymerix™ analysis software.

Reference:
(1) Liang Li, "MALDI Mass Spectrometry for Synthetic Polymer Analysis", John Wiley & Sons, Inc., United States of America (2010).

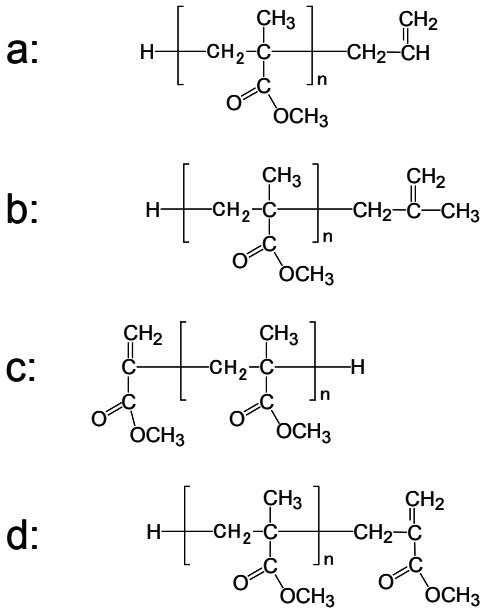

Figure 3. Structural formula of product ions series.

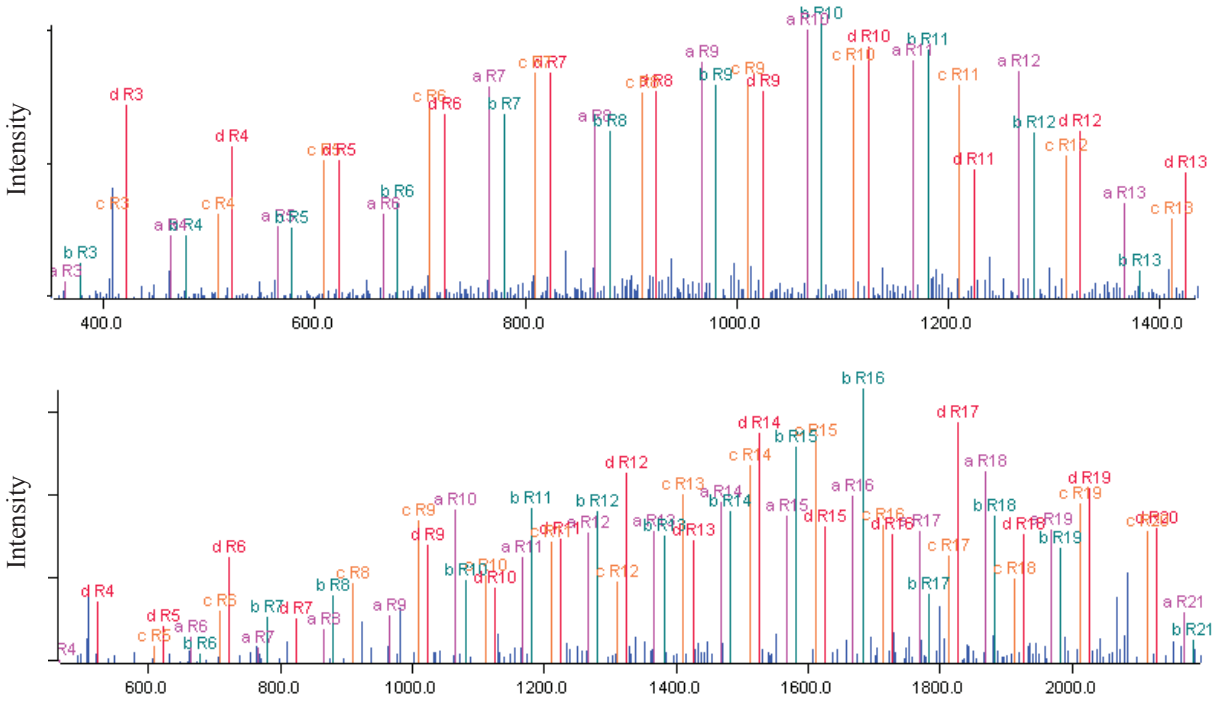

Figure 4. Polymerix analysis results of *m/z* 1525.8 (n=15, $[M+Na]^+$) (upper) and *m/z* 2326.2 (n=23, $[M+Na]^+$) (lower).

Structure analysis of a polymer additive using high-energy collision–induced dissociation mass spectra acquired by JMS-S3000 with TOF/TOF option

Product used: Mass Spectrometer (MS)

Various kinds of additives are used in a polymer, such as an antioxidant, a light stabilizer, and an ultraviolet absorber. Because a polymer's properties depend on the additives in the raw material, it is important to understand these additives. Matrix-assistance laser desorption/ ionization time-of-flight mass spectrometer (MALDI-TOFMS) JMS-S3000 SpiralTOF™ is widely used in polymer analysis. High-energy collision–induced dissociation (HE-CID) measurement with the TOF/TOF option is also useful in analyzing the structures of additives. SpiralTOF™ can achieve a high precursor ion selection with a revolution of 17 m. Fragmentation derived from HE-CID can be observed only due to the ions from post-source decay (PSD), these fragment ions can be eliminated by the four electrostatic sectors that constitute the spiral trajectory. In this Applications Note, we report on polymer structural analysis by comparing fragmentation patterns in the product ion spectra of IRGANOX 1076 (BASF) $M^{+\cdot}$ and $[M+Na]^+$.

Experiment

For the sample, we used the additive IRGANOX 1076 (10 mg/ml in tetrahydrofuran [THF]) in a commercially available additive kit. For the matrix, we used 2,5-hydroxybenzoic acid (DHB; 20 mg/ml in THF). HE-CID measurements were carried out for all ion species ($M^{+\cdot}$ and $[M+Na]^+$) confirmed by the mass spectrum, and the product ion spectra were acquired.

Results

The mass spectrum of IRGANOX 1076 is shown in Figure 1. We observed ion species corresponding to $M^{+\cdot}$ and $[M+Na]^+$ at *m/z* 530 and 553, respectively. Two kinds of monoisotope ions were selected to obtain a product ion spectrum.

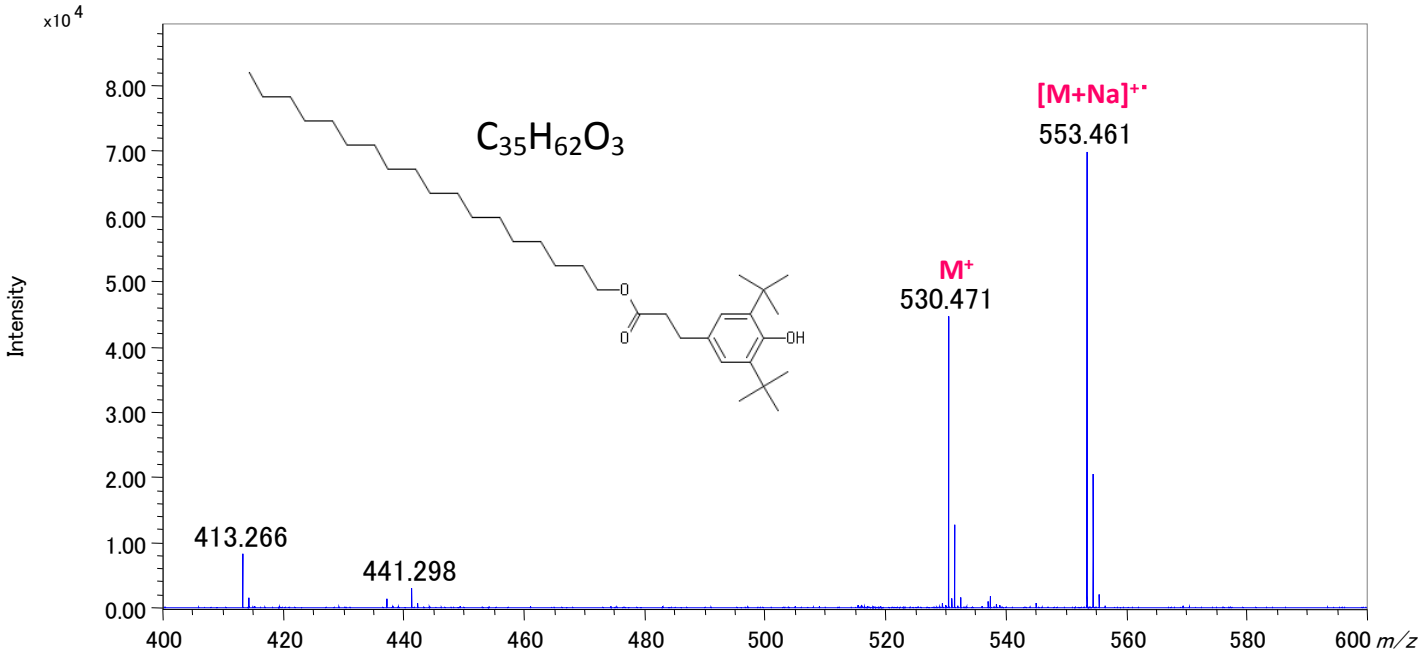

Figure 1. Mass spectrum of IRGANOX 1076.

Product ion spectra of IRGANOX 1076 *m/z* 530.5 ($M^{+\cdot}$) and *m/z* 553 ($[M + Na]^+$) measured with HE-CID are shown in Figure 2(a) and (b). We compared the fragmentation channels of both types of ions. Peaks observed below *m/z* 219 are indicated by the dotted red line, common fragmentation channels from $M^{+\cdot}$ and $[M+Na]^+$ by the solid red line. We estimated the peaks to be fragment ions without sodium. In particular, the peak at *m/z* 219 was estimated to be a fragment ion from the phenolic side with a tert-butyl group (t-Bu). Those observed at *m/z* 233 and 259 in Figure 2(a) and (b) have a mass difference of 23 u. It is understood that these fragment ions indicate the same fragmentation channel from $M^{+\cdot}$ and $[M+Na]^+$. Furthermore, in the product ion spectrum of $[M+Na]^+$, we observed peaks at intervals of 14 u at *m/z* 320–540. These are peaks were derived from alkyl chain cleavage by charge remote fragmentation (CRF), which is characteristic of HE-CID. We regularly observed mass differences at intervals of 14 u, suggesting that there was no unsaturated bond in the alkyl chain.

Conclusions

Obtaining product ion spectra of different ion species of the same compound observed in the mass spectrum is effective in two ways. First, the ion species of fragment ions can be estimated by comparing the mass differences of peaks appearing in the product ion spectrum, which aids in structural analysis. Second, alkyl chain fragmentation can be observed via CRF.

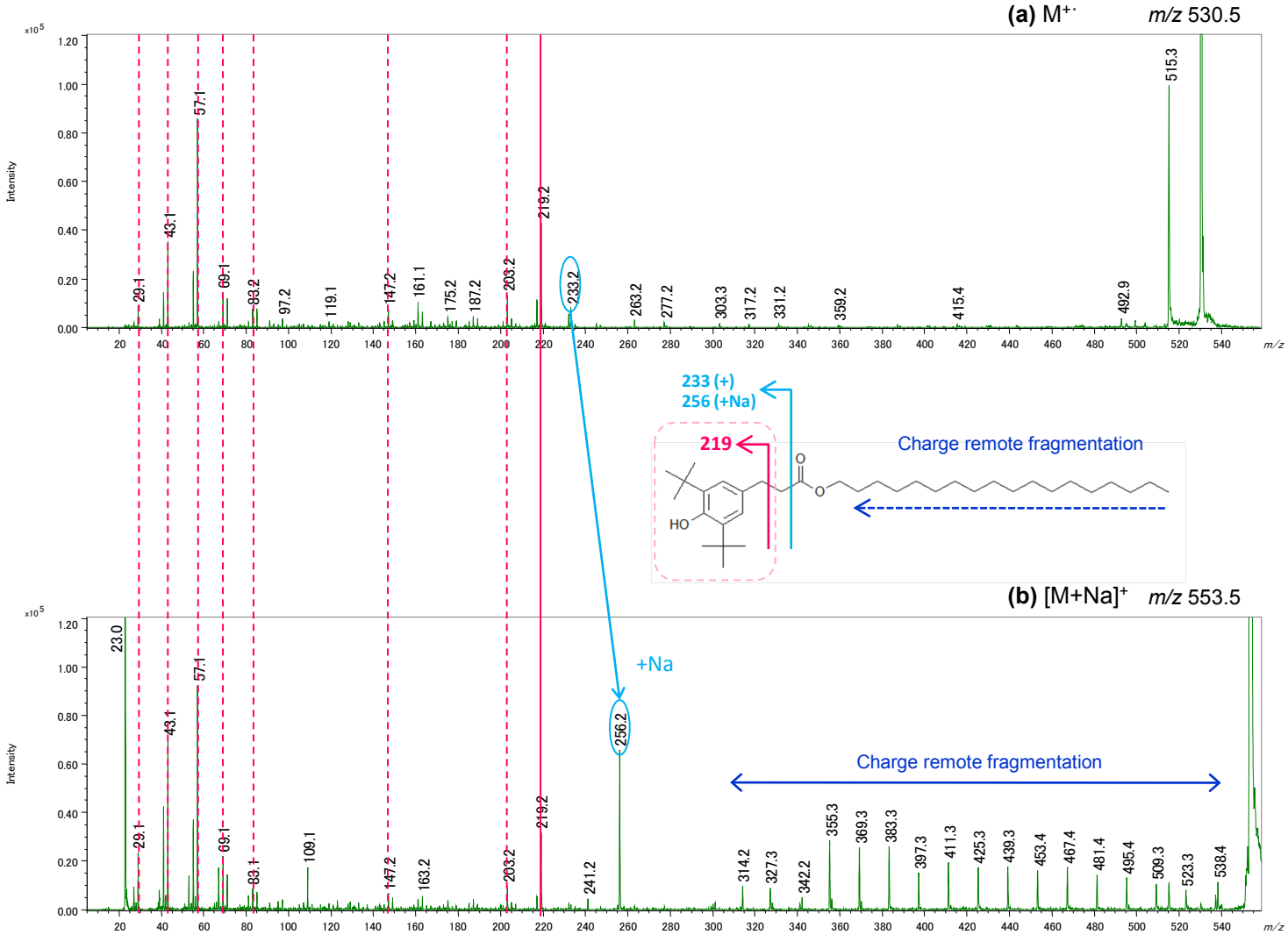

Figure 2. Product ion spectra of IRGANOX 1076 with different ion species. (a) *m/z* 530 $M^{+\cdot}$. **(b)** *m/z* 553 $[M+Na]^+$.

JEOL Ltd.
3-1-2 Musashino Akishima Tokyo 196-8558 Japan Sales Division Tel. +81-3-6262-3560 Fax. +81-3-6262-3577
www.jeol.com ISO 9001 • ISO 14001 Certified
▼Local offces
• AUSTRALIA & NEW ZEALAND • BELGIUM • BRAZIL • CANADA • CHINA • EGYPT • FRANCE • GERMANY • GREAT BRITAIN & IRELAND • ITALY • KOREA • MALAYSIA • MEXICO • RUSSIA • SCANDINAVIA
• SINGAPORE • TAIWAN • THE NETHERLANDS • USA

Analysis of medicinal properties in a combination cold remedy by using JMS-S3000 “SpiralTOF™”

Product used：Mass Spectrometer (MS)

Matrix assisted laser desorption ionization (MALDI) is a soft ionization method that uses laser energy absorbing “matrix” compounds to assist with the ionization process. Typically, the molecular weight for these matrice ions are in the low *m/z* range (typically 100-300Da range). The MALDI ion source is typically combined with reflectron type time-of-flight mass spectrometers (TOFMS), which offer insufficient mass resolving power for separating matrix and contamination peaks from analyte peaks of interest with low molecular weights. The JMS-S3000 “SpiralTOF™” (Figure 1) is a MALDI-TOFMS that has a spiral ion trajectory that folds a 17m flight path into a one meter box by using four electrostatic sectors. As a result, the SpiralTOF™ has a five times longer flight path than conventional reflectron TOFMS systems thus allowing it to achieve the highest mass resolution commercially available for a MALDI-TOFMS system. Additionally, interference from chemical background are reduced by eliminating post source decay ions in the electrostatic sectors. These features allow the SpiralTOF™ to easily detect low molecular weight ions. In this report, we will discuss the analysis of medicinal components in a combination cold remedy.

Experiments

A commercially available combination cold remedy tablet was dissolved in 13.4 ml of water. The seven medicinal ingredients in the tablet were acetaminophen, tranexamic acid, dl-methylephedrine hydrochloride, anhydrous caffeine, d-chlorpheniramine maleic acid, dihydrocodeine phosphate and isopropamide iodide. Sinapic acid ($C_{11}H_{12}O_5$) was used for matrix. The SpiralTOF™ was used in positive ion mode to acquire the sample mass spectra.

Results

The mass spectrum of the combination cold remedy is shown in Figure 2. All of the ions related to the seven medicinal components were observed as $[M+H]^+$. The mass correction for accurate mass analysis was performed by using two peaks related to the sinapic acid matrix compound $[M-H_2O+H]^+$ (*m/z* 207.0659, ▼ in Figure 2) and $[2M+Na]^+$ (*m/z* 471.1262, not shown). The observed and calculated mass for the ions related to seven medicinal components are listed in Table 1. The mass error for each measured ion was within 0.001 u of the calculated value. Additionally, high mass accuracy was achieved even for the low intensity ions such as d-chlorpheniramine and dihydrocodeine, as a result of the high mass resolution and reduction of background interferences in the low mass region.

Conclusion

In this work, we analyzed the medicinal components in a combination cold remedy tablet by using JMS-S3000 “SpiralTOF™” and showed high accuracy mass analysis in the low mass region, which is difficult to do using a conventional reflectron type TOFMS. Furthermore, we showed an easy method for getting high mass accuracy in the low mass region by using matrix peaks for internal mass correction.

a) b)

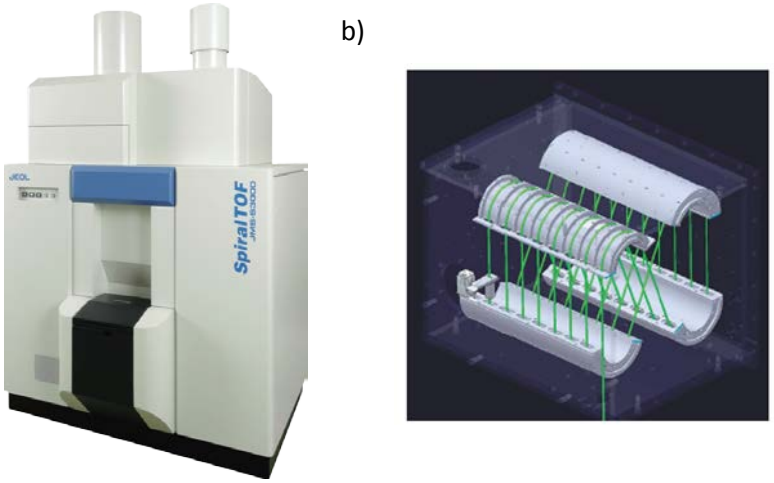

Figure 1. a) JMS-S3000 “SpiralTOF™” and b) spiral ion trajectory.

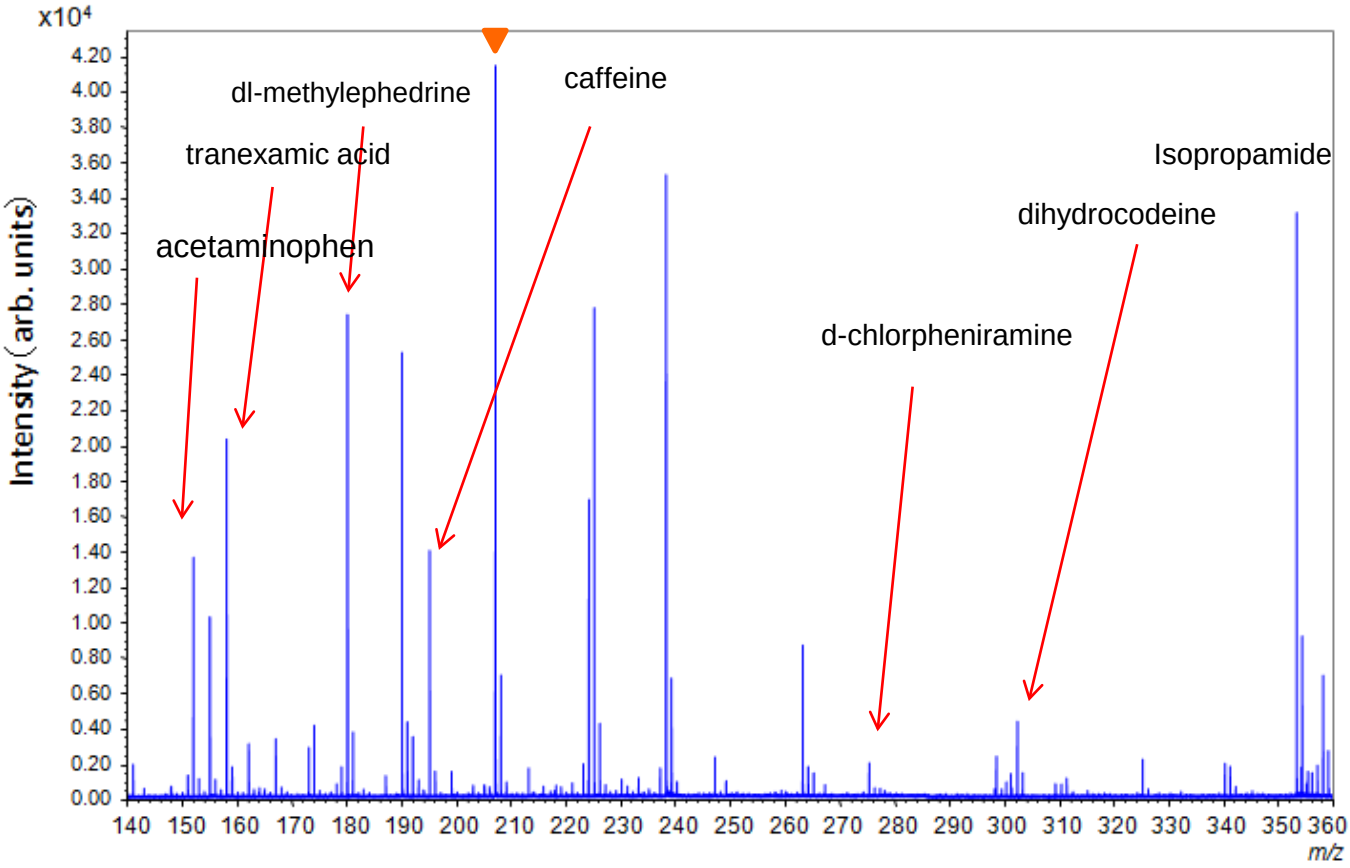

Figure 2. Mass spectrum of the combination cold remedy

Table1. Mass accuracy of the medicinal components in the combination cold remedy.

Medicinal properties	Chemical formula	Calc.[M+H]⁺ (u)	Observed (u)	Error (u)
acetaminophen	$C_8H_9NO_2$	152.0706	152.0707	+0.0001
tranexamic acid	$C_8H_{15}NO_2$	158.1176	158.1166	-0.0010
methylephedrine	$C_{11}H_{17}NO$	180.1383	180.1375	-0.0008
caffeine	$C_8H_{10}N_4O_2$	195.0877	195.0880	+0.0003
hlorpheniramine	$C_{16}H_{19}ClN_2$	275.1310	275.1300	-0.0010
dihydrocodeine	$C_{18}H_{23}NO_3$	302.1751	302.1747	-0.0004
Isopropamide	$C_{23}H_{32}N_2O$	353.2587	353.2573	-0.0014

JEOL Ltd.
3-1-2 Musashino Akishima Tokyo 196-8558 Japan Sales Division Tel. +81-3-6262-3560 Fax. +81-3-6262-3577
www.jeol.com ISO 9001 • ISO 14001 Certified
▼ Local offces
• AUSTRALIA & NEW ZEALAND • BELGIUM • BRAZIL • CANADA • CHINA • EGYPT • FRANCE • GERMANY • GREAT BRITAIN & IRELAND • ITALY • KOREA • MALAYSIA • MEXICO • RUSSIA • SCANDINAVIA
• SINGAPORE • TAIWAN • THE NETHERLANDS • USA

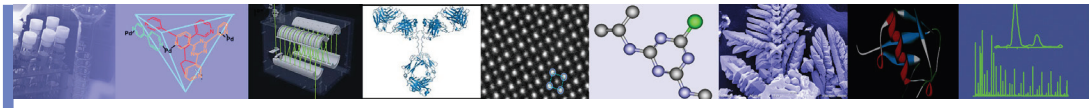

Applications Note

SpiralTOF-TOF

MALDI for Polymer Analysis: Synthetic Polymers and Additives

Introduction:

A high-resolution MALDI/TOF-TOF system with unique ion optics is applied to the identification of polymers and polymer additives. Exact mass measurements and isotopic abundances were used to identify elemental compositions. High-energy collision-induced dissociation with monoisotopic precursor selection provided structural information for additives and polymers. The mass accuracy for the sodiated molecule of Irganox 1010 in polymethyl methacrylate (PMMA) was within 1ppm of the calculated *m/z* (*m/z* 1199.7733, $C_{73}H_{108}O_{12}Na^+$). The high-energy CID product-ion mass spectrum for sodiated Irganox 1010 shows bond cleavage with little or no rearrangement. Four types of product ions are identified for the high-energy CID product-ion mass spectra of sodiated PMMA ions.

Experimental:

Samples were analyzed by using a MALDI/TOF-TOF (JEOL JMS-S3000 "Spiral TOF™ MS") mass spectrometer with multi-turn ion optics that fit a 17-meter flight path within a 1 meter space. Electrostatic sectors are used to continuously refocus the ion beam to minimize ion losses.

The MS-I resolving power is sufficiently high (60,000 FWHM) that monoisotopic precursor selection can be achieved by using a simple deflector. Ions with 20 keV kinetic energies undergo collisions with helium and a 9 keV post-acceleration combined with an offset parabolic reflector provides a wide energy acceptance for product ions.

Irganox1010 added to PMMA solution was used as a model sample, which included 5000 ppm as concentration of Irganox1010. 2,5-Dihydroxybenzoic acid (DHB) was used as the MALDI matrix and sodium iodide (NaI) was used as cationization agent.

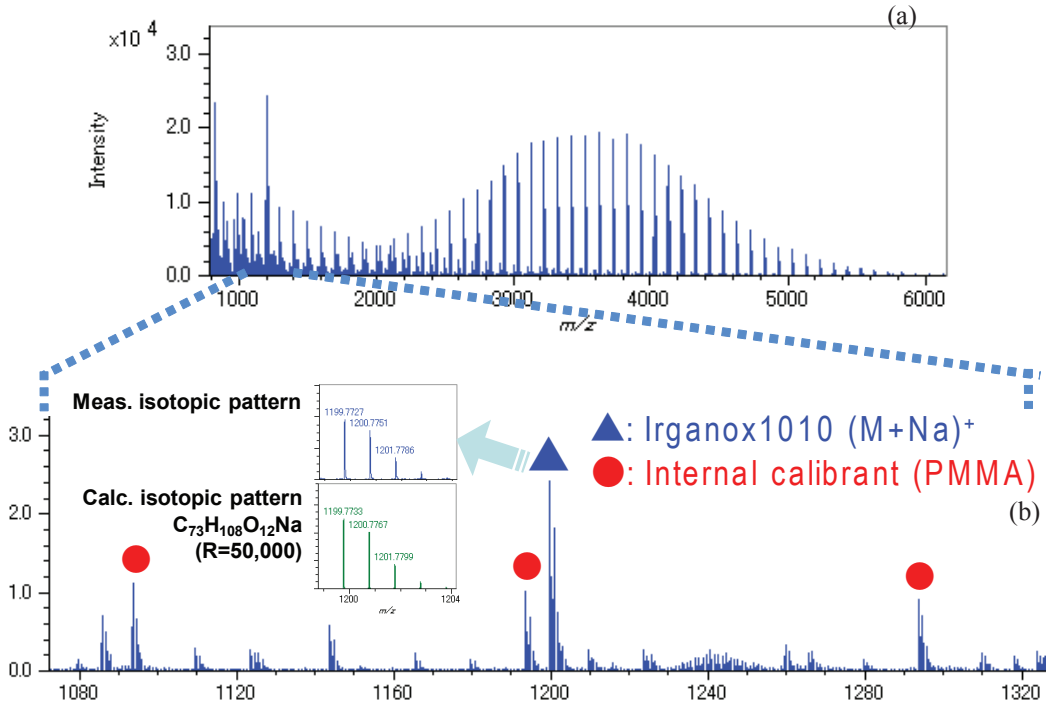

Figure 1. MALDI mass spectra of Irganox 1010 in PMMA solution (a) over all, (b) enlarged.

MS-110624A

Table 1. Accurate mass measurement results for sodium-cationized molecule of Irganox1010.

No.	Resolution @ *m/z* 1199.7733	Mass error (ppm)	
		Internal calib.	External calib.
1	52,762	-0.31	-1.23
2	48,061	-0.71	-0.72
3	49,726	-0.54	-1.20
4	51,716	-0.61	-2.10
5	50,911	-1.02	5.46
6	47,648	-0.16	5.41
7	49,394	0.13	3.19
8	51,403	0.35	3.62
9	53,594	-0.47	5.64
10	46,463	-0.28	2.13
Ave.	50,635	0.46	3.07

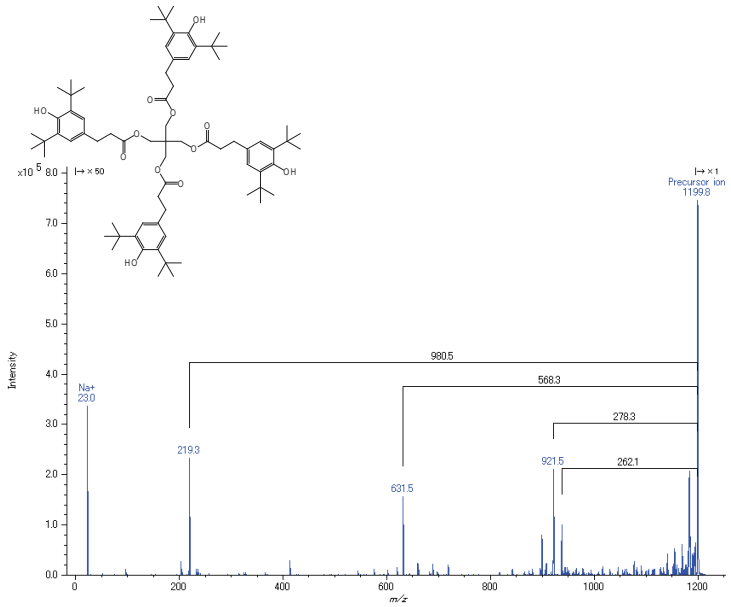

Figure 2. Product-ion spectrum and fragment ions of Irganox1010 in model sample (m/z 1199.8 ($[M+Na]^+$)).

Results:

(1) Additives

The phenolic antioxidant Irganox 1010 was detected as the sodiated molecule (*m/z* 1199.7733, $C_{73}H_{108}O_{12}Na^+$) in the model sample. The resolving power (FWHM) was approximately 50,000 for the $[M + Na]^+$ peak, well in excess of that needed to separate isotope peaks.

Accurate mass values of the monoisotopic ion of the sodiated molecule of Irganox 1010 were determined by using PMMA as either internal or external calibrant. The average mass errors were 0.46 ppm using internal calibration and 3.07 ppm using external calibration, respectively. Mass accuracy and isotopic abundances were sufficient to confirm the elemental composition of a sodiated molecule as $C_{73}H_{108}O_{12}Na$.

High-energy CID product-ion mass spectra were obtained with monoisotopic precursor selection for sodiated Irganox in the PMMA mass spectrum. All product ions were monoisotopic. The product-ion mass spectrum of sodiated Irganox 1010 was relatively simple due to the symmetric structure of the molecule.

(2) PMMA

High-energy CID product-ion mass spectra were obtained with monoisotopic precursor selection for the sodiated n=15 and n=23 species in the PMMA mass spectrum. All product ions were monoisotopic. Product-ion assignments corresponded to direct bond cleavage with minimal rearrangement. Four major fragment classes were observed in the high-energy CID product-ion mass spectra of sodiated PMMA (Fig,5). The *m/z* range for the product-ion mass spectra extended from the precursor *m/z* to *m/z* 23 (Na^+).

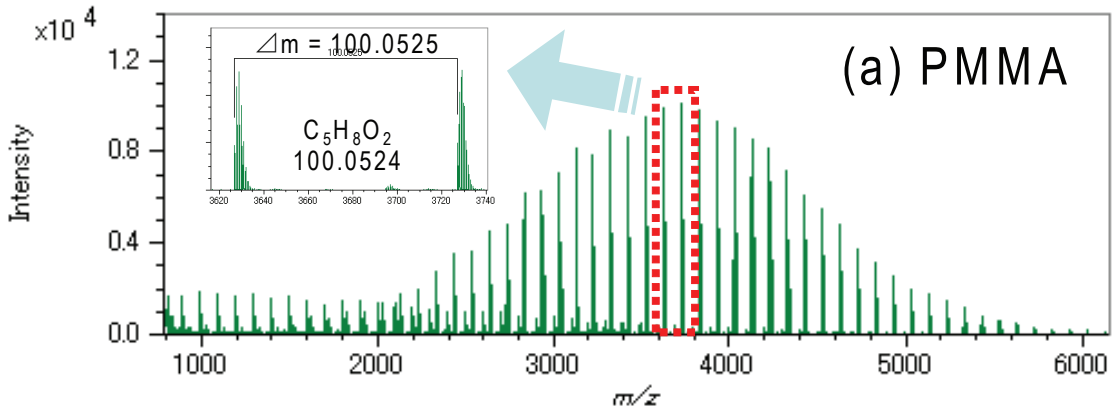

Figure 3. MALDI mass spectrum of PMMA.

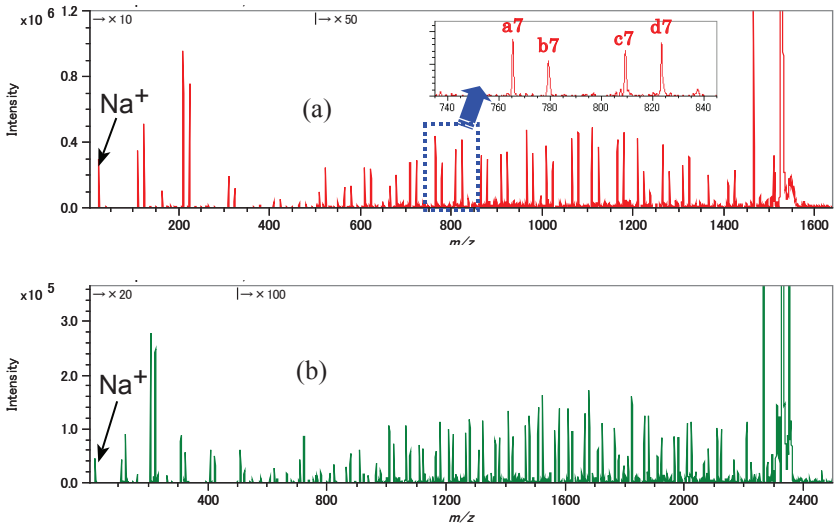

Figure 4. Product-ion spectra of PMMA,
(a) m/z 1525.8 (n=15, $[M+Na]^+$), (b) m/z 2326.2 (n=23, $[M+Na]^+$).

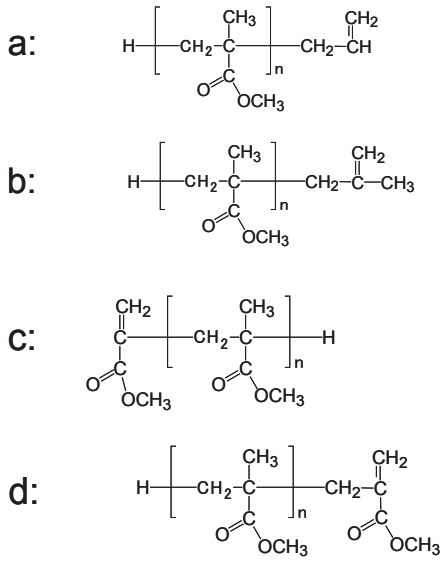

Figure 5. Structural formula of four major fragment classes.

Conclusion:
In this study we demonstrate accurate mass measurement for the polymer additive Irganox 1010 and structural analysis for PMMA and Irganox 1010.

- The SpiralTOF system provides ultra high resolution and high mass accuracy. It is very easy to perform accurate mass measurements. The sodium-cationized molecule of Irganox 1010 was detected with a mass accuracy of less than 1 ppm.

- MS/MS spectra were obtained by using the TOF-TOF option to provide structural information for PMMA

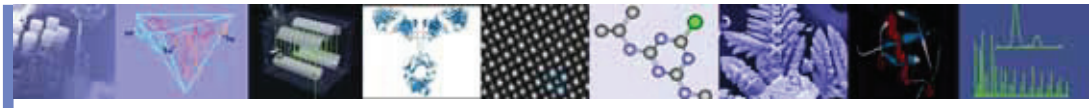

JEOL

Applications Note

SpiralTOF™

MALDI for Small Molecule Analysis: Triazine Pesticides

Introduction:

Matrix-Assisted Laser Desorption Ionization (MALDI) has been applied to a wide range of analyses and is particularly suitable for the qualitative analysis of high molecular weight samples. On the other hand, MALDI is generally considered unsuitable for low molecular weight compounds because the matrix ions interfere with sample ion detection in the low mass region. However, if these low *m/z* ions can be separated from each other and distinguished with sufficiently high mass resolving power, then MALDI can be expanded to the analysis of low-molecular-weight compounds. We have demonstrated this by using the JEOL MALDI SpiralTOF mass spectrometer The innovative Spiral orbital technology consisting of 4 sets of toroidal electrical sector and Matsuda plates provides ultra-high mass resolving power combined with high ion transmission.

Here we report the use of Spiral technology to collect high mass-resolving power and high mass-accuracy data for eight triazine compounds. Additionally, we report TOF-TOF data obtained with monoisotopic precursor ion selection to provide clear product-ion mass spectra for each compound.

Experimental:

Stock solutions of each of the triazine compounds listed in Table 1 were prepared at concentrations of 1 mg/ml in 2:1 methanol/water. Alpha-Cyano-4-hydroxyxinnamic acid (CHCA, formula = $C_{10}H_7NO_3$) was used as the MALDI matrix. CHCA was dissolved in 1:1 water/acetonitrile containing 0.1% trifluoroacetic acid at a concentration of 10 mg/mL. A 0.5 µL mixture of sample and CHCA (1/1, v/v) was deposited and dried on the MALDI target plate.

The SpiralTOF was operated in positive-ion mode using the full 17-meter flight path. Matrix peaks were used as internal mass reference standards for calibration with the native MS Tornado software.

Results:

(1) SpiralTOF

Accurate mass measurements for the compounds are shown in Table 1.The resolving power (FWHM) for each triazine was approximately 38,000 for the $[M+H]^+$ peak, well in excess of that needed to separate isotope peaks.

Accurate mass values for the protonated molecule of Triazines were determined by using CHCA matrix ions as an internal calibrant. The average mass errors were 0.55 ppm using internal calibration. Mass accuracy and isotopic abundances were sufficient to confirm the elemental composition of protonated molecules.

Table 1. Accurate mass measurement results for protonated molecule of Triazines.

No.	Name	Formula (M+H)	Meas. *m/z*	Error (mDa)	Error (ppm)	Mass resolving power
1	Ametryn	$C_9H_{17}N_5S + H$	228.12774	0.01	0.04	38,361
2	Atrazine	$C_8H_{14}ClN_5 + H$	216.10105	0.04	0.18	37,049
3	Prometon	$C_{10}H_{19}N_5O + H$	226.16624	-0.19	-0.84	36,062
4	Prometryn	$C_{10}H_{19}N_5S + H$	242.14339	0.06	0.24	36,481
5	Propazine	$C_9H_{16}N_5Cl + H$	230.11670	-0.18	-0.78	38,717
6	Simazine	$C_7H_{12}ClN_5 + H$	202.08540	0.21	1.02	37,754
7	Simetryn	$C_8H_{15}N_5S + H$	214.11209	-0.16	-0.73	38,330
8	Terbutryn	$C_{10}H_{19}N_5S + H$	242.14339	-0.14	-0.59	43,185
Average				0.12	0.55	38,242

MS-111020

(2) TOF-TOF

The TOF-TOF product-ion mass spectra are shown in Figures1-8, and are compared with the corresponding EI mass spectra from the 2011 NIST/EPA/NIH Mass Spectral database. High-energy collision-induced dissociation (CID) mass spectra obtained in the TOF/TOF mode are rich in structurally-significant fragments and show less rearrangement than low-energy CID spectra measured on other types of mass spectrometers. Almost all fragment ions were generated by simple cleavage of chemical bonds by 20 kV high-energy CID.

All of the protonated molecules for the triazines showed a loss of CH_4 (16), *m/z* 15 (CH_3), *m/z* 27 (C_2H_3) and *m/z* 43 (C_3H_7) in the TOF-TOF spectra. Loss of C_3H_6 (42) and loss of C_3H_8N (58) were observed in all of the triazines except simazine, simetryn and terbutryn because these compounds do not have the $NHCH(CH_3)_2$ functional group in their structure. The simazine and simetryn spectra show a losses of C_2H_5 (29) and C_2H_6N (44) from the $NHCH_2CH_3$ functional group. In the atrazine, propazine and simazine mass spectra loss of Cl (35) was observed. Terbutryn showed a loss of C_4H_8 (56) .

Conclusion:

In this study we have demonstrated the potential of TOF/TOF high-energy CID for structural analysis for small molecules.

"SpiralTOF" mode provides

- Ultra high resolving power sufficient to separate analyte ions and matrix ions.
- Routine high mass accuracy (less than 1ppm)

"SpiralTOF-TOF" mode provides

- Monoisotopic precursor selection
- True high-energy (20 kV) CID
- Absence of artifacts from post-source decay (PSD)

Structural analysis of small molecules is easily performed by using the TOF-TOF method. The high-energy CID provided by the JEOL Spiral TOF-TOF produces information-rich structurally significant fragmentation for small molecules that is often directly comparable to EI mass spectra.

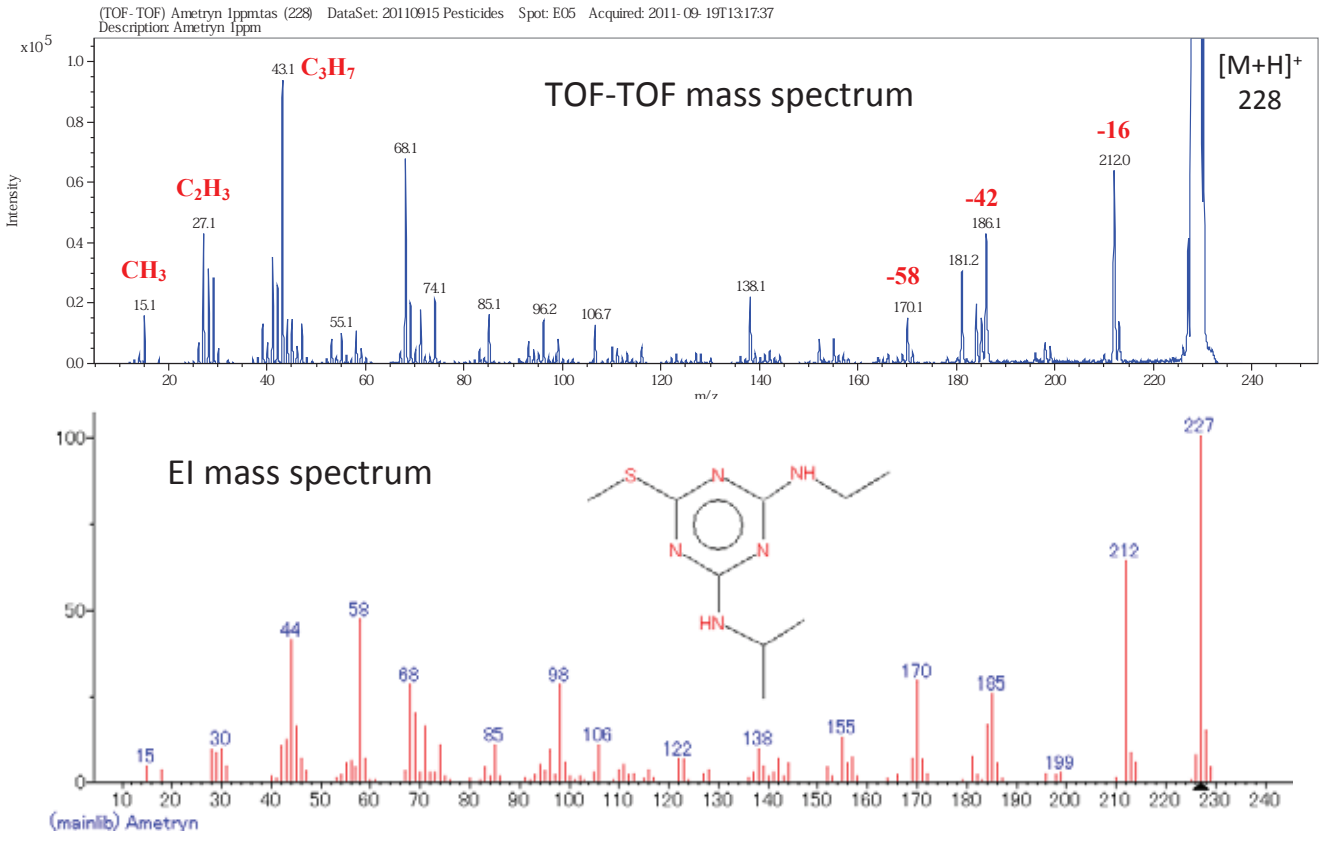

Figure 1. Mass spectra of Ametryn. Top: MALDI TOF-TOF spectrum Bottom: EI Spectrum

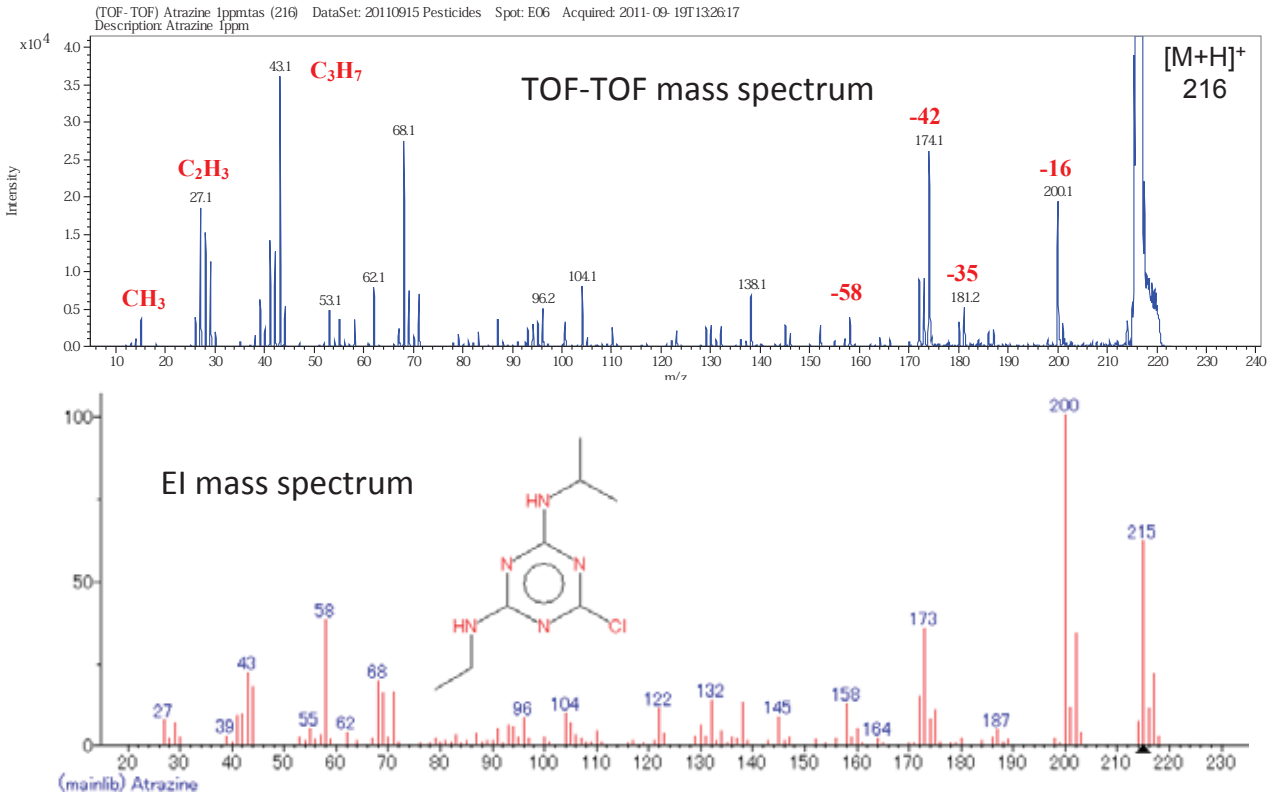

Figure 2. Mass spectra of Atrazine. Top: MALDI TOF-TOF spectrum Bottom: EI Spectrum

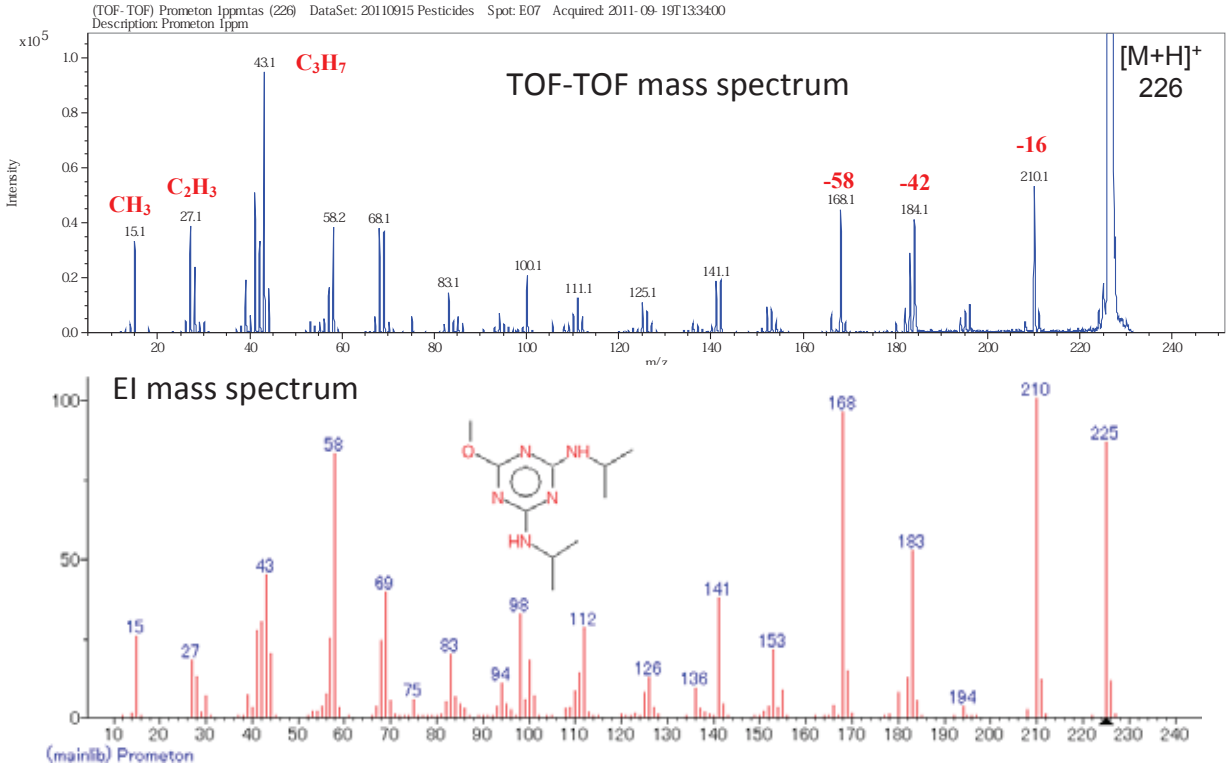

Figure 3. Mass spectra of Prometon. Top: MALDI TOF-TOF spectrum Bottom: EI Spectrum

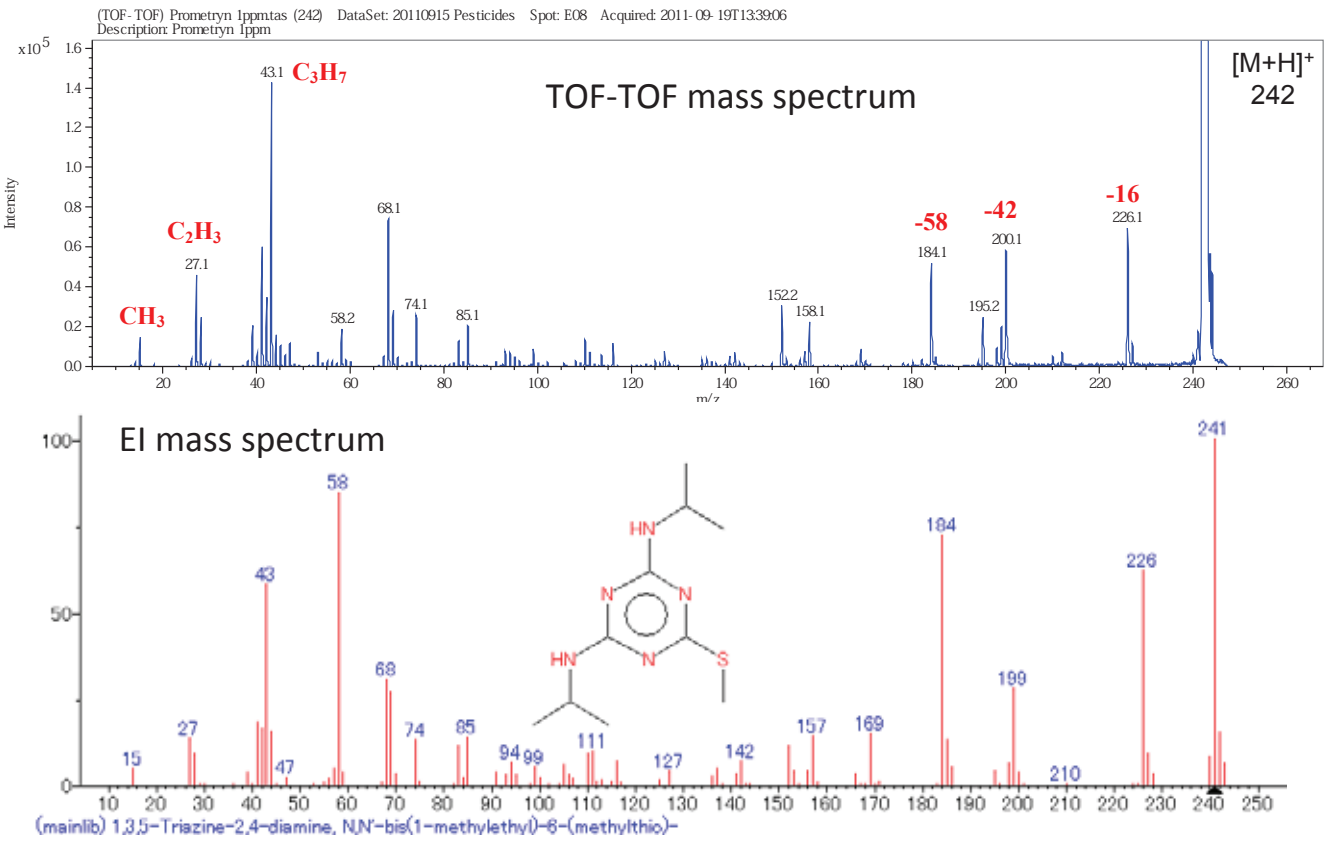

Figure 4. Mass spectra of Prometryn. Top: MALDI TOF-TOF spectrum Bottom: EI Spectrum

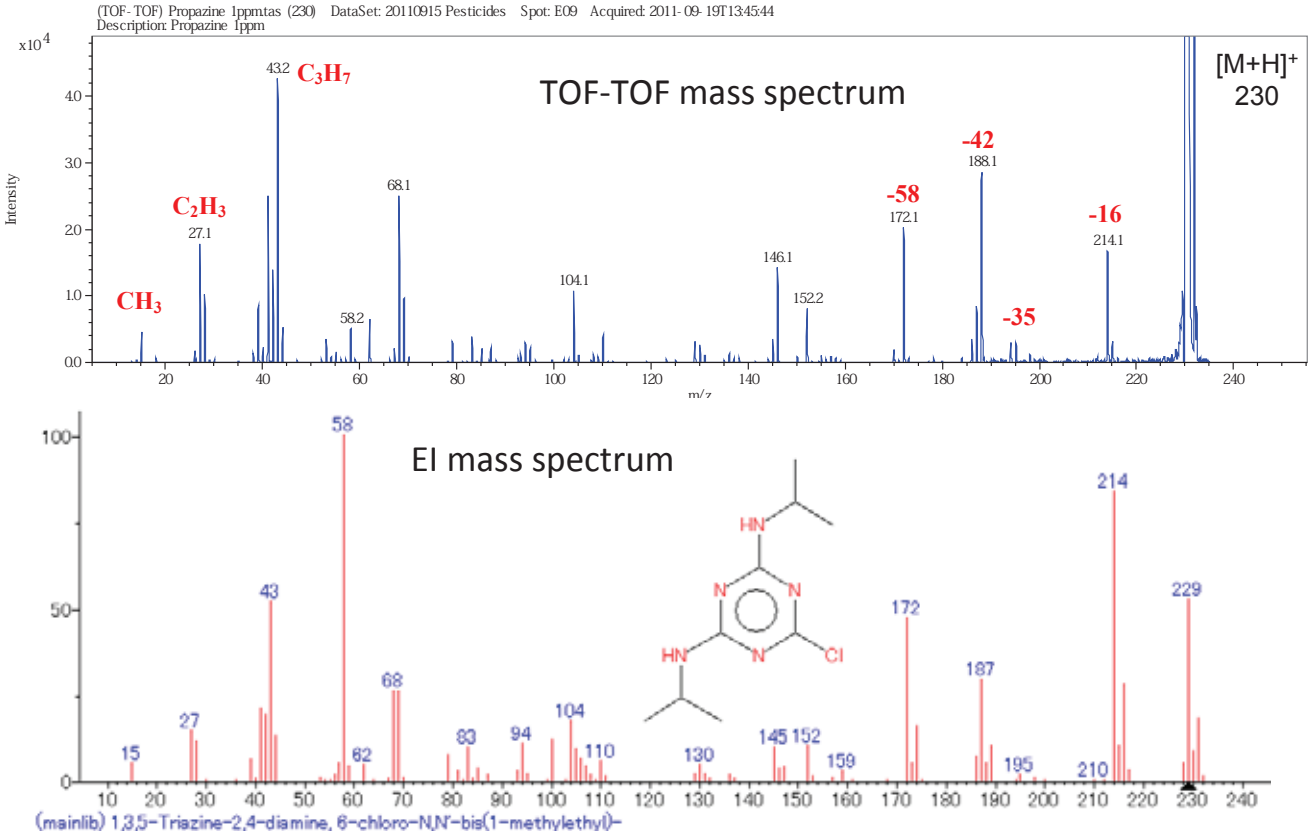

Figure 5. Mass spectra of Propazine. Top: MALDI TOF-TOF spectrum Bottom: EI Spectrum

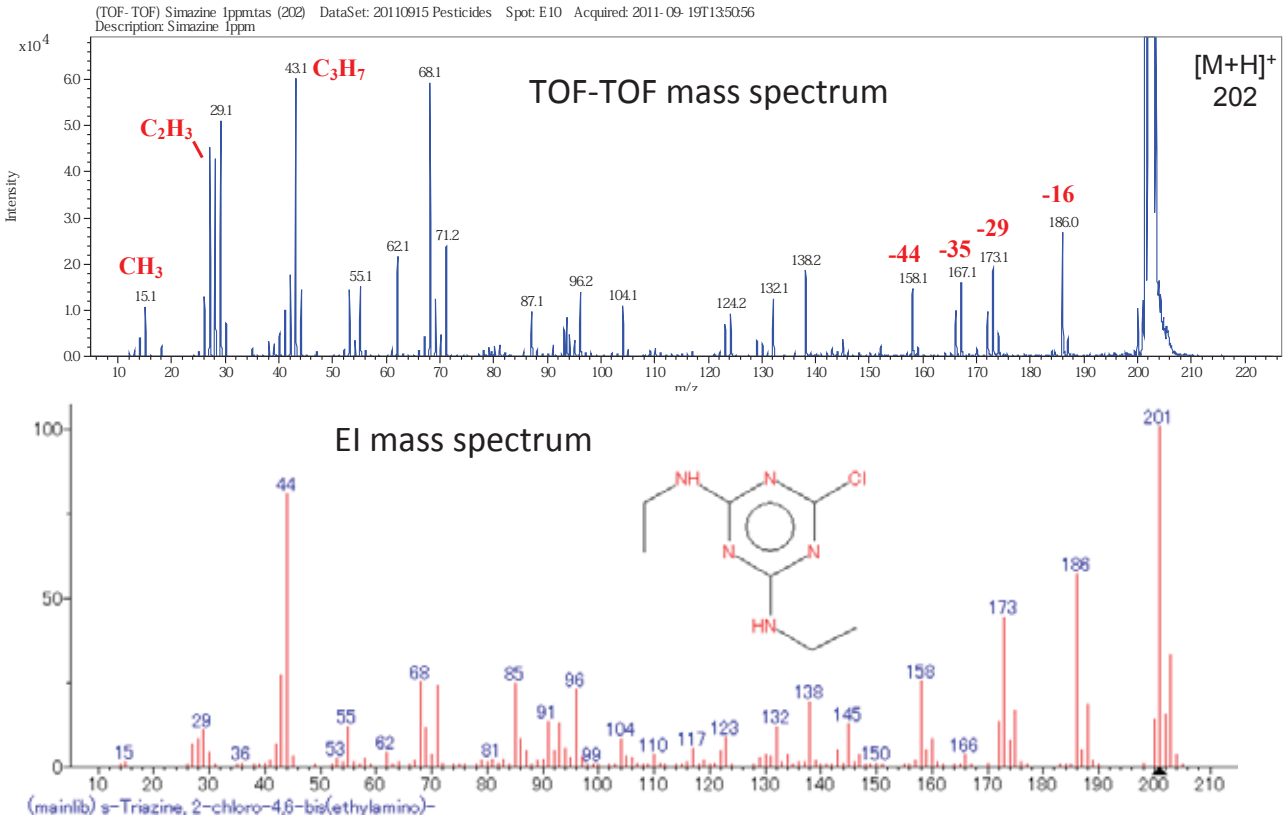

Figure 6. Mass spectra of Simazine. Top: MALDI TOF-TOF spectrum Bottom: EI Spectrum

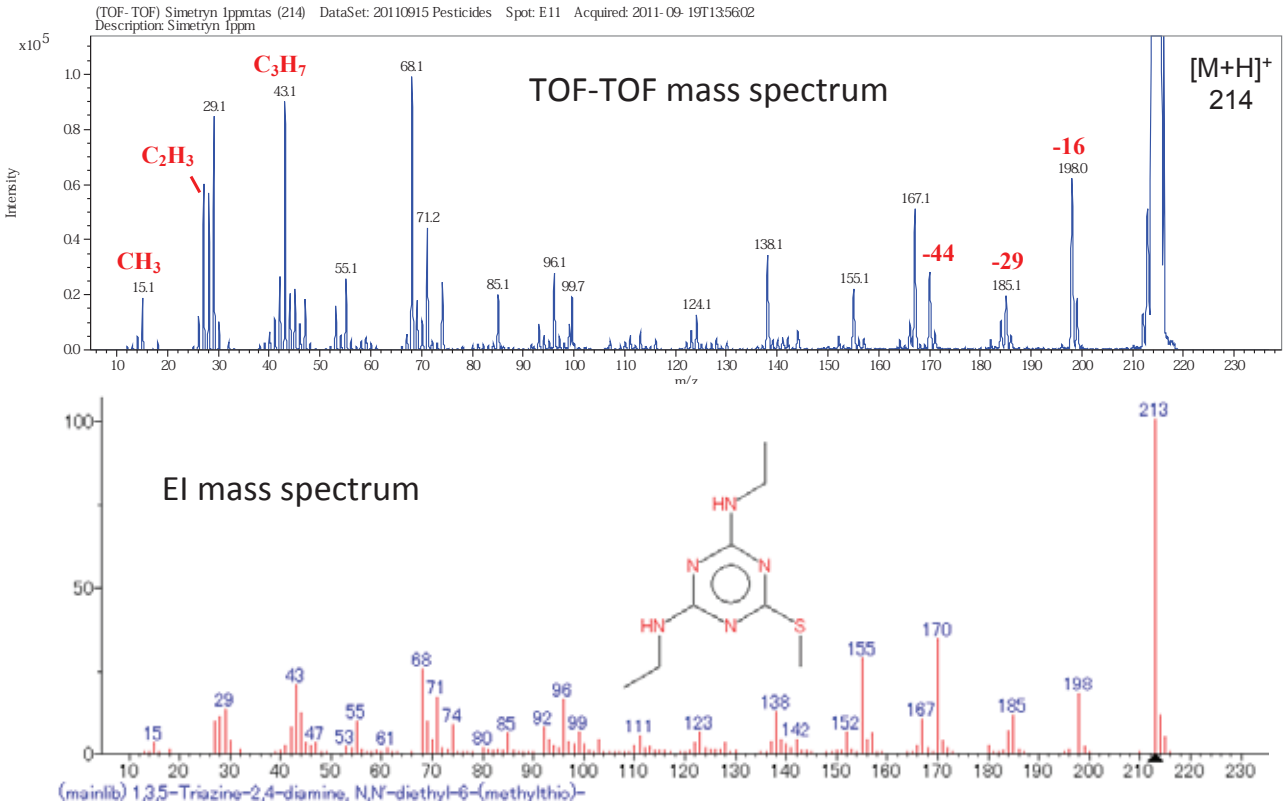

Figure 7. Mass spectra of Simetryn. Top: MALDI TOF-TOF spectrum Bottom: EI Spectrum

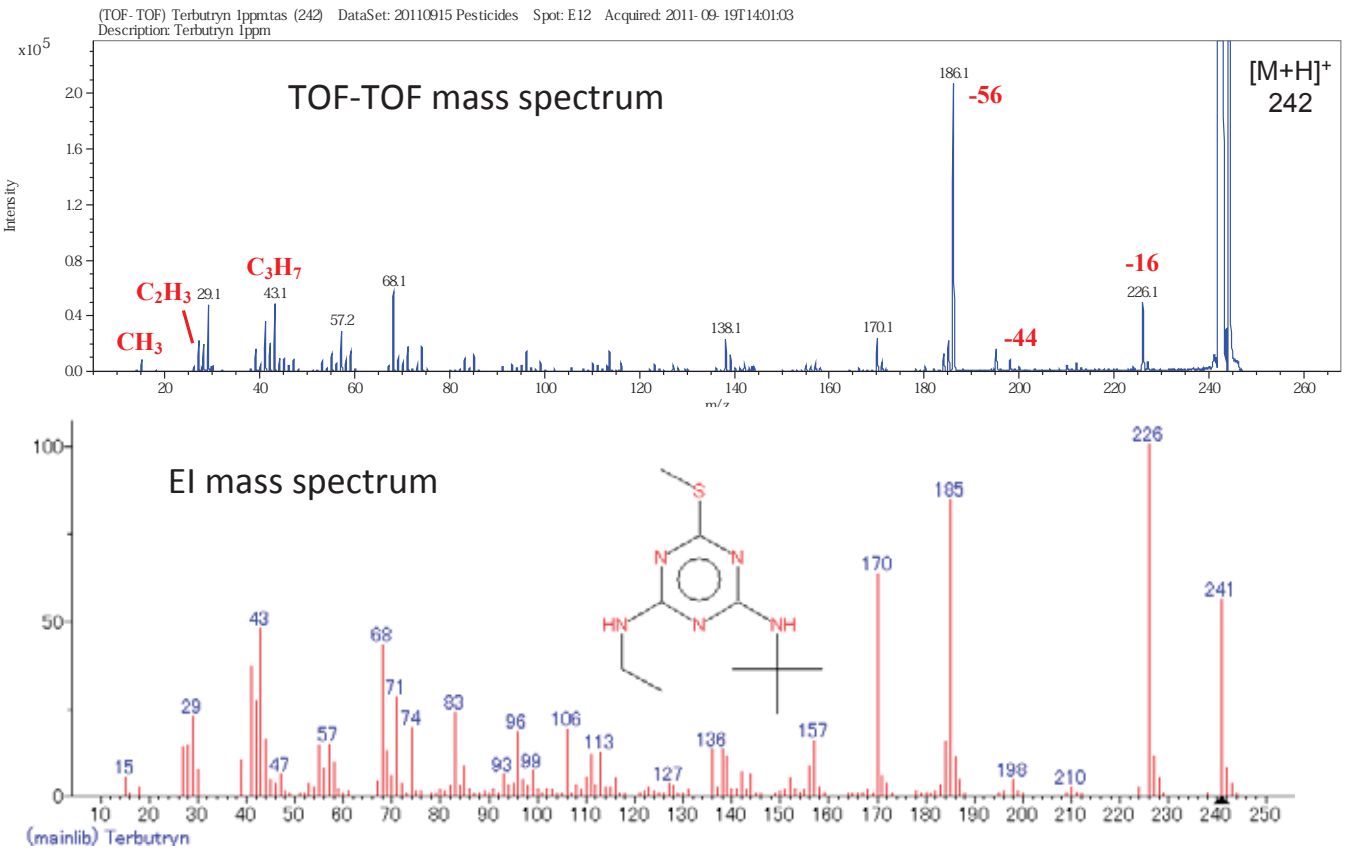

Figure 8. Mass spectra of Terbutryn. Top: MALDI TOF-TOF spectrum Bottom: EI Spectrum

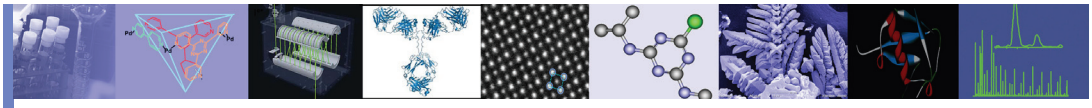

JEOL

Applications Note

SpiralTOF-TOF

High-Energy CID MS/MS Analysis of Small Organic Molecules

Introduction

The JMS-S3000 SpiralTOF™ is a MALDI-TOF MS that uses an innovative spiral ion optics system to achieve the highest resolution currently available for a MALDI instrument. As a result, small organic molecules can be analyzed on this system with minimal interferences from the matrix peaks. Additionally, the JMS-S3000 is available with a TOF-TOF option that can acquire high-energy collision-induced dissociation (CID) product ion spectra for monoisotopically selected precursor ions. In this work, we analyzed several small organic molecules by using the JMS-S3000 with the TOF-TOF option.

Results and Discussion

The proline sample was measured using positive ion mode which produced an $[M+H]^+$ ion at *m/z* 116. This ion was monoisotopically selected as the precursor ion for TOF-TOF analysis. The resulting high-energy CID product ion spectrum is shown in Fig. 2a. The overall MS/MS spectrum was very simple for this sample with the low mass ions *m/z* 43 and *m/z* 70 attributed to the fragments shown in Fig. 3.

[Samples]

Compound1	Proline
Compound2	Stearic acid

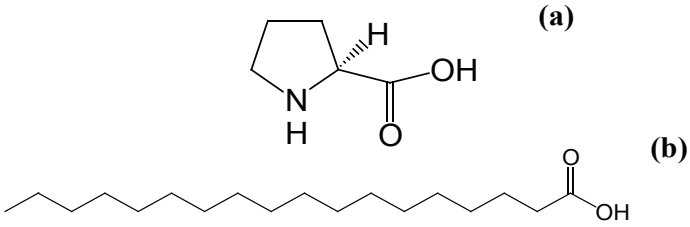

Figure 1. Structural formula of (a) Proline and (b) Stearic acid.

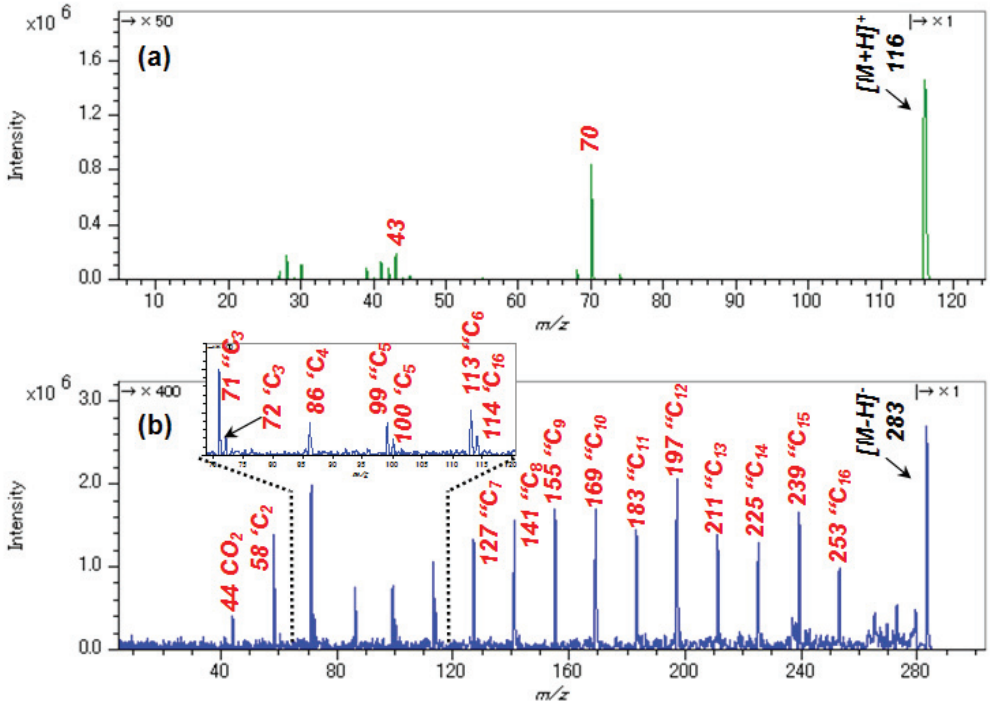

Figure 2. Product ion spectra of (a) Proline (*m/z* 116 $[M+H]^+$) and (b) Stearic acid (*m/z* 283 $[M-H]^-$).

MS Tips 173

The stearic acid sample was then measured using negative ion mode which produced an $[M-H]^-$ ion at *m/z* 283. This ion was monoisotopically selected as the precursor ion for TOF-TOF analysis. The resulting high-energy CID product ion spectrum is shown in Fig. 2b. This spectrum showed a mass spectral pattern that was attributed to charge remote fragmentation (CRF) by high-energy CID. CRF occurs during CID when the charge is localized to a particular location on the molecule (in this case on the $–COO^-$) and the bonds that are cleaved are located at positions away from this charge.[1,2] This technique is very useful for structural analysis. Fig. 4 shows the identity of each peak based on the overall structure of stearic acid.

Conclusions

The JMS-S3000 "SpiralTOF" with TOF-TOF option can be used to measure both the $[M+H]^+$ and $[M-H]^-$ precursor ions even for small organic molecules. Furthermore, this technique can be used to acquire high-energy CID product ion spectra that show CRF which involves the systematic cleavage of C-C bonds within the molecular structure.

Reference

1) W. J. Griffiths, Y. Yang, J. A. Lindgren, and J. Sjövall, Rapid Commun. Mass Spectrom., 10, 21-28, (1996).
2) M. Gross, Int. J. of Mass Spectrom., 200(1–3), 611–624, (2000).

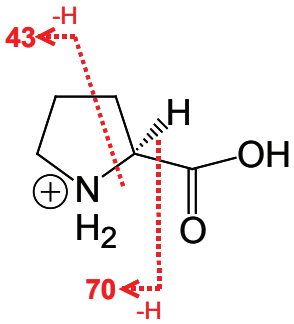

Figure 3. Fragment ions of Proline (*m/z* 116 [M+H]+).

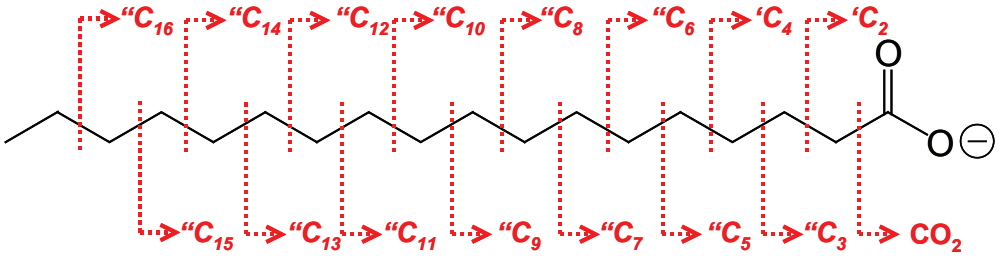

Figure 4. MASCOT MS/MS Ion search result of tBSA by TOF-TOF mode.

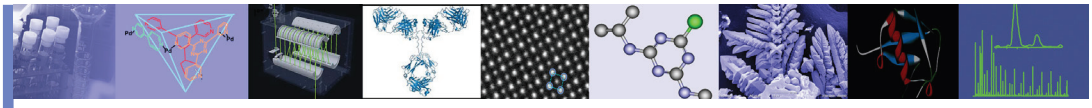

Applications Note

SpiralTOF™

MALDI for Small Molecule Analysis: A Complex Drug Mixture

Introduction: Matrix-Assisted Laser Desorption Ionization (MALDI) applications to small molecule analysis are often considered to be limited by low-mass matrix ions that can be isobaric with the target analytes. However, with sufficient resolving power, matrix ions and analyte ions can be separated. Additionally, these resolved matrix ions can serve as internal mass reference standards for exact mass measurements.

The SpiralTOF's unique multi-turn ion optics package a very long (17-meter) flight path within a 1-meter space. Electric sectors and Matsuda plates provide perfect focusing to eliminate ion loss due to beam divergence. Post-source decay fragments occurring in the flight path are eliminated by the ion optics, providing a clean and artifact-free background.

This is shown here for the high-resolution analysis of a mixture of 32 small-molecule drugs analyzed by MALDI with the JEOL SpiralTOF mass spectrometer.

Table 1. Compounds analyzed.

Solution	Compound	Formula
Benzodiazepines Mix #1 (0.25 mg/ml)	Alprazolam	C17H13ClN4
	Clonazepam	C15H10ClN3O3
	Diazepam	C16H13ClN2O
	Flunitrazepam	C16H12FN3O3
	Lorazepam	C15H10Cl2N2O2
	Nitrazepam	C15H11N3O3
	Oxazepam	C15H11ClN2O2
	Temazepam	C16H13ClN2O2
Capillary Drug Mix #1 (0.1 mg/ml)	Caffeine	C8H10N4O2
	Carbamazepine	C15H12N2O
	Cocaine	C17H21NO4
	Despiramine	C18H22N2
	EDDP	C20H24N
	Glutethimide	C13H15NO2
	Lidocaine	C14H22N2O
	Methadone	C21H27NO
	Methaqualone	C16H14N2O
	Phenobarbital	C12H12N2O3
Stimulants Mix (0.1 mg/ml)	*d*-Amphetamine	C9H13N
	d-Methamphetamine	C10H15N
	Caffeine	C8H10N4O2
	Methylphenidate	C14H19NO2
	Cocaine	C17H21NO4
Opiates Mix #1 (0.1 mg/ml)	Codeine	C18H21NO3
	Ethyl morphine	C19H23NO3
	Meperidine	C15H21NO2
	Methadone	C21H27NO
	Morphine	C17H19NO3
Opiates Mix #2 (0.1 mg/ml)	Codeine	C18H21NO3
	Diacetylmorphine	C21H23NO5
	Hydromorphone	C17H19NO3
	Morphine	C17H19NO3
	Nalorphine	C19H21NO3
	Oxycodone	C18H21NO4

MS-110623A

Experimental: Grace Quik-Chek™ DEA-exempt drug standards were used to create the drug mixture. One µl of each of the following drug mixtures was added to a vial: Benzodiazepines Mix #1, Opiates Mix #1, Opiates Mix #2, Stimulants Mix and Capillary Drug Mix. A list of compounds, formulas and concentrations is given in Table 1. 25 µl of a 10 mg/ml solution of the MALDI matrix α-cyano-4-hydroxycinnamic acid (CHCA, formula = $C_{10}H_7NO_3$) in 1:1 water/acetonitrile containing 0.1% trifluoroacetic acid was added to the vial, and a 0.5 µl aliquot was applied to the MALDI plate and allowed to dry.

The SpiralTOF was operated in positive-ion mode using the full 17-meter flight path, a MALDI delayed extraction time of 20 ns and a laser power attenuation of 31%. Matrix peaks were used as internal mass reference standards for calibration with the native MS Tornado software. Mass spectra were exported in plain text format for further processing with Mass Spec Tools II software (version 1.0.5.2). A Microsoft Excel spreadsheet was created with the names and elemental compositions of the target compounds to permit compound searching by the Mass Spec Tools II software based on exact mass measurements.

Results: All but two of the 32 compounds in the target mass list were identified as protonated or sodiated molecules with measured exact masses within 0.001 of the expected *m/z* (Figure 1, Table II). The two exceptions were phenobarbital and glutethimide. Phenobarbital is a weak acid, and it is possible that it does not protonate under these conditions. Glutethimide has a similar chemical structure to phenobarbital.

High resolving power is required to separate target compounds from interfering isobaric peaks. For example, the ^{35}Cl peak for protonated oxazepam occurs at *m/z* 287.0587 and the ^{37}Cl peak for protonated diazepam occurs at 287.0770. These peaks are well separated with a resolving power in excess of 40,000 (Figure 2).

Conclusion: The high resolving power available from the SpiralTOF's multi-turn 17-meter flight path permitted the detection of all but two compounds in the 32-component mixture without interference from matrix peaks or post-source decay. The remaining two compounds are apparently not ionized under these conditions. Two isomeric pairs of compounds (morphine/hydromorphone and codeine/hydrocodone) cannot be distinguished solely by high-resolution exact mass measurements. All of the compounds were detected with measured masses within 0.001 of the calculated values.

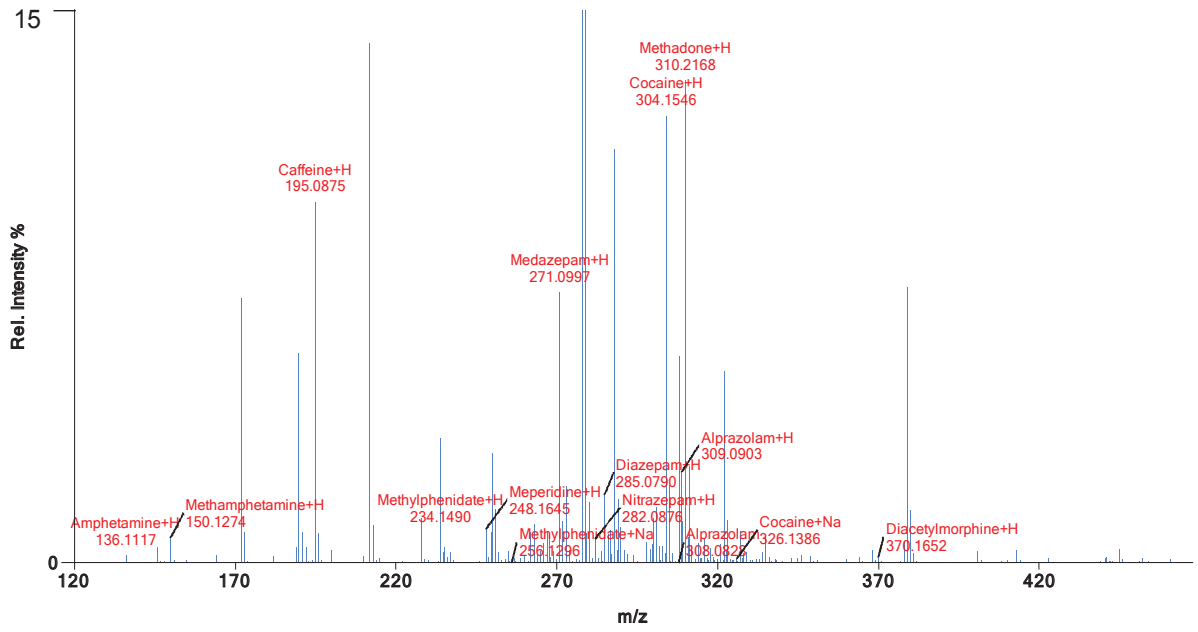

Figure 1. Enlarged view of the mass spectrum of the 32-drug mixture. The base peak is for EDDP at *m/z* 278.1906.

Table 2. Assignments for compounds detected in the drug mixture.

Name	Composition	Adduct	Measured	Calculated	mmu	Abund.
Alprazolam	C17H13ClN4	+H	309.09033	309.09071	0.38	2.631
Alprazolam	C17H13ClN4	+Na	331.07220	331.07265	0.45	0.089
Alprazolam	C17H13ClN4		308.08279	308.08289	0.09	0.012
Amphetamine	C9H13N	+H	136.11168	136.11262	0.94	0.228
Bromazepam	C14H10BrN3O	+H	316.00836	316.00856	0.20	0.403
Bromazepam	C14H10BrN3O		315.00269	315.00073	-1.95	0.009
Caffeine	C8H10N4O2	+H	195.08751	195.08819	0.68	10.431
Caffeine	C8H10N4O2		409.16174	409.16100	-0.74	0.012
Carbamazepine	C15H12N2O	+H	237.10271	237.10278	0.07	0.299
Carbamazepine	C15H12N2O	+Na	259.08472	259.08472	0.01	0.147
Carbamazepine	C15H12N2O		236.09561	236.09496	-0.66	0.023
Clonazepam	C15H10ClN3O3	+H	316.04871	316.04890	0.20	0.668
Cocaine	C17H21NO4	+H	304.15463	304.15489	0.26	12.930
Cocaine	C17H21NO4	+Na	326.13858	326.13683	-1.75	0.118
Codeine	C18H21NO3	+H	300.15982	300.15996	0.13	1.303
Codeine	C18H21NO3	+Na	322.14267	322.14190	-0.77	0.091
Despiramine	C18H22N2	+H	267.18558	267.18611	0.53	0.927
Diacetylmorphine	C21H23NO5	+H	370.16522	370.16545	0.23	0.160
Diacetylmorphine	C21H23NO5	+Na	392.14761	392.14739	-0.22	0.020
Diazepam	C16H13ClN2O	+H	285.07904	285.07948	0.44	1.975
Diazepam	C16H13ClN2O	+Na	307.06247	307.06142	-1.05	0.031
EDDP	C20H24N		278.19061	278.19089	0.27	100.000
Ethyl morphine	C19H23NO3	+H	314.17581	314.17561	-0.20	0.575
Ethyl morphine	C19H23NO3	+Na	336.15683	336.15755	0.72	0.048
Flunitrazepam	C16H12FN3O3	+H	314.09390	314.09410	0.20	0.572
Hydrocodone	C18H21NO3	+H	300.15982	300.15996	0.13	1.303
Hydrocodone	C18H21NO3	+Na	322.14267	322.14190	-0.77	0.091
Hydromorphone	C17H19NO3	+H	286.14413	286.14433	0.20	0.821
Hydromorphone	C17H19NO3	+Na	308.12628	308.12627	-0.01	0.127
Lidocaine	C14H22N2O	+H	235.18031	235.18104	0.73	0.469
Lidocaine	C14H22N2O	+Na	257.16263	257.16299	0.36	0.066
Lorazepam	C15H10Cl2N2O2	+H	321.01965	321.01976	0.10	0.546
Lorazepam	C15H10Cl2N2O2	+Na	343.00116	343.00170	0.54	0.144
Medazepam	C16H15ClN2	+H	271.09970	271.10020	0.50	7.822
Meperidine	C15H21NO2	+H	248.16452	248.16505	0.53	0.980
Meperidine	C15H21NO2	+Na	270.14542	270.14700	1.58	0.021
Methadone	C21H27NO	+H	310.21683	310.21708	0.26	13.963
Methamphetamine	C10H15N	+H	150.12743	150.12828	0.85	0.736
Methaqualone	C16H14N2O	+H	251.11768	251.11844	0.76	1.553
Methylphenidate	C14H19NO2	+H	234.14902	234.14941	0.39	0.863
Methylphenidate	C14H19NO2	+Na	256.12961	256.13136	1.75	0.008
Morphine	C17H19NO3	+H	286.14413	286.14433	0.20	0.821
Morphine	C17H19NO3	+Na	308.12628	308.12627	-0.01	0.127
Nalorphine	C19H21NO3	+H	312.15970	312.15996	0.26	0.521
Nalorphine	C19H21NO3	+Na	334.14178	334.14190	0.11	0.033
Nitrazepam	C15H11N3O3	+H	282.08759	282.08787	0.29	0.692
Nitrazepam	C15H11N3O3	+Na	304.06805	304.06982	1.76	0.259
Oxazepam	C15H11ClN2O2	+H	287.05865	287.05873	0.07	0.946
Oxazepam	C15H11ClN2O2	+Na	309.04092	309.04067	-0.25	0.147
Oxycodone	C18H21NO4	+H	316.15509	316.15489	-0.20	0.406
Oxycodone	C18H21NO4	+Na	338.13562	338.13683	1.21	0.069
Temazepam	C16H13ClN2O2	+H	301.07379	301.07438	0.59	1.591
Temazepam	C16H13ClN2O2	+Na	323.05618	323.05633	0.14	0.252

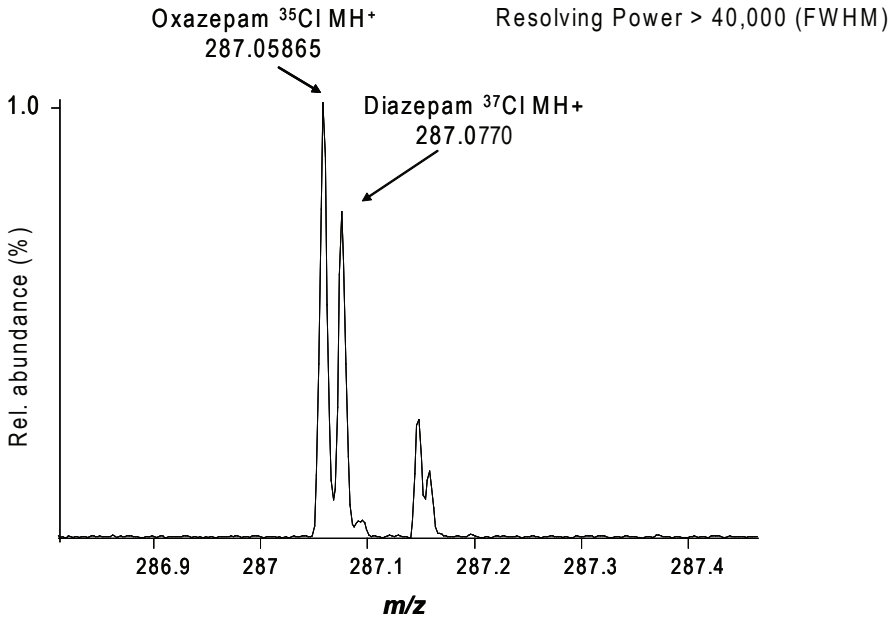

Figure 2. Separation of isotopic peaks for oxazepam and diazepam.

JEOL MS Data Sheet

MS Tips

Mass Spectrometry Application Group
Mass Spectrometry Business Unit
JEOL Ltd. www.jeol.com

No. 168 (1, 04/10)

JMS-S3000 Application Data

Accurate mass measurement of small organic molecules using JMS-S3000 "SpiralTOF™"

While MALDI-TOFMS are widely used for the analysis of high molecular weight analytes (e.g., biopolymers, synthetic polymers), analysis of small molecules are also possible. The JMS-S3000 is a MALDI-TOFMS employing an unique SpiralTOF™ ion optical system and can provide highly accurate mass measurement over wide *m/z* range. An accurate mass measurement and elemental composition calculation of a small molecule is demonstrated in this application note.

Diphenhydramine was used as an "unknown" sample and α-Cyano-4-hydroxycinnamic acid (CHCA) was used as the matrix. The data was processed using "msTornado Analysis", the data reduction software program for JMS-S3000, as shown in Fig. 1.

The mass spectrum (Fig. 1 [A]) shows peaks derived from CHCA as well as that derived from diphenhydramine at *m/z* 256. The accurate m/z of the monoisotopic protonated diphennydramine was determined as 256.1687 by performing a *m/z* calibration using $[M+H]^+$ and $[2M+H]^+$ ions of CHCA as internal *m/z* references. Possible elemental composition was calculated using the constraints shown in Fig. 1 [B] and a unique result of $C_{17}H_{22}NO$ was obtained with the error below 0.001 (u) (Fig. 1 [C]). This agrees with the elemental formula of protonated diphenhydramine (Fig. 2).

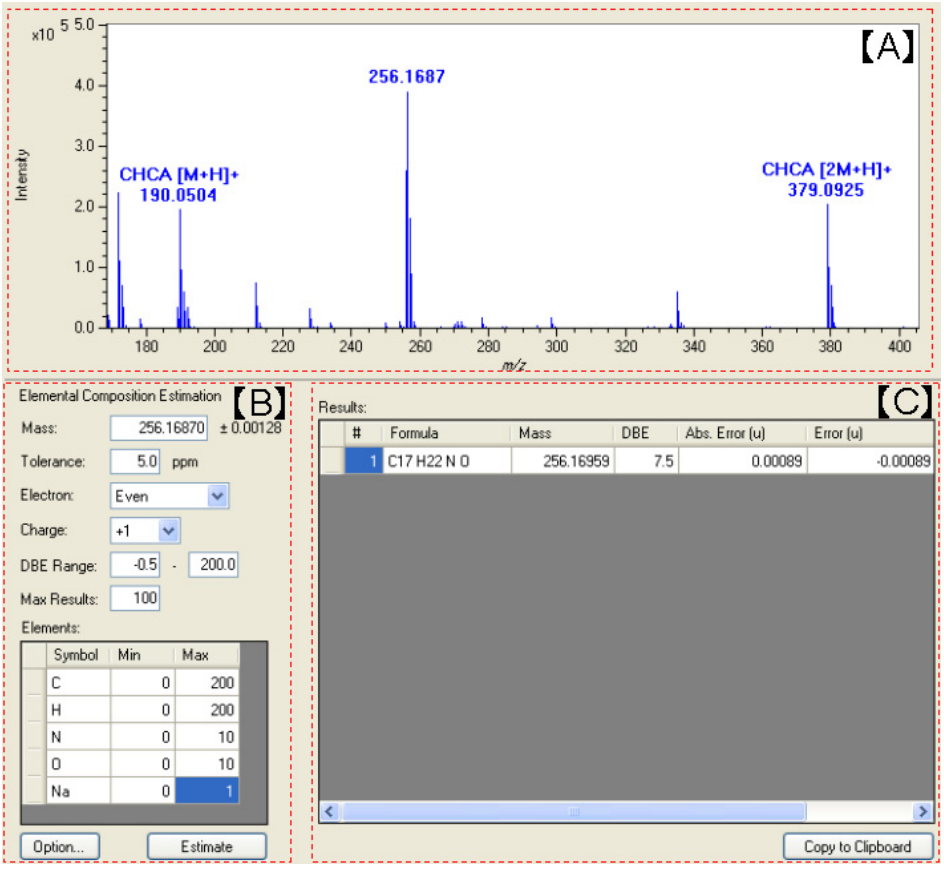

Fig.1 "msTornado Analysis" software windows

The JMS-S3000 "SpiralTOF" can provide sufficient mass accuracy for determining elemental compositions of "unknown" small molecules.

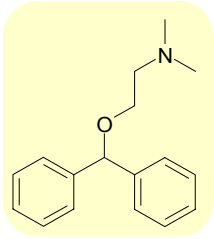

Fig.2 The structure of Diphenhydramine **($C_{17}H_{21}NO$)**

Certain products in this brochure are controlled under the "Foreign Exchange and Foreign Trade Law" of Japan in compliance with international security export control. JEOL Ltd. must provide the Japanese Government with "End-user's Statement of Assurance" and "End-use Certificate" in order to obtain the export license needed for export from Japan. If the product to be exported is in this category, the end user will be asked to fill in these certificate forms.

JEOL Ltd.

3-1-2 Musashino Akishima Tokyo 196-8558 Japan Sales Division Tel. +81-3-6262-3560 Fax. +81-3-6262-3577

www.jeol.com ISO 9001 • ISO 14001 Certified

• **AUSTRALIA & NEW ZEALAND** /JEOL (AUSTRALASIA) Pty.Ltd, Suite 1, L2 18 Aquatic Drive - Frenchs Forest NSW 2086 Australia • **BELGIUM** /JEOL (EUROPE) B.V, Planet II, Gebouw B Leuvensesteenweg 542, B-1930 Zaventem Belgium • **BRAZIL** /JEOL Brasil Instrumentos Cientificos Ltda. Av. Jabaquara, 2958 5º andar conjunto 52 ; 04046-500 Sao Paulo, SP Brazil • **CANADA** /JEOL CANADA, INC. 3275 1ere Rue, Local #8 St-Hubert, QC J3Y-8Y6, Canada • **CHINA** /JEOL (BEIJING) CO., LTD. Zhongkeziyuan Building South Tower 2F, Zhongguancun Nansanjie Street No. 6, Haidian District, Beijing, P.R.China • **EGYPT** /JEOL SERVICE BUREAU 3rd Fl. Nile Center Bldg., Nawal Street, Dokki, (Cairo), Egypt • **FRANCE** /JEOL (EUROPE) SAS Espace Claude Monet, 1 Allee de Giverny 78290, Croissy-sur-Seine, France • **GERMANY** /JEOL (GERMANY) GmbH Gute Aenger 30 85356 Freising, Germany • **GREAT BRITAIN & IRELAND** /JEOL (U.K.) LTD. JEOL House, Silver Court, Watchmead, Welwyn Garden City, Herts AL7 1LT, U.K. • **INDIA** /JEOL INDIA PVT. LTD. Unit No.305, 3rd Floor, ABW Elegance Tower, Jasola District Centre, New Delhi 110 025, India /JEOL INDIA PVT. LTD. Hyderabad Office 422, Regus Solitaire Business centre, 1-10-39 to 44, level 4, Gumidelli Towers, Old Airport Road, Begumpet, Hyderabad - 500016, India • **ITALY** /JEOL (ITALIA) S.p.A. Palazzo Pacinotti - Milano 3 City, Via Ludovico il Moro, 6/A 20080 Basiglio(MI) Italy • **KOREA** /JEOL KOREA LTD. Dongwoo Bldg. 7F. 1443, Yangjae Daero, Gangdong-Gu, Seoul, 05355, Korea • **MALAYSIA** /JEOL (MALAYSIA) SDN.BHD. 508, Block A, Level 5, Kelana Business Center, 97, Jalan SS 7/2, Kelana Jaya, 47301 Petaling Jaya, Selangor, Malaysia • **MEXICO** /JEOL DE MEXICO S.A. DE C.V. Arkansas 11 Piso 2 Colonia Napoles Delegacion Benito Juarez, C.P. 03810 Mexico D.F., Mexico • **QATAR** /Mannai Trading Company W.L.L., ALI Emadi Complex, Salwa Road P.O.Box 76, Doha, Qatar • **RUSSIA** /JEOL (RUS) LLC Krasnoproletarskaya Street, 16, Bld. 2, 127473, Moscow, Russian Federation • **SCANDINAVIA** /SWEDEN JEOL (Nordic) AB Hammarbacken 6A, Box 716, 191 27 Sollentuna Sweden • **SINGAPORE** /JEOL ASIA PTE.LTD. 2 Corporation Road #01-12 Corporation Place Singapore 618494 • **TAIWAN** /JIE DONG CO., LTD. 7F, 112, Chung Hsiao East Road, Section 1, Taipei, Taiwan 10023 (R.O.C.) • **THE NETHERLANDS** /JEOL (EUROPE) B.V. Lireweg 4, NL-2153 PH Nieuw-Vennep, The Netherlands • **USA** /JEOL USA, INC. 11 Dearborn Road, Peabody, MA 01960, U.S.A.